School of Civil and Mechanical Engineering
Department of Civil Engineering

Development of Hybrid Fibre Ferrocement Panels as Permanent Formwork of Concrete Slabs with Lightweight Blocks Infill

Nadim Frhat Abushawashi

This thesis is presented for the Degree of
Doctor of Philosophy
of
Curtin University

July 2015

DECLARATION

To the best of my knowledge and belief this thesis contains no material previously published by any other person except where due acknowledgment has been made.
This thesis contains no material which has been accepted for the award of any other degree or diploma in any university.

Signature:

Nadim Abushawashi
Date: July 2015

ABSTRACT

The structural performance of conventional ferrocement as a thin cementitious composite has been enhanced by using hybrid PVA fibre. The method used to achieve high performance in deflection, strain and strength capacity is through the enhancement of the matrix toughness. Consequently, deflection hardening, strain hardening behaviour, and multiple crack formation were achieved by adding two different PVA fibres to ferrocement.

The structural performance of Hybrid PVA fibre ferrocement (HFF) with various PVA fibre combinations was investigated using different volume fractions of fibres in mixtures. Two types of PVA fibres short (8 mm) and long (30 mm), were used. The volume fraction of the fibres was in a range of 0.75 to 1.5% of the total sample's volume. The best fibres combination and content were determined testing the performance of HFF panels. To enhance the workability, different water to cement ratio and additives, such as fly ash, silica fume, and superplasticizer, was added to the matrix. Moreover, the composition impact on the structural performance was also determined using statistical approaches.

The structural behaviour of HFF panels was further examined to determine the composite properties. The tested composite properties were the compressive, tensile, flexural and shear strengths, as well as the fibre pullout strength. Furthermore, phase properties of the composites, which are the elastic modulus, hardness, and packing density, were determined using nanoindentation technique.

The impact of elevated temperature and carbonation were experimentally examined to investigate the durability properties of HFF composites. The effect of higher temperatures on the HFF panel on the microstructure, flexural, and compressive strength was evaluated. Furthermore, the carbonation impact on the structural performance was determined. The changes in microstructure, chemical components, and structural performance were observed using XRD, and SEM. The composites showed excellent behaviour in resisting heat and carbonation impacts.

HFF panels were then used in a novel reinforced concrete slab composite. The panels acted as permanent formwork in combination with one-way concrete slabs using autoclaved aerated blocks as infill material. The flexural test of 13 composite slabs was conducted. The slabs achieved full composite action. The tests

have shown that the concept of using HFF panels as permanent formwork is a success in term of structural performance.

Finally, finite element modelling and analyses were carried out. The materials properties of the HFF composite used in the model were from the obtained test data. The fibre effect was also considered by applying the fibre properties using the smeared method. The analytical results agree well with the test results. On the other hand, a similar approach was used to model the slab composite. The finite element model gave a relative underestimated stiffness of the overall composites, but the stresses at the first crack and ultimate state were found comparable with the experimental results. Further works were recommended.

In general, the new produced structural composite enhance the quality and performance of an efficient, low-cost construction material and improve its ability as a high performance material to compete with other structure materials in the construction industry.

Keywords: *Hybrid PVA fibre ferrocement, Deflection hardening, strain hardening, High performance, permanent formwork, Slab composite.*

ACKNOWLEDGMENT

This thesis is the result of the research carried out from February 2011 till July 2015 at the Department of Civil Engineering at Curtin University of Technology.

Iwould, first of all, want to express my deepest gratitude and sincere appreciation to my supervisor, Dr Vanissorn Vimonsatit, for her guidance, support, and patience. In particular, I am grateful for her encouragement, empathy and guidance throughout the period of research.

I wish also to thank Dr Faiz Shaikh Ahmed (Co-supervisor), Professor Hamid Nikraz, Mr Gorge Hopkins, and Professor Pichai Nimityongskul for their support and advice.

The sincere thanks are extended to my colleagues Hyuk Lee, and Peng Loy Chow for their fruitful discussions and advice. Also my greetings to the technical staff and data acquisition stuff of the Civil Engineering workshop and laboratories, for their assistance and attention in the experimental work.

Special appreciation and greetings are addressed to Dr. Kornkanok Boonserm and Mr. Niti Kongsin from Department of Management Engineering, Rajabhat Mahasarakam University in Thailand, for their assistance in microstructure analysis of carbonated samples. Thanks are also extended to Chi Chung (Kelvin Siew) and Hong Hui (Johnny Sim) for conducting part of the carbonation experimental work as a final year project. Also a special thanks to Elite Editing for editing the thesis, using editorial intervention to Standards D and E of the *Australian Standards for Editing Practice.*

I would like also to acknowledge the Libyan Ministry for Higher Education for their scholarship which gives me the opportunity to study at Curtin University.

At the end, I have to say that the largest support came from my family, wife and children, through their support, understanding, and patience. Although I have not forgotten my family members, which were a bit far away but have encouragedme through the whole study period. God be thanked in the beginning and the end.

PUBLICATION LIST

Journal Publication:

Abushawashi, N., and V. Vimonsatit. 2014. "Influence of mixture, wire mesh and thickness on the flexural performance of hybrid PVA fibre ferrocement panels." *International Journal of Innovative Research in Science Engineering and Technology* 3 (9).

Abushawashi, N., and V. Vimonsatit. 2015a. "Flexural behaviour of hybrid polyvinyl alcohol fibre reinforced ferrocement containing different fibre types and volume fractions." *Australian Journal of Structural Engineering*: Accepted for publication.

Abushawashi, N., and V. Vimonsatit. 2015b. "Material classification and composite elastic modulus of hybrid PVA fiber ferrocement." *Journal of Materials in Civil Engineering*: Accepted for publication.

Abushawashi, N.F., V. Vimonsatit, and F.U.A. Shaikh. 2015. "In situ flexural behaviour of hybrid PVA fibre reinforced ferrocement panels at elevated temperatures." *Construction and Building Materials* Submitted under review.

Conference Publication

Abushawashi, N., V. Vimonsatit, and G. Hopkins. 2012. "Shotcrete prefabricated ferrocement panels by using WA mixture materials." Research, Development, and Practice in Structural Engineering and Construction, Perth, Australia.

Abushawashi, N., and V. Vimonsatit. 2014b. "Use of ferrocement panel as reinforced concrete slabs with lightweight blocks infill." Sustainable Solutions in Structural Engineering and Construction., Bangkok, Thailand.

Table of Contents

List of Figures

List of Tables

List of Abbreviations

AAC	autoclaved aerated concrete
ACI	American Concrete Institute
ASTM	American Society for Testing and Materials
CC	cement clinker
CDF	cumulative distribution function
C-S-H	calcium silicate hydrates
ECC	engineered cementitious composite
EF	Engineered ferrocement with mono PVA fibre
FA	fly ash
FE	finite element
FEM	finite element model
FRC	fibre-reinforced concrete
FRCC	fibre-reinforced cementitious composite
HD	high density
HFF	hybrid fibre ferrocement
HFF-OWC	hybrid fibre ferrocement combined with one way concrete slab
HFRC	hybrid fibre-reinforced concrete
HPFRCC	high performance fibre-reinforced cementitious composite
LB	larger is better function
LD	low density
LVDT	linear variable differential transformer
OA	orthogonal array
OPC	ordinary Portland cement
PDF	probability density function
PE	polyethylene

R/ECC	Reinforced engineered cementitious composite
RC	reinforced concrete
RVE	representative volume element
S/N	signal to noise function
SEM	scanning electron microscope
SF	silica fume
SFRC	steel fibre-reinforced concrete
SHCC	strain hardening cementitious composite
SNT	statistical nanoindentation technique
UHPFRCC	ultra-high performance fibre-reinforced cementitious composite
XRD	X-ray diffraction

Chapter 1: Introduction

1.1 Defining the problem

In recent decades, many so-called cementitious composite materials—a type of thin-walled material—have been developed by materials scientists. These materials include ferrocement, engineered cementitious composites (ECCs), high performance fibre-reinforced cementitious composites (HPFRCCs) and ultra-high performance fibre-reinforced cementitious composites (UHPFRCCs). Such materials present a unique opportunity for civil engineers to reduce construction costs in the form of both labour and materials. Labour costs can be controlled by mechanising construction methods or eliminating construction steps and material cost reduction can be achieved by using alternative materials, such as lightweight construction technology. The investigation and development of lightweight and thin-walled construction elements is a growing trend. Due to the excellent properties of cement composite materials, their application has increased enormously. This is especially true for wire mesh- and fibre-reinforced cementitious composites (FRCCs), because their production is similar to that of traditional construction materials and their application in construction is straightforward. Several of these materials, such as ferrocement and ECC, have been the subject of intensive research for application possibilities, whereas others, such as hybrid fibre cementitious materials, are currently under development and are the subject of ongoing research.

Ferrocement is an adaptable composite of a reinforced cement product. Its low material cost components have stimulated interest in this construction material in developing countries in recent decades (Brown 1973). The application of this thin shell, wire mesh-reinforced cementitious construction material has been progressively studied to identify its potential as a structural element in several types of construction. Despite this wide range of applications in developing countries, the conventional construction method using ferrocement panels is labour intensive. This disadvantage generally discourages the integration of this less capital-intensive material in construction material lists. It is also the main reason why ferrocement is

not widely adopted in developed countries, where labour costs are a significant factor in construction costs. High labour costs can be overcome by introducing rapid production methods such as shotcrete or spray techniques, or precast production.

Another important way to reduce construction costs involves using cheaper, lightweight construction materials, or by using smart applications to reduce some construction steps. For example, ferrocement panels can be used as a permanent formwork in slabs and beams, thereby reducing the stripping of the form. To inspire the application of ferrocement, the utilisation of the lightweight propriety of this thin cementitious composite could be a satisfactory method. The use of this material as a lightweight structural component of construction systems, or in permanent formwork, can provide economic benefits for the entire construction industry.

One possible reason for the slow uptake of ferrocement into construction material lists in developed countries may be its relatively low strength capacity in comparison with newly developed high performance cementitious composites. The superior material properties of high performance cementitious materials have been achieved by modifying their microstructural properties. One way to achieve high performance properties is to increase the packing density of microminerals such as silica powder and silica fume (SF) (Ranade et al. 2013), which generally increases the compressive strength of the material. Another method is through the enhancement of a matrix's toughness by using fibre reinforcement to improve its strain hardening behaviour in tension, ductility and tensile strength (Swamy and Hussin 1990). The interaction of fibre in cement products including ferrocement may act as secondary reinforcement, leading to high performance specifications. This could be the key solution to promoting the use of ferrocement in the construction industry.

The current research investigates whether using two types of polyvinyl alcohol (PVA) fibre in ferrocement panels will enhance the performance of the ferrocement and its interaction with a developed material. Accordingly, the main research questions are (i) Does the addition of hybrid fibre significantly improve conventional ferrocement? and (ii) Will hybrid PVA fibre ferrocement panels function as a permanent formwork in a reinforced one-way concrete slab?

1.2 Research aims and objectives

The primary aim of this research is to extend the application of ferrocement via developments that improve its tensile capacity and provide more weight reduction, in a novel slab construction system. The extension of improved ferrocement applications may stimulate its use more intensively in developed countries. The elimination of the traditional slab formwork in the construction step, and self-weight reduction, has the potential to be of huge benefit in the construction industry. The investigation of structural behaviours in applications of hybrid PVA fibre ferrocement in autoclaved aerated concrete (AAC) one-way reinforced concrete (RC) slabs will be a substantial component of this research. Towards achieving the aims mentioned above, the related objectives are as follows:

- The first stage of the research will involve conventional ferrocement improvement:
    1. Conventional ferrocement will be enhanced by the addition of hybrid PVA fibre. The improvements will include tensile and ductility capacity by the interaction of two different types of PVA fibre (‘hybrid fibre’). The fibres act as a secondary reinforcement with wire mesh as the primary reinforcement, to create hybrid fibre ferrocement (HFF).
    2. Structural performance will be examined using flexure, tensile, compressive and shear tests. The experimental results will be compared with conventional ferrocement structural behaviour to evaluate the improvement level.
    3. The results from structural tests will provide additional structural information about the composite’s properties, which are very important in the design of the composite slab.
    4. The addition of hybrid fibre is expected to improve the flexure strength and increase the ductility of ferrocement and will influence its function in the proposed application (a slab system). The aim at this stage is to investigate the characteristics of the enhanced, modified ferrocement.
    5. This study will begin by experimenting with the mortar mixture, adding hybrid PVA fibre. The matrix will be further modified using other

additive materials such as fly ash (FA) and SF, with the goal of achieving high performance and excellent workability.

6. The composite will be classified according its structural behaviour. The classification process will consider strain hardening behaviour according to the tensile test. The toughness index will be calculated on the basis of flexural tests and the cracking behaviour of the tested specimens. The classification will place the composite into a particular material group, which will provide an overall better understanding of its structural behaviour.
7. The study will include an investigation of the composite's characteristics at the microstructural level. This will provide important information about its micromechanical material properties, providing further evaluation of the composite.

- The proposed application of the HFF panel is as a permanent formwork in concrete slabs using AAC lightweight blocks as infill material. The objectives of this part of the research are:
  1. To investigate the potential structural application of the HFF as part of a one-way AAC concrete slab. The viability of the proposed use in a slab system will be experimentally investigated. The test will examine whether the panels can be successfully used in the tension zone of slabs.
  2. To investigate slab behaviour during and after the test to determine whether the composite slab is exhibiting full composite action and can therefore act as a composite slab.
  3. To achieve any additional improvement to the structural performance of the composite slab, the research will investigate the influence of parameters such as the use of shear studs—a variation of the permanent formwork thickness.

1.3 Significance of the research

The research findings will encourage the use of a new approach to producing lightweight composite slab roofing systems for industrial low-cost housing construction. Moreover, they will promote better quality construction and use of

innovative systems in the industry. The research project represents an important step in the right direction to achieve the development of quality products. Accordingly, this project will:

- contribute to ferrocement application acceptance and improve its ability as a high performance material to compete with other structure materials in the construction industry;
- produce a new structural composite with potential as an alternative construction material in the housing and building industries;
- contribute to the decline in risk and in the cost of construction by using permanent formworks in slabs, which will be beneficial for the whole construction industry;
- encourage the production and use of ferrocement in modular housing and building systems, which can be developed and marketed nationally and internationally;
- enhance the quality and performance of an efficient, low-cost construction composite and make the information available for ferrocement constructors in developing countries.

1.4 Overview

This thesis encompasses two major topics. The first is the development of ferrocement by the addition of hybrid PVA fibre, and the second is the application of fibre ferrocement in the tensile zone of a lightweight slab. The thesis is organisedas follows.

Chapter 2 presents a review of the existing literature on the development and application of cementitious composites as high performance materials, including an overview of cementitious composites, ferrocement strength capacity and its applications, the effect of mono and hybrid fibre on crack bridging, the durability of thin-walled cementitious composites and the microstructural behaviour of this material.

Chapter 3 describes the experimental programme for assessing HFF behaviour using flexural, direct tensile, indirect tensile and compressive testing procedures, the equipment setup used, and the parameters investigated.

Chapter 4 examines the effect of different PVA fibre types and volume fractions (0.75%, 1.0% and 1.5%) added to ferrocement, and panel thickness, on strength capacity. Statistical analysis is used to determine the contribution of fibre type in the HFF to strength capacity. The effect of adding FA and SF in different proportions is evaluated.

Chapter 5 describes the structural and micromechanical material properties of HFF, including the flexural, tensile and maximum compressive strength capacity of the mixture matrix and composite element. An overview of the shear capacity and the fibre bond capacity according to the pullout testis provided. The microstructural behaviour of the mortar mixture including the hybrid PVA fibre is an important component of this chapter. Finally, the determination of the elastic modulus using different methods is described.

Chapter 6 examines the fire resistance of the HFF material and the effect of carbonation on material structural performance. To evaluate the heat impact on the HFF panels, a novel test setup was used. The samples were tested inside the Kiln oven while the designated temperature was achieved. On the other hand, the carbonation impact was studied by storing the samples in a chamber with ideal environmental properties for carbonation. The assessment of both impacts (elevated temperature and carbonation) followed in the structural and microstructural level.

Chapter 7 demonstrates the application of the HFF panels as a permanent formwork in a one-way AAC concrete slab. The effect of several variables on slab performance (e.g. HFF panel thickness, a slip of composite slab with and without shear studs) is examined. The results are compared with simple one-way concrete slabs (no panels in the tension zone) and a control slab using conventional ferrocement as a permanent formwork.

Chapter 8 presents a numerical model for HFF and the composite slab, after having tested all of the materials and structural elements. The models consider both the microstructural and structural levels. HFF panels are then incorporated in a numerical model applied to simulate a four-point bending test. An extensive finite element model (FEM), validating the results obtained from testing the composite slabs, is also used. The process is performed by comparing the computational and experimental results.

Chapter 9 summarises the overall research outcomes and related conclusions, and makes future research recommendations.

Chapter 2: Mono and Hybrid Fibre Cementitious Composite Materials

2.1 Introduction

With growing research efforts to enhance construction materials properties and invent, in particular, lightweight and high performance structural materials, an area of interest is to develop fibre-reinforced thin cementitious composite materials. The structural specifications of these materials vary depending on the additives used and in what proportions, and the type of reinforcement. The flow chart presented in Figure2.1 places thin cement composites and ferrocement within this family and shows that each member can stand alone or in combination with other members. An introduction to cementitious composite material development is provided in this section. Special attention is given to ferrocement, ECC and fibre-reinforced concrete (FRC) in the mono and hybrid reinforcement cases. Excellent overviews of ferrocement and ECC can be found in Naaman (2000), Naaman (2007) and Li 1993). Before providing a general overview of these composites, fibre effect, strain hardening, quasi-brittleness, and their relationship with high performance specifications are discussed. In particular, the definition and illustration of the effect of hybridisation of reinforcement on material characteristics areessential. This chapter will also focus on the theoretical background of cementitious material and its proposed application as composite slabs.

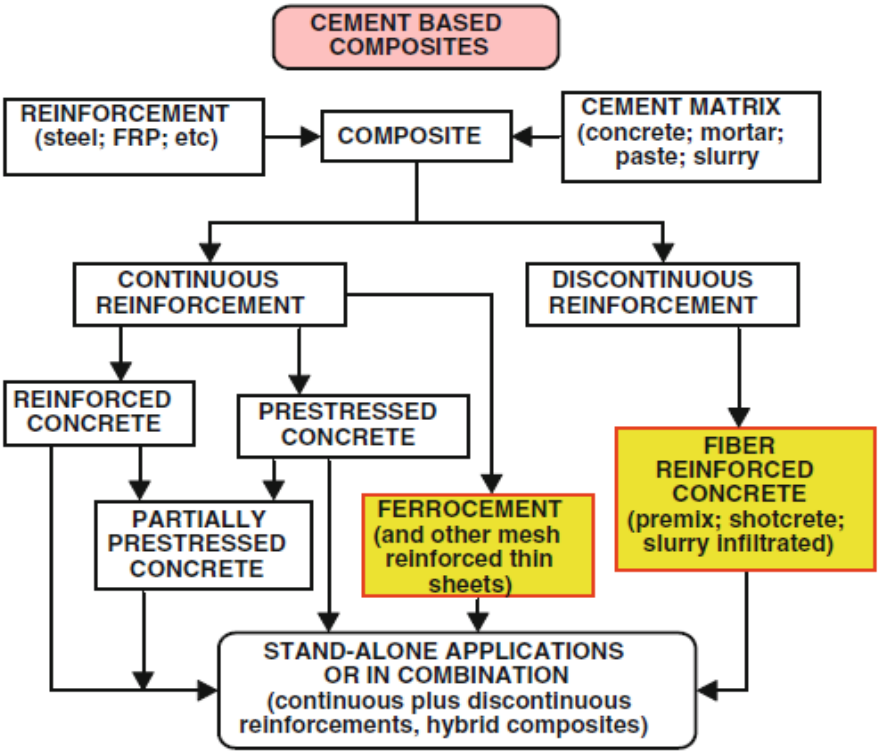

Figure 2.1 Cement-based composite and hybrid combination (source: Naaman 2013)

2.2 Fibres in cement-based composites

2.2.1 Fibre types and forms

An enormous variety of fibre products is produced from several industry branches for different purposes. Only a few types of discontinues fibre have proven to be compatible with use in cementitious composites. The suitability of fibres for cement paste relates to the bond between the fibre and the matrix. Discontinuous fibres are characterised in different ways(Altun, Haktanir and Ari 2007), according to: (1) source—natural organic, such as cellulose, horse hair and bamboo; natural mineral,such as rock wool and asbestos; produced, such as steel, carbon, glass, synthetic and polymers; (2) specifications (chemical, physical or mechanical).This could include density, non-reactivity with the cement matrix, elastic modulus, stiffness and ductility, among others; (3) geometric properties of the fibre, including length, diameter and cross-sectional shape (Naaman 2007). The American Society for Testing and Materials standard (ASTM Standard 2011a) classified the fibre used in concrete into four main types: steel fibre, glass, synthetic and natural fibre. The

following is a short overview of the fibres most frequently used in reinforcing of cement-based materials.

2.2.1.1 Steel fibres

Steel fibres have relatively high strength and modulus of elasticity, and are protected from corrosion by a highly alkaline matrix. ASTM A820 (ASTM Standard 2011b) establishes the minimum mechanical requirements for steel fibres employed in reinforcing concrete. The enhancement of the bond between fibre and matrix can be achieved through the improvement of its mechanical anchorage. One way to accomplish this is by deforming the fibre or increasing the surface roughness. Deformed shapes to enhance the bond are shown in Figure 2.2.

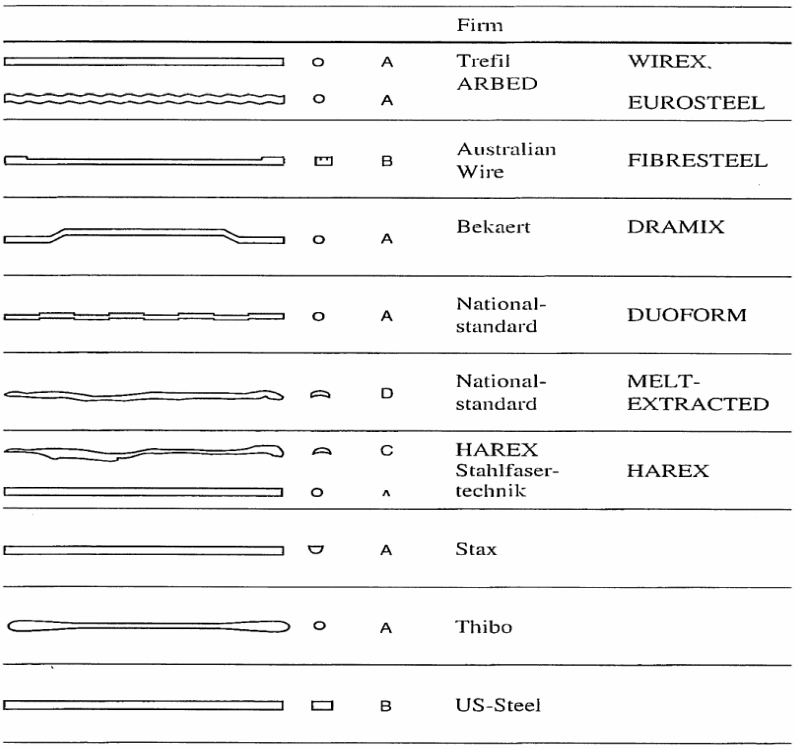

Figure 2.2 Steel fibre forms according to Grübl, Weigler and Karl (2001)

However, the primary known modified steel fibres are as described below.

Hooked steel fibre (Dramix): One type of hooked steel fibre is 'Dramix'. Dramix was developed and industrialised in Belgium by Berkaert. The fibre is produced from cold-drawn, high-tensile-strength steel wire with hooked ends that drive the mechanical bond. The deformed ends contribute to bond strength through

the work required to straighten the fibre during pullout (Xu, Ju and Shi 2011). The straightening mechanism for hooked steel fibre during the pullout test is divided into the three main stages shown in Figure 2.3.

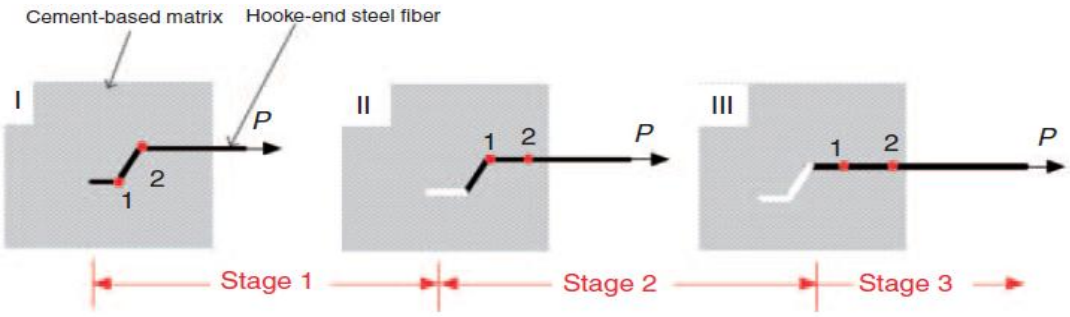

Figure 2.3 The Schematic pullout process for a hooked steel fibre in a cement matrix (Xu, Ju and Shi 2011)

Twisted polygonal steel fibres (Torex): In 1999, Naaman developed a twisted polygonal steel fibre known commercially as 'Torex' (Naaman 1999). The fibre is engineered to achieve optimal properties in terms of mechanical properties and compatibility with a matrix. Torex fibre is produced from a twisted polygonal high-strength steel wire along its length (see Figure 2.4). The main advantage of Torex fibres is their large contact sectional area providing a direct increase in adhesive and frictional components of the bond. Another significant advantage of Torex fibre is its excellence in pullout resistance, which increases with increases in slip while being pulled out from the matrix. This confers a high level of resistance, achieving 70–80% slip over the total embedded length (Naaman 2003b).

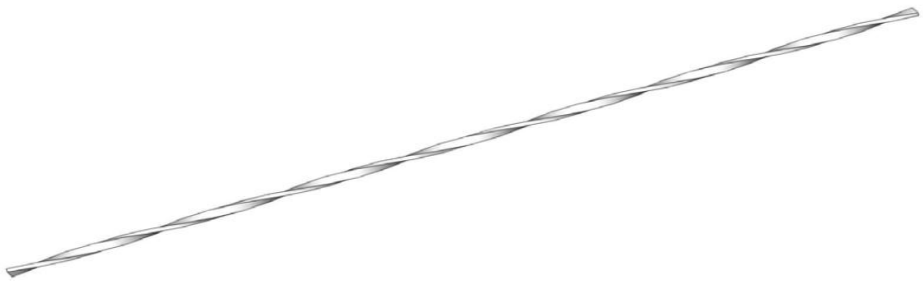

Figure 2.4 Torex steel fibre (Suwannakarn 2009)

2.2.1.2 Glass fibres

Short-length glass has been widely used in the construction industry for non-structural elements such as facade sheets, architectural precast concrete, pipes and channels (Shakor and Pimplika 2011). A significant requirement for glass fibres is a minimum content of 16% zirconia for alkaline resistance (Banthia et al. 2012). Other glass fibres, like E-glass fibres, are recommended for uses other than concrete reinforcement. Glass fibres have high modulus and high strength, and develop a strong bond with the concrete. One shortcoming of using glass fibre is its high cost due to the high required content in the concrete: ~ 4–6% volume fraction. A fibre content of 1–2% volume fraction is more typical in FRCCs.

2.2.1.3 Synthetic fibres

Synthetic fibres are mainly developed from petrochemical and textile products, and are non-metallic fibres. Some of the commonly used synthetic fibres in cement-based composite are described below.

***Carbon fibre*:** The use of carbon fibre in cement-based composites began in the early 1970s (Ali, Majumdar and Rayment 1972). High-modulus, short polyacrylonitrile fibres were used and significantly improved the mechanical properties of the cement matrix. However, the high cost of polyacrylonitrile-based fibres limited their employment in FRC. More cost-efficient carbon fibre was produced in the 1980s from pitch-based carbon fibres, developed and studied for their appropriateness in cement-based composites (Banthia 1992). Carbon fibre is distinguished from other fibres by its high elastic modulus, heat resistance and chemical stability in an aggressive alkaline environment.

***Polypropylene*:** This fibre was produced from homopolymer polypropylene resin that can be found in two types of cementitious composite reinforcements. These two fibre types are monofilament and fibrillated, both characterised by small elastic modulus, low melting point and reduced bond development (Banthia et al. 2012).

***Polyvinyl alcohol*:** Since the 1980s, PVA fibre has been applied to cement-based composites. This highly stiff and insoluble fibre was produced during manufacturing of petrochemical PVA resin. Its relatively lowcost and high chemical

bond strength, due to the hydrophilic nature of PVA fibre, have led to considerable interest in using PVA fibre in cementitious composites.At the molecular level, hydrogen bonds result in high mechanical bond strength between the PVA fibre surface and the cement matrix (Horikoshi et al. 2006). However, PVA fibres tend to rupture due to their high bond strength and relatively low tensile strength as cracks open, rather than exhibiting pullout failure. Consequently, the fibre surface is treated with an oiling agent to reduce the bond strength (Li, Wang and Wu 2001).

***Polyethylene (Spectra)*:** The material known as 'Spectra' is made from ultra-high-molecular-weight polyethylene (PE). Concrete reinforced with high-modulus PE fibre has high strength, toughness and very high impact resistance. Unfortunately, Spectra fibre shows weak bond strength in a cement matrix (Soroushian, Khan and Hsu 1992). Despite this, it exhibits slip hardening behaviour during fibre pullout, which is due to the abrasion effect (Suwannakarn 2009). In addition, Spectra-reinforced, cement-based material exhibits a slip hardening response. This is due to damage to the Spectra fibre surface after it is pulled out from a cementitious matrix. The fibre is brittle so breaks into small fibrils which gather around the fibre; this prevents the fibre from being pulled out smoothly. This mechanism grows the fractional bond strength between the Spectra fibre and cement matrix. This creates a fibre that has similar tensile strength to steel fibre but is several times lighter—another significant advantage in using Spectra fibre as reinforcement.

2.2.2 Fibre effects on cementitious composites

Fibres in reinforcing cementitious composites are classified according to their content in the composite: low (<1%), moderate (1–2%) or high-volume fraction (>2%). This classification allows the determination of fibre contribution and its effect on the strength capacity, toughness, energy absorption and strain capacity of the composite.

To understand the mechanism of a single fibre in a matrix, it is necessary to understand the effect of fibre on load transfer behaviour in uncracked and cracked composites. In uncracked composite subjected to tensile load, the tensile stress is transferred to the fibre. The adhesive bond carries a small load and there is no relative slip between the fibre and matrix. As pressure increases, chemical adhesive

bonds break. Simultaneously, shear bonds control the transfer of stresses to the fibre reinforcement. The uncracked composite moves stresses back from the matrix into the reinforcement in a cyclical way. As the load increases and the composite cracks, the load is carried by the fibres bridging the crack. The shear bond leads to the transfer of the load back into the uncracked zones of the composite. At this stage, the shear bond still resists the pullout of the fibre from the matrix. When the load reaches the maximum load capacity for the material, post-cracking occurs and the fibres bridging a crack are pulled out. These are the main factors affecting the mechanism of failure and defining its mode. In general, there are two types of shear bonds: the elastic shear bond that includes adhesion (depends on fibre type), and the frictional shear bond (Naaman et al. 1989).

A fibre's pullout mechanism is responsible for its high toughness, which is dictated by its contribution in transmission stress between the fibre and matrix (Naaman et al. 1991), whereby the tensile load applied to a fibre embedded in a cement-based matrix causes an extension in the fibre length at the penetration point of the fibre into the matrix. This is full elastic bonding at this stage. After that, the fibre gets partially de-bonded and begins a process of plastic deformation. As the load increases, complete fibre debonding occurs and the fibre becomes kinematically pulled out (Alwan, Naaman and Hansen 1991). The typical relationship between the pullout load and the slip is shown in Figure 2.5. Note that the slipbehaviour of synthetic fibre–cement illustrates slip hardening due to fibre surface abrasion (Lin and Li 1997).

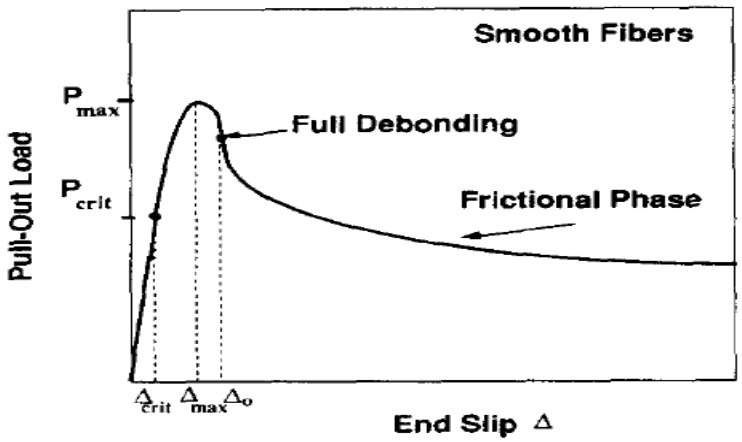

Figure 2.5 Typical pullout load–slip relationship (source: Alwan, Naaman and Hansen 1991)

To improve the mechanical bond between the fibre and the matrix, fibre can be modified by roughening its surface along its length by persuading mechanical deformations: fibres can be deformed, coiled, twisted and hooked. Another method is mixing a high density (HD) cement matrix. The bond at the microscopic level is improved using the more subtle particle material in the matrix mixture. This increases the packing density on the surrounding surface area of the fibre and increases the interfacial friction, as seen in Figure 2.6 (adhesive elastic shear bond) (Shannag, Brincker and Hansen 1997).

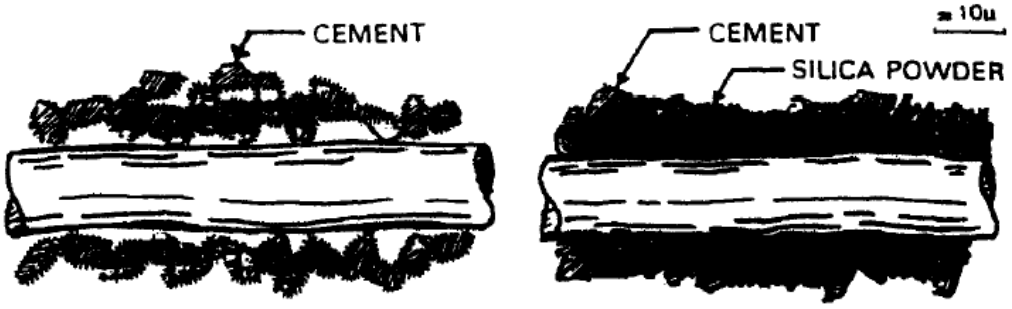

Figure 2.6 The effect of a high packing density matrix (Shannag, Brincker and Hansen 1997)

Analytical methods to calculate pullout strength and bridging load have been developed, involving models predicted under the reflection of multiple cracking behaviours (Kullaa 1996). To improve those models, fibre bridging due to pullout stress, debonding stress and debonding displacement has been predicted considering the influence of cracks, strain hardening behaviour, matrix micro spalling and the Cook–Gordon effect (Kullaa 1998). The Cook–Gordon effect describes a de-bonding normal-to-fibre axis caused by a tensile load in the fibre–matrix interface. The revised model promises greatly improved design technologies for fibre-reinforced cementitious materials (Yang et al. 2008). Pullout behaviour has been furhter investigatedto determine parameters all neededto calculate the average shear stress. The designated shear stress occurs during an applied pullout load on a single fibre (known as bond strength) (see Figure 2.7). In Yang et al. (2008) investigation, the effect of different fibre shapes was also included as one of the studied parameters. It was evident that deformed shapes contributed to different pullout mechanisms with

additional generated loads (Figure 2.8). The test results indicated an equivalent bond strength using twisted or hooked steel fibres, which was found to be four to five times stronger than smooth steel fibre (Wille and Naaman 2012).

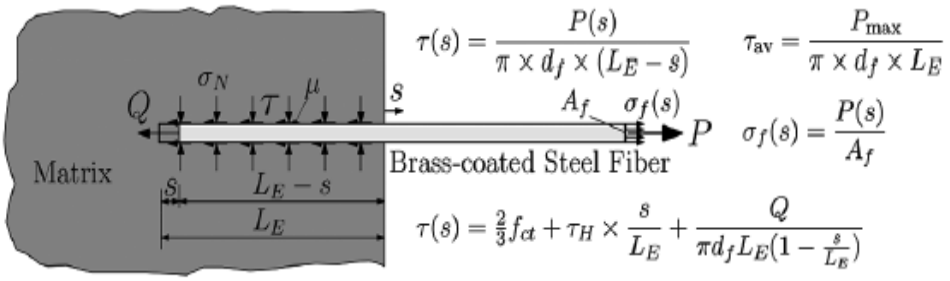

Figure 2.7 Definition of average shear stress τ(s) at a given slip (source: Wille and Naaman 2013)

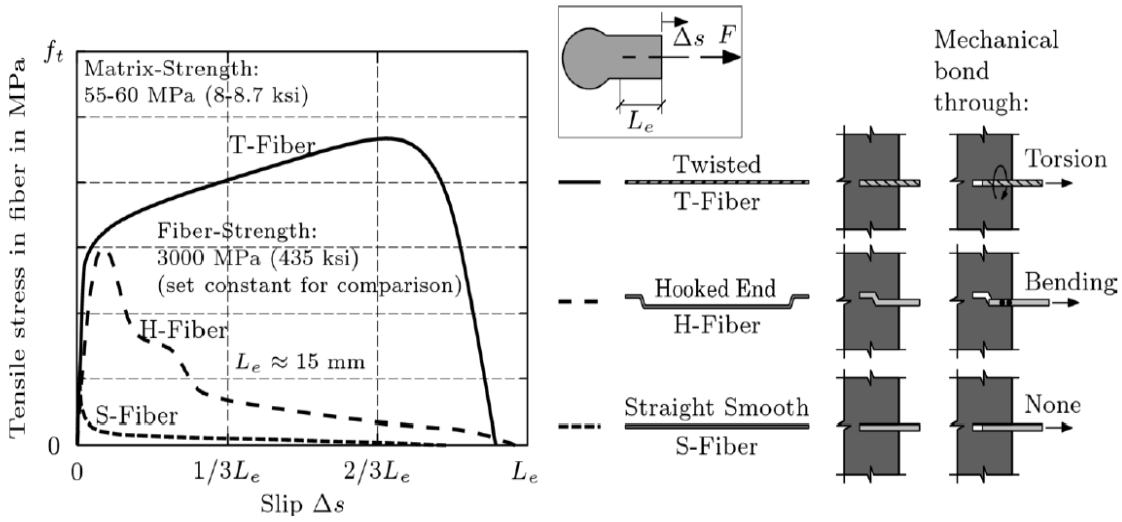

Figure 2.8 Comparison between pullout behaviours of straight, hooked and twisted fibres (source: Wille and Naaman 2012)

2.3 Hybridisation of reinforcement

The term ‘hybrid’ indicates that two or more different types of reinforcement are used. The hybridisation process of fibres in cementitious composites occurs by combining fibres that differ in geometry, and structural and mechanical properties, in a cement matrix (Ravichandran, Suguna and Ragunath 2009). Hybridisation of fibres provides superior mechanical properties of composites compared with their mono counterparts. Hybridisation of fibres can be achieved in several ways. For instance,

by using different types (metallic and polymeric), modulus, lengths or diameters (Ahmed, Maalej and Paramasivam 2003; Ahmed and Mihashi 2011).

Developments have been made to further enhance the performance of FRCCs such as ECC, through the interaction of two different fibre types with different lengths and tensile strengths. A significant increase in strength and ductility, exhibiting strain hardening behaviour and multiple cracking was observed by using hybrid fibres compared to a single fibre in ECC (Ahmed and Maalej 2009). The use of hybrid fibres shows that different length scales can activate the bridging stress during different cracking processes undergone by ECC with its multiple crack behaviours (American Concrete Institute (ACI) Committee 549-R97). This bridging stress process would allow shorter fibres to be active at microcrack formations until rupture or pullout (Li and Wang 2006).

A better understanding of the hybridisation effect in a matrix can be achieved through detailed consideration of fibre function at the micro- and macrocracking level. Using short fibres (micro fibres) combined with longer fibres (macro fibres), leads to short fibre bridging microcracks, as propagation is closely spaced. This makes the micro fibres responsible for the enhancement of the first cracking tensile strength of the composite, as seen in Figure 2.9. However, as microcracks extend with increasing load to macrocracks, the micro fibres are shorter and therefore pulled out, constituting rupture. After macrocracksare formed, longer fibres become active. At first, they capture due to the effective propagation of macrocracks, leading to strain hardening behaviour and multiple crack formation. When the macrocrack opening increases to large cracks in the localisation phase, the longer fibre still bridges those cracks until strain softening and ductile failure occurs (Betterman, Ouyang and Shah 1995; van Mier 2004). This hybrid fibre crack bridging effect is as seen in Figure 2.10.

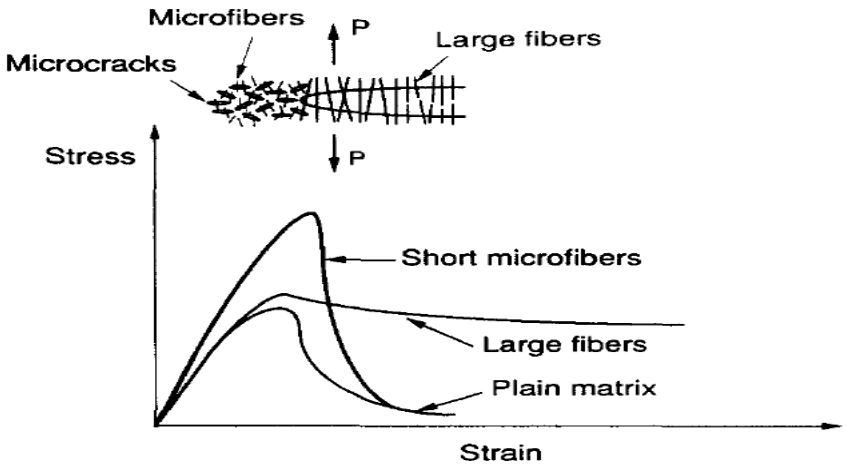

Figure 2.9 Influence of different fibres on tensile strength and crack behaviour (Betterman, Ouyang and Shah 1995)

In a separate investigation of hybrid fibre-reinforced cement composites, it was found that the tensile stress–crack opening responses indicate that different fibres are activated at different length scales of the cracking process. The smalldiameter fibres are more efficient at minuscule crack openings. However, multiple hardening composites are showing differentiated contribution of the fibres to cracks at different scales of the cracking process (Pereira, Fischer and Barros 2012a).

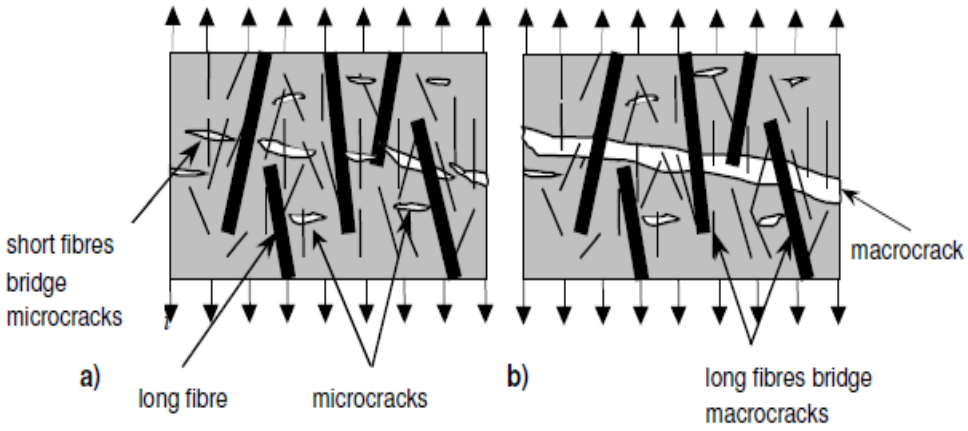

Figure 2.10 Effect of short and long fibres in a matrix (Markovic 2006)

Ahmed, Maalej and Paramasivam (2007a) performed several studies on hybrid fibres in ECC in their investigation of the flexural response of hybrid fibre cement composites. They found that the modification of ECC with hybrid fibre allowed particular pseudo-strain hardening ability under tension (strain hardening). This has the effect of increasing ductility, post-cracking strength and energy

absorption capacity (Ahmed and Maalej 2009; Pereira, Fischer and Barros 2012a). Mixtures of hybrid fibre with 1.5–2% volume fraction (V_f) with high-volume FA shows HPFRCC behaviour (Ahmed, Maalej and Paramasivam 2007b). Moreover, they developed a design concept for the critical fibre volume fraction on the basis of fracture and deformation mechanism using the effect of hybrid fibres (Figure 2.11), and an analytical equation to calculate the maximum bridging stress of hybrid fibres in a cement matrix (Equation 2.1).

$$\sigma_{cu} = g_1\sigma_{o1}\left[1 - \frac{2\delta_2^*}{L_{f1}}\right]^2 + g_2\sigma_{o2} \qquad (2.1)$$

where g is the snubbing factor; L_{f1} is the length of the shortest fibre; δ^* is the maximum slip at full bonding; and σ_o (1,2) is the fibre tensile strength. The theoretical principals are taken from the composite bridging law as seen in Figure 2.12.

However, the predicted critical fibre volume fraction is a conservative estimate for ECC hybrid fibres only. Another significant finding in this study was that low-modulus fibres contribute more effectively to strain hardening and multiple cracking behaviour than do high-modulus fibres (Ahmed, Maalej and Paramasivam 2007a).

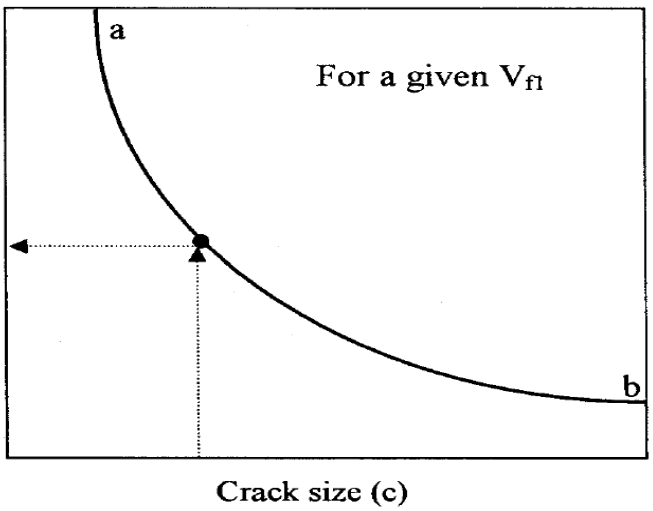

Figure 2.11 Design curve for critical volume fractions of hybrid fibre (source: Ahmed, Maalej and Paramasivam 2007a)

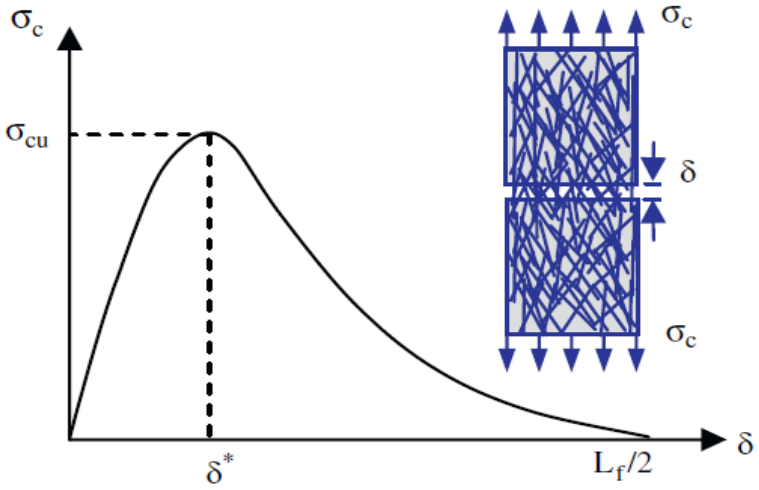

Figure 2.12 The bridging law of composites (Maalej et al. 2012)

2.4 High performancecementitious composite classification

A large variety of cement-based composites can be found today in practical construction use, including structural elements. Therefore, it is necessary to classify structural materials in accordance with their performance. The link between structural engineering and materials engineering is recognised because of material models and related material parameters. This reflects a material's behaviour through its physical specifications, which direct its structural and mechanical behaviours (Stang and Li 2004). The properties of cement-based composites that are significant for material performance classification are their compression strength, tensile strain behaviour, flexural response, toughness and energy absorption. Compressive strength is an important characteristic in concrete design, because of potential failure due to crashing in the compression zone (known as brittle failure). However, FRCCs exhibit quasi-brittle or strain hardening behaviour, so compression strength is not a relevant design parameter.

Types of failure are presented in Figure 2.13. Brittle failure behaviour occurs at a stage when the cement paste is hardened. Linear stress–strain behaviour is followed by an abrupt stress loss at the first crack, which is no longer able to resist any stress (curve A). In contrast, fibre concrete and some other fibre-reinforced cementitious materials exhibit quasi-brittle failure. This is observed as linear stress–strain behaviour followed by softening behaviour, as seen in curve B. On the other

hand, strain hardening materials are specified by their ability to resist stress after the linear elastic behaviour. Directly after reaching the first crack load an increase in strain will occur (large deformation) due to increasing levels of loading (curve C). The maximum strain value of a strain hardening material is usually higher than that of brittle or quasi-brittle material (Li 1997). A transition from quasi-brittle to strain hardening failure is only possible under conditions of 'steady-state' cracking, which arises under two conditions: (1) the stress at the crack must equal the first crack peak; and (2) the crack opening displacement must be less than the fibre slip caused by the bridging stress (Li and Leung 1992).

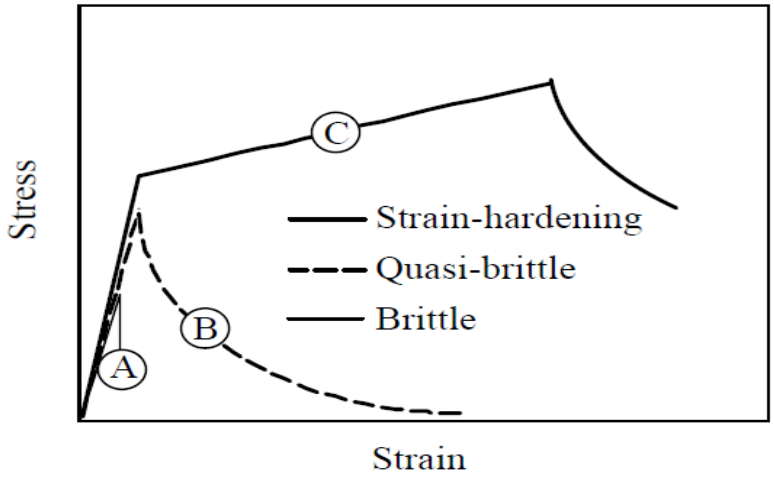

Figure 2.13 Model for type of failure in cementitious composites (Li 1997)

In general, the classification of fibre-reinforced materials relates to the strain hardening behaviour of the tensile strain response accompanied by multiple cracking behaviour. Although multiple cracking may infrequent not developed in strain hardening or deflection hardening depending on specimen size, test procedure or scale effect (Naaman 2003a). Other quantification methods can be used to classify the behaviour of fibre cement materials, such as flexural toughness indices, flexural load–crack opening relationships or tensile stress–crack opening relationships (Fischer 2004).

2.4.1 Strain hardening

The term ‘high performance’ has been used since the mid-1980s by Naaman to describe ‘strain hardening’ for fibre-reinforced, cement-based composites. According to Naaman (2007), high performance, fibre-reinforced cement composites are ‘a class of FRC composites characterised by a strain hardening behaviour in tension after first cracking, accompanied by multiple cracking up to relatively high strain levels’. He preferred ‘strain hardening’ over ‘high performance’ because the latter can be understood in different ways by different individuals.

It is clear that fibre-reinforced materials as thin walled materials with strain hardening behaviours have significantly better structural performance than conventional contra counters (Naaman and Jeong 1995). This isprimarily related to the enhancement of tensile stress and strain capacity. Therefore, the most appropriate mechanical classification method for strain hardening behaviour consists of tensile stress–strain response. An important indication of strain hardening is that the stress in the inelastic stage is higher than that at the first crack. In contrast to localised deformation in conventional cement materials, the deformation of HPFRCC is uniform on a macroscale and considered to be pseudo-strain behaviour. Pseudo-strain hardening, according to Fischer (2004), is used to ‘distinguish the cracking based deformation behaviour in HPFRCC from strain hardening in metals due to dislocation micromechanics’. On the other hand, bending tests showing deflection hardening in combination with toughness can be used for classification of high performance (Naaman 2003a). However, the direct uniaxial tensile test still represents the best way to confirm strain hardening behaviour (Li, Wang and Wu 2001). Moreover, the volume fraction in a cement matrix plays a significant role in strain hardening behaviour. The relationship between strain hardening and deflection hardening, and the critical fibre volume fraction in HPFRCC materials, is best described in Figure 2.14. However, fibre-reinforced composites showing strain hardening in tensile, and also deflection hardening in flexure are identified as HPFRCC materials.

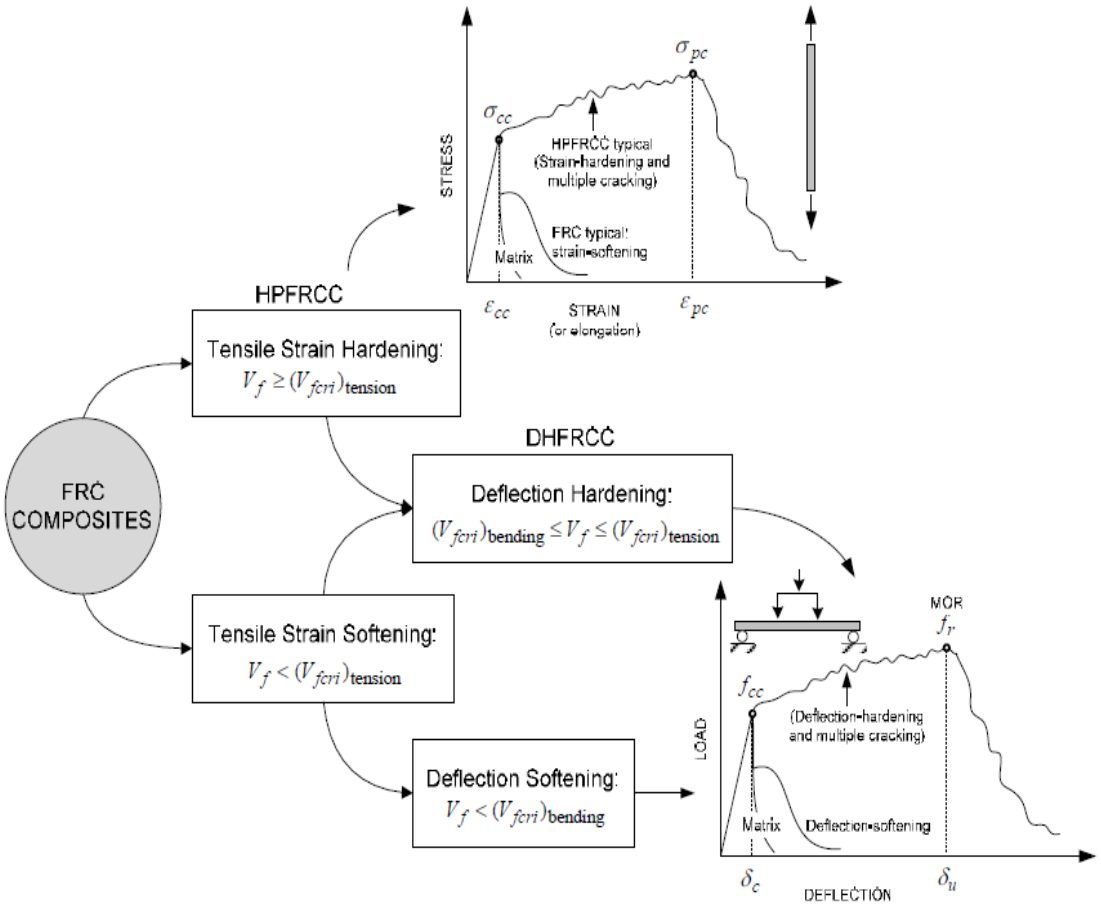

Figure 2.14 Classification of HPFRCC based on their tensile stress–strain response (Naaman and Reinhardt 2006)

2.4.2 Multiple crack behaviours

One of the most significant classification factors for high performance material behaviour is multiple crack formation. However, the fibre volume fraction must be properly designed, and the fibre must be in proportion with crack sizing. Under these conditions, the fibre effectively bridges developed macrocracks and transfers sufficient load after first cracking to allow the composite to undergo multiple cracking. At this stage of strain, hardening behaviour is developed (Lin and Li 1997). Fibre distribution is an important aspect governing the bridging behaviour of cracks. The second is the matrix flow size distribution, which affects the number of cracks at the multiple cracking stage. The relationship between microstructure and composite tensile behaviour describing multiple crack formation is shown in Figure 2.15. Pullout behaviour is dependent on the single fibre interface specification, which contributes significantly to the bridging capacity of fibres to cross the crack. Multiple

cracks are formed at this stage if steady-state cracking dominates the crack behaviour (Li and Wang 2006).

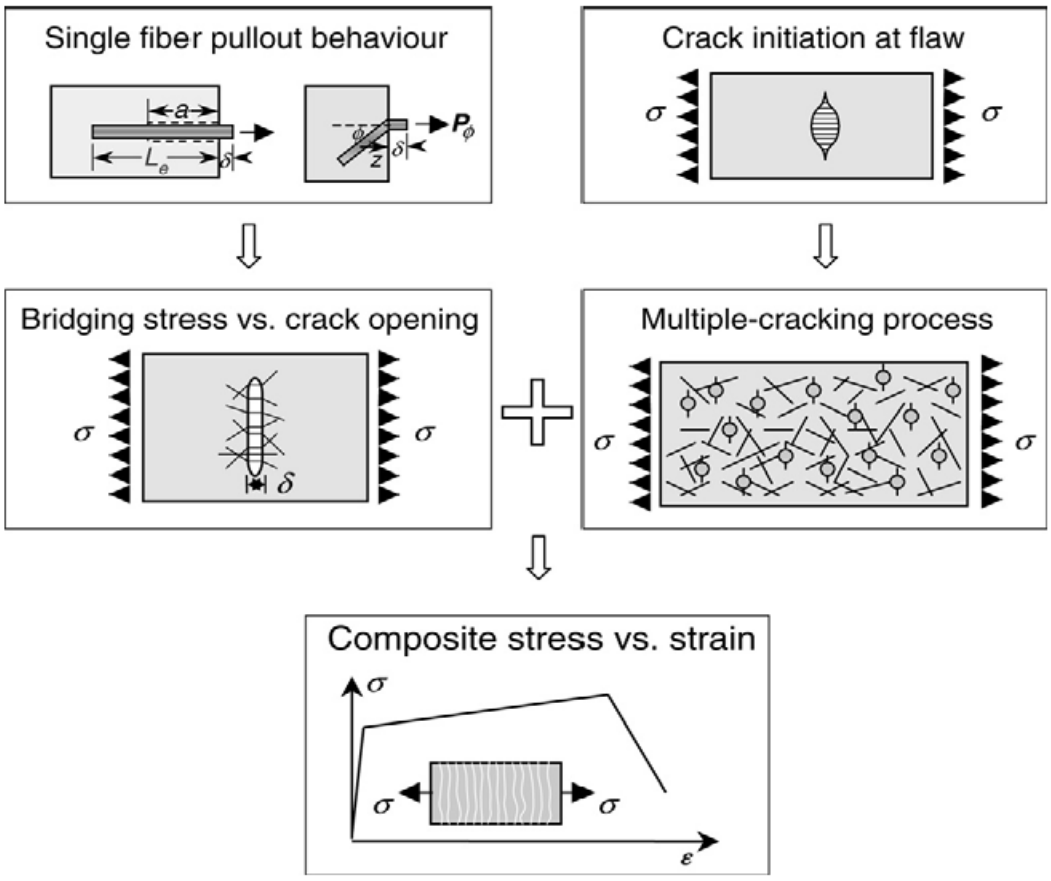

Figure 2.15 Multiple crack formation in ECC materials (Li and Wang 2006)

To explain multiple cracking behaviours in strain hardening materials, research was performed under the assumption that the first crack is also the failure crack. It was found that if the required energy to extend the critical cracks exceeds the energy needed to form a new crack, then as multiple cracks could be formed. The total strain at the peak of the localisation zone (after peak stress) represents the combined strain of elastic and inelastic strain (Tjiptobroto and Hansen 1991). Another study proposed an approach to predict the stress–strain relationship in a pseudo-strain hardening model emphasising fundamental micromechanics and experimental observations of multiple cracking (Kanda, Lin and Li 2000). The predicted model matched with the experimental results, which confirmed that bilinear behaviour in multiple cracking stages between the first cracking and the maximum tensile can be used for simplicity.

2.4.3 Toughness and toughness index

Fibre in a cement matrix not only enhances its ductility and tensile strength capacity, but also improves its toughness. The influence of fracture mechanics in the design of cement-based materials is substantial. This hasbeen recognisedbecause fibres in conventional concrete mainly increase toughness (Stang 2004). However, plain concrete and cement materials have shown a weak point in their inelastic energy absorption during fracture development, which is well described in their tensile stress–crack opening relationships. Thus, in concrete the fibre–matrix interface de-bonding energy is insignificant; it is more important in straining–hardening cementitious composites as a supplementary absorption capacity (Li and Maalej 1996b). The rules for fibre toughening a cement-based material can be seen in Figure 2.16, which shows the different crack stages and the interaction of fibre in aggregate bridging zones.

Accordingly, high performance materials subjected to flexural load usually show deflection hardening behaviour. Therefore, classification of high performance behaviour in fibre cementitious composites due to the flexure–deflection relationship can be achieved using toughness indices (Naaman and Reinhardt 1995). The toughness index is described in ASTM Standard (1997) as representing the area under the load–deflection curve up to a given deflection, divided by the area under the same curve up to first cracking. Different toughness indices (I_5, I_{10}, I_{30}, I_{50}, I_{100} *and* $I_{failure}$) can be determined depending on the deflection capacity of the materials. Ahmed, Maalej and Paramasivam (2007b) successfully used this method to illustrate strain hardening of a hybrid fibre ECC. Further, the high bond strength in hybrid fibre-reinforced cement-based composites is responsible for increasing their pullout resistance and therefore toughness, due to increasing the energy absorption and the fracture energy. This was experimentally examined by Mihashi and Ohno (2007).

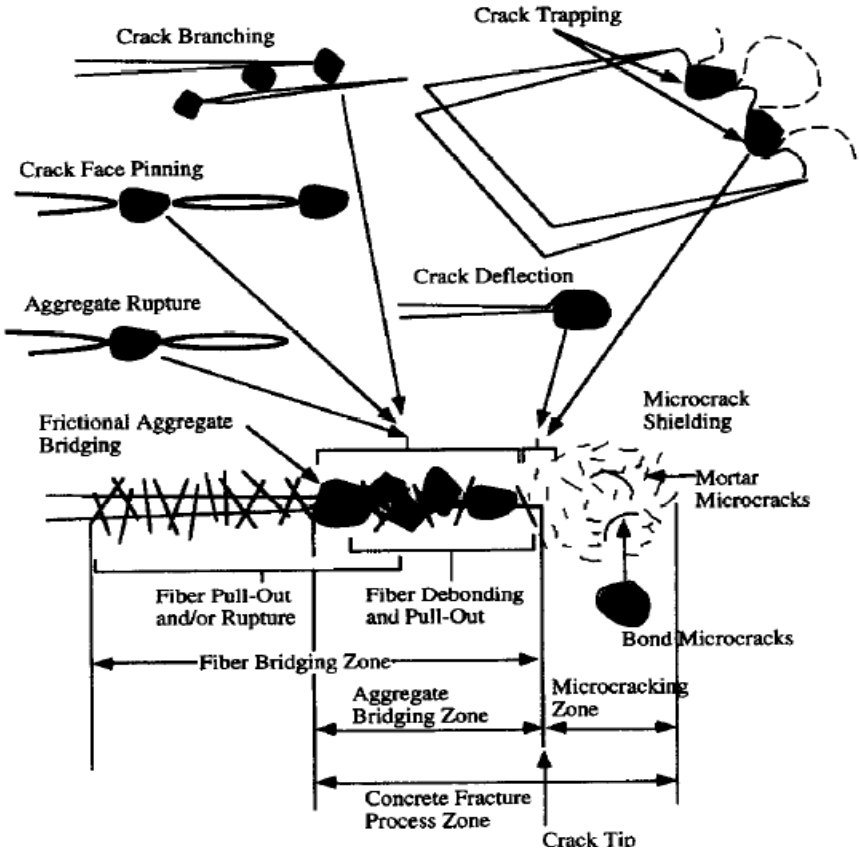

Figure 2.16 Possible toughening mechanisms in a fibre-reinforced cement composite (Li and Maalej 1996a)

2.5 Mono reinforced cementitious composites

2.5.1 Ferrocement

2.5.1.1 Material description and specification

In 1852, a landscaper applied for a patent under the name of 'Ferciment' when he experimented with wire meshes and plastered them with sand and cement mortar to build a boat (Paul and Pama 1978). Since then, ferrocement has become more attractive in other applications.

Ferrocement is a simple, flexible composite of reinforced mortar produced from cement, water, sand and wire mesh (see Figure 2.17). Committee 549 of the ACI (ACI Committee 549-R97 1997) defines ferrocement as 'a type of thin wall reinforced concrete construction where usually hydraulic cement is reinforced with layers of continuous and relatively small diameter mesh. Mesh may be made of metallic material or other suitable materials'. However, this construction material

differs from conventional reinforced or pre-stressed concrete by the method of the reinforcement (ACI Committee 549.2 R-04 2004), which is according to Naaman's only book of ferrocement more in detail described (Naaman 2000). Specific guidelines for wire mesh properties and the design of ferrocement are also reported in ACI Committee 549-R93 (2009).

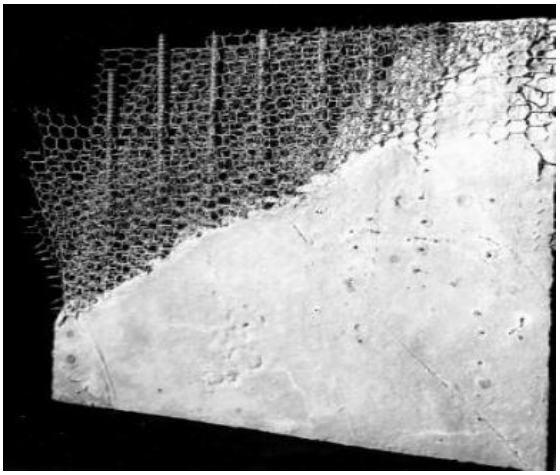

Figure 2.17 A typical ferrocement section (source: R.B. Williamson, University of California, Berkeley ACI 549-97)

Intensive tests have been conducted in recent decades to determine the structural capacity and general performance of ferrocement. The material shows excellent strength behaviour in bending and tensile tests. Both bending and tensile strength is reliant on several factors, such as the wire mesh volume fraction, the composite thickness and the mortar compressive strength (Sasiekalaa and Malathy 2012). The tensile strength at first cracking in ferrocement is directly proportional to the volume fraction of reinforcement (or layer number) (Mansur and Paramasivam 1985), although an equivalent elastic bending stress up to 50 MPa can be achieved using 7% wire mesh content (Naaman 2013). However, the tensile strength of ferrocement is more related to mesh orientation and the orientation in which the load is applied, in the uniaxial or biaxial direction. This isdue to the change in volume fraction regarding the loading direction (Arif, Pankaj and Kaushik 1999; Abdullah and Mansur 2001). Therefore, the wire mesh content of ferrocement has a significant effect on its flexural strength, modulus of rupture, toughness and energy absorption ability, as seen in Figure 2.18. This means that the increase of wire mesh layers up to a particular content and their arrangement in the panels increases the overall

structural capacity of ferrocement (Paramasivam and Sri Ravindrarajah 1988). Further investigation revealed that flexural and tensile strength capacity varies with different types of steel wire mesh. This is related to the effect of mesh orientation (Nanni and Zollo 1987; Hossain, Rokonuzzaman and Inoue 2005; Masood et al. 2003; Ibrahim 2011b).

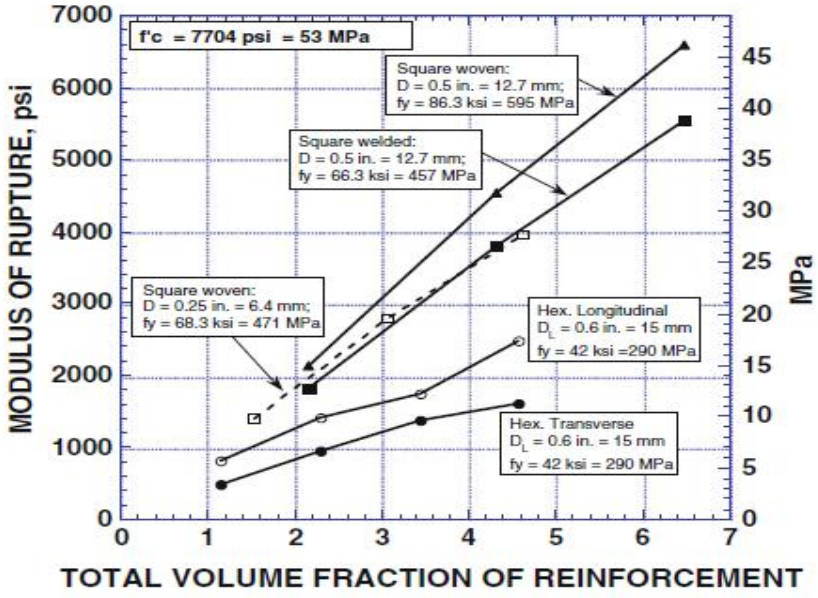

Figure 2.18 Relationship between modulus of rupture and wire mesh volume fraction (source: Naaman 2013)

Thorough investigations have been performed on ferrocement to provide an understanding of its flexural behaviour. This required development of an explicit design equation for the modulus of elasticity in flexure. Hossain and Awal (2011) developed such an equation using explicitly defined mesh factors for the different types of wire mesh. Moreover, efforts have been made to study the shear capacity of ferrocement, which proved to be almost identical to that of deep concrete beams (Ibrahim 2011a).

A simplified method based on the assumption that reinforcement yield at nominal moment resistance is recommended in the design of ferrocement. In this approach, strain distribution is assumed to be linear, and the compatibility of the cross-section and the stress–strain relationship is considered to be the most significant factor. Figure 2.19 shows the idealised stress–strain relationship for maximum strength of a ferrocement section. This assumption has provided useful

results compared to experimental data determining maximum strength (Paramasivam and Sri Ravindrarajah 1988; Swamy and Hussin 1990).

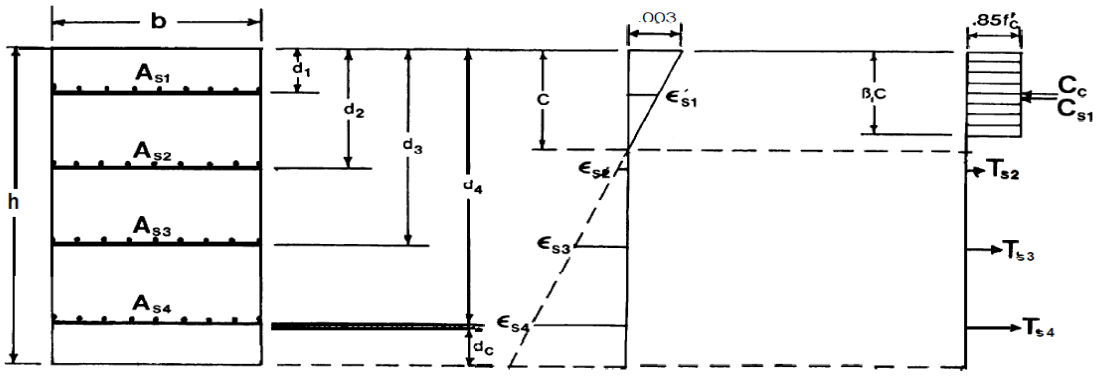

Figure 2.19 Idealised stress–strain diagram at maximum strength in a ferrocement section (adopted from ACI Committee 549.2 R-04 2004)

The crack characteristics of ferrocement can be categorised into three phases (Hago et al. 2005). The first is the pre-cracking stage, at which the mortar matrix and the wire mesh are inelastic. In this phase the load–deflection relationship is linear, and the first crack occurs. In Phase 2, multiple cracking begins after the cracking of the mortar matrix. The cracking mechanism in this phase is a load transfer from the mortar to the wire mesh, during which the wire mesh elongates and transfers the load back to the cement matrix. The reversed load produces new cracks. In Phase 3, failure occurs due to an increase in depth of the existing cracks. A crack after failure is shown in Figure 2.20.

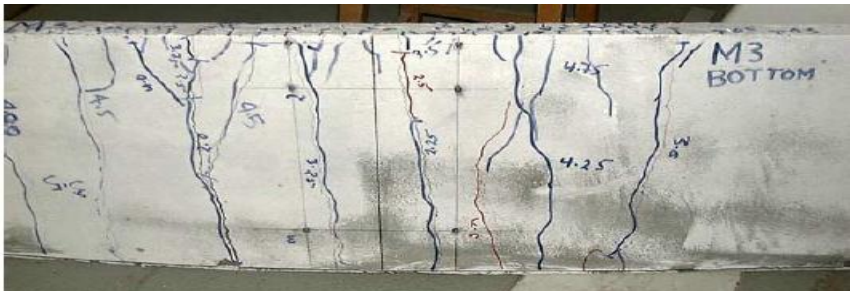

Figure 2.20 Crack pattern at maximum load (source: Hago et al. 2005)

In addition to the conventional wire mesh used in ferrocement, such as hexagonal (chicken mesh), woven and square wire mesh, researchers have developed more advanced steel reinforcements for ferrocement. In Belgium, Berkaert produced

a mesh-like product called Fleximat® (Naaman 2006), which incorporates high-strength fine steel strands in a longitudinal direction, and low-end polymeric line in the transverse direction. Another product promoted in the US market is a very high-strength, steel-based product with the tradename of Hardwire© (Naaman 2005, 2006), which exhibits a different way of reinforcing ferrocement. In addition, three-dimensional reinforcements suitable for ferrocement using steel or polymeric meshes (as seen in Figure 2.21), or a combination of both, have also been developed (Naaman 2013).

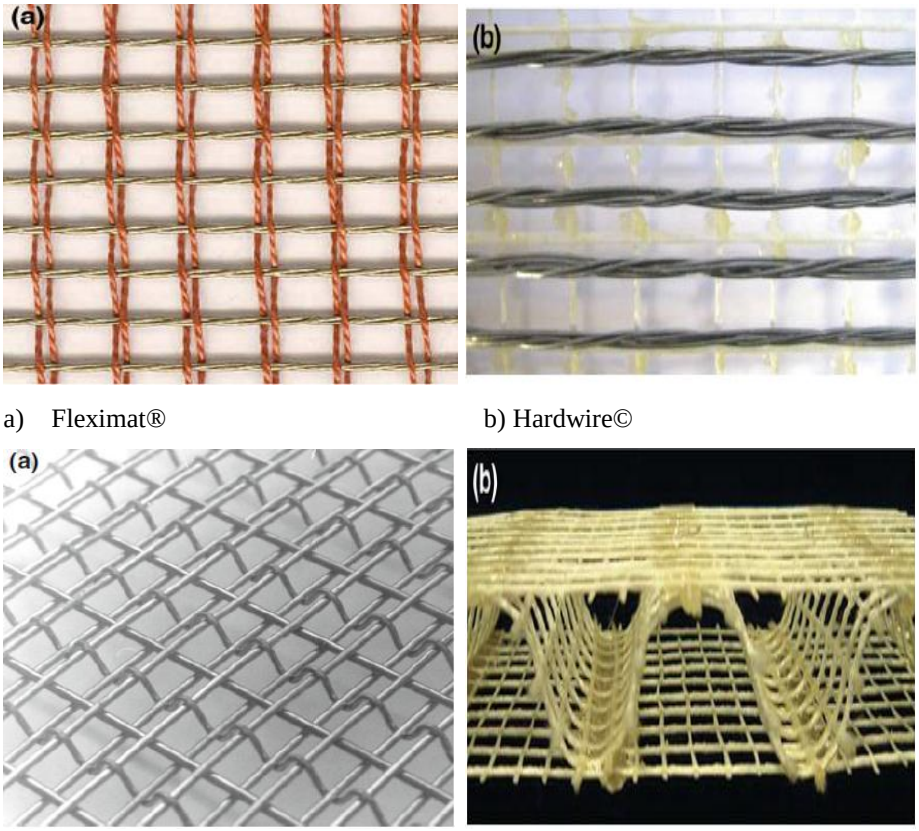

a) Fleximat® b) Hardwire©

a) Three-dimensional steel mesh b) Three-dimensional spacer stiff textile

Figure 2.21 Examples of advanced reinforcement (source: Naaman 2013)

2.5.1.2 Ferrocement durability

In general, ferrocement is recognised as a durable construction material that can last for many decades. The durability of this thin cementitious composite depends on numerous factors including mortar composition, corrosion of reinforcement, permeability, environment and construction application (Masood et al. 2003; Naaman 2000; Mansur, Maalej and Ismail 2008; Shannag 2008).

An important factor with respect to structural applications is the fire resistance of the construction material. More understanding of this by engineers in relation to ferrocement is required. There is a chance of fire in buildings and other structures due to accidents or other causes. Very high temperatures (up to~800 °C) can develop within 30 minutes (Cruz and Gillen 1980, Purkiss 2007) of fire and this can damage structural integrity. Therefore, it is important to understand the fire resistance of ferrocement if it is to be used for structural applications. The degradation of the mechanical properties of mortar at elevated temperatures due to fire is well established and widely researched (Kodur, 2002; Kong and Sanjayan 2010; Saemann and Washa 1997; Schneider 1988). Significant damage of RC structures is seen as spalling of cover concrete during fire. This spalling leads to direct exposure of the reinforcement to fire and causes a substantial reduction in the load-carrying capacity and stiffness of the structure (Balázs and Lublóy 2012; Şahmaran et al. 2011).

It has been shown that the ability of ferrocement to resist fire is not related to its wire mesh content (Greepala and Nimithyongskul 2006). The mechanical properties of ferrocement alone are not very good when it is exposed to fire, because it is a thin material with a thin cover over the reinforcement (Naaman 2000). However, the use of jacketed ferrocement with other structural components such as RC, or pre-stressed concrete may enhance the fire resistance of the composite element due to its ability to absorb more heat compared to concrete cover (Greepala, Parichatprecha and Tanchaisawat 2011). As mortar is an excellent insulator, the reinforcing mesh can reduce the spalling of the ferrocement matrix and probable collapse of concrete structures during a fire. However, the use of ferrocement as a cover on structural members to protect from damage associated with fire has not been well researched and to date has included only an examination of the residual flexural behaviour of ferrocement made with pure cement mortar, after exposure to fire (Greepala and Nimityongskul 2008). This showed that the increase of wire mesh volume fraction after exposure to fire is less significant than at ambient temperature, and the mortar cover has a negligible influence on the strength capacity of ferrocement.

2.5.1.3 Ferrocement applications

Cast-in-place ferrocement has inspired the adoption of this material in the construction world (Arif, Pankaj and Kaushik 1999; Naaman 2000; Paramasivam 2001; Brown 1973). The advantage of very easily constructing ferrocement in any desired shape allows its modern use for various complex architectural shapes including, for example, domes, curved building elements, water tanks or boats, which have been progressively studied (Paramasivam and Nathan 1984; Paramasivam 2001; Paul and Pama 1978). A significant application as a structural element is in roofing systems, where the use of ferrocement panels as slabs has been implemented as a domestic low-cost solution, for example in Egypt (Ibrahim 2011b) and the Caribbean (Clarke 2010). Full-scalemodel housing systems were tested and applied successfully using ferrocement elements to resist earthquakes and hurricanes (Adajar, Hogue and Jordan 2006; Saleem and Ashraf 2008). The use of ferrocement is not restricted to small-scale elements; its low permeability provides high ductility that allows its use in large-scale water tanks (United Nations High Commissioner for Refugees (UNHCR) 2006).

2.5.2 ECCs

2.5.2.1 Material description and specification

ECCs were first discovered in 1971 by the IPC group (Aveston, Cooper and Kelly 1971). Since then, great efforts have been made to develop this fibre cementitious composite. The most significant advantages of ECCs are their high tensile ductility (strain hardening), toughness index, strength and multiple cracking (Naaman and Reinhardt 1995). Li (2003) defined ECCs as a class of ‘ultra-ductile fibre reinforced cementitious composites developed for applications in the large volume usage, cost sensitive construction industry’.

The high-ductile material shows an extraordinary tensile strain capacity exceeding 4% (and up to 5%) before softening sets in, as seen in Figure 2.22 (Li, Wang and Wu 2001). The tensile strength of ECCs is between 2 and 8 MPa depending on the fibre type, fibre volume fraction and the components of the matrix. For typical mix designs it is around 4 MPa (Trueb 2011). Significant deflection

hardening can be seen in flexural tests, and the corresponding flexural strength ranges from 11 to 16 MPa (Wang and Li 2006). The flexural strength depends on both the tensile strength and compressive characteristics. A relationship between the flexural and tensile strength was experimentally and analytically demonstrated by Maalej and Li (1994), who showed that the modulus of rupture for ECCs can be as high as five times the first cracking stress in direct tension.

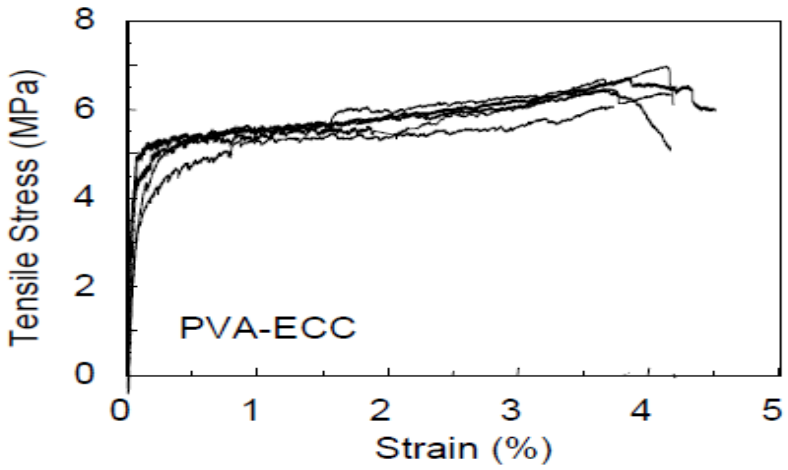

Figure 2.22 Tensile stress–strain curves of PVA–ECC (Li 2008)

Compressive strength of ECCs varies from 50 to 80 MPa, depending on the mixture proportion, which classifies them as high-strength materials similar to concrete materials but without the brittleness (Özbay et al. 2012).

Dramix fibres used to reinforce ECCs exhibited a maximum shear stress of 9.89 MPa, which is ~81% higher than that for RC (Li et al. 1994). Spectra fibre ECC showed a moderate load-carrying capacity and failed at a stress of 5.09 MPa, which is slightly lower than that of RC, by ~7% (Li et al. 1994). Another study examining shear capacity under a reversed cyclic load of steel fibre ECC members showed sufficient shear resistance; additional shear reinforcement was ineffective (Fischer and Li 2002a).

Notably, several fibres have been successfully employed in ECCs, but a large number of studies have focused on ECCs based on PVA fibre, commonly known as PVA–ECC (Li 2008). PVA fibre is a synthetic fibre made of PVA resin when a multi-step, high-elasticity production process creates a product with high stiffness and water insolubility (Hikasa, Genba and Mizobe 1986). Unfortunately, PVA fibre in a cement mortar matrix tends to rupture instead of pullout, because of its robust

bonding to cement hydrates and slip hardening response during the pull. This prompted the development of REC 15, a type of PVA fibre developed specifically for ECC (Wang and Li 2003). This PVA fibre improves fibre dispersion in a cement matrix through use of a special surface treatment (1.2% oil surface coating), which has the effect of dropping the fibre volume fraction to minimum of 2% optimum content (Li et al. 2002).

The primary mechanical specification distinguishing ECCs is that they strain harden (Li, Wang, and Wu 2001) more willingly than they tension soften, after first cracking. After the formation of first cracking, ECCs are designed to increase their composite tensile stress up to 500 times higher than concrete (Li 2003). This is followed by growing stress with simultaneously increasing strain. This strain hardening response gives way to the typical tension-softening response and achieves a stress–strain relationship similar to that of a ductile metal (Li and Kanda 1998). A multiple crack formation as seen in Figure 2.23 is formed at this stage. Closely related to the strain hardening behaviour is the high fracture toughness of ECCs—approximately 30 kJ/m^2—which is comparable to that of aluminium(Maalej, Hashidaand Li 1995). Moreover, the ability of flexural load–deflection curvesto distinguish the behaviour of mortar reinforced with various fibre types and volume fractions, and the ability of flexural toughness indices to characterise the load–deflection curve was demonstrated by Ward and Li (1991).

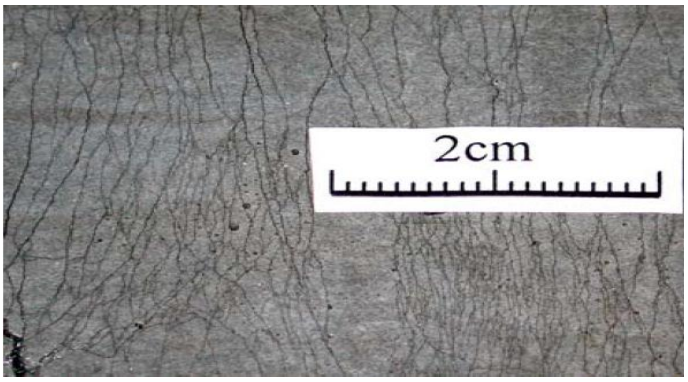

Figure 2.23 Crack pattern of PVA–ECC (Wang and Li 2006)

Another remarkable mechanical property of ECC material is its energy dissipation capacity, which is higher than that for plain concrete due to its fibre pullout and multiple cracking behaviour (Fischer and Li 2007). All of these remarkable specifications have led to the production of some unique by-products of

ECCs. Regardless of their characteristic high ductility, these ECC materials also fulfil other specific requirements such as high early strength lightweight ECCs (Li 2003), and self-consolidating ECCs (Kong, Bike and Li 2003).

2.5.2.2 Durability

For structural applications of materials in construction, excellent mechanical performance alone is not enough. It is also important that the applied material is designed for reliable performance in different environments and that its mechanical specifications should not degrade over time and decrease the designed strength capacity below its minimum. In the case of ECCs, with their strain hardening behaviour and multiple cracking, it is more likely that the material will be used as a structural element. This makes important the examination of ECCs under long-term conditions such as cyclic load, or exposure to different environments.

Several tests of ECC performance in response to reversed cyclic load have conducted to study their capacity under these conditions (Fischer and Li 2003b; Kesner, Billington and Douglas 2003). The results indicate nonlinear elastic behaviour with relatively small residual deflections due to flexure crack; reversed cyclic tension and compression loading did not reduce tensile strain capacity, as seen in Figure 2.24. For complete validation of ECCs with respect to long-term efficiency, tensile tests were performed to determine strain capacity during the hydration process (Li et al. 2004a). It was found that as hydration continues (typically to cement products), the increasing matrix toughness leads to reduced composite ductility. When an ECC is new, a maximum strain capacity of approximately 5% can be achieved. After the matrix mature had been treated for 180 days, the long-term strain capacity dropped by only 3%, and remained steady.

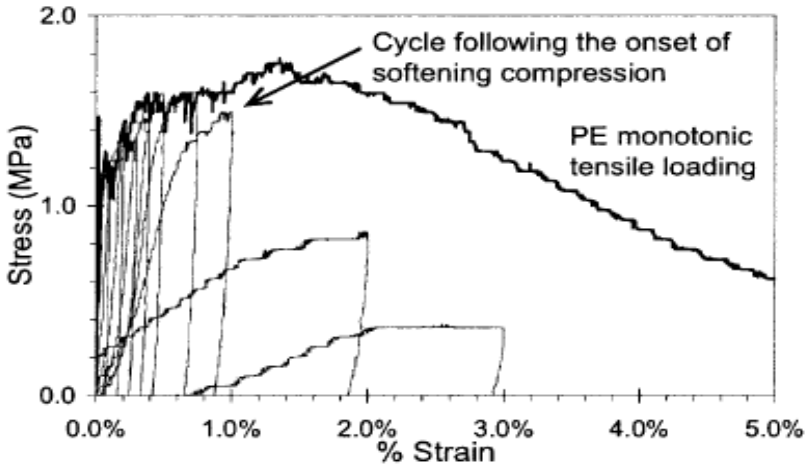

Figure 2.24 Tensile response of PE–ECC under cycling load (source: Kesner, Billington and Douglas 2003)

ECC is a cementitious material with the ability to self-heal (Wua, Johannesson and Geiker 2012). This prompted an investigation of the self-healing phenomenon under wet–dry cycles. Uniaxial tensile tests after the exposure of an ECC to a wet–dry cycle to simulate a tropical environment (Yang et al. 2009) showed that the ECC had the ability to recover 76–100% of its initial resonant frequency value (non-destructive test method), with a slight change in stiffness. Also, the temperature during the environmental cycles led to an increase in maximum strength, with a slight decrease in tensile strain capacity. Another experimental study was conducted to examine the durability of ECCs with respect to cracking and healing under the combination of load and environmental influences. The tested ECC specimens were pre-loaded under uniaxial tension then exposed to an alkaline environment. The ECC in both cases (virgin and microcracked) remained durable (Şahmaran and Li 2008).

One significant shortcoming of using PVA for ECCs is the coefficient of thermal expansion, which causes shrinkage in length of up to 4% at a temperature of 200°C (Banthia et al. 2012). Essential data on the mechanical properties and microstructure of PVA–ECC exposed to high temperatures (up to 800°C) have been reported by Şahmaran, Lachemi and Li (2010). Their test results demonstrated minor changes in the mechanical properties for specimens after exposure to temperatures up to 400°C for one hour. At the micromechanical level, the material showed an increase in porosity and empty channels, due to the melting process of the PVA fibre at a temperature of 200–400°C. In contrast, at 600–800°C, the tested specimen

showed a significant drop in compressive strength and stiffness, but the overall mechanical performance was still higher than that of concrete at similar temperatures.

2.5.2.3 Application

The advantages of flexibility in the fresh casting stage and high ductility in the hard stage have made ECCs attractive for structural applications (Li 2008), including on their own, or in a composite (hybrid) form to support other structural materials (Naaman 2007). The unique properties of ECCs as strain hardening cementitious composites (SHCCs) have been successfully tested for their ability to protect structural elements made of RC in an aggressive environment, by reducing crack width (Maalej and Li 1995). The application of ECCs for repair and retrofitting of concrete structures was studied by Li et al. (2000). The investigation showed that use of ECCs was not restricted to existing structures; they were also suitable for protecting structures with specific requirements, such as high impact resistance, crack width control, aggressive environment and large damage tolerance.

Fischer (2010) successfully used stand-alone PVA–ECC panels as floor slabs in modular housing. The tested panel slabs exhibited beneficial characteristics with relatively high flexural stiffness, ductility, maximum strength failure and low cost. Additional to the mechanical and economic advantages are the environmental benefits. The use of waste materials including FA or slag as filler in the mixture matrix of the ECC floor slab made this slab system more attractive and sustainable.

The development of green ECCs for sustainable infrastructure is feasible (Li et al. 2004b) for a range of applications including pipes, cement boards, electrical shafts, pavements and as overlay systems in bridge decks (Zhanga and Li 2002).

2.5.3 FRC

2.5.3.1 Material description

Concrete is still the most used construction material because it has the lowest cost-strength ratio. The problem with concrete is its low tensile strength and brittle behaviour, which causes failure and collapse shortly after the first crack occurs. This

issue led researchers to investigate property enhancements for concrete. In the early 1960s, steel fibre-reinforced concrete (SFRC) was established as a form of hybrid-reinforced cementitious material. Steel fibre addition provided significant enhancement in tensile splitting strength, flexural strength, first cracking strength, toughness, stiffness and impact resistance. In addition, deflection, crack width, shrinkage and creep were reduced (Tejchman and Kozicki 2010). Guidelines for design and specification of material properties are provided in ACI Committee 544 (2002). As noted above, the ASTM Standard (2011a) classified FRC according to fibre type: steel, glass, syntheticand natural fibre.

2.5.3.2 Mechanical properties and behaviour

Experimental investigations of steel fibre-reinforced beams with varying fibre content (0, 30 or 60 kg/m^3) were conducted under flexural testing (Altun, Haktanirand Ari 2007). The properties included compression, elastic modulus and toughness. The results revealed in insignificant decline in the compressive strength due to the increase of the fibre content, and excellent flexural strength capacity was achieved by using 30 kg/m^3 (1.25% volume fraction)

Shear tests on SFRC beams were performed using different stirrups and fibre content. The experiment, by Lim and Oh (1999), indicated that in SFRC, additional shear reinforcement is not required. However, similar tests showed that excellent shear strength capacities are achieved by using 1.5 % fibre volume fraction (Juárez et al. 2007).

Uniaxial tension tests are usually conducted on SFRC specimens with conventional longitudinal reinforcement, to study their tension stiffening and cracking behaviour. An increase in the post-load yielding capacity, and the development of multiple crack formation behaviours, compared to conventional RC were reported (Deluce and Vecchio 2013). Note that the fibre content of the mixture matrix has a significant influence on the tensile strength capacity of FRC (Sujivorakul 2012). Similar crack behaviour under tensile testing was observed using synthetic FRC (Wang, Li and Backer 1990).

Thus, the behaviour of FRC under tension depends on the fibre content. Low fibre volume fraction FRC still exhibits quasi-brittle failure and does not show any strain hardening behaviour. However, failure is more ductile and shows a gradual

strain softening behaviour, as seen in Figure 2.25. On the other hand, using a high fibre volume fraction in FRC resulted in strain hardening behaviour similar to that of HPFRCC (Naaman and Reinhardt 2006).

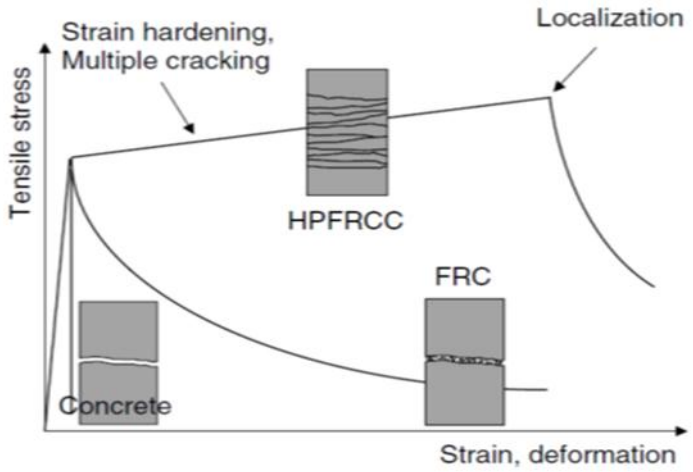

Figure 2.25 Schematic tensile stress–strain behaviour of cementitious materials (source: Fischer and Li 2007)

2.5.3.3 Material durability and application

From the structural point of view, the application of a material in construction is dependent on its mechanical performance and durability. Cementitious materials exhibit a close link between durability and ductility at the structural level (Li and Stang 2004). Steel rebars are subject to corrosion due to inadequate concrete cover or by increased permeability of crack formations. Fibre in concrete improves crack resistance and reduces crack width. Therefore, a reduction in the permeability of concrete and an enhancement of the overall environmental impact are observed in comparison with traditional RC (Banthia and Bhargava 2007; Bentur, Diamond and Berke 1997).

A durability performance study of FRC in an aggressive environment using cracked fibre-reinforced shotcrete showed durability problems due to attack by sulphate and salt solutions (Kaufmann 2014). The test provided similar environmental conditions are found in tunnel construction. It was shown that steel fibres in cracks corrode, resulting in loss of the residual strength capacity. However,

uncracked samples showed more resistance behaviour over a given period. In addition, it was observed that polymer fibre was more durable in such environments.

The ability to produce FRC by shotcrete or pre-casting processes provides several application opportunities. FRCs are used in pipeline trench applications, sewage channels, permanent formwork for beams, tunnel lining, railroad track beams for high-speed trains, and precast concrete fence panels (Banthia et al. 2012). These are the general applications of FRC; more specific applications of matrix-modified FRC can be found in structures subjected to blast or impact loading. For example, Bindiganavile, Banthia and Aarup (2002) examined the effect of impact load response of ultra-high-strength compact steel FRC. The matrix contained Portland cement, SF (24% by weight of cement) and 6% steel fibre volume fraction and was experimentally examined under drop-weight impact load (quasi-static loading). The material exhibited three times' greater strength and energy absorption than standard FRC. This shows that due to its high impact resistance, the material is suitable for use in strategic important structures such as military or high-security structures.

2.6 Hybrid-reinforced cementitious materials

2.6.1 Hybrid FRC

2.6.1.1 Material description

Hybrid fibre-reinforced concrete (HFRC) is a newly developed form of UHPFRCC (Markovic, Walraven and van Mier 2003). The composition of HFRC includes mainly short fibres in interaction with longer fibres. This combination in a well-balanced mixture can significantly improve mechanical properties compared to mono fibre-reinforced FRC. The use of two or more types of fibre in a suitable combination improves the overall performance, and results in production synergy (Banthia and Gupta 2004). A more detailed material description, development and microstructural component behaviour can be found in van Mier (2003).

2.6.1.2 Mechanical behaviour and material properties

The idea of adding different fibre types in various volume contents makes the design of HFRC very flexible. UHPFRCC shows high tensile capacity and exhibits strain

hardening behaviour in a way that demonstrates maximum synergy in terms of flexural toughness. Although the addition of steel macro fibres and polypropylene micro fibres does not enhance the compressive strength of the mix, it clearly enhances the modulus of rupture (Banthia and Gupta 2004).

These developed properties are dependent on the fibre combination, type and content. This was made clear in a study to investigate the effect of blending macro and micro fibres on the tensile stress–strain response (Park et al. 2012), employing four types of high-strength steel macro fibres, each at 1.0%, and micro steel fibres at 0.0, 0.5, 1.0 and 1.5%. The macro fibres included long smooth, two types of hooked, and a twisted fibre. The materials' responses depended on the volume fraction of the micro fibre and the type of the macro fibre, as seen in Figure 2.26. Strain hardening and multiple cracking behaviourswere affected according to these factors. A maximum strength of 18.6 MPa, with average crack spacing of 3.8 mm, was obtained. Similar material behaviours were achieved using a 2% steel fibre volume fraction and 0.5% polypropylene (PP) fibres (Jayakumar and Anandan 2014). In addition, flexural behaviour was analogous to the tensile response of HFRC, and was significantly dependent on the type of fibre and the fibre mix proportions (Yao, Li and Wu 2003).

Moreover, using natural cellulose fibres combined with steel fibre increased the flexural strength capacity, but due to the loss of cellulose fibre efficiency at high load applications, an increase of crack opening and large shear deformation were observed (Banthia et al. 2014). In contrast, the use of steel fibre with polyolefin fibres enhanced properties related to compressive and splitting flexural strength, and reduced the crack opening (Ravichandran, Suguna and Ragunath 2009).

It is important to understand crack formation in hybrid fibre composites, which is exemplified by the tensile response of HFRC shown in Figure 2.27, in which tensile behaviour is divided into four phases. Phase 0 is the linear elastic behaviour of uncracked concrete. Further linear elastic behaviour combined with the first microcracks is represented in Phase A. At this stage, the short fibre becomes mobilised due to its propagation and high first crack strength is developed. Section B characterises itself with first macrocrack, formation followed by multiple cracking; strain hardening dominates at this stage. The final stage, Phase C, exhibits strain softening.

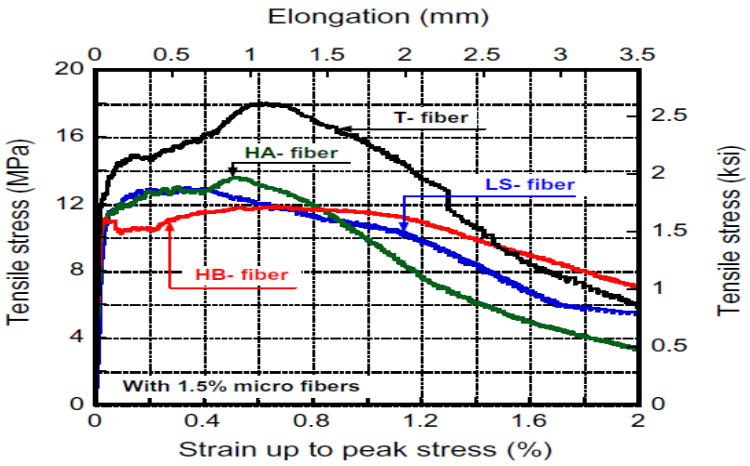

Figure 2.26 Tensile response of HFRCs with 1.5% micro fibres and1.0% macro fibres, for different macro fibre types: LS, long smooth; HA and HB, two types of hooked fibre; T, twisted (Park et al. 2012)

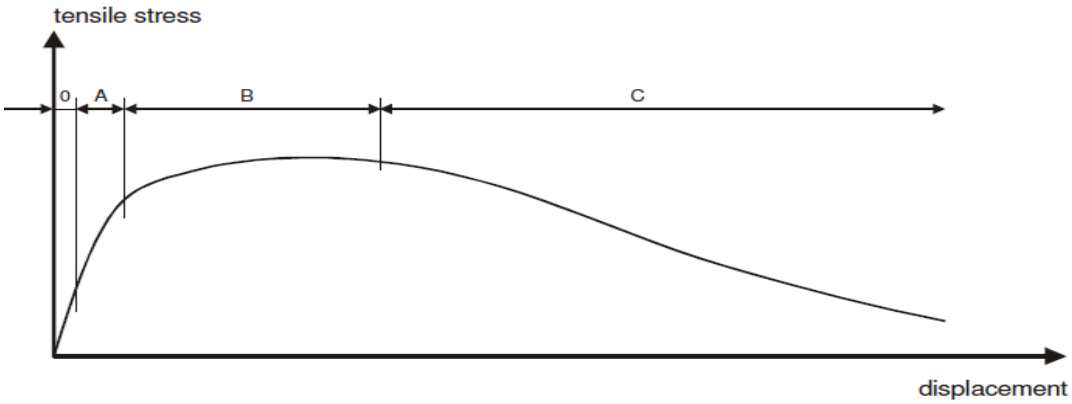

Figure 2.27 Stages in the tensile fracture of hybrid fibre concrete: 0, elastic stage; A, microcracking; B, macrocrack growth; C, bridging of macrocrack (Markovic 2006)

2.6.1.3 Material durability and application

The desired durability characteristic is the reduction of permeability, and therefore the increase in corrosion resistance. This could be realised in loaded structural elements if cracks could be controlled by reducing the crack opening. The use of micro and macro fibres has this effect, as illustrated in a research investigation by Banthia and Nandakumar (2003).

Fire resistance of construction materials is a significant requirement of building constructions. An experiment using synthetic fibre (PP) in interaction with steel fibre under a range of evaluated temperatures indicated an increase in porosity due to alow melting point of 160–170°C and vaporisation at 340°C, leading to an

increase in permeability (Suhaendi and Horiguchi 2006). The mechanical properties of HFRC after exposure to high temperature show a general drop in compressive strength to ~50% of tensile capacity at a temperature of 400°C, but still exhibits better results than FRC (Chen and Liu 2004).

The applications of HFRC are still in their infancy due to its rather recent development. An application study using HFRC as earthquake-resistant structural walls was performed due to the excellent performance of HFRC under cyclic load. The tests showed composite excellent vibration resistant (Dazio, Buzzini and Trüb 2008).

2.6.2 Hybrid ECCs

2.6.2.1 Material description

The hybridisation of ECCs (to produce HECCs) can be achieved in two ways. The first is by using two or more fibres of synthetic, steel, natural or a combination of types. The highest advantage of the hybridisation effect (Section 2.3) is accomplished by blending micro fibres combined with macro fibre. The second way to create HECCs is through the interaction of reinforced steel rebars with a mono fibre ECC. Li (2003) referred to ECCs replacing concrete in reinforced structures as R/ECC. However, mechanical properties of two types of available hybrid ECCs will provide entirely different structural behaviours.

2.6.2.2 Mechanical behaviour and material properties

In steel-reinforced ECC, the replacement of brittle concrete with a strain hardening material like ECC improves overall structural behaviour. R/ECC does not fail through interface delamination or bond splitting (Fischer and Li 2003b). The interaction of structural steel reinforcement and fibre-reinforced cement composite (R/ECC) in uniaxial tension was examined in an experimental study (Fischer and Li 2002b). The comparison of RC and R/ECC specimens indicated performance improvements in the form of energy dissipation, maximum strength and shear capacity, resulting from the ductile deformation behaviour of ECC, as seen in Figure

2.28. Due to its high shear resistance, no transverse steel reinforcement is required in R/ECC flexural members.

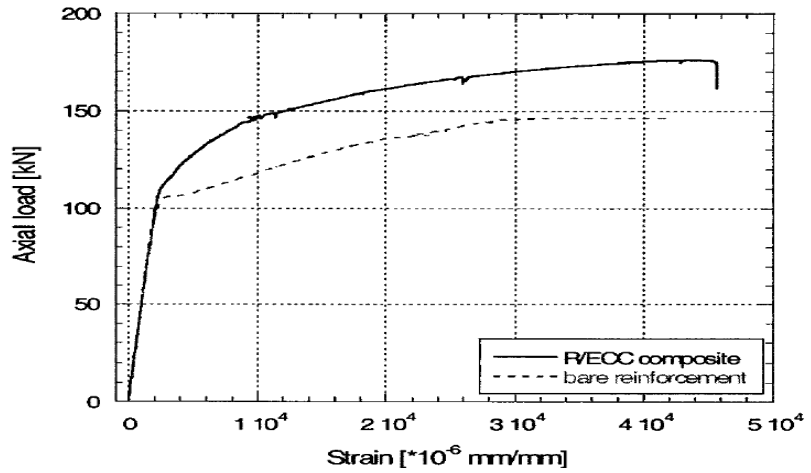

Figure 2.28 Compression of shear load–deformation response of R/ECC and RC (Fischer and Li 2002b)

On the other hand, HECC is a very ductile, strain hardening material showing multiple cracking behaviours. The effect on strain hardening behaviour of using hybrid fibre is shown in Figure 2.29. This research programme found that PE fibres contribute to enhancement of tensile strain capacity, whereas steel fibres improved the maximum tensile strength of hybrid fibre composites (Ahmed and Maalej 2009). In addition, increasing the fibre length led to significant increases in tensile strain capacity as well as improvements in strain hardening and multiple cracking behaviours of HECCs. This is an important finding on the influence of different fibre types and the length of overall structural behaviour.

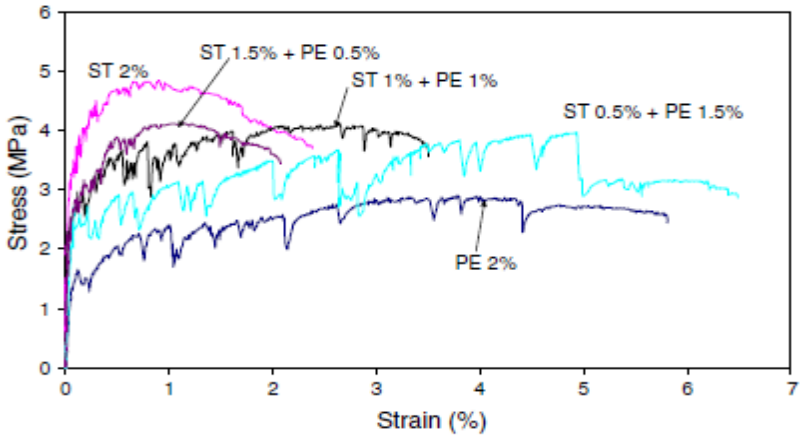

Figure 2.29 Effect of hybrid reinforcement using steel fibre (ST) and PE (source: Ahmed and Maalej 2009)

The flexural response of HECC using hybrid steel–PVA and steel–PE fibre composites with different fibre volume fractions were evaluated in a serial test (Ahmed, Maalej and Paramasivam 2007b). The steel–PE HECC exhibited lower flexural strength but higher deflection capacity than steel–PVA HECC. In general, using the toughness index method described in Section2.4.3, both hybrid composites exhibited strain hardening behaviour and multiple crack formation. The study employed different FA contents (50, 60 and 70%) to evaluate the effect of cement replacement by high-volume FA in the matrix. The optimal FA content in terms of flexure behaviour was 50%. Similar experimental results on the strain hardening and multiple cracking behaviours of hybrid PVA HECC under bending were reported by Ahmed and Mihashi (2011). That research also examined the effect of combining different PVA fibre volume fraction and fibre lengths (6, 8, 12 and 24 mm). The HECCs containing 2% of 24-mm, or 1% of 6-mm-length fibres performed best, with the highest maximum load, largest crack mouth opening displacement and multiple crack behaviour.

Studies of different fibres in hybrid composites have shown that they contribute different functions to the overall performance of the composite. An analytical model agreed well with experimental data by Ahmed, Maalej and Paramasivam (2007a). The model predicts first crack strength, the maximum bridging strength of hybrid fibre ECC, and the minimum critical volume fraction of fibres required to exhibit strain hardening and multiple crack behaviours in uniaxial tension. Using this information, the fibre bridging contribution can be calculated.

2.6.2.3 Material durability and application

The durability of HECCs is usually similar to that of conventional ECCs in terms of fire resistance and aggressive environmental influences, but the additional improvement of permeability resistance of HECCs compared to ECCs could enhance corrosion resistance (Li 2003). This is a result of hybridisation in terms of resisting crack formation and crack depth growth. This advantage has led to the use of the hybrid form of ECC as a concrete cover.

An important use of R/ECC is in column members designed for earthquake resistance (Fischer and Li 2003a). Such columns are found to provide better ductility and energy dissipation capacity, and less shear reinforcement compared with RC

columns. The columns at failure show no spalling or interface delamination (Fischer and Li 2003b). Similar behaviours were observed as R/ECC was applied to shear beam members (Fukuyama et al. 1999). High damage tolerance in structural elements with high-stress concentration suggests its use in other applications, for example, in beam–column systems (Parra-Montesinos and Wight 2000). The use of HECC and R/ECC in the construction industry is likely to increase in the future, as a result of their superior material behaviour and high durability (Maalej et al. 2012).

2.6.3 Hybrid-reinforced ferrocement

2.6.3.1 Material description

Naaman (2000) has extended the definition of ferrocement to include that 'The fineness of the mortar matrix and its composition should be compatible with the mesh and armature systems it is meant to encapsulate. The matrix may contain discontinuous fibres'. This definition was intended to highlight the compatibility of the matrix with the reinforcement that builds a composite, and to present the opportunity to use discontinuous fibres or micro fibres to improve the mechanical performance of ferrocement as hybrid composites, if necessary. Known fibrous ferrocement is a type of hybrid reinforcement in which the primary reinforcement is wire mesh and the secondary reinforcement is mono fibre.

Since Naaman's (2000) work, efforts have been made to develop ferrocement as a high performance material or, as Naaman prefers to call it, a strain hardening material (Naaman 2007). Fibre enhances the structural proprieties of ferrocement composites due to the interaction of fibres with the wire mesh (Shannag and Bin Ziyyad 2007). The fibres can be used in mono (one type) as well as in hybrid (two types) forms.

2.6.3.2 Mechanical behaviour

Improvements in ferrocement structural specifications have been made by the enhancement of the mortar mixtures using additives, and FA as a partial replacement of cement (Arif et al. 2001). Improvements in ferrocement properties have also been made by changing the type and ratio of reinforcement.

The addition of PVA mono discontinuous fibre to ferrocement with only one layer of steel mesh, but with various wire spacing, produces better overall performance in terms of cracking behaviour, yield and maximum strengths, than does normal ferrocement (El Debs and Naaman 1995). Another experimental investigation showed that increasing the number of steel mesh layers from two to four in combination with a 1.5–2% volume fraction of steel fibres in ferrocement increases the flexural strength by up to 2.6 times, and the energy absorption of the panels until failure by up to 3.85 times (Shannag and Bin Ziyyad 2007). Other experiments resulted in similar increases in flexure strength capacity and a decrease in crack widths when compared to conventional ferrocement (Wang, Naaman and Li 2004; Prakash, Desayi and EI-Kholy 1991).

A flexure and compression test series of fibrous ferrocement identified an increase of flexure strength by 28% compared to traditional ferrocement (Wegian 2010). At the same time, it increased impact strength by increasing steel fibre content to an average of 77%. Three layers of wire mesh, 1% of steel fibres and a superplasticiser content of 0.5% provided the best results in term of strength capacity. A similar study examined the flexural behaviour of self-compacting, mortar-reinforced fibre ferrocement panels, revealing a reduction in crack width, increase in number of cracks (multiple crack formation) and a delay in crack growth (Shri and Thenmozhi 2012).

Tests showed that 12.5-mm-thick PVA fibre ferrocement plates reinforced with only two layers of Hardwire© had the effect of increasing the modulus of a rupture in bending up to 105 MPa, as seen in Figure 2.30. The volume fraction of Hardwire© reinforcement (two extreme layers) was only 1.76%, and of PVA fibre, 1% (Naaman 2005). Similar results were obtained using Fleximat® mesh; a modulus of rupture of 127 MPa with an equivalent total volume of reinforcement of 3.7% was achieved. In general, the performance enhancement of ferrocement due to the addition of fibres is apparent, but research on HFF performance, durability and its applications is limited in the literature.

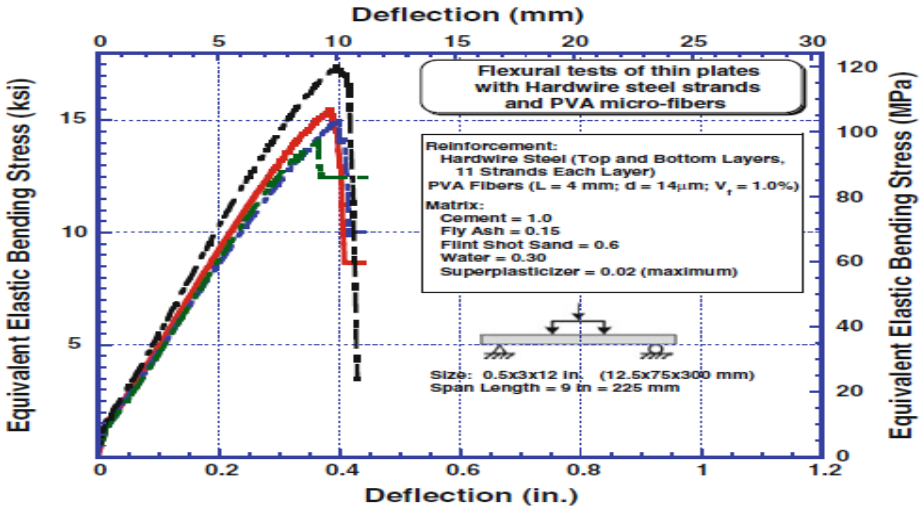

Figure 2.30 Bending response of hybrid ferrocement reinforced with Hardwire© wire mesh and PVA fibre (source: Naaman 2013)

2.7 Comparison between mono and hybrid materials

A comparison of the most important mono FRCC and its hybrid versions is presented in Table 2.1, which shows the material's name, and reinforcement type and volume fraction.

The main criterion that distinguishes the mono from the hybrid FRCCs is high tensile strength with adequate strain capacity. This characteristic is achieved due to the effect of using different fibre types, as described in Section 2.3. The effect of hybridisation is not only seen on strain hardening behaviour; also the fibre bond and the bridging capacity in different crack stages is significantly improved. When considering hybrid fibre-reinforced cement materials including different fibre geometries and mechanics, the material properties vary depending on the fibre blend used. For example, mixtures with a large fibre volume fraction of short fibres and low content of long fibres will provide different mechanical properties than the reversefibre proportions. This emphasises the fact that fibre cocktails can be individually tailored to achieve the mechanical properties required for a particular application. Figure 2.31 shows the effect of combining different fibre properties. Note that the mechanical improvement not only affects hybrid fibre reinforcement, but also materials with combined steel fibre in forcements, such as ferrocement and R/ECC.

There are many different mechanical specifications that distinguish materials. Comparisons of the most significant specifications of FRCCs required for structural design and application are made below

Tensile and flexural strength: If the FRC application requires high tensile strength a better choice would be HFRC. The highest possible tensile strength that can be achieved is ~18 MPa. Further, even ECCs exhibit higher tensile strength than that of FRC—as much as 8 MPa. Similar behaviour is observed in ferrocement and its hybrid-reinforced version with respect to flexural strength. The fibre/wire mesh-reinforced ferrocement exhibits an equivalent flexural stress of 26 MPa, whereas the traditional form achieves only 6 MPa (El Debs and Naaman 1995).

Table 2.1 Summary of cementitious composite abbreviations and reinforcements

Type	Name	Abbreviation	Reinforcement	Fibre content	Reinforcement classification
Mono reinforcement	Ferrocement	F	Wire mesh	-	-
	Engineered cementitious composite	ECC	Fibre	$V_f \leq 2\%$	Moderate
	Fibre-reinforced concrete	FRC	Fibre/steel	$1\% \leq V_f \leq 6\%$	Low–high
Hybrid reinforcement	Fibre ferrocement	HFF	Wire mesh fibre	$0.5 \leq V_f \leq 2\%$	Moderate
	Hybrid fibre engineered cementitious composite	HF-ECC/ R-ECC	Fibre/steel	$1.5\% \leq V_f \leq 2.5\%$	Moderate–high
	Hybrid fibre-reinforced concrete	HFRC	Fibre/steel	$1\% \leq V_f \leq 8\%$	Low–high

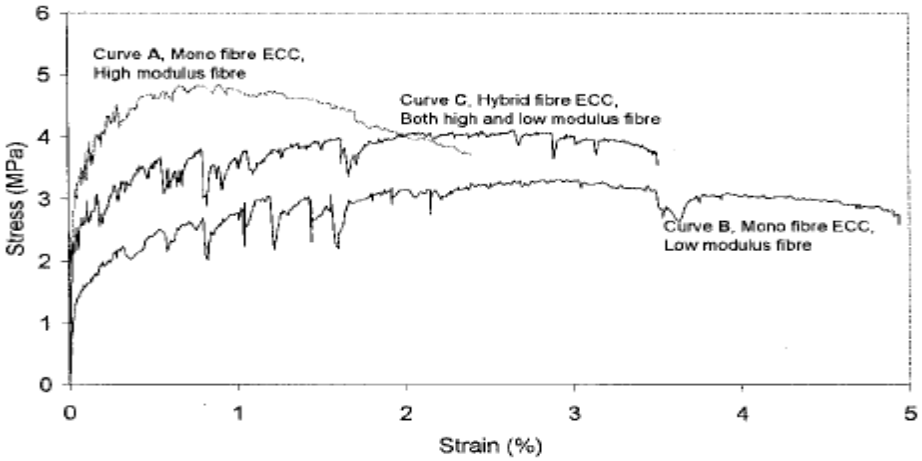

Figure 2.31 Comparison of hybrid and mono ECCs (Ahmed, Maalej and Paramasivam 2007a)

Ductility: Fibre reinforcement reduces or eliminates brittleness and increases ductility. Ductility is a specification manifested through strain hardening. Structural ductile materials are the preferred engineering materials for earthquake-resistant structural elements, because materials without strain hardening damage suddenly after reaching first cracking, and there will be no spread of cracking unless structural reinforcement is used. Only mono fibre ECCs and all hybrid forms referred to in this chapter exhibit high performance behaviour and therefore show strain hardening to some degree. Specifically, this behaviour is dependent on the fibre type and cocktail used in materials. The longer fibres in FRCCs generate a clearly identifiable strain hardening phase; hence the most effective fibre blend in ECCs, HFRCs or HFFs involves medium to long fibres.

Bond strength: An important specification is good bonding behaviour of the matrix. High bond strength in FRCCs depends on several characteristics. The main character is a highly dense matrix that increases frictional forces. Another aspect influencing the bond is ductility, which assures a favourable stress and microcrack distribution. Additionally, in steel-reinforced composites, the bond will be increased if the matrix shows high tensile strength because this will delay crack formation in the contact area between the matrix and the steel reinforcement. These characteristics can be found by HFRC, HFF and R/ECC.

Energy dissipation/toughness: FRCCs exhibit higher energy dissipation capacity than concrete. The energy dissipation depends on the load type; however, describing toughness in this case is more appropriate. The high toughness (energy

dissipation) of strain hardening makes materials suitable for high-security and military buildings. HFRCs have been tested for such applications.

Compressive strength: Compressive strength is not an important strength characteristic in FRCC, but if high compressive strength is the desired property in an application then a compact matrix is necessary. The fibre combination requires a moderate amount of medium-sized fibres in order to avoid brittle failure. However, the UHPFRCCs such as HFRC can be considered as high performance materials with high compressive strength. On the other hand, the compressive strengths of thin cementitious materials such as ECC, ferrocement and HFF are comparable with conventional concrete.

Spalling prevention: Toughness is the main factor preventing the FRCC from spalling. Due to the increased tensile strength, which is necessary to prevent spalling, HFRCC is more suitable for seismic applications. It is sufficient that FRCC members do not fail in a brittle manner, and maintain their reliability even after reaching the maximum tensile strength usually known for all HPFRCCs.

2.8 Microstructure and micromechanical properties of fibre-reinforced cement composites

Understanding the microstructure of fibre cement composites is essential to describe their mechanical behaviour in terms of crack initiation, bond capacity and multiple crack formation. Hence, material performance can be improved due to microstructure modification such as increasing the packing density, which has effects at the micromechanical level. Micromechanical properties are relayed to the macroscopic structure of a composite, which forms the skeleton of materials property and design theory. Specifically, it allows systematic microstructure tailoring of FRCCs. For now, it is evident that microstructure tailoring can lead to extreme composite ductility and increases in material toughening. Figure 2.32 shows a density-modified fibre-reinforced cement composite.

At the microscopic level, it is evident that the microstructure of cement phases is heterogeneous material. The cement paste mass seems to be very dense in some areas of the whole matrix, whereas in other parts of the same mortar it is highly porous. In concrete, for instance, behaviour under stress can be described more

precisely when the cement paste–aggregate interface is considered as a third phase of the concrete microstructure (Mehta and Monteiro 2006). To provide more understanding, we may need to observe the whole picture of the microstructure components of cement paste. The chemical mineral composition of clinkers is C_3S, C_2S, C_3A and C_4AF. The calcium sulphate dissolves in water and produces heat. The heat generated accelerates the chemical reaction of all cement components, and at this stage, needle-shaped crystals of calcium trisulfoaluminate hydrate (or ettringite) are formed. Hours later, large prismatic crystals of calcium hydroxide and tiny fibrous crystals of calcium silicate hydrate (C–S–H) start filling the spaces in the matrix. When the hydration process is at a developed stage, the ettringite becomes unstable and decomposes to hexagonal plates. The microcrystals are as seen in Figure 2.33.

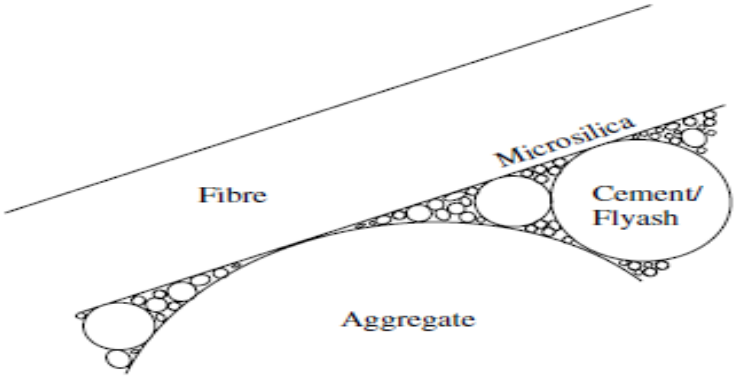

Figure 2.32 Modified packing density of concrete components with fibre (adopted from Staehli and Van Mier 2007)

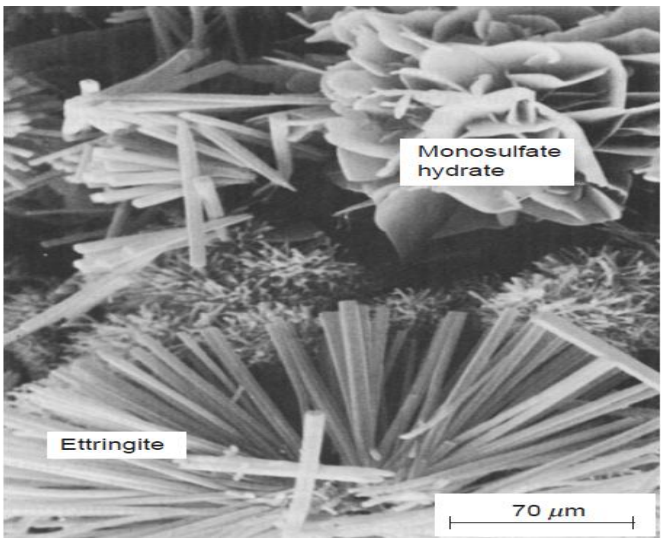

Figure 2.33 Microstructure of a hydrated cement paste (Mehta and Monteiro 2006)

A full range of superior material properties of HPFRCC has been achieved through modifying their packing density, by filling the empty space between the morphological crystals with microminerals (increasing packing density) such as silica powder and SF (Ranade et al. 2013). Another method, mentioned previously, is by enhancing matrix toughness through the use of fibres (Banthia et al. 2012). Methods to determine these material properties usually involve conducting mechanical testing at a structural scale level.

A recently developed method to determine microstructural properties is nanoindentation. This technique is adopted and used to specify nanomechanical behaviour (Constantinides and Ulm 2007; Constantinides, Ulm, and van Vliet 2003; Ulm et al. 2007). This method allows governing of the mechanical properties on a microscale level in cementitious composites. The method for determining the packing density, hardness and elastic properties of materials requires statistical analysis of the results obtained from nanoindentation tests. The use of this technique on cement-based materials has led to the identification of the basic properties of the representative morphological arrangements of C–S–H. The nanoindentation test methodology will be discussed further in the next chapter. In general, nanoindentation is performed over a tiny area, and is therefore related to the principal of a representative volume element (RVE). According to Deluce and Vecchio (2013) the RVE is ‘the smallest material volume element of the composite for which the usual spatially constant (overall modulus) macroscopic constitutive representation is a sufficiently accurate model to represent mean constitutive response’. This means that the RVE primarily includes a large number of composite micro-heterogeneities, such as grains, voids, inclusions and fibres (Kanit et al. 2003).

2.9 Multiple functional applications of thin cementitious composite

To employ FRCC on a regular basis as structural elements, a framework for strain hardening material models identifying relevant material parameters needs to be established. It is proposed that such a framework should include material information like unloading, fatigue, creep or relaxation, and durability (Fischer 2004). Further, to convince material suppliers and the construction industry using these materials, an

assessment of structure and economic benefit must be available. This can be achieved by selecting materials from the perspective of weight reduction, or those with multiple functions reducing a working step and therefore decreasing construction costs.

Slabs are structural elements subjected to initial and superimposed loads. Minimising the dead load of slabs, for instance, could be achieved using lightweight concrete or reducing the cross-section weight by using lightweight infill materials. An example of lightweight infill materials is AAC blocks, whose worldwide use was first proposed in Sweden in the 1920s. The efficient use of this type of slab was first experimentally investigated by Wahyuni, Vimonsatit and Nikraz (2012). Weight-saving advantages and reductions in construction effort were gained using these blocks. They weigh around a quarter as much as normal concrete and provide remarkable fire resistance, and excellent sound and thermal insulation (Yardim et al. 2011). On the other hand, AAC concrete members are limited in their structural application due to their low strength capacity in comparison with ordinary concrete (Vimonsatit, Mazlan and Nikraz 2011).

Multiple applications can be found for thin cementitious composites in combination with other materials; for example, using ferrocement as a repair structure element in the form of jackets or as formwork for beams and slabs (Nassif and Najm 2004; Memon, Sumadi and Ramli 2007; Yardim et al. 2011). Ferrocement has been applied in the tension zone cover area of concrete slabs. It is evident that the panel cover can be successfully used for reinforcing concrete slabs (Al-Kubaisy and Jumaat 2000). An additional study proposed weight reduction using AAC blocks as infill material and ferrocement panels in the tension zone of a concrete slab, which achieved the desired weight loss with simultaneously good performance (Yardim et al. 2013). One downfall of this application is the slip due to the horizontal shear bond, or ‘shear transfer’, of the different materials at the interface connection areas (Abdullah and Easterling 2009). This could be remedied using shear studs to connect both slabs, but this will generate tensile pressure in the ferrocement panel in the area surrounding the studs, due to frictional shear transfer and dowel action. These generated tensile stresses affect the brittle matrix of ferrocement and could lead to a sudden failure at the connection points. The application of ductile materials with strain hardening behaviour and enhanced tensile strength capacity, such as HFF, may resolve this issue.

2.10 Summary

The literature suggests that mechanical properties of brittle, cement-based materials—such as tensile strength capacity, energy absorption and ductility—can be significantly improved by reinforcing with fibres. High performance, or strain hardening behaviour, is achieved due to toughness enhancement afforded by adding certain amounts of fibre to cement-based matrixes. Hybridisation of these composites has an even stronger influence, enhancing pullout and crack bridging mechanisms, and thereby mechanical properties such as tensile strength, strain capacity and toughness. Examples of materials containing mono, or ‘single’, fibres that have been improved by adding another fibre type are ferrocement, ECC and FRC. All these materials provide satisfactory durability accompanied by excellent mechanical behaviour, which has encouraged their use in structural applications. This allows the use of such materials in a multifunctional form, but reconsideration of the chosen materials to tailor their performance to applications nonetheless is required.

Chapter 3: Experimental Programme for Strength Behaviour of Hybrid Fibre Ferrocement

3.1 Introduction

As described in Chapter 2, substantial research has been carried out to determine the mechanical properties and structural behaviour of FRCCs and their related hybrid materials. However, a complete model for hybrid PVA fibre ferrocement's structural and mechanical behaviour, describing maximum strength, strain capacity, ductility, and toughness behaviour, is not yet available. To determine the mechanical behaviour of HFF, an experimental investigation is carried out here. On the basis of the availability of resources and utilities, the study is limited to the following tests: direct tensile test, indirect tensile test, bending test, shear test, nanoindentation, pullout test and elastic modulus. For the purposes of this experimental investigation, a microscale model involving fibre, matrix and interface zone is introduced.

The primary objective of this work is to enhance the overall structural performance of ferrocement by adding hybrid PVA fibre. However, it is necessary to determine the PVA fibre type and content that provides optimal structural performance. Assessments of the combination volume fraction and type are conducted by the flexure test. The use of short fibres leads to stiffening of the mixture and a compact composite, such that full penetration through the wire mesh is not guaranteed. To improve workability and retention of the desired structural behaviour, experimental manipulation of the mixture matrix by the addition of mineral additives is required. The effect of these additives on the mortar is assessed by the compression test and visual observation of casting quality.

The HFF requires a detailed material analysis to obtain its specifications. First, a material classification is required to provide a better understanding of the composite's behaviour, requiring a test series using methods developed for high

performance materials grouping. Prior to this, the tensile stress–strain relationships must exhibit strain hardening behaviour properties. Toughness calculated from the flexure response of a composite, and its multiple crack development, are strong indicators of a high performance material. Specification of composite properties is a significant part of this study. The tensile strength test measures not only tensile strength but also strain capacity; it is also used to analyse the contribution of the material's composition to its tensile behaviour. Other tests such as the shear, pullout, compression and indirect tensile tests, along with nanoindentation, are conducted to determine the individual material properties of the composite.

The HFF panels are then used as permanent formwork in one-way concrete slabs (HFF–OWS). The main investigation of the slab composite occurs via three-point flexure test. Additional calculations are performed to demonstrate the composite's complete action and predict some design-related values. This is followed by finite element (FE) modelling to validate the experimental results. The overall research procedure is shown in Figure 3.1.

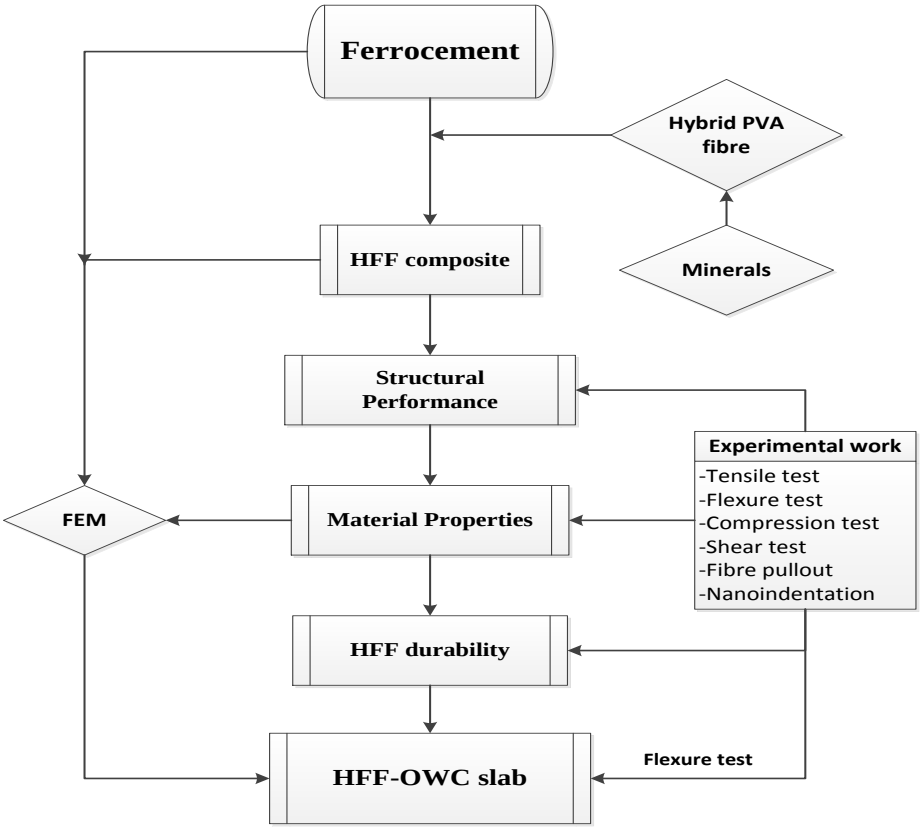

Figure 3.1 Schematic diagram of the procedures followed in the study

3.2 Hybrid fibre ferrocement materials

3.2.1 Mortar

The cementitious composite used throughout this study was regular mortar with an unconfined compressive strength of ~56 MPa. Cement used in this research was commercially available Type III Portland cement classified according to AS 3972 (Australian Standard 2010), having specified chemical substances as shown in Table 3.1.

All mixtures were designed to have a cement content of 400 kg/m^3. The weight-based mixture ratios of cement, sand, FA and water are described in subsequent chapters. Some mixtures were modified by a superplasticiser to improve their workability. Superplasticisers in cement-based mixtures may enhance workability and increase compressive strength. Weigan (2010) showed that superplasticiser added to fibre ferrocement concrete increases its compressive strength by ~7%. Flexural strength is also increased. In addition, superplasticiser addition reduces water in the mixture and has a significant effect on the cement's hydration and setting time (Weigan 2010).

Locally available natural silica sand known as yellow 'Baldivis' sand was used for the mixture. All chunks of clay and other external materials were separated from the aggregate. Grading of the sand was in accordance with AS 1152 (Australian Standard 1993). In a previous study (Abushawashi, Vimonsatit, and Hopkins 2012), the available sand was not suitable for producing ferrocement panels in a test series using the shotcrete method because it caused congestion in the pump. Therefore, to reduce production costs, superior graded sand referred to as 'Gingin' sand was used to provide a pumpable mixture. The grading of the yellow and Gingin sand is shown in Figure 3.2.

Local FA (type F according to ASTM C-618) and SF were used in the preparation of the HFF panels. A chemical analysis of these materials provided by the manufacturer is shown in Table 3.2.

Table 3.1 Chemical analysis of GP cement according to AS3972

Chemical	Content (%)	AS3972 limits
SiO_2	21.1	
Al_2O_3	4.7	
Fe_2O_3	2.7	
CaO	63.6	
MgO	2.6	
SO_3	2.5	3.5% maximum
LOI	2	
Chloride	0.01	
Na_2O	0.5	

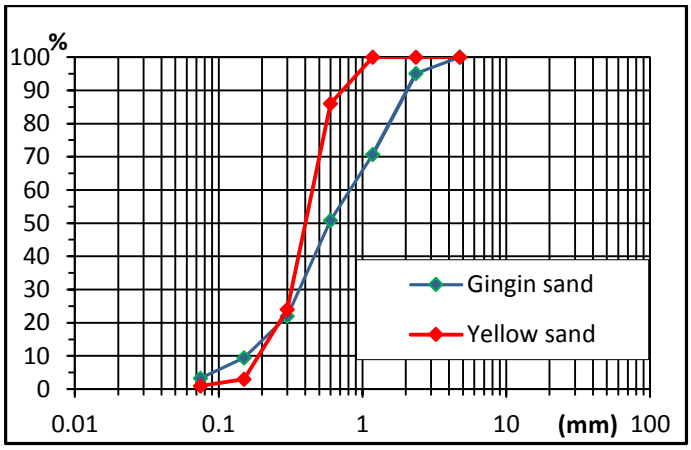

Figure 3.2 Sieve analyses of Gingin and yellow sand

Table 3.2 Chemical analysis (%) of FA and SF

Chemical	FA	SF
SiO_2	55.2	93
Al_2O_3	25.3	0.2
Fe_2O_3	8.34	0.05
CaO	2.65	–
MgO	1.56	0.51
SO_3	0.09	0.05
LOI	1.6	4.15
Chloride	1.39	0.22
Na_2O	0.58	0.2

3.2.2 Polyvinyl alcohol fibre

Two types of monofilament PVA fibre were combined in the mortar mixture for this study. Thus, four combinations were considered (see Figure 3.3), to determine the best performing blend. The specifications of the four types of PVA fibres including their trade names, lengths, and tensile and flexural strength capacities are provided in Table 3.3. Short (two types) and long (two types) were combined, and the mixture that gave the best results was used in all subsequent tests. PVA fibre provides high chemical bond strength due to hydrogen bonds between the PVA fibre and the cement paste. However, PVA fibres tend to rupture instead of pulling out during the extension of crack openings, because of their relatively low tensile strength. Treatment with an oiling agent during the production process effectively eliminates this behaviour and leads to pullout failure instead of rupture (Li et al. 2002).

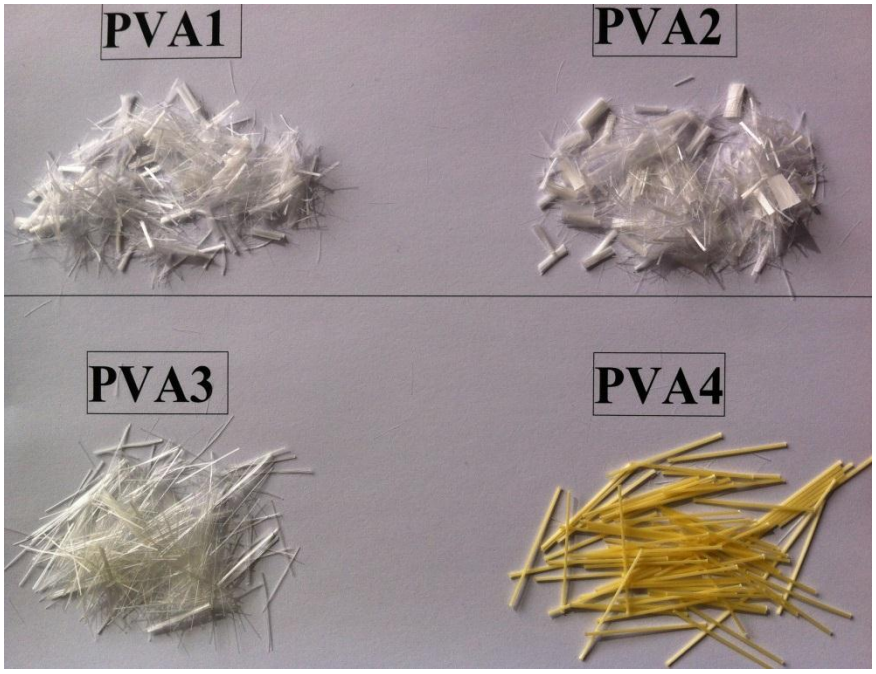

Figure 3.3 The appearance of PVA fibres used in this study

Table 3.3 PVA fibre specifications

Fibre type	Tread name	Diameter (μm)	Length (mm)	Tensile strength(MPa)	Fibre elastic modulus (GPa)	Fibre density (g/cm^3)
PVA1	RSC15	38	8	1400	30	1.3
PVA2	RECS15	38	8	1600	40	1.3
PVA3	RFS400	200	19	1000	29	1.3
PVA4	RF4000	660	30	800	23	1.3

3.2.3 Wire mesh

The ACI Committee 549-R93 (2009) outlines requirements for the condition of wire mesh used in ferrocement. It should be clean and free from dust, rust, paint, oil and similar substances. Two types of flexible galvanised wire mesh were used in this experimental investigation. The first was hexagonal woven wire mesh (chicken mesh) with a diameter of 1.4 mm and wire spacing of 40 mm. The second type was flexible galvanised welded square mesh of 1.24-mm diameter and 25x25-mm holes. Both wire meshes are shown in Figure 3.4. The wire mesh and mortar mixture matrix followed guidelines presented in the ferrocement report by the ACI Committee 549-R93 (2009).

Figure 3.4 Square and hexagonal wire mesh used in the slabs produced for this study

3.3 One-way concrete slab materials

The one-way concrete slabs used AAC blocks as infill material in the free web of the slabs. The use of AAC blocks first began in Sweden in the 1920s. This type of material has been used in the form of lightweight RC slabs. The efficient use of this type of slab was first experimentally investigated in the previous study (Wahyuni, Vimonsatit and Nikraz 2012), revealing its weight-saving proprieties that provided an additional reduction in construction effort. However, AAC concrete members have only limited structural application due to their low strength capacity compared to ordinary concrete (Vimonsatit, Mazlan and Nikraz 2011; Vimonsatit, Wahyuni and Nikraz 2012).

The concrete slabs were cast using Portland cement, natural local sand and crushed granite aggregate with a combined maximum size of 10–20 mm. The cement:sand:aggregate ratio was 1.0:2.1:3.2, and the water-cement ratio was 0.4. The concrete mix was designed to provide a compressive strength of 30 MPa after 28 days.

Three AAC blocks of size 600x200x75 mm were tested to determine flexural strength. The average maximum flexural strength was 0.7 MPa, the density of the aerated autoclaved concrete was 550 kg/m^3 and its compressive strength was only 3.5 MPa. This suggested that AAC blocks have a negligible structural influence on slab composites under bending, and are only useful as infill. A slab cross-section and AAC block are shown in Figure 3.5.

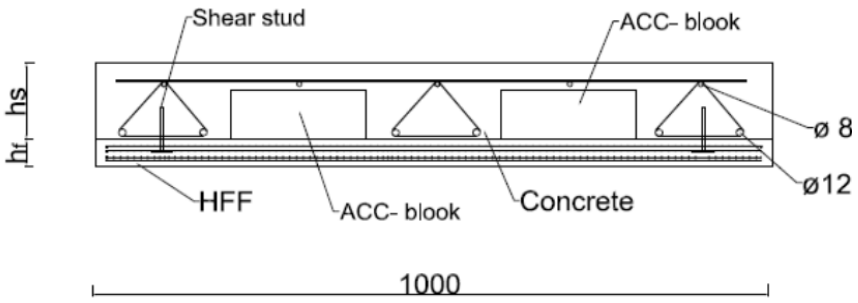

Figure 3.5 Slab cross-section (top) and AAC block (bottom)

3.4 Mixing procedure and specimen preparation

A horizontal mixing pan was used to perform the mixing process because vertical rotating mixing machines produce fibre balls, in a process known as the 'balling effect'. The mixing sequence for materials for the matrix was adapted from Zhou et al. (2012), and involved first mixing the appropriate amount of cement and all other powder materials with water and the proposed liquid materials. Fibre was then slowly added to the paste during the mixing process, followed by the remaining powder material. This process created a uniform distribution of fibre throughout the matrix, and the order of mixing increased the maximum tensile strength. This procedure was followed for all fibre-reinforced specimens prepared in this study.

All tensile test specimens were prepared in Plexiglas® moulds; panels were cast in wooden moulds for flexure tests. To prevent clumping of fibre and mortar, the moulds were oiled. After casting, the specimens in the moulds were covered for 24 hours then removed from the moulds and cured in a water tank for 28 days. One day before testing, specimens were removed from the water tank to dry. Large-scale specimens were covered by a plastic sheet for the first 24 hours; panels removed from plywood moulds were covered with wet burlap for seven days. Figure 3.6 shows the formwork used to prepare all test samples.

(a) Dogbone moulds

(b) HFF panels moulds

(c) Slab composite moulds and casting procedure

Figure 3.6 Moulds and casting procedure for test samples

The 620x200x40-mm HFF panels were cast by pouring a thin layer of the cement paste into the mould, then laying the first wire mesh, followed by more cement paste; this continued until all layers were placed, finishing with a certain cement cover. The AAC concrete–HFF composite slabs of size 1220x1000x155 mm

were made in three stages: (1) placement of the bottom zone layer (HFF panel), (2) placement of AAC blocks and reinforcement, and (3) casting of the concrete.

3.5 Test method

3.5.1 Flexure (bending test)

A four-point bending test with a constant bending moment at the mid-span was carried out to determine flexure response, producing load–deflection curves or the equivalent stress–deflection curve. A primary advantage of this test is its relatively easy setup and the information it provides about a material's mechanical behaviour is adequate. The goal in this study was to use the load or equivalent flexure stress–deflection curves to describe first cracking, ultimate flexure strength and deflection behaviour, which involves a relatively simple structural analysis technique. Moreover, data obtained from the flexural test can be used to invert stress–strain curves for tested materials, by simplifying tensile behaviour to perfect elastic-plastic behaviour with a 'first crack yield strength' (Stang and Li 2004).

The tests were performed with the INSTRON testing machine located in the Curtin University concrete laboratory, which allowed application of the load under displacement control at a loading rate of 1 mm/min for all tested panels. A representation of the flexural test setup is shown in Figure 3.7. Deflection and load data were documented to display the load *vs*. deflection. The load test was completed when there was an 85% load drop or a maximum machine displacement of 50 mm, whichever occurred first. A similar test setup was used for shear testing of the HFF panels.

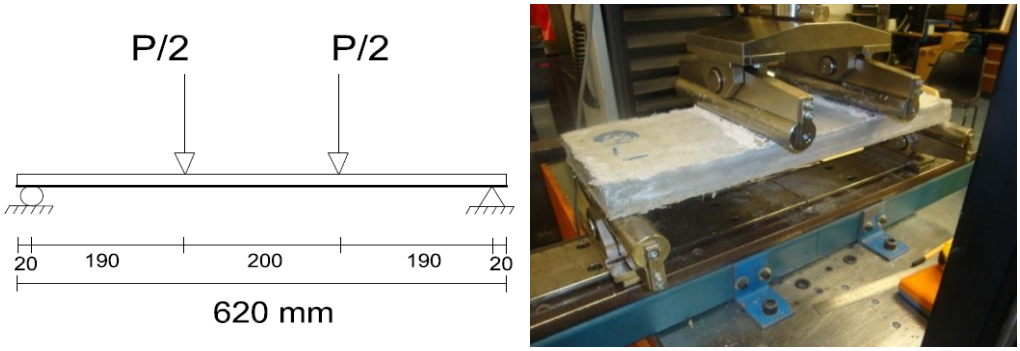

Figure 3.7 Four-point bending test setup

To achieve the required comparisons and evaluations of tested panels, the load was transferred as an equivalent elastic bending stress, to allow for the assumption of uncracked section behaviour. As a result of this assumption, equivalent flexural stresses were calculated using the following equation:

$$\sigma = {}^{M}/_{Z} \qquad (3.1)$$

where M is the bending moment and z is the section modulus. According to the geometry of the tested panel, an equivalent elastic bending stress can be calculated using the following equation:

$$\sigma = P \times 0.00178 \qquad (3.2)$$

for σ in MPa, and P is the applied load, in N.

In addition, to classify the mixture matrix, a four-point loading test was used to test the flexure performance of a non-mesh-reinforced beam. The test was conducted according to ASTM C 1609 (ASTM 2013) to determine toughness of each 350x100x100-mm specimen in the test setup shown in Figure 3.8.

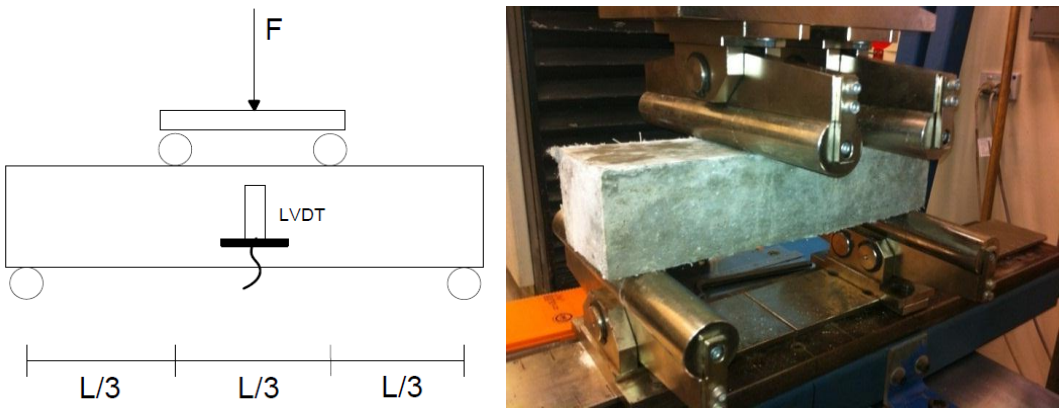

Figure 3.8 Four-point test setup to determine mixture toughness

A unique test setup was developed to perform a four-point flexure tests at different temperatures, with the primary objective of evaluating the flexure behaviour of HFF panels at elevated temperature. A locally manufactured kiln (Appendix B) was used to heat the HFF specimens to the desired temperature at a rate of 6.67°C/min (400°C/hour), and to hold that temperature for one hour to ensure that the panels reached the required temperature. This relatively high heating rate was chosen because fires in buildings can reach temperatures up to 600°C in only 15 minutes (Allen 2006).

The temperature was measured using two thermocouples attached to the specimen surface inside the oven. Two other thermocouples measured the air temperature inside the kiln. All four thermocouples, the load cell and a wire linear variable differential transformer (LVDT) were connected to a Quantum data logger to record the temperature data. To allow multiple testing in one day, the testing process was sped up by placing some specimens in the Kiln while it was still warm from the previous test (slightly above room temperature). The slightly elevated starting temperature had no effect on the HFF panels as all specimens were preheated to 100°C (24 hours) for the drying process.

The four-point bending test setup of HFF panels inside the kiln is shown in Figure 3.9, and a detailed diagram of the test setup is shown in Figure 3.10. A constant moment zone was used to determine the flexure strength of the panels. The kiln was positioned under a load jack with a 50-kN load cell connected to the top of a steel loading frame. A circular opening at the top of the kiln provided access to the loading cylinders (see Figure 3.9). During the heating process, the hole in the kiln was sealed using rock wool.

To perform a large-scale bending test on the applied HFF panels as a permanent formwork on AAC block slabs. A simply supported slab with one load point and a clear testing span of 1000 mm was set up to determine and compare results for the control specimen. Twelve LVDTs were used to measure the deflection at spacing of 200 mm: six for the top and six for the bottom slab. A 400-kN load cell and all LVDTs were connected to the Quantum data logger to record the data. To provide simple support, two Teflon® sheets were used on one support side to eliminate horizontal load caused by the friction between the slab and the steel support beam (see Figure 3.11).

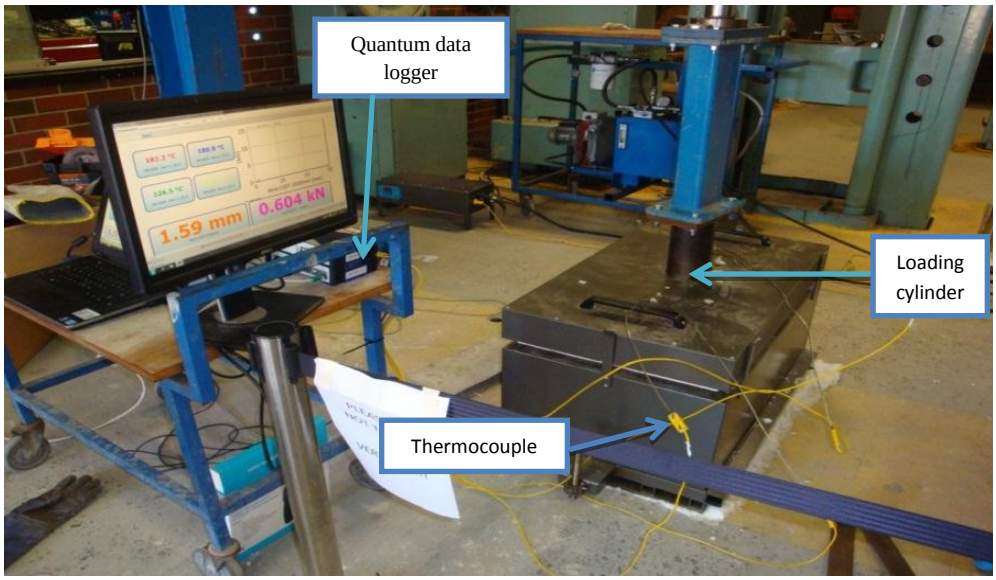

Figure 3.9 Experimental setup of *in situ* four-point bending test at elevated temperatures

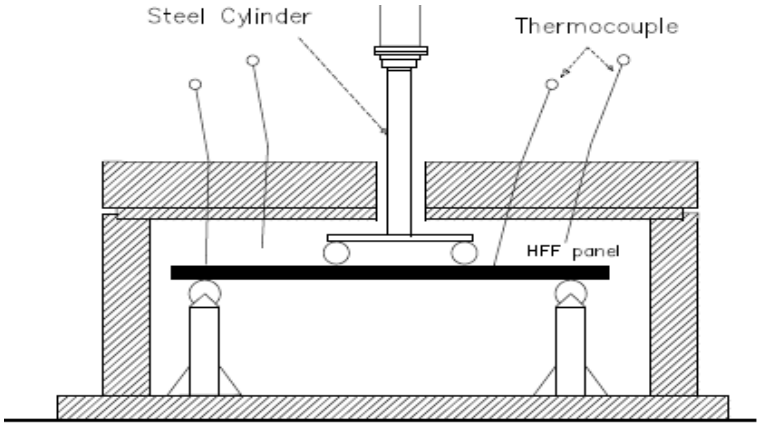

Figure 3.10 *Insitu* four-point bending test on HFF panels inside the kiln at elevated temperatures

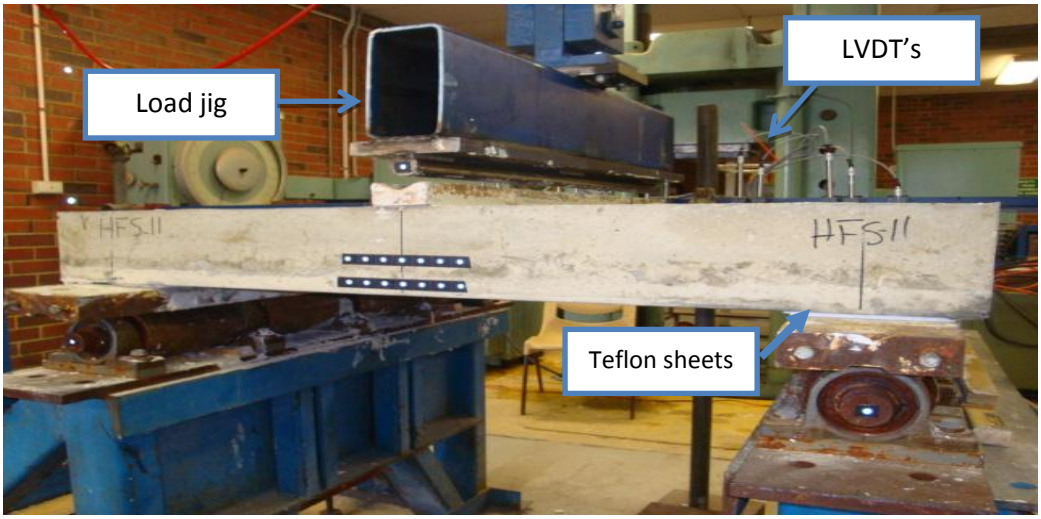

Figure 3.11 Slab testing setup

3.5.2 Direct tensile test

Conventional 'dogbone'-shaped specimens (Figure 3.12) were tested under direct tensile load to understand the HFF material's behaviour. Specimen size was chosen according to the Japanese Industrial Standard (2006), which recommends a minimum size of at least the fibre length and twice the maximum aggregate size.

An extensometer was employed to measure the elongation occurring during the load application. The specimen ends were held by purpose-made grips attached to the test machine. The test setup is shown in Figure 3.13. The strain was calculated from elongation measured with the extensometer. The tensile stress σ_t and tensile strain ε were calculated using the following equations:

$$\sigma_t = P/A \quad (3.3)$$

$$\varepsilon_t = \Delta L/L \quad (3.4)$$

where P is the load applied during the test, A is the cross-sectional area, ΔL is the elongation of the tensile specimen and L is the gauge length (distance between both grip ends) of the tensile specimen (80 mm). A hydraulic testing machine was used for all the direct tensile tests. A deformation-controlled procedure was used to capture the tensile response at a rate of five data points per second. A loading rate of 0.75 kN /mm/min was applied in the test.

The tensile test results were used to determine not only tensile strength and strain capacity, but also the contribution of fibre type and wire mesh content, using the Taguchi method test design (see Chapter 4).

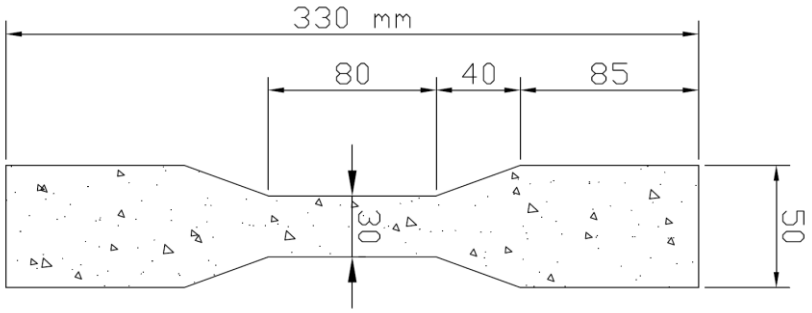

Figure 3.12 Dogbone specimen dimensions

Figure3.13 Tensile test setup

3.5.3 Indirect tensile test

The indirect tensile test, originally known as the Brazilian test for determining the tensile strength of concrete, was used on the HFF composite by applying a compressive load on opposite generators of a cylindrical specimen. The specimen fails in tension along the diametric plane containing the load. The test was conducted according to AS 1012.10 (Australian Standard 2000a) on all cylinder samples in an MCC8 testing machine. The use of soft strips of material between the specimen and the plates of the testing machine was necessary. Plywood strips 4 mm thick and 15–20 mm wide along the specimen were used. The indirect tensile test setup is shown in Figure 3.14.

Figure 3.14 Indirect tensile test setup

3.5.4 Standard compressive strength (static modulus of elasticity and Poisson's ratio)

A standard compression test according to AS 1012.8.1(Australian Standard 2000b) at 7, 21 and 28 days of curing were conducted for quality control and determination of the compressive strength of all mixtures, using 50x50x50-mm cubes.

To determine the elastic modulus, the standard test for static modulus of elasticity and Poisson's ratio for testing cylinders under compression was employed, as shown in Figure 3.15. The test started by repeating the loading and unloading process three times. The load was applied to achieve 40% of the maximum load capacity. The test involved applying a compression load to the specimens and measuring longitudinal elongation for calculating the elastic modulus, and transverse elongation for calculating the Poisson's ratio. The test procedure and the related equations to calculate the modulus were as recommended by ASTM (2010).

Figure 3.15 Test setup to determine (a) elastic modulus and (b) Poisson's ratio

3.5.5 Single fibre pullout test

In fibre composites, fibre–matrix interface properties can dictate mechanical behaviour because such properties have a significant effect on crack formation, stress values and strain capacity. Interface properties also a significant influence on the failure mode. Consequently, predicting composite strength in a micromechanical

model can be achieved using the bond between the fibre and matrix—known as the adhesive strength. One test proposed to measure the adhesive strength of the fibre–matrix interface is the single fibre pullout test, as seen in Figure 3.16. The testing machine used in this experiment could not connect to a data logging instrument. Therefore, only maximum pullout force could be measured.

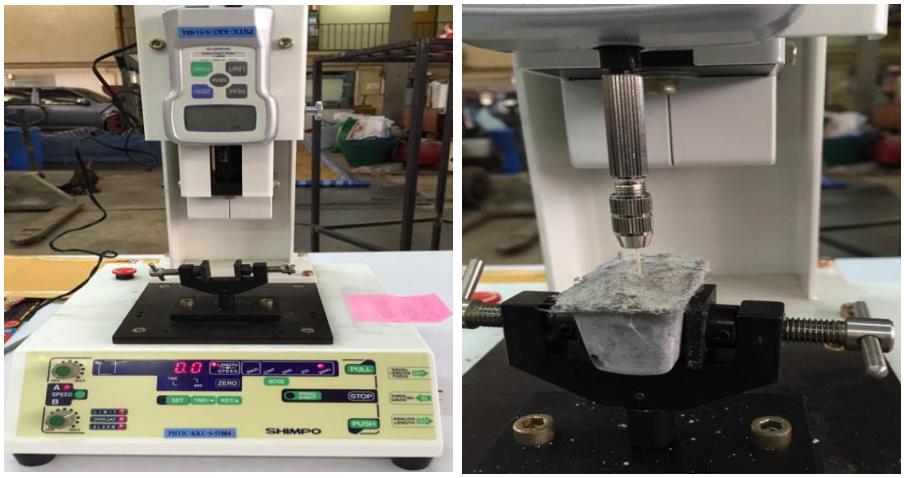

Figure 3.16 Single fibre pullout test machine and setup

3.5.5 Nanoindentation

The primary goal of nanoindentation tests is to determine the elastic modulus and hardness of the specimen material via experimental analyses of indenter load and depth during the indenter's penetration of the sample. The penetration depth of the nanoindenter into the specimen's surface is measured as the required load. One way to determine the elastic modulus is to measure the material's stiffness due to the changed rate of load and penetration depth. The curve resulting from the load and unload in relation to depth is shown in Figure 3.17. The total elastic module was as the sum of the elastic modules of each matrix phase calculated.

In small-scale studies, a Berkovich indenter is preferable (Fisher 2004) because its edges meet at a single point more precisely than do those of other indenters, such as the four-sided Vickers pyramid. The test was performed by applying a load from zero to a particular maximum force, then back to zero. At this point, plastic deformation may occur in the form of creep (Bahr and Morris 2008). The load–depth curve describing this process is shown in Figure 3.17.

For the nanoindentation tests, slices from the HFF panels were cut (using a diamond precision saw) into square specimens 10 mm long, 10 mm wide and 8 mm thick. The wire mesh was avoided in cutting out the samples. To prevent hydration, the samples were treated with isopropanol solvent for two days. Nanoindentation experiments were performed using an Agilent G200 Nano Indenter located at Curtin University. The specimen and nanoindentation machine are as seen in Figure 3.18.

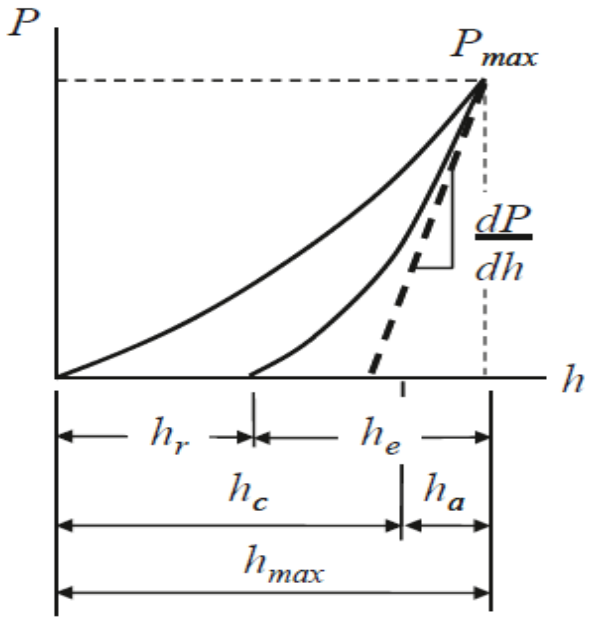

Figure 3.17 Load–depth curve for the penetration of an indentation tip into a solid (source: Oliver and Pharr 2004)

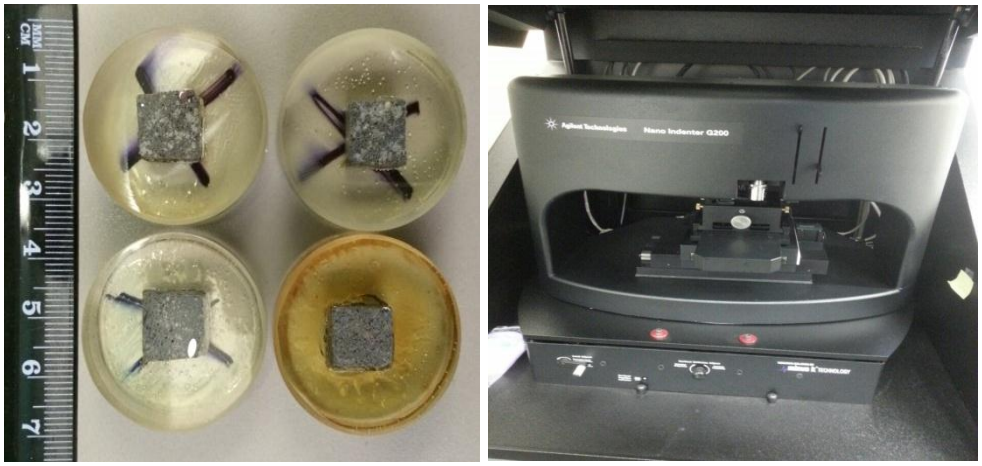

Figure 3.18 Specimens and nanoindentation testing machine

The penetration depth *h* of the nanoindenter was consistently recorded by the change in the capacitance of a parallel plate capacitor. The load–depth (*P*–*h*)

relationship was recorded through a certain load and displacement range. A loading history curve was prescribed, defined by a loading, holding and unloading time. A three-sided pyramidal Berkovich indenter with a semi-vertical angle of 65.27º was used in this test. Examinations were carried out by randomly choosing the positions for 500 indentations on the surface of each specimen.

An effective elastic modulus E_{eff} (MPa) can be calculated from the load–displacement slope provided by the *P–h* curve (Lukovic et al. 2014; Oliver and Pharr 2004). The Young's modulus of the indented sample E_s (MPa) can be calculated from E_{eff} (MPa) by:

$$\frac{1}{E_{eff}} = \frac{1-{v_s}^2}{E_s} + \frac{1-v_i^2}{E_i} \qquad (3.5)$$

The effective elastic modulus concedes the combined elastic displacements, with Young's modulus E_s and Poisson's ratio v_s, and the indenter elastic constants E_i and v_i. For the diamond Berkovich indenter in this investigation, the properties of the indenter (E_i=1000 GPa, v_i =0.07) are at least an order of magnitude greater than most cementitious constituents (Constantinides, Ulm and van Vliet 2003), so that:

$$E_{eff} \approx E_s/(1-v_s^2) \qquad (3.6)$$

The vertical displacement of the contact margin follows from the geometry of the depth of the indent from the contact surface of the specimen, once the contact area is determined, and the peak load (milli Newton) is known. The hardness (H) is estimated from the maximum indentation load P_{max} over the cross-sectional area of the indenter *A* as:

$$H = \frac{P_{max}}{A} \qquad (3.7)$$

The data obtained from the tests were analysed using the statistical nanoindentation technique (SNT) according to the method of Ulm et al. (2007). The results were analysed based on the deconvolution method to generate the experimental cumulative distribution function (CDF) by estimating the mean and standard deviation of the indentation modulus, and hardness for each phase level of the materials. The data were analysed using a MATLAB program developed at Curtin University.

The multiple scale considers four primary levels (Sorelli et al. 2008) of the microstructure of HFF composite, as seen in Figure 3.19. Level I consist of low density and HD C–S–H, with an estimated size of 10^{-8}–10^{-6} m. The C–S–H matrix, with calcium hydratecrystals, cement clinker (CC), micro quartz from SF and empty

microvoids, forms the cement paste (Level II), which is at alarger scale (estimated at 10^{-4}–10^{-3}m)than Level I. The mortar paste (Level III) is in the estimated size range of 10^{-3}–10^{-1}m and represents the composite material of the cement paste matrix, sand particle and fibre. This is the appropriate scale for numerical structural modelling of the RVE (Garboczi and Berryman 2001; Li et al. 1999).

3.5.6 Scanning electron microscope

Microstructural analysis using scanning electron microscope (SEM) observations was conducted on samples taken from the cores of the HFF panels. SEM delivers advanced high-resolution images of the sample surface and near-surface. It is a widely used analytical method because of the extremely detailed images it can quickly provide. A Zeiss NEON high-resolution SEM with GEMINI lens is located at Curtin University of Technology (see Figure 3.20). The SEM was used to examine the surface of the specimens, which were coated with gold. A high-resolution surface inspection of samples afforded microstructural examination and provided images of different HFF mixtures, including under evaluated temperature.

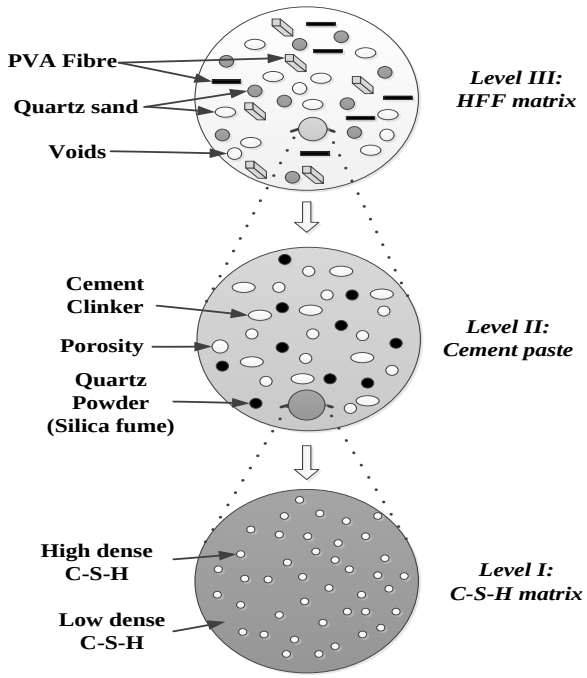

Figure 3.19 Microstructure levels of HFF matrix

Figure 3.20 SEM located at Curtin University

3.6 Data acquisition system

The experimental results from the flexure and direct tensile tests are in the form of load *vs*. displacement. The data were obtained using LVDTs and extensometers connected to a QuantumX MX840A data acquisition logger (Figure 3.21), an eight-channel universal amplifier to record the data immediately at 24 bits. The data were stored, and used to plot the relationship between a load and its related displacement. To maximise the accuracy of the data, the reading rate was set to five readings per second. The LVDT sensors and load cell were attached to the QuantumX logger to process the signal. The load–displacement data obtained from the LVDTs and the load cell were then displayed in real time during the test. If more than eight channels was required, two or more data loggers could be connected.

Figure 3.21 Quantum MX 840A data acquisition logger

3.7 Numerical modelling

Several cementitious composites are quasi-brittle or exhibit strain hardening behaviour with nonlinear strength and deformation behaviour. Two different types of modelling were used in this study to account for this. The first method was applied to determine HFF material properties, and the second involved building a model to examine the structural behaviour of HFF panels and slabs.

A numerical model of hybrid fibre cementitious composites was developed by Pereira, Fischer and Barros (2012b) for application to the material properties obtained from mechanical testing. Developing an FEM for hybrid fibre in HFF is very complex because of the randomly distributed fibres—which show transverse isotropic behaviours (Barbero and Luciano 1995; Barbero 2014)—and the variety of assumptions necessary to deal with the missing material properties of the matrix. To validate the structural material specifications achieved in this investigation and the local intensification of the stress induced by the fibre, a three-dimensional FEM was created using the ANSYS mechanical program (ANSYS 2015). The numerical model represents a valuable contribution to calculate the dominant micromechanical properties using an RVE. The microstructural variation due to fibre, sites of flaws (where cracks are initiated) and size distribution in the matrix has a significant influence on ductility (Li and Wang 2006). Therefore, the assumption in this study was that the indented specimen, in this case RVE, was composed of the complete cementitious matrix including mortar and hybrid fibre.

Two numerical modules were modelled using FE software by ANSYS (2015). One model represents HFF panels to validate the results obtained from the test data. The second was built to simulate HFF in its application as an AAC block slab composite. The purpose of this model was to determine the stress concentration, slip and transverse shear behaviour of both slabs at the contact interface. In general, the modelling distinguished between concrete (brittle material) and the HFF matrix (strain hardening). For concrete, a conventional model was developed using a SOLID 65, eight-node brick element accomplished by simulating the cracking and crushing of brittle materials. This included the application of the concrete specifications for the material properties. The rebar reinforcements were separately modelled using LINK 180, and all rebar properties were applied.

To include the effect of fibre addition on the strain behaviour of HFF material, the nonlinear elasticity model was based on the concept of a variable module by expressing the stresses and strains obtained from the test results using a SOLID 65 element. Consideration of strain hardening behaviour due to multiple cracking is important as crack opening contributes to the total strain. In other words, the strain must be divided into elastic strain and plastic cracking strain. This can be achieved by applying a shear transfer coefficient for open cracks, representing the crack conditions, an approach known as a smeared crack model (Trueb 2011). The wire mesh is modelled similarly to the concrete reinforcement. A more detailed description of the numerical FE method will be presented in Chapter 8.

3.8 Research limitations

The structural and mechanical behaviour of cementitious composite is primarily dependent on its reinforcement. The range of fibre types used for reinforcing cementitious composites is so vast that they cannot all be included in one study. The current study is limited to an investigation of synthetic PVA fibre. However, the limitations of the conducted tests are dependent from the available test machines and the materials from the resources.

In addition, the study considers only the structural and mechanical behaviour of the HFF, and does not take into account any cost comparisons. The cost reduction claimed as a significant advantage of HFF panels as permanent formwork is based solely on the fact that weight reduction and elimination of a construction step will in theory reduce overall construction costs.

3.9 Summary and concluding remarks

This chapter outlined the methodology employed in the research programme. This was followed by a material description of the components under study, and an introduction to the test equipment and procedures employed. The explanation included a detailed illustration of mixture composition, fibre properties, specimen preparation, specimen curing conditions, testing arrangement, data acquisition and

key parameters in the testing programme. The objective of the study is to evaluate the behaviour of HFF over its structural and mechanical properties. It is worth noting that the research programme was limited by the available resources and time.

Chapter 4: Composition Variation and Material Contribution to Strength Capacity

4.1 Introduction

Several factors affect the performance of FRCCs. Mixture composition is one critical factor contributing to performance: increasing matrix packing density improves mechanical behaviour. However, an FRCC's structural response to loads in tension is mainly driven by its reinforcement type and volume fraction. Another important factor influencing the structural behaviour of thin cementitious composites is the cross-section, specifically the thickness. However, composites such as HFF, in which the reinforcement is a combination of wire mesh and two types of fibre, are more complex and hence their structural performance requires examination.

In this chapter, the structural performance of HFF with various PVA fibre combinations is investigated using different volume fractions of each blend. The PVA fibre combinations are 0.75, 1.0 and 1.5% volume fractions. These fibre combinations were proposed to evaluate the structural response, which allows the choice of the best fibre combination and content with respect to performance. The investigation focuses mainly on the flexure response of this composite because it reflects all generated actions in the composite due to the acting force.

Next, a research programme is undertaken to examine the effect of using different ratios of additives to water in the HFF mortar mixture, on the flexural performance of ferrocement panels. Admixtures used are superplasticisers and SF. The aim is to achieve the desired strength development while maintaining mixture flowability, which has a significant influence on casting of the wire-reinforced panels. The effect of increasing FA content from 0% to 50% on the flexure behaviour of HFF composite is also evaluated. Other significant efforts are made to optimise the wire steel mesh content and HFF panel thickness. The optimal mixture

proportions, wire mesh content, fibre type and volume fractions are used for the remainder of this study. Noticeably, a part of the work presented in this chapter has been published in Australian Journal of Structural Engineering and International Journal of Innovative Research in Science, Engineering and Technology.

4.2 PVA fibre type

Four PVA fibre types were used to determine the structural performance of the ferrocement composite (see Table 3.3andSection 3.2.2). The primary test conducted in this examination was the flexure test. A detailed description of the test setup and specimen size was provided in Section 3.5.1.

4.2.1 Flexural response of different PVA fibre type combinations in HFF composites

To determine the most suitable PVA fibre combination, four fibre combinations were tested (see Table 4.1). The mix was designed for a cement content of 400 kg/m^3. The mortar mix proportions were equal for all specimens, with a ratio of 1:0.45:1 by weight of cement, water and sand. Control mixtures with the same mix proportions but without the addition of fibre were usedto cast ferrocement panels. ECC panels without wire mesh reinforcement and panels with one mono fibre type (PVA1) (EF panels) were also cast. To enable a reasonable comparison with the same mix proportion used for ferrocement, the ECC mixture proportions did not follow the normal ECC specification. The mixture sequence used in the fibre composite followed Zhou et al. (2012). Notably, the volume fraction of 2% was not used in these test mixtures, to maintain workability without admixtures, which allows full penetration of the mixtures between the wire mesh layers during casting, and to avoid the balling effect mentioned in Chapter 3.

The data were obtained in the form of load *vs*. deflection, which were used to calculate the equivalent elastic bending stress using Equation 3.2 to provide the relevant stress–deflection curve. For each mixture, three panels were cast and tested; the equivalent stress–deflection curves presented here are the average of the three curves resulting from the test.

Table 4.1 PVA fibre combination

Combination	Tread	Fibre ID	Volume fraction (V_f)	Specimen size (mm)	Number of wire mesh layers
HFF1	RSC 15+RF4000	PVA1+PVA4	1.5%	620×200×40	4
HFF2	RSC15+ RFS400	PVA1+PVA3	1.5%	620×200×40	4
HFF3	RECS15+FS4000	PVA2+PVA4	1.5%	620×200×40	4
HFF4	RECS15+RF400	PVA2+PVA3	1.5%	620×200×40	4
Ferrocement	-		-	620×200× 40	4
ECC	RSC 15	PVA1	1.5%	620×200×40	-
EF	RSC 15	PVA1	1.5%	620×200×40	4

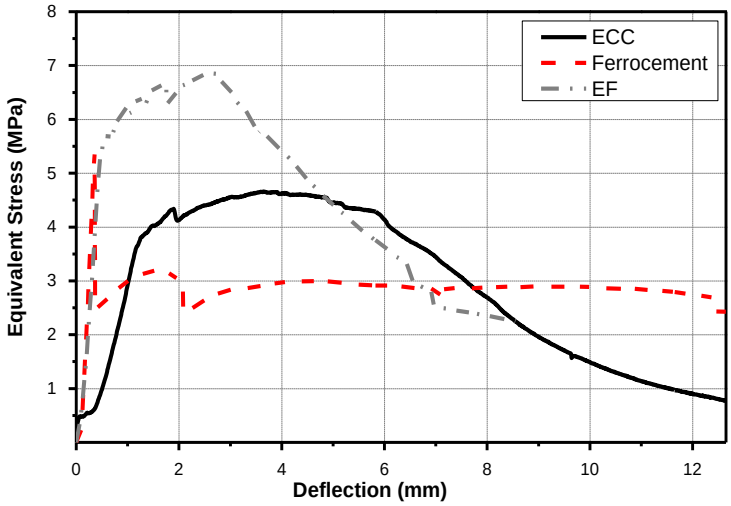

Figure 4.1 Equivalent flexure stress–deflection of control specimens

The effect of a single fibre on the flexural performance of cement-based composite, conventional ferrocement and ECC is evident in Figure 4.1. The mono PVA fibre-modified ferrocement (EF in Figure 4.1) exhibited deflection hardening similar to that of ECC, but with higher maximum load and lower deflection capacity; whereas ferrocement tended to behave in a quasi-brittle fashion, as seen by its higher first crack stress followed by more or less strain softening behaviour. Notably, the ferrocement control panels presented equivalent stress–deflection behaviour similar to that reported in the literature (Naaman 2000;Arif, Pankaj and Kaushik 1999; El

Debs and Naaman 1995). The curve shows an elastic behaviour in the initial phase followed by an extended progressively inelastic behaviour as the stress increases. A sudden load drop at the transition point from the elastic to the inelastic phase distinguishes this regime, which is an indication of first cracking. Beyond this point, in the same region, the slope of the load–deflection curve gradually decreases, showing some sudden decreases due to microcracking extension in the matrix. Further, the wire meshes in tension were undergoing a straightening effect; the first wire mesh layer might yield, leading to further crack widening. Continued increases in the load on the specimens mobilised the internal wire meshes to start carrying loads until failure.

The comprehensive equivalent stress–deflection curves of hybrid fibre composites and mono fibre-reinforced ferrocement with a fibre content of 1.5% are shown in Figure 4.2. In this direct comparison of the four hybrid blends, it is evident that the hybrid fibre exhibits, in general, higher structural performance than its mono fibre ferrocement counterpart (Figure 4.2). PVA hybrid composites, depending on the fibre combination, show an increase in maximum flexural stress, and a higher deflection capacity, compared to EF composites. The maximum stress ranges from 8% in mix HFF2 to 32% in mix HFF1. The lower flexural strength of the mono fibre control panels can be related to the tensile resistance activation of the hybrid PVA fibre used. The effect of hybrid PVA fibres is that the shorter fibres act in the earlier load stages to bridge microcracks, whereas the longer fibres act at the stage of macrocracks with additional tensile capacity provided by the wire mesh. The higher tensile strength and length of the PVA3 and PVA4 fibres compared to PVA1 and PVA2 resulted in an increase in the binding stress and post-yield strain capacity of these specimens.

Additionally, all tested HFF panels showed multiple crack formation due to the maximum load being greater than the first cracking load. After the first crack, the panels continued to sustain the load due to the tensile capacity provided by the fibres. Further development of multiple cracks in the constant moment region of the panel span continued until the maximum bending moment was reached. However, the multiple cracking observed was an additional phenomenon related to the use of hybrid fibres. As soon as the cracks widened, shorter PVA fibres ruptured or were pulled out. Longer fibres continued bridging the extensions of those cracks. This was evident during the tests as continuing rupture sounds after the first crack. At this

stage, the wire mesh contributed by resisting the tensile stress until failure occurred. The mono fibre-reinforced ferrocement also exhibited multiple cracks, but these were fewer in number than in the hybrid composite, as seen in Figure 4.3.

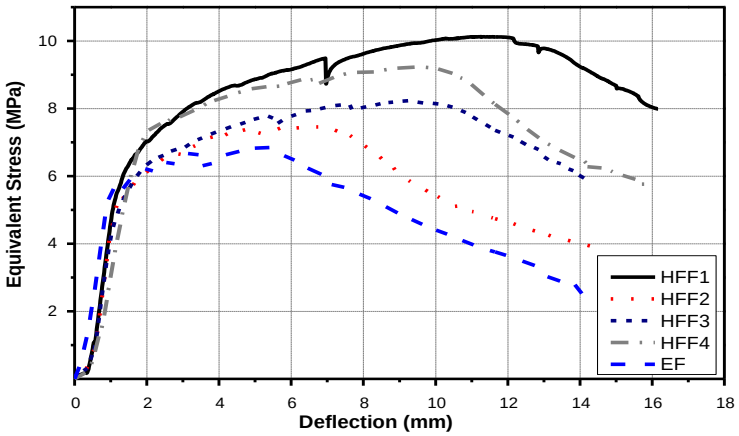

Figure 4.2 Stress–deflection curves of specimens with different hybrid combinations

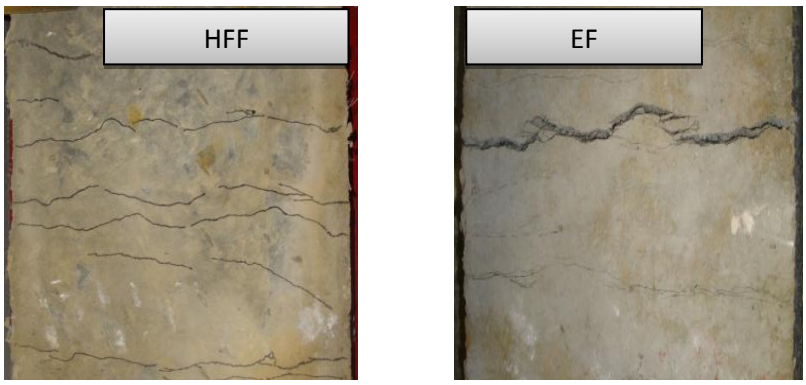

Figure 4.3 Crack formation in mono and hybrid PVA fibre ferrocement

4.2.2 Effect of hybrid PVA fibre volume fraction in HFF

For this test, similar mixture proportions were used as in Section 4.2.1. The only variable in the mixture was the fibre volume fraction (V_f): mixture types A, B and C, had V_f of 0.75, 1.0 and 1.5% respectively. Numbers 1–4 associated with each A–C mix corresponded to the PVA type in the mixture. For example, A1, B1 and C1 had the same type of PVA fibre but at different volume fractions. In total, 36 panels were fabricated to examine the effect of volume fraction for different PVA fibre combinations. Table 4.2 identifies the tested panels and their fibre type combination and content. It was assumed that different fibres contributed equally to structural

performance. Therefore, ~50% of each fibre type was used in the mixture to achieve the required volume fraction.

Table 4.2 Reinforcement and fibre content

Combination	Mix	Reinforcement					
		Fibre and volume fraction V_f(%)					Wire mesh
		PVA1	PVA2	PVA3	PVA4	Total	Number of layers
HFF1	A1	0.37	-	-	0.38	0.75	4
	B1	0.46	-	-	0.54	1	4
	C1	0.73	-	-	0.77	1.5	4
HFF2	A2	0.37	-	0.38	-	0.75	4
	B2	0.46	-	0.54	-	1	4
	C2	0.73	-	0.77	-	1.5	4
HFF3	A3	-	0.37	-	0.38	0.75	4
	B3	-	0.46	-	0.54	1	4
	C3	-	0.73	-	0.77	1.5	4
HFF4	A4	-	0.37	0.38	-	0.75	4
	B4	-	0.46	0.54	-	1	4
	C4	-	0.73	0.77	-	1.5	4

The panels were tested under bending. The equivalent bending stresses *v.* deflection curves in hybrid fibre composites with different fibre types and content are shown in Figure 4.4. The test results for all hybrid fibre composites showed increased capacity for both first crack and maximum strength with increasing volume fraction of PVA fibres. The flexural strength of HFF composites with a fibre volume fraction of 1.5% was greater than that of the composites with lower fibre volume fractions. Deflection capacity was also found to increase with fibre volume content, and showed deflection hardening. However, the hybrid PVA fibre C1 and C4 mixes exhibited better performance in terms of flexural strength and deflection capacity compared to their counterpart C2 and C3 mixes. Similar behaviours in term of stress and deflection were observed in B1 and B4 in relation to B2 and B3 fibre mix combinations. In contrast, (A) mixes did not differ significantly from each other in maximum flexural strength or deflection capacity (except that A4 exhibited

deflection softening). This might suggest that the fibre content in (A) mixes was too low to influence performance.

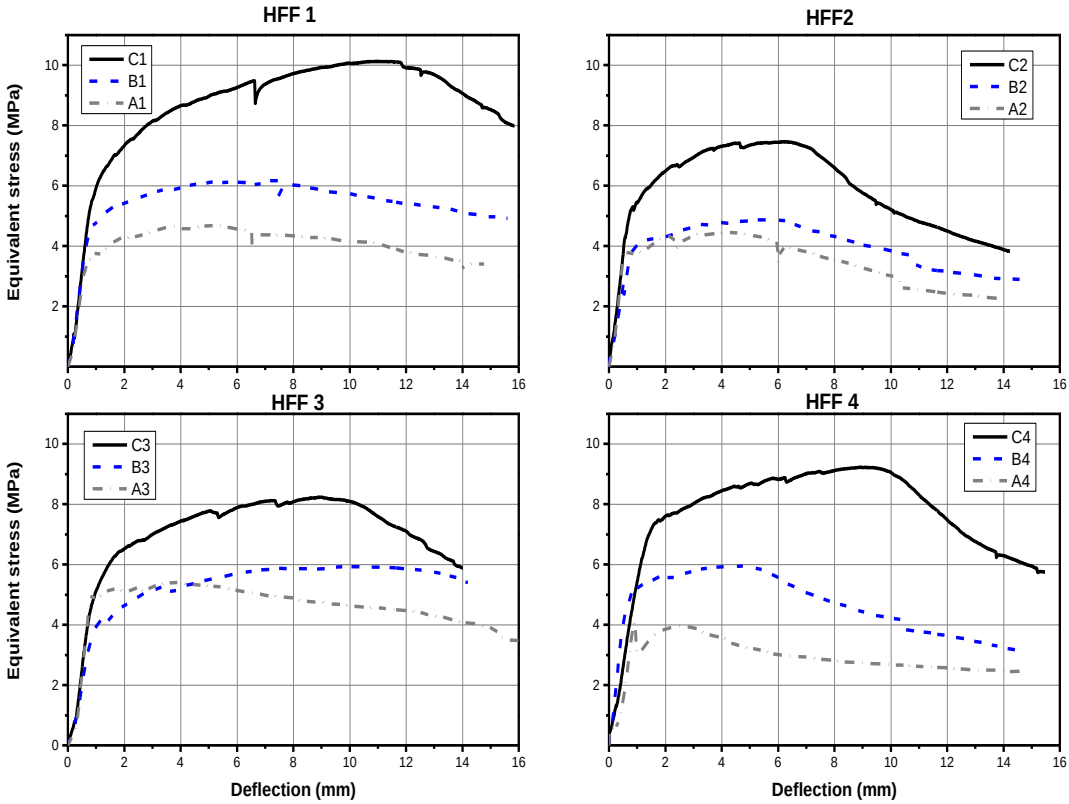

Figure 4.4 Equivalent flexural stresses for HFF panels with 0.75, 1.0 and 1.5%fibre volume fraction

Table 4.3 summarises the results obtained at the first cracking and maximum stress of all tested HFF specimens. As expected, structural performance in terms of flexural response depended on fibre content. This relationship is particularly evident in Figure 4.5. However, low fibre content had little effect on the maximum strength achieved and its deflection capacity, which is illustrated in some cases such as for A4, whose stress–deflection behaviour was similar to that of ferrocement. The influence of hybrid PVA fibres in ferrocement began to be evident at the moderate hybrid fibre content of 1.0%. The 1.5% fibre volume fraction of HFF1 showed, in general, the best performance. Therefore, further investigations of hybrid PVA fibre were conducted using the fibre combinations PVA1 and PVA4.

Table 4.3 Summary of the first peak and maximum values

Specimen ID	Cracking (first peak)			Ultimate		
	Deflection Δ_{cr} (mm)	Load P_{cr} (N)	Stress σ_{cr} (MPa)	Deflection Δ_u (mm)	Load P_u (N)	Stress σ_u (MPa)
A1	0.9	2106	3.8	5.2	2635	4.7
A2	0.5	2099	3.7	4.2	2502	4.5
A3	0.8	2788	5.0	3.7	3039	5.4
A4	0.9	2296	4.1	2.6	2231	4.0
B1	0.8	2007	3.6	7.4	3480	6.2
B2	0.4	1112	2.0	5.6	2741	4.9
B3	1.3	2374	4.2	7.1	3340	5.9
B4	0.8	2850	5.1	4.7	3346	6.0
C1	1.0	3363	6.0	10.9	5691	10.1
C2	0.9	3010	5.4	6.2	4193	7.5
C3	1.6	3442	6.1	9.0	4626	8.2
C4	1.6	4100	7.3	8.9	5184	9.2

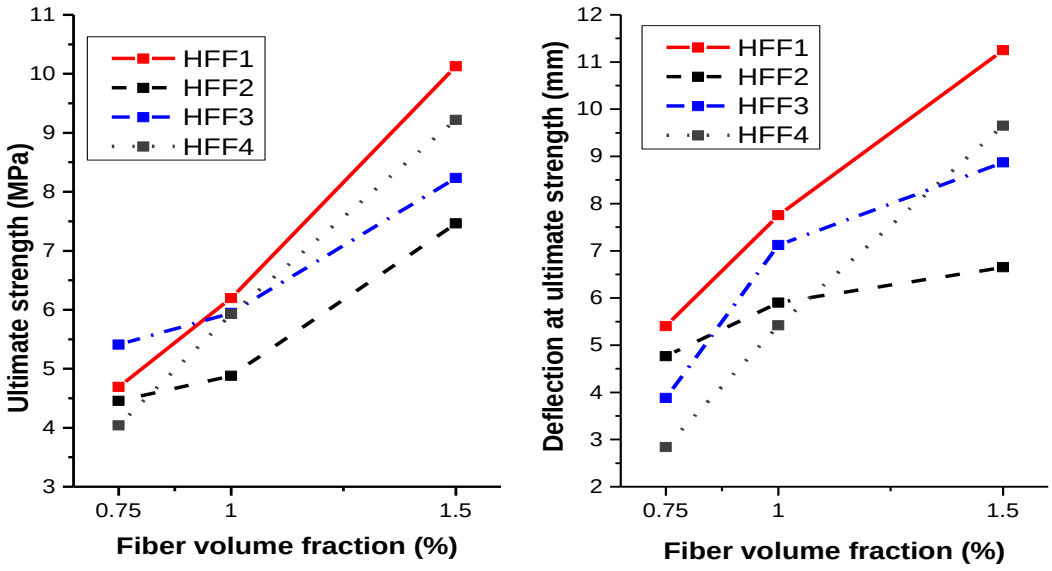

Figure 4.5 Flexural capacity of HFF panels with different fibre volume fractions

The compression of control specimens with low hybrid fibre content provided additional understanding of the fibre amount in cement-based composites influenced structural performance. For example, the average maximum stress obtained from the

FE specimen was 6.9 MPa, which is larger than that of HFF with a 0.75 or 1% V_f. However, the HFF with 1% V_f exhibited greater post-yield strain capacity, as seen in Figure 4.6, which could be associated with the hybrid effect due to the crack binding mechanism of those composites, as described in Chapter 3.

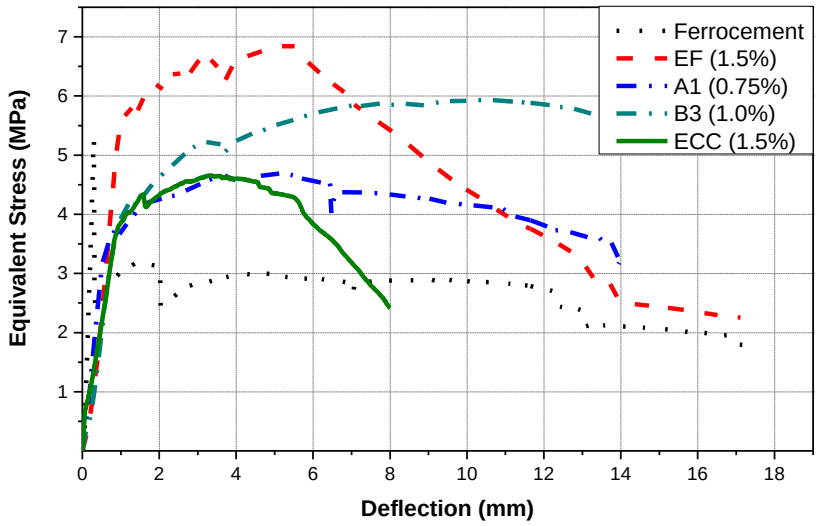

Figure 4.6 Flexure performance of ferrocement and HFF panelswith low fibre content

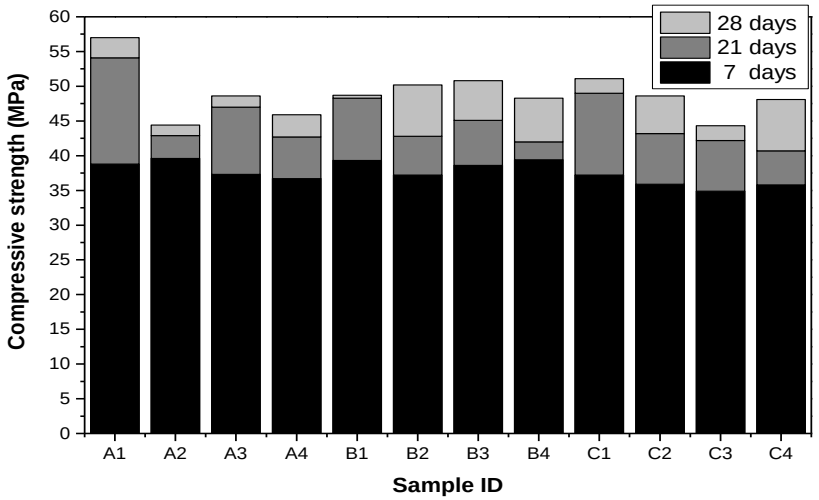

Figure 4.7 Average compressive strength development of all specimens at 7, 21 and 28 days

The compressive strength of different composite mixtures was compared. A standard compressive strength test was conducted 7, 21 and 28 days after casting, as seen in Figure 4.7. The average compressive strength of ferrocement with the ordinary mortar mix was ~54 MPa. The fibre-reinforced mortars with different

volume fractions of hybrid PVA are according to Table 4.2. It should be noted that the addition of fibres to a mortar mixture generally leads to a reduction in compressive strength, which might be largely due to air bubbles forming during addition of the fibres during mixing (El Debs and Naaman 1995). However, the cubes containing 1.0 and 1.5 % V_f exhibited converged compressive strengths.

Notably, all tested specimens exhibited multiple crack formation, although differing in crack width and number. In general, crack number increased with fibre volume fraction, as seen in Figure 4.8. Samples with 0.75% V_f showed minuscule multiple crack openings in comparison with specimens with higher volume fractions.

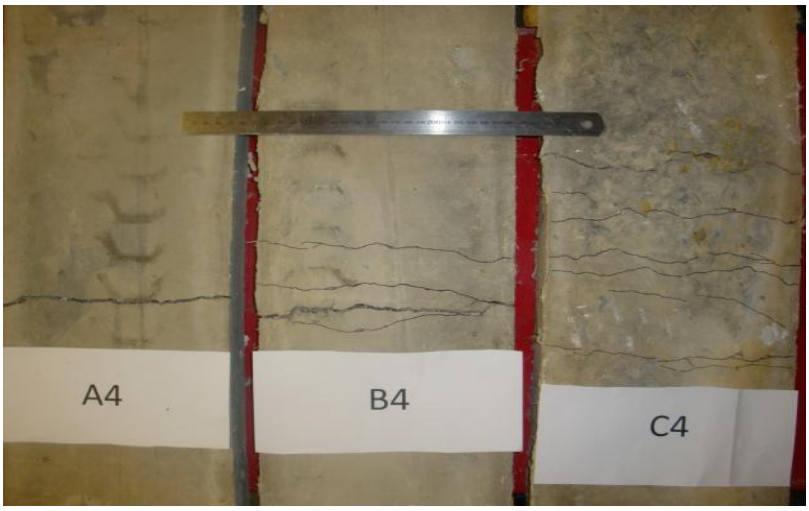

Figure 4.8 Crack formation and crack quantity with increased fibre volume fraction

4.3 Effect of the mixture on the structural performance of HFF composites

Relatively low workability as a result of the addition of fibre was observed in some mixes, which may create a system of defect zones. The air bubbles and partial penetration of the mortar between the wire mesh throughout the system due to the very stiff matrix led to significant defect areas. To avoid these imperfections, improved workability is required, and the most suitable mix was tested by comparing several HFF composite mixes. The mortar mix proportions of all mixes were as shown in Table 4.4. Three 50-mm cubes and three 620x200x40-mm panels with four layers of wire mesh were produced from each mix. FA, SF and superplasticiser were used in the mixtures to increase workability and improve compressive strength

(Alsadey 2012). Mix C1 is a control mix with no additives; CM, CN and CL were the mixes with FA, SF and various amount of superplasticiser; CX and CY had no superplasticiser, with and without SF. The FA content in all mixes was 25% cement replacement, except that CG and CZ had 50% replacement, and CZ also had added SF. The water content in these mixes was adjusted to improve the workability of the materials.

Table 4.4 Mixture proportions* and compressive strength

Mixture type	Binder		Sand	water	Silica fume	Superplasticiser
	Cement	FA				ml /100 Kg cement
C1	1	-	1	0.45	-	-
CM	0.75	0.25	1	0.40	0.05	400
CN	0.75	0.25	1	0.35	0.05	600
CL	0.75	0.25	1	0.30	0.05	800
CX	0.75	0.25	1	0.45	-	-
CY	0.75	0.25	1	0.45	0.05	-
CG	0.50	0.50	1	0.45	-	-
CZ	0.50	0.50	1	0.45	0.05	-

**All ratios are by weight.*

The average compressive strength of hybrid fibre-reinforced mortar with 1.5% volume fractions of PVA fibres was obtained via standard compression tests according to AS 1012.8.1 (Australian Standard 2000b), at the age of 28 days, with results presented in Figure 4.9. These results suggest that all mixtures with 0.25 FA ratios developed excellent compressive strength values similar to the control mix. Mix CL provided the highest compressive strength, greater than the C1 strength value. All mixtures with 0.5 FA ratios exhibited relatively low strength, which suggests that this ratio is appropriate only when high strength is not essential.

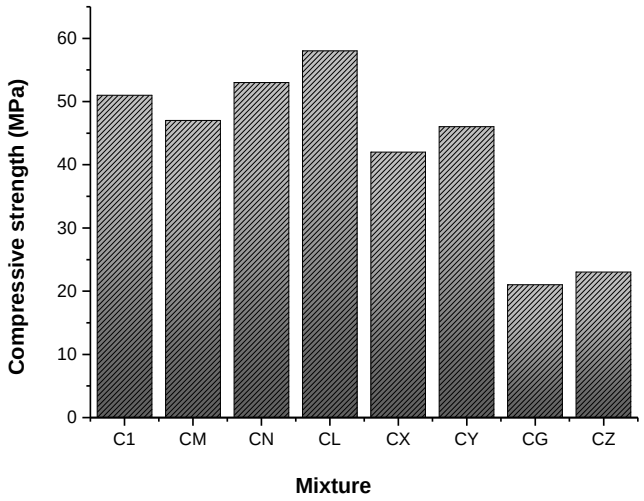

Figure 4.9 Compressive strength of different HFF mixtures

The stress–deflection curves for all tested panels are shown in Figure 4.10. It is apparent that a decrease in the water-cement ratio, and the addition of SF and FA can improve the compressive strength value of tested specimens. The specimens with relatively high compressive strength also performed best in terms of flexural strength.

Based on these results, panel CL provides the best flexure strength, which is consistent with the material's cube strength. However, the CL mix was very stiff compared to all other mixtures in this test. The low workability due to the low water content of the CL mix made it difficult to cast the panel because of poor penetration between the wire mesh layers. On the other hand, mixes CM and CN flowed better (i.e. showed higher workability) but resulted in slightly lower compressive and flexural strength than those of the CL mix. The high workability and improvement in strength capacity may relate to the superplasticiser, as mentioned in Chapter 3. Both the first peak stress and the ultimate strength of the CN specimen were greater than those for most other mixes. However, its post-yield strain capacity was approximately 13% lower than that for the C1control mix. Nonetheless, this had not effect on ductility and energy absorption of this composite material. Overall, the CN mix (Appendix B) produced excellent results with reasonable workability, so was chosen for all further tests in this study.

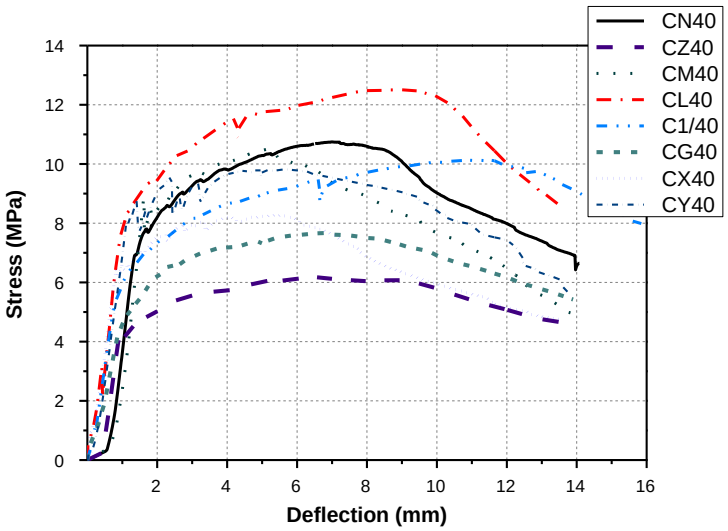

Figure 4.10 Stress–deflection curves of specimens with different water:cement ratios and FA content

Comparisons of CX and CY with control mix C1 showed that the use of 25% FA as a cement replacement without SF has no positive influence on strength capacity. Adding SF to the mixture improved its flexural capacity. After the first crack, CX and CY panels appeared to develop multiple cracks in the lower deflection range and attained lower maximum strength values than for the C1 panel. The large amount of FA in CG and CZ panels resulted in relatively large reductions in the flexure strength and strain capacity of the HFF specimens. Similar results have been reported in several other studies on the effect of FA content in ferrocement and ECC materials (Bhikshma, Ravandekishore and Srinivas 2011; Özbay et al. 2012). The equivalent stress at the first crack and the ultimate strength are the lowest for panels with high FA contents, which caused ~50% decrease in values compared to other tested specimens.

4.4 Influence of wire mesh

4.4.1 Wire mesh content

To determine the effect of wire mesh volume fraction on the flexural behaviour of HFF composites, a test series using different wire mesh volume fractions was conducted. The CN mixture proportions were used to produce the required number of panels. All panels were made with similar size and fibre volume fractions as in the

previous test. Note that wire mesh content (hexagonal mesh) is counted as layer numbers, which can be used to determine the wire mesh volume fraction according to the following equation (ACI Committee 549-R93 2009):

$$V_r = \frac{N\pi d_b^2}{4h}\left(\frac{1}{D_l} + \frac{1}{D_t}\right) \qquad (4.1)$$

where N is the number of layers; d_b is the diameter of the mesh wire; h is the thickness of the ferrocement panel; D_l is the spacing of wires aligned longitudinally in reinforcing mesh from centre to centre; and D_t is the centre-to-centre spacing of wires aligned transversely in the reinforcing mesh.

Figure 4.11 shows the maximum strength obtained by the tested panels, which decreased with decreasing numbers of wire mesh layers, except for panels with six mesh layers. Panels with four mesh layers (0.67% V_r) exhibited the highest ultimate strength. The panel using three layers had similar flexural behaviour, with a slightly lower first crack stress and maximum strength than the four-layer panel. Specimen CN, which had only two layers (0.33% V_r) of wire mesh, provided a similar stress–strain curve trend as observed for the high performance fibre-reinforced materials in Suwannakarn (2009), but with a lower strength development compared with the three- to six-layer wire mesh-reinforced panels.

The equivalent stress–deflection curves for all tested samples also show supplementary growth in yield deflection and strength capacity for panels with one or two layers of wire mesh reinforcement. This behaviour is due to the reinforcement effect of hybrid PVA fibre, in addition to the wire mesh. It was expected that the combination of wire mesh and 1.5% hybrid PVA fibre would provide improved strength and high strain capacity. It is significant in strain hardening materials that, after reaching the first stress peak, the stresses growth until reaching the maximum strength (Naaman 2007). This behaviour is due to the phenomenon of discontinuous reinforcement and the effect of fibre hybridisation (Ahmed 2003). Different continuous reinforcement content affects the values but has very little effect on the ductile behaviour of HFF. Insensitivity to this parameter, while maintaining strain hardening behaviours, indicates better prospects for the use of such hybrid ferrocement composites.

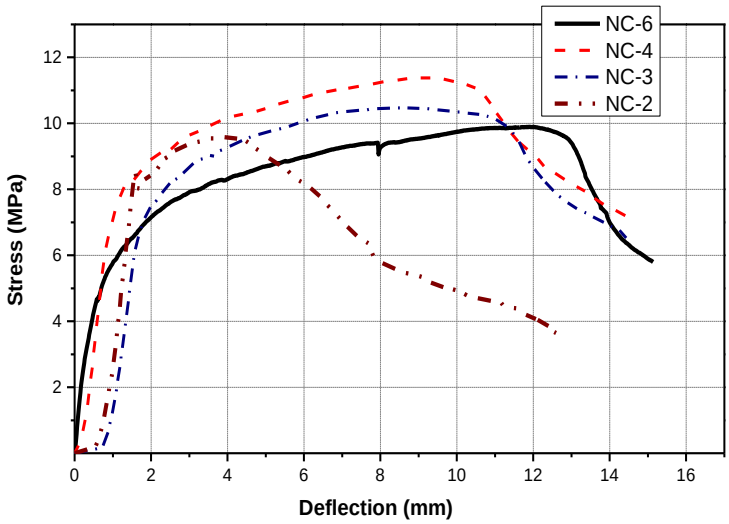

Figure 4.11 Stress–deflection curves of panels with different wire mesh content

Another important observation was the multiple crack formation in flexure-tested specimens, as seen in Figure 4.12. In HFF panels with different hexagonal wire mesh content and 1.5% volume fraction fibre, multiple cracks were formed. Small cracks closed considerably after removal of load. This could reflect a self-healing effect due to the use of different lengths of fibre in a mixture matrix, which increases the bridging stress–crack relationship. However, this phenomenon is related to the activation of different fibres at different crack scales in the material's structure (Li, Wang and Wu 2001), so the wire mesh content had an insignificant effect on the multiple crack behaviour observed in those specimens.

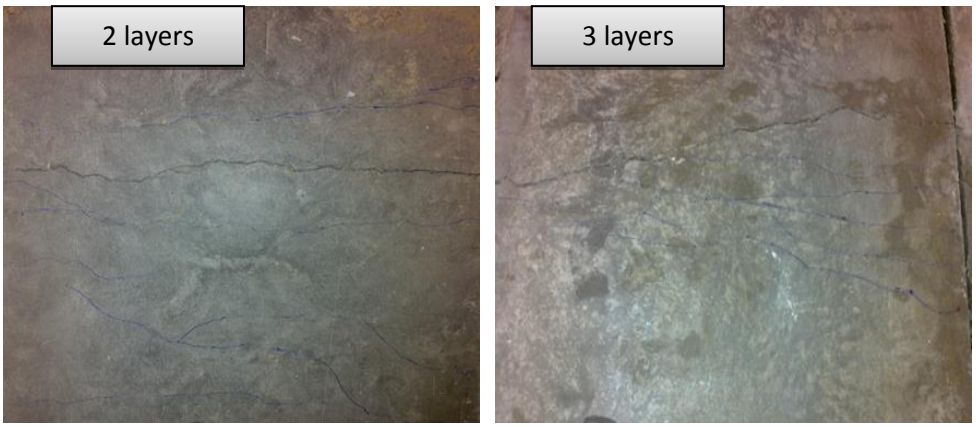

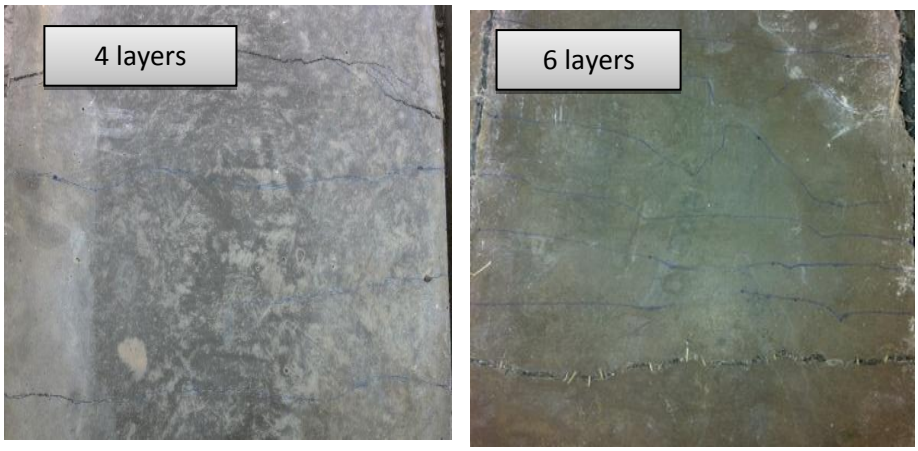

Figure 4.12 Cracking in HFF panels with different wire mesh content

4.4.2 Wire mesh type

The flexure results were compared between specimens made with two wire mesh types (Figure 3.4); a galvanised square wire mesh with a spacing of 25x25 mm and 1.24-mm wire diameter, and a galvanised hexagonal mesh with 1.4-mm wire diameter. The panels were made by using the same mixture composition as in CN panels. The wire mesh volume fraction was held constant at ~0.67%. The results presented in Figure 4.13 suggest astonishingly higher strength capacity using the square mesh. However, HFF with hexagonal wire meshexhibited a steadily increased plastic deformation after first crack, which provided a smoother strain course at the multiple crack stage. The higher strength of HFF with square mesh could be related to the longitudinal and transverse arrangement of the wire mesh, which allows transfer of the tension loads occurring in the panels due to the applied load in bending. This is because ferrocement is more on the mesh direction and the way of applying the load in uniaxial or biaxial direction oriented. This confirms that the flexural and tensile strength capacity depends on the type of steel wire mesh because of the effect of mesh orientation, as observed in other studies (see Section 2.5.1).

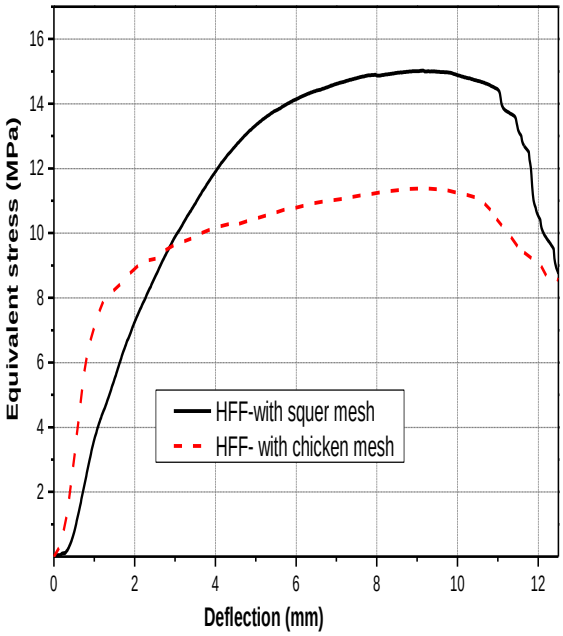

Figure 4.13 Stress–deflection of HFF with different wire mesh

4.5 Influence of panel thickness

To determine the effect of panel thickness on the structural performance of HFF, 27 panels with three different panel thicknesses (25, 30 and 40 mm) were cast. An illustration of the stress *vs*. deflection curve is provided in Figures 4.10 and 4.14. Note that thinner panels were reinforced with smaller numbers of wire mesh layers to avoid overcrowding in the smaller space available. All panels exhibited a similar flexure response showing strain hardening behaviour. The values depended on the panel thickness and reinforcement content. All tested samples under bending showed deflection hardening behaviour. The experimental results for the CN30 samples showed that panels with three mesh layers performed better than those with two and four layers. Although there were minor differences, these results show that the optimum wire mesh content is not necessarily related to the maximum volume fraction of the reinforcement. Remarkable stress values were achieved in the CN25-3 specimen, which had 41% higher strength capacity than the peak strength of CN25-2. This exceptional performance for CN25-3 suggests that it is possible to determine optimum thickness and wire mesh content of HFF panels.

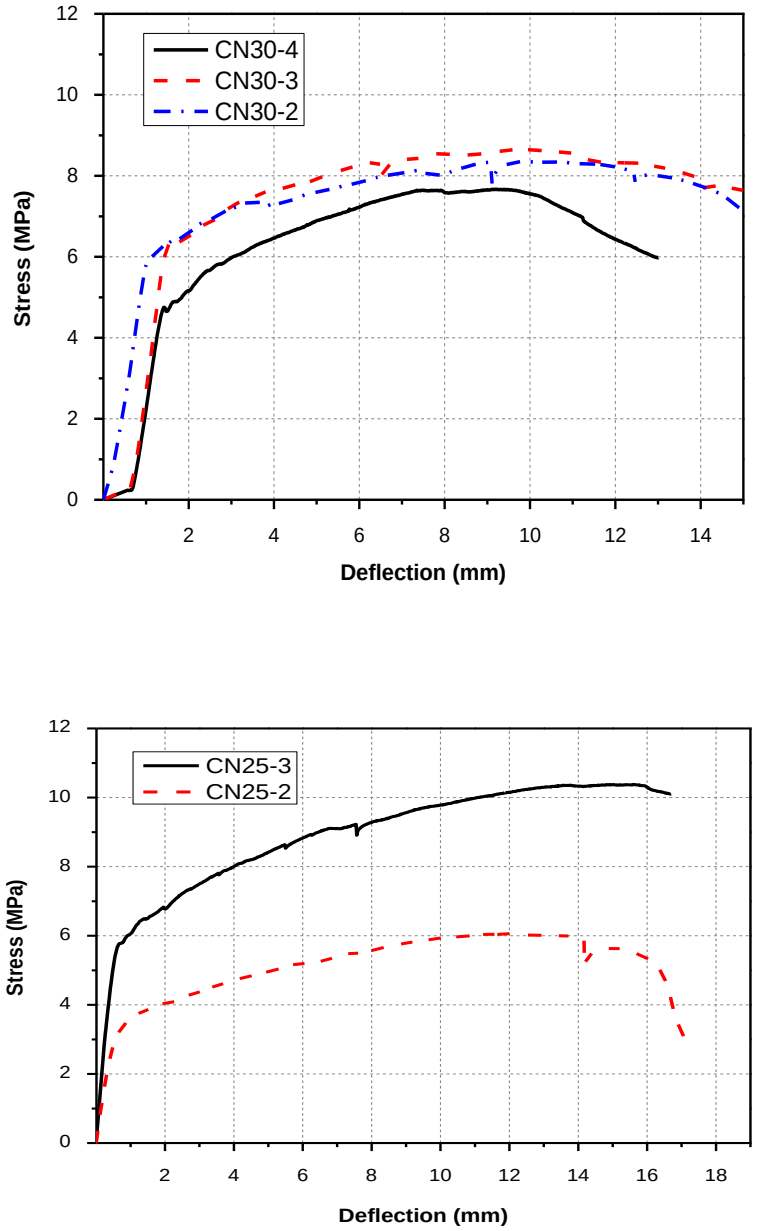

Figure 4.14 Flexure behaviour of HFF panels with different thicknesses (25 and 30 mm) and reinforcement content

To provide a better overall understanding of the effect of panel thickness in conjunction with wire mesh content, the ultimate strength and energy absorption values related to specimen thicknesses were compared (see Figure 4.15). Mixture CN40-4, with a reinforcement content of 0.67% (four mesh layers), exhibited greater maximum strength than all other tested panels with different reinforcement contents and thicknesses. The use of three wire mesh layers in all panel thicknesses also yielded relatively high strength values. The stress results at maximum loads showed

that the 25-mm thick panel with three mesh layers had relatively high strength results, comparable to the 40-mm thick panel. This behaviour is important in considering the best weight reduction for these cementitious composite materials. As might be expected, all panels with two layers of wire mesh reinforcement had the lowest maximum strength in this test series.

Similarly, the insignificant energy absorption in 40-mm thick panels with two wire mesh layers can be explained by the inadequate reinforcement content afforded by 0.33% V_r and an extensive cover limiting free flow during the energy dissipation procedure. The 40-mm thick specimens with two, three and four mesh layers showed energy absorption of 6.25, 27.50 and 39.92 J respectively. For 25-mm thick specimens, post cracks began at a very high energy level of around 88 J when three layers were used. This could be due to better reinforcement content (0.80 % V_r) in the hybrid PVA fibre cementitious matrix.

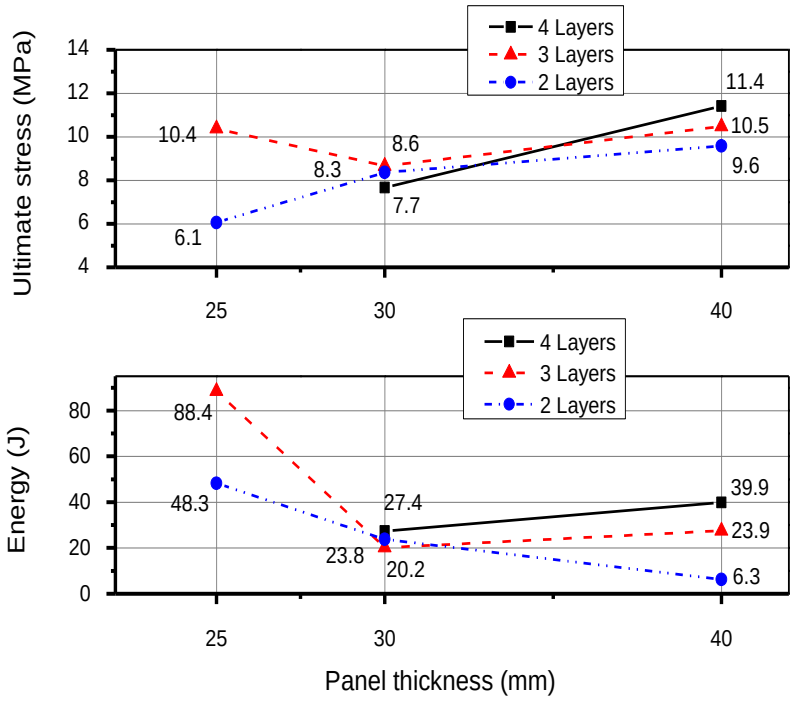

Figure 4.15 Stresses at ultimate loads and energy absorption for different thicknesses

According to Barr and colleagues (Barr, Liu and Dowers 1982; Barret al.1996), the toughness index can be used to ration the energy absorption of fibre-reinforced cement composites. The toughness index based on the load–deflection curve was calculated according to the ASTM C1609- Standard test method for

flexural performance of FRC (using a beam with four-point loading) (ASTM 2012). This guideline defines toughness as the area under the load–deflection curve up to a given deflection, divided by the area under the same curve up to first cracking deflection. Table 4.5 summarises the results for all tested panels. The toughness values for the CN25-2 and CN40-4 specimens (15.8 J and 11.9 J) were the highest calculated at L/150, according to ASTM 1609. The toughness results confirm all other results related to energy absorption at the post-cracking points. These results suggest that increasing the reinforcement content from 0.67% to 0.80% V_r allows a larger area of load transfer and correspondingly increases the energy absorption level.

The primary benefit is achieved in weight reduction with excellent structural performance. For example, the CN25-3 specimens showed a weight reduction of ~40% compared with the CN40 specimens, which did not affect the energy absorption values. However, with a suitable content of steel mesh in terms of flexural strength, energy absorption is delivered by using only three layers in 25-mm thick ferrocement panels. The number of mesh layers could not be increased beyond three layers in this tested thickness as mentioned before, because of the high density of steel reinforcement content.

Table 4.5 Strength summary for tested specimens

Panel designation ID	Specimen weight (kg)	First crack stress (MPa)	Deflection at first crack (mm)	Maximum strength (MPa)	Deflection at maximum stress (mm)	Ratio of maximum to first crack load	Toughness (J)
CN25-3	6.62	5.48	0.57	10.38	15.62	1.89	15.8
CN25-2	6.60	3.16	0.63	6.06	12.13	1.92	11.6
CN30-4	7.39	4.75	0.87	7.67	8.67	1.61	9.8
CN30-3	7.33	6.38	1.02	8.66	9.40	1.36	6.9
CN30-2	7.10	5.94	1.08	8.36	10.60	1.41	6.4
CN40-6	11.18	4.61	0.57	9.89	11.83	2.15	15.4
CN40-4	11.12	6.19	1.18	11.41	9.47	1.84	11.9
CN40-3	10.96	6.16	0.92	10.47	7.68	1.70	11.4
CN40-2	10.87	8.51	1.12	9.59	3.42	1.13	7.3

All tested specimens exhibited strain hardening behaviour, and continuous reinforcement content and specimen thickness had very little effect on this behaviour.

4.6 Composition contribution to structural performance

In hybrid fibre-reinforced cementitious materials, different fibre types are activated at different reaction stages. This means that each fibre type contributes differently to the structural performance of those materials. For example, when both short and long fibres are present, shorter fibres bridge microcracks particularly and macrocracks are bridged only by longer fibres. Hence, each fibre has its own, specific function in the bridging mechanism, and different types have their own effect on overall structural performance. However, HFF materials have an additional mechanism for resisting tension loads: wire mesh makes the consideration of the whole structure behaviour of the material more complex. This complexity makes it essential to determine the influence of each reinforcement type on structural performance, to enable better understanding of the individual reinforcement mechanisms. To obtain this type of information, an enormous effort is required to produce a large number of samples incorporating all parameters to determine the effect of each reinforcement type. A method that reduces testing effort is thus required.

The Taguchi method has been successfully used for test design and analysis of mechanical behaviour. Previous applications of this approach have been in studying the effect of mix proportion in cement-based materials (Özbay et al. 2009; Tanyildizi 2013; Xu et al. 2012; Chatterjee and Das 2013). In such cases, a statistical approach was required to identify the individual effects of reinforcement and their corresponding response. Here, the main aim was to determine which reinforcement component has the most significant influence on post-tensile strength, first crack strength and strain at both strengths. The experimental trials were designed to provide the best possible performance conditions for the parameters affecting mechanical properties, using the Taguchi and ANOVA Method.

4.6.1 Method and test design

The Taguchi method provides the best approach in a parametric study for the efficient determination of the most optimal design. Through use of this method, the robustness of the required results is guaranteed by selecting test conditions that capture the effect of various noise factors. Taguchi's model is based on 'noise factors' considered the source of variability in terms of performance, and the reason for material failure, for example. A noise factor is any measurable characteristic leading a material composition to deviate from its proposed target (Rao et al. 2013). To achieve the designated material specification robustness in relation to the noise factor, the selection of the main parameters influencing the material components is required. Orthogonal arrays (OA) are then used to provide an experimental design that investigates a large number of variables with a small number of tests. The OAs significantly reduced the number of trials required. The results obtained from small-scale experiments are transferable over the whole project (Ross 1996).

In this study, the parameters to be investigated are the effect of FA replacement ratio, water content, PVA fibre ratio (optimum fibre volume fraction of each type) and wire mesh content. The factors and their variation levels are shown in Table 4.6, and the L9 OA is chosen. The standard L9 OA is shown in Table 4.7. This means that only nine different mixtures are needed to perform this test; otherwise, 81 (3^4) mixes would be necessary to determine the effects by considering all four parameters.

Table 4.6 Factors and factor levels

	Factors			
Level	**FA/C**	**W/B**	**PVA1/PVA$_{tot}$**	**Wire (%)**
1	0.25	0.38	0.25	0.50
2	0.12	0.40	0.50	0.67
3	0.00	0.45	0.75	0.85

Table 4.7 Taguchi's L9 orthogonal array

Standard L9 orthogonal array				
Mix number	**FA/C**	**W/B**	**PVA1/PVA$_{tot}$**	**Wire (%)**
B1	0.25	0.38	0.25	0.50
B2	0.25	0.40	0.50	0.67
B3	0.25	0.45	0.75	0.85
B4	0.12	0.38	0.5	0.85
B5	0.12	0.40	0.75	0.50
B6	0.12	0.45	0.25	0.67
B7	0	0.38	0.75	0.67
B8	0	0.40	0.25	0.85
B9	0	0.45	0.50	0.50

A 400 kg/m^3 of cement or binder content (cement (OPC), and FA) to sand ratio of 1:1 was used for all mixtures. A constant total fibre volume fraction (V_f) of 1.5% as in the CN mix was used; PVA1 indicates the shorter fibre and PVA2, the longer fibre. The PVA1 fibre proportion of the total fibre quantity indicates the amount of shorter fibre, and the proportion of longer fibre can be determined from this. The mixture proportions for this test were derived by applying the parameters in Table 4.6 to the L9 OA in Table 4.7. The resulting tests and their proportions are outlined in Table 4.8. The total amount for each batch was 10 kg.

Table 4.8 Mix proportions for test HFF according to the Taguchi method

Mix number	**Specimen ID**	**OPC**	**FA**	**PVA1**	**PVA2**	**Wire**	**W**	**Total binder**
		(g)	**(g)**	**(g)**	**(g)**	**%**	**ml**	**(g)**
B1	**HFF1**	7,500	2,500	121.9	365.6	0.5	3800	10,000
B2	**HFF2**	7,500	2,500	243.8	243.8	0.67	4000	10,000
B3	**HFF3**	7,500	2,500	365.6	121.9	0.85	4500	10,000
B4	**HFF4**	8,800	1,200	243.8	243.8	0.85	3800	10,000
B5	**HFF5**	8,800	1,200	365.6	121.9	0.5	4000	10,000
B6	**HFF6**	8,800	1,200	121.9	365.6	0.67	4500	10,000
B7	**HFF7**	10,000	0	365.6	121.9	0.67	3800	10,000
B8	**HFF8**	10,000	0	121.9	365.6	0.85	4000	10,000
B9	**HFF9**	10,000	0	243.8	243.8	0.5	4500	10,000

ANOVA analyses were also undertaken, using a loss function to explain the variance among the obtained test results and the desired results. Once a performance statistics signal to noise ratio (*S/N*) was determined, the contributions of the studied parameters were determined in the final stage of the Taguchi method. Each parameter's effect on performance is assessed by the division of the primary target values into three categories:

- Smaller is better: this category must be chosen when the goal is minimising the response, for instance, when material weight reduction is required. The relevant *S/N* ratio can be calculated as follows:

$$S/_N = -10 \times log_{10}\left(\frac{1}{n}\sum_{i=1}^{n} Y_i^2\right) \quad (4.2)$$

- Larger is better: this category is considered when the goal is maximising the response, for example, if optimal strength capacity of materials is required. The *S/N* ratio is calculated as:

$$S/_N = -10 \times log_{10}\left(\frac{1}{n}\sum_{i=1}^{n} \frac{1}{Y_i^2}\right) \quad (4.3)$$

- Nominal is better: this category should be chosen when the goal is to target the response. The *S/N* ratio is calculated according to:

$$S/_N = -10 \times log_{10}\left(\frac{1}{n}\sum_{i=1}^{n} (Y_i - Y_0)^2\right) \quad (4.4)$$

where in all equations Y_i are the experimental results, and Y_0 is the target sample showing the measured value of each response when the variable occurs.

As the required characteristics of HFF, such as tensile strength and compressive strength, are not negative values, the 'larger is better' (LB) relationship describes the quality characteristic. The expectation is that LB characteristics will provide better compressive strength performance in terms of adjusted mix proportions, such as FA content and water ratio. The same relationship provides the best results in terms of the volume fraction of each fibre and wire mesh content, which are more likely to be associated with the tensile strength of HFF as a response variable. Therefore, the LB loss function for tensile and compressive strength was chosen to identify the optimal conditions, and Equation 4.3 will apply in this case.

4.6.2 Response values

In this investigation, the strength capacities of HFF composites with various mixtures (Table 4.8) were considered response values for the statistical approach used. A test series for tensile, flexure, and compressive strength was conducted. For the tensile and flexure test, the required average and maximum stress and strain at the first crack are summarised in Table 4.9. The data used in the Taguchi and ANOVA analyses as a response to the factors defined provided all tensile test results from the 27 tested specimens (three of each mixture), as seen in Figure 4.16.

To identify the short and long fibre mobilisation stages, the first crack results were used because they represent a transfer point from microcracks to macrocracks. The results from ultimate strength are characterised as the point at which the macrocracks become more extended and strain softening behaviour occurs.

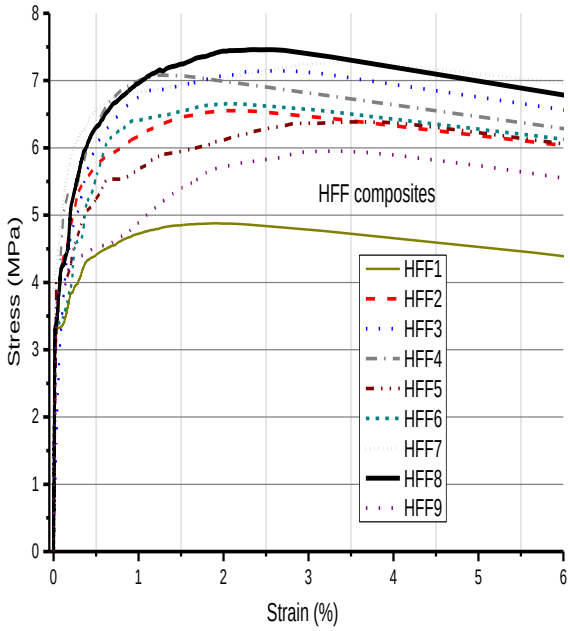

Figure 4.16 Tensile stress–strain curves for all tested samples

First crack strength was defined as the tensile stress that acted on the crack as the crack spread throughout a cross-section (Naaman, Moavenzadeh and McGarry 1974). In this investigation, the position of the first crack point was chosen for the transition from the elastic stage to the inelastic stage. Figure 4.17 shows the transition point suggested as the first crack.

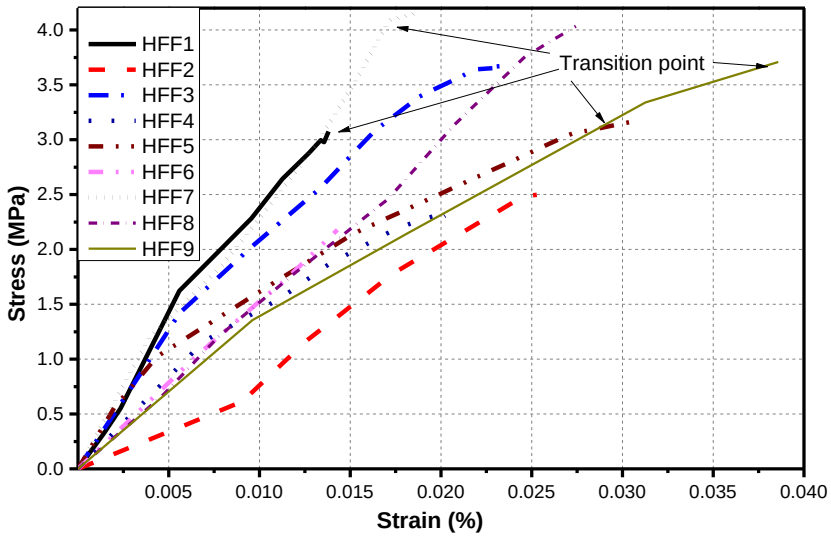

Figure 4.17 Stress–strain at first crack

The samples tested under bending also showed strain hardening behaviour. Multiple cracks were observed in all samples. The equivalent flexure strength *vs*. deflection of all tested samples is shown in Figure 4.18. The average strengths are summarised in Table 4.9.

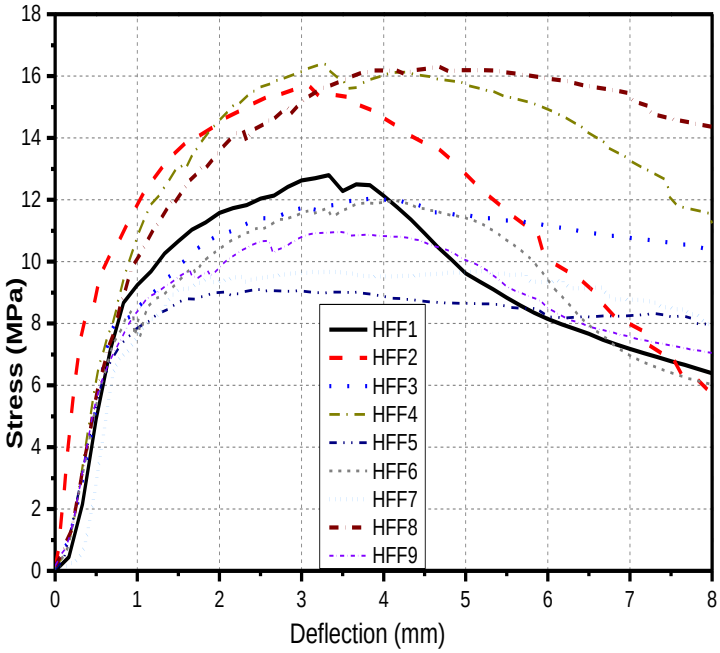

Figure 4.18 Flexure–deflection behaviour of the HFF panels

Table 4.9 Average stress and strain for the tensile and flexural tests

ID	At first crack				At maximum crack			
	Tensile		Flexure		Tensile		Flexure	
	Strain %	Stress MPa	Deflection mm	Stress MPa	Strain %	Stress MPa	Deflection mm	Stress MPa
HFF1	0.054	2.63	0.67	7.83	1.93	4.83	3.71	12.23
HFF2	0.024	3.34	0.53	7.94	2.33	6.65	3.07	14.61
HFF3	0.029	2.87	0.89	7.03	3.27	6.49	5.27	11.63
HFF4	0.039	3.97	0.78	8.01	1.48	7.34	3.26	15.69
HFF5	0.04	3.87	0.91	8.10	2.71	6.54	2.73	9.95
HFF6	0.027	3.37	1.03	7.32	1.76	6.59	3.82	13.57
HFF7	0.025	4.47	0.75	7.48	2.08	7.07	3.15	10.23
HFF8	0.02	4.31	1.14	10.26	2.77	7.06	4.13	15.36
HFF9	0.032	3.84	1.10	8.40	1.98	5.81	2.89	11.04

The average compression strength at a cure of 28 days is shown in Figure 4.19. The results were obtained by testing five cubes of each mixture. HFF composites with no FA (HFF7–9) showed better compression strength than samples with FA. In general, the decline in compression strength was clearly related to increasing FA content.

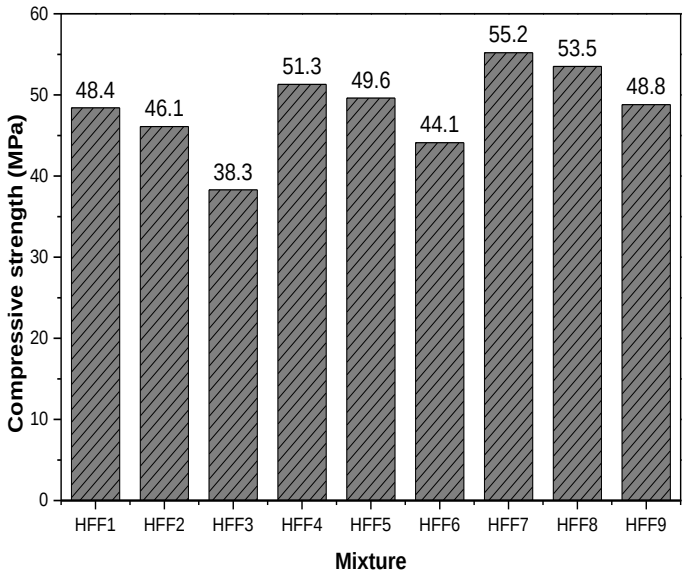

Figure 4.19 Average compressive strength of all tested mixtures

4.6.3 Test parameter contributions to tensile behaviour of HFF

Use of the Taguchi and ANOVA approaches identified the effects of fibre and wire mesh on first crack stress. At this crack stage, the crack bridging effect of shorter fibres dominates in terms of efficiency. Shorter fibres are more efficient at bridging microcracks and initial cracks until crack openings increase to the point where their propagation exceeds the fibre length; in this phase, the fibre is being pulled out or the the material is rupturing, which means that shorter fibre should be more efficient at bridging initial cracks, which are relatively small. One possible way to confirm this suggestion is to apply the Taguchi and ANOVA methods in an observation of fibres under first crack stress and strain at the first crack. After analysing the data, the *S/N* was calculated, as seen in Figure 4.20(a). It became obvious that 0.75% fibre resulted in a component that produced the highest stress at first crack. At this percentage, the shorter fibre dominates fibre content. Other components such as FA, water –binder ratio (w/b) and steel wire mesh content also contribute to the stress at first crack.

The *S/N* of the ultimate tensile strength was calculated for each level of the experimental parameters. This allowed a detailed analysis of which component contributed most to the results. From the results shown in Figure 4.20(b), it is apparent that (1) the highest tensile strength was achieved by 0.12% FA, 0.4 w/b, 0.75% PVA1/PVA_{tot} and 0.85% wire mesh volume fraction; (2) Noticeably, the shorter fibre appeared to more efficiently contribute to the tensile strength than did the longer fibre, and equal content of both fibre types gave superior results compared with dominant proportions of the longer fibre; and (3) wire mesh appeared to control the ultimate tensile strength performance in this composite.

The results of the ANOVA analysis are presented in Table 4.10. The FA had a less adhesive effect on the matrix component, so its content was an important factor affecting the stress at first crack. This means that mixtures without FA exhibit the greatest first crack strength. Figure 4.10 shows the detailed contribution of all factors to the first crack strength. The results for maximum strength obtained from the variance calculation using the ANOVA approach are presented in Figure 4.21 and Table 4.11. There is no doubt that wire mesh content, which had a 57.4% contribution, was the most significant factor in tensile strength. FA was an unexpected second factor, with a 24.8% contribution. PVA fibre ranked only third in

overall tensile strength performance. This could be due to the adherence of FA particles in the surrounding matrix, and the 0.12% by weight cement replacement appeared to be the value that provided the highest results for strength.

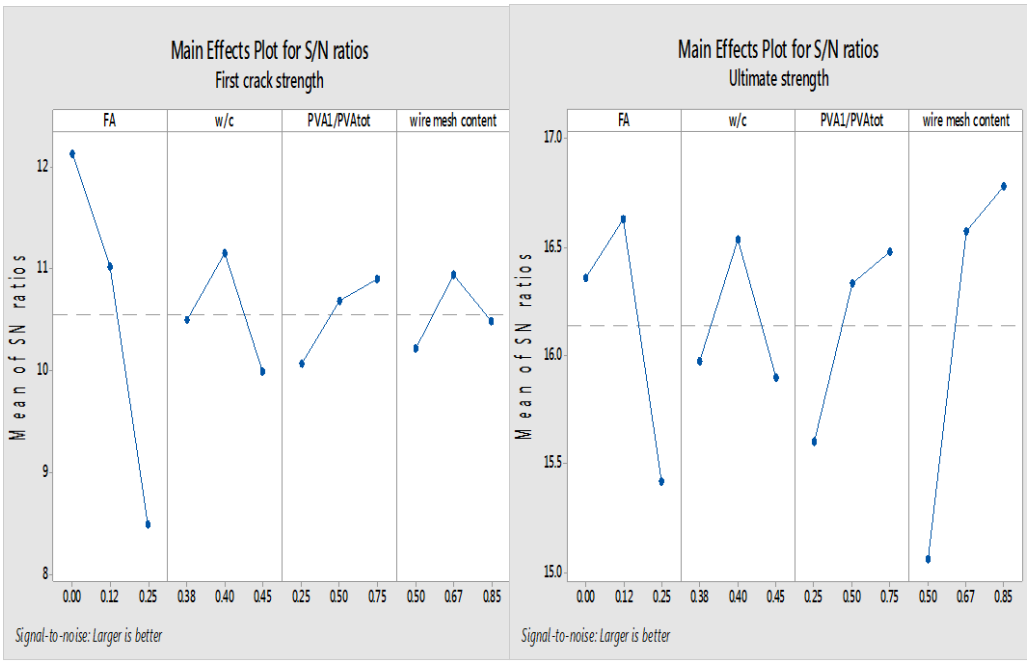

(a) (b)

Figure 4.20 Main *S/N* plot showing the effect of the tested factors on tensile capacity: (a) at first crack; (b) at ultimate crack

Table 4.10 Results of ANOVA for first crack strength

Control factor	Degrees of freedom (f)	Sum of squares (SS_A)	Variance (V_A)	Contribution (%)
FA	2	2.45	1.23	78.2
w/b	2	0.36	0.18	11.5
PVA_1/PVA_{tot}	2	0.17	0.08	5.4
Wire mesh	2	0.15	0.08	4.9
Error		-	-	-
Total	8	3	-	100

Table 4.11 Results of ANOVA for ultimate tensile strength

Control factor	Degrees of freedom (f)	Sum of squares (SS_A)	Variance (V_A)	Contribution (%)
FA	2	1.15	0.58	24.8
w/b	2	0.33	0.17	7.2
PVA_1/PVA_{tot}	2	0.49	0.25	10.6
Wire mesh	2	2.66	1.33	57.4
Error	-	-	-	-
Total	8	5		100

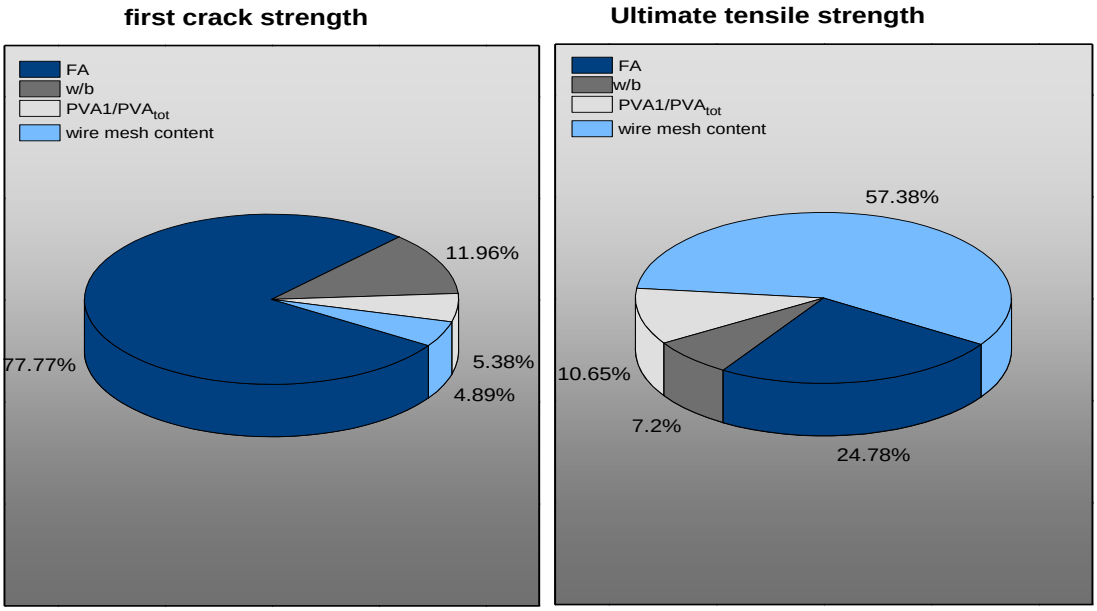

Figure 4.21 The effect of experimental parameters on strength

The strain at first crack was more affected by the shorter fibre than the longer fibre, as can be seen in Figure 4.22(a). In contrast, the results obtained in relation to the contribution of factors to strain at maximum strength—in this case, the wire mesh—contributed more to the value of strain at first crack. Despite the relatively small contribution of the PVA ratio on performance, the effect of the fibre itself was still significant for the overall structural performance during the first crack phase. The concern in this examination was only the ratio of short to long fibre content, not the fibre's contribution to strength.

The parameters' effects on the strain at maximum tensile stress can be observed in Figure 4.22(b). The average strain obtained from the tested data is

presented in Table 4.9. In contrast, the maximum strength shows that the PVA fibre contributed significantly to the strain at maximum stress. The best ductility in the inelastic stage was achieved when the quantity of the longer PVA fibre was higher than the shorter. The more remarkable results related to an FA content of 0.12, which appeared optimum for this stage. The other obvious components were a w/b of 0.4 and a wire reinforcement content of 0.85%. All these factors contributed individually to the strain at maximum stress, highlighting that the composition of HFF composites determines their quantitative properties. In other words, the optimal material proportions of HFF are dependent on its ultimate application. If an application required resistance against high-tension loads, for instance, the material design would be different than if it required more flexibility and the ability to absorb energy.

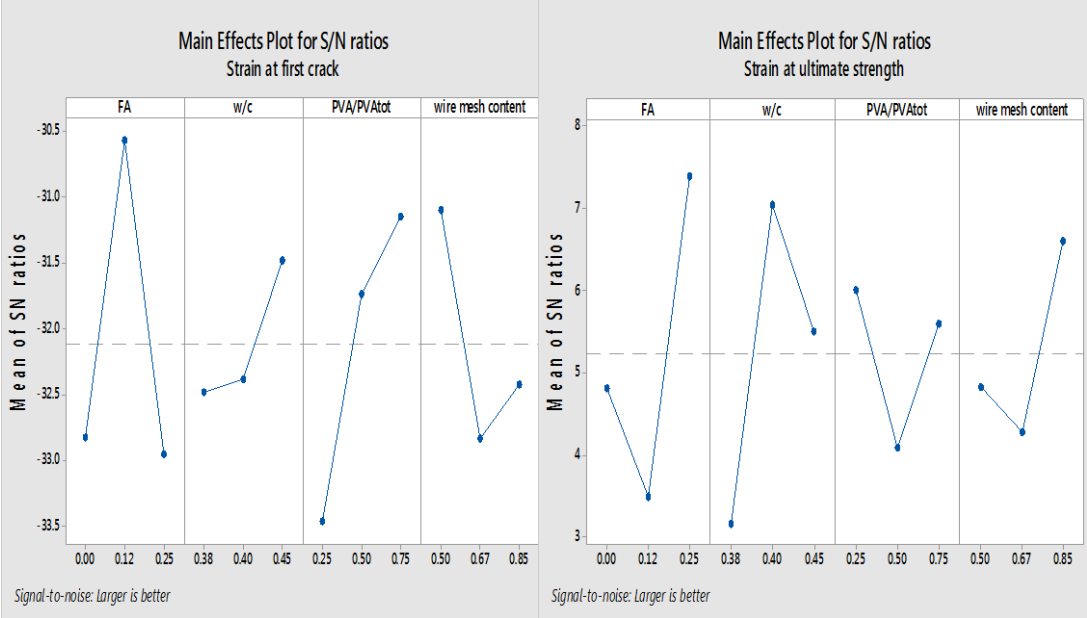

(a) **(b)**

Figure 4.22 Main effect plot of the strain: (a) strain at crack; (b) strain at ultimate strength

ANOVA using the variance calculation was used to determine the total component contributions. The overall influence of the factors on strain is illustrated in Tables 4.12 and 4.13. After examination of the results in Figure 4.23, it was clear that wire mesh had an insignificant effect on the strain at maximum tensile stress

when compared to all other factors. On the other hand, the effect of wire mesh was significant at the first crack, which indicates that the wire mesh is mobilised earlier in resisting tensile strain than previously thought. Shorter fibres, however, contributed more in the first crack phase and longer fibres, in the maximum crack phase.

Table 4.12 Results of ANOVA for strain at first crack

Control factor	Degrees of freedom (f)	Sum of squares (SS_A)	Variance (V_A)	Contribution (%)
FA	2	0.00020	0.00010	21.9
w/b	2	0.00024	0.00012	26.1
PVA_1/PVA_{tot}	2	0.00001	0.00001	1.3
Wire mesh	2	0.00046	0.00023	50.7
Error	-	-	-	-
Total	8	0.00090	-	100

Table 4.13 Results of ANOVA for strain at maximum tensile stress

Control factor	Degrees of freedom (f)	Sum of squares (SS_A)	Variance (V_A)	Contribution (%)
FA	2	0.42	0.21	16.22
w/b	2	0.93	0.47	36.34
PVA_1/PVA_{tot}	2	0.91	0.45	35.33
Wire mesh	2	0.31	0.16	12.12
Error	0	0	-	-
Total	8	2.57	-	100

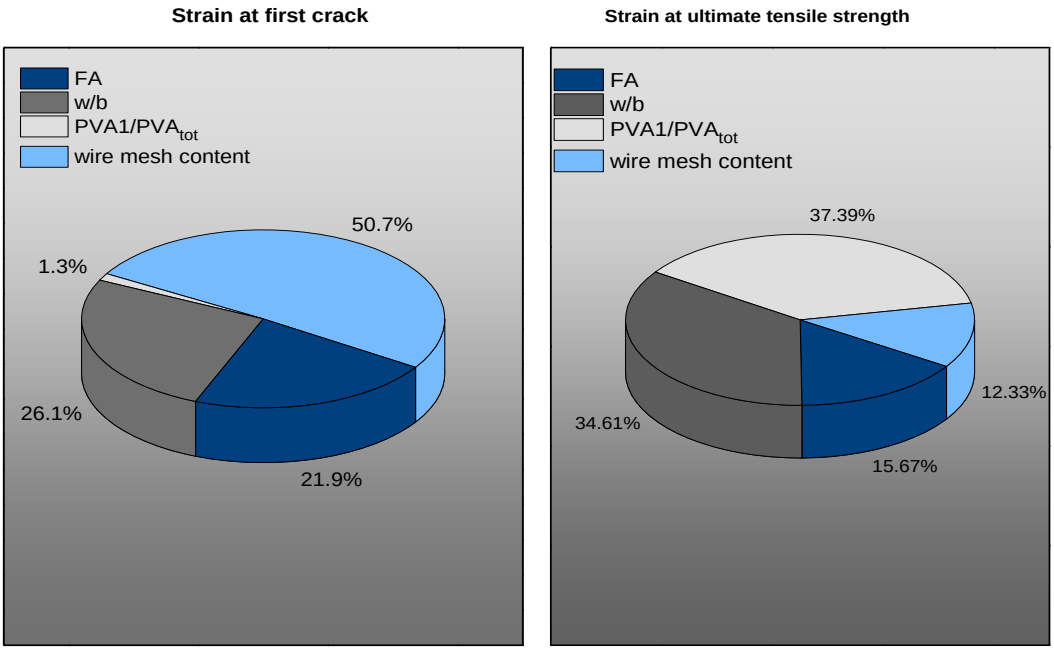

Figure 4.23 The effect of experimental parameters on the strain

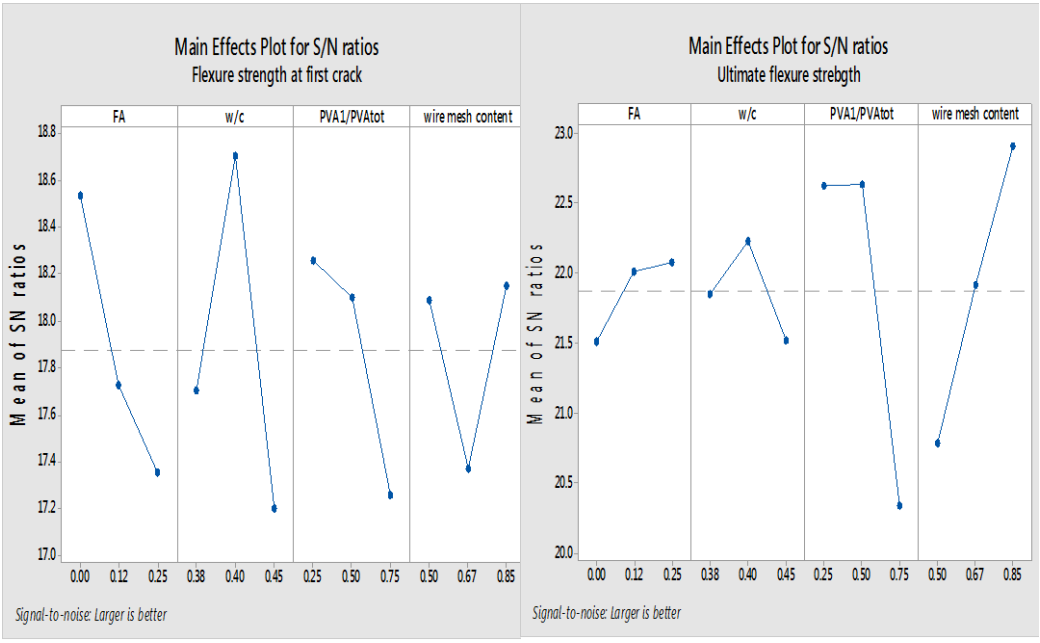

(a) (b)

Figure 4.24 Main effects *S/N* plot showing the effect of tested factors on flexure capacity: (a) flexure strength at first crack; (b) ultimate flexure strength

Table 4.14 Results of ANOVA for flexure strength at first crack

Control factor	Degrees of freedom (f)	Sum of squares (SS_A)	Variance (V_A)	Contribution (%)
FA	2	2.10	1.05	30.1
w/b	2	2.43	1.21	34.8
PVA_1/PVA_{tot}	2	1.33	0.67	19.1
Wire mesh	2	1.11	0.56	15.9
Error		-	-	-
Total	8	7	-	100

Table 4.15 Results of ANOVA for flexure strength at maximum

Control factor	Degrees of freedom (f)	Sum of squares (SS_A)	Variance (V_A)	Contribution (%)
FA	2	1.18	0.59	3.1
w/b	2	2.27	1.13	5.9
PVA_1/PVA_{tot}	2	19.86	9.93	51.9
Wire mesh	2	14.92	7.46	39.0
Error	-	-	-	-
Total	8	38	-	100

The influence of the test PVA fibre on deflection was slightly different than on flexure strength. The longer fibre (PVA2) dominated the effect of fibre on deflection at the first crack. The main effect for *S/N* of the deflection is as seen in Figure 4.25. The shorter fibre (PVA1) also contributed by providing relatively high deflection capacities at first crack. PVA2, however, actively contributed by providing large deflections at maximum stress. Higher wire mesh content provided the best deflection results at both stages. The effect of the compounds on deflection is shown in Tables 4.16 and 4.17.

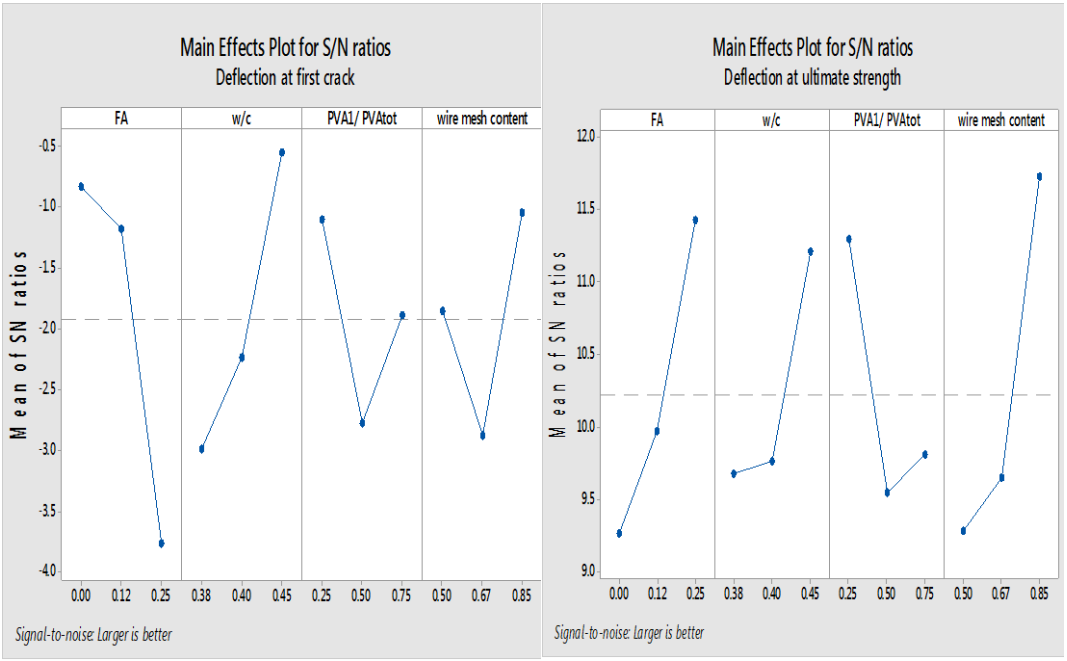

Figure 4.25 Main effects *S/N* plot showing the effect of tested factors on deflection capacity

Table 4.16 Results of ANOVA for deflection at first crack

Control factor	Degrees of freedom (f)	Sum of squares (SS_A)	Variance (V_A)	Contribution (%)
FA	2	0.140	0.070	42.5
w/b	2	0.114	0.057	34.7
PVA_1/PVA_{tot}	2	0.031	0.015	9.3
Wire mesh	2	0.045	0.022	13.5
Error	-	-	-	-
Total	8	0.3298	-	100

Table 4.17 Results of ANOVA for deflection at maximum flexure strength

Control factor	Degrees of freedom (f)	Sum of squares (SS_A)	Variance (V_A)	Contribution (%)
FA	2	0.96	0.48	19.3
w/b	2	0.87	0.43	17.4
PVA_1/PVA_{tot}	2	1.10	0.55	22.1
Wire mesh (V_r)	2	2.05	1.02	41.1
Error	0	0	-	-
Total	8	4.98	-	100

4.6.4 Test parameter contributions to the compressive strength of the HFF composite

The contributions of w/c, FA content and fibre ratio to compressive strength were analysed. Through the Taguchi and ANOVA, the effect of the individual material components was examined. The best mixture composition of the HFF materials in terms of compressive strength was: no addition of FA, w/b of 0.38 and equal short and long PVA fibre content, at 1.5% of total volume. However, the fibre appeared to have an insignificant effect on compressive strength (see Figure 4.26). The ANOVA results (Table 4.18) show that w/b is the primary factor affecting compression strength, with a 45.9% contribution. FA is the second most significant factor, and fibre content was not significant, as seen in Figure 4.27.

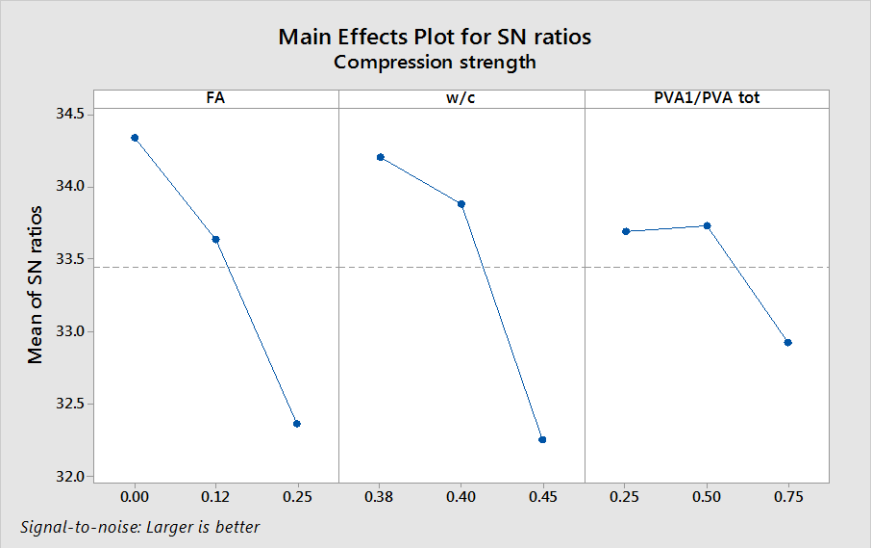

Figure 4.26 Effect of factors on compressive strength at 28 days

Table 4.18. Results of ANOVA for compressive strength

Control factor	Degrees of freedom (f)	Sum of squares (SS_A)	Variance (V_A)	Contribution (%)
FA	2	158.0	79	44.03
w/b	2	165.0	82	45.90
PVA1 /PVA_{tot}	2	18.0	9	4.93
Error	2	18.5	9	5.14
Total	8	359	-	100

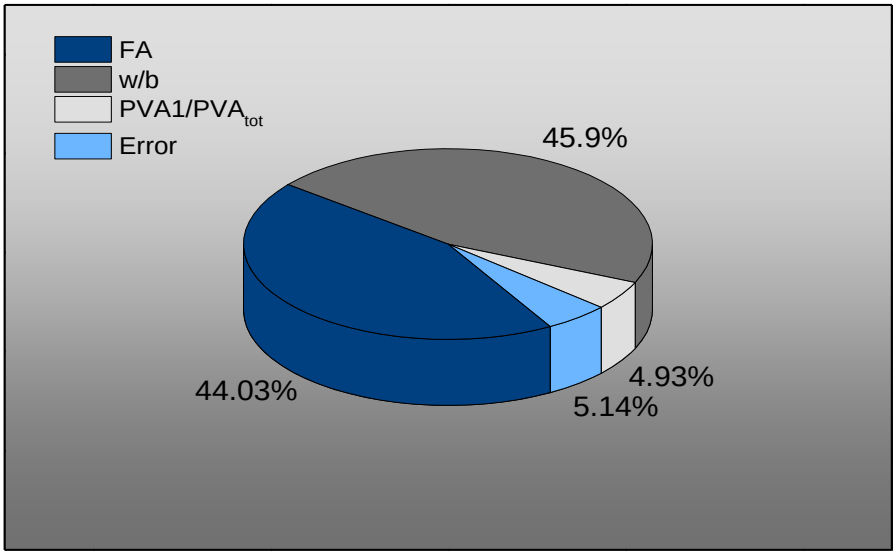

Figure 4.27 Material component contributions to the compressive strength of HFF

The results show that the individual material proportions affect the overall performance of the HFF composite. Table 4.19 summarises the material proportions leading to the best structural performance.

Table 4.19 Mix proportions of HFF composite leading to the best results

	Behaviour	OPC	FA	PVA1	PVA2	W	Wire mesh	Total binder
		(g)	(g)	(g)	(g)	ml	%	(g)
First crack	Tensile strength	10,000	0	365.6	121.9	4,000	0.67	10,000
	Flexure strength	10,000	0	121.9	365.6	4,000	0.85	10,000
	Strain	8,800	1,200	365.6	121.9	4,500	0.50	10,000
	Deflection	10,000	0	121.9	365.6	4,500	0.85	10,000
Ultimate strength	Tensile strength	8,800	1,200	365.6	121.9	4,000	0.85	10,000
	Flexure strength	7,500	2,500	243.8	243.8	4,000	0.85	10,000
	Strain	7,500	2,500	121.9	365.6	4,000	0.85	10,000
	Deflection	7,500	2,500	121.9	365.6	4,500	0.85	10,000
	Compressive strength	10,000	0	243.8	243.8	3,800	-	10,000

Note that the calculations of Taguchi and ANOVA are in Appendix A presented.

4.7 Concluding remarks

The addition of hybrid fibre to ferrocement panels is extremely desirable to improve their flexural behaviour and energy absorption capabilities. The enhancement of flexural strength through the addition of fibre to the mixture contributes to an increase in strain hardening and maximum post-crack stresses. The most suitable composition in terms of flexural performance and workability is 1.5% hybrid PVA fibre, four layers of wire mesh and mixture proportion as in CN with a 40-mm-thick panel. The Taguchi and ANOVA analyses showed that the proportion of the material components is important and depends on the ultimate application and structural function. Therefore, the material amounts can be designed regarding the load that will face the composite in its application. Further, the study has shown that shorter fibres are activated at propagation at the crack scale, whereas longer fibres are slightly more active at the inelastic strain stage of the deformed composite. Wire mesh also has a significant effect on maximum tensile strength and strain at first crack, which contributes to the overall performance of HFF composites.

Chapter 5: HFF Structural Behaviour and Mechanical Properties

5.1 Introduction

The most suitable material composition with respect to HFF structural behaviour and corresponding materials such as ECC, ferrocement and mono fibre-reinforced ferrocement was discussed in Chapter 4. The present chapter is mainly concerned with the translation to the structural level of HFF, of strain hardening properties at the materials level. It is evident that an improvement in flexural strength through the fibre matrix leads to growth in terms of maximum post-crack stresses and strain hardening behaviour. It is important in strain hardening materials that the load, or the stress–deflection behaviour, after reaching the first stress peak, the stresses continue to increase until maximum strength is reached (Naaman 2007). This behaviour of the composite is due to the process of adding discontinuous reinforcement and the effect of fibre hybridisation (Ahmed 2003). Insensitivity to these parameters, while retaining strain hardening behaviours, indicates better prospects for the use of such hybrid ferrocement composites.

The stress *vs.* strain and the equivalent flexural stress *vs*. deflection curves exhibit strain hardening behaviour, which primarily depends on the bridging mechanism and the bond of the hybrid fibre, in addition to the wire mesh effect on resisting the tension loads. To precisely classify the HFF into a material category due to its structural and mechanical properties, a wide range of experimental investigations are required.

In the research described in this chapter, experiments to study tensile, flexure and microstructure behaviour of HFF specimens were carried out. To provide a material definition based on structural behaviour, a classification method to confirm strain hardening (and therefore designation as an HPFRCC material) was used. Further investigations were conducted to determine the elastic modulus and

Poisson's ratio. The values obtained were then compared and the materials further evaluated in a microstructural study.

5.2 Experimental determination of the maximum strength capacity of HFF composites

5.2.1 Tensile strength capacity and behaviour of HFF composites

One of the most distinctive features of HFFs is that their tensile behaviour can be represented by stress–strain relations, which is important for predicting structural response and determining post-peak capacities. The typical tensile strength behaviour of HFF and control samples is shown in Figure 5.1. The HFF mixture was made using B2 mix proportions as in Table 4.8. The control sample (WM) representing ferrocement is from the same mixture as HFF, but with only wire mesh and no fibre. In contrast, FM has fibre but no wire mesh reinforcement. The HFF exhibits both higher tensile strength and improved ductility compared with the control specimens (WM), whereas the FM samples show similar behaviour to HFF composites, but with lower stress values. After initial loading, the ferrocement showed an elastic trend until first cracking, followed by a sudden decline in the curve and then a slight increase in tensile strength, which is remarkable for this stage. After a certain amount of strength increase (although still lower than the first crack value), the behaviour exhibited a smooth strain softening.

In HFF panels, the first part of the stress–strain curve illustrated a linear slope up to the first crack, after which small fluctuations were observed in strength, possibly as a result of load transition from the pulled out or ruptured shorter fibre to the longer fibre. Further increases were observed in tensile strength with a simultaneous rise in strain. As the load increased, the tensile strength also grew and formed greater strength values compared to first cracking, representing strain hardening behaviour. At this point, additional load increase activated the wire mesh, which resisted the tension loads developed in the specimens. This part of strain hardening behaviour, as described in Chapter 4, is dependent on the fibre type and volume fraction, and wire mesh content and type. After maximum tensile strength was reached, a decrease in strength was observed as a steady flattening of the stress–strain curve until failure. The softening stage is not a true strain but reflects the

increasing crack opening of the tested specimen. A similar curve for mono fibre ferrocement in tension was reported by Desayi and EI-Kholy (1991).

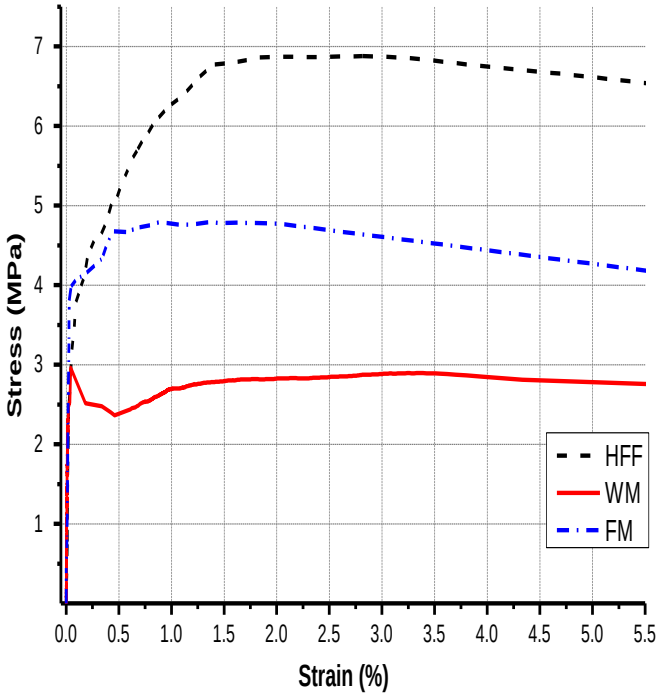

Figure 5.1 Stress–strain curve of HFF and control samples in the direct tensile test

Observations suggest that during the strain hardening stage (in real time) a large number of small multiple cracks develop across the dogbone. At peak stress, this results in a transition to the localised crack extension stage followed by loss of the fibre bridging effect, until wire mesh rupture and rapid failure. The relatively large number of small cracks is radically reduced to a small number through self-healing, such that only cracks with extended openings remain visible. The crack behaviour of tested samples is shown in Figure 5.2, and Appendix B.

The effects of parameters such as hybrid fibre volume fraction and wire mesh content were evaluated in term of their quantitative proportions in Chapter 4. The stress–strain curves for the remaining mixtures from Table 4.8 are shown here in Figure 5.3, revealing stress–strain behaviour similar to the samples in Figure 5.1, where an increase of the inelastic phase after the transition from the elastic trend was observed for all tested samples. The parameters introduced in the previous chapter in general affected the first crack strength, post-crack strength and ductility.

Figure 5.2 Crack pattern of HFF after failure in tensile test

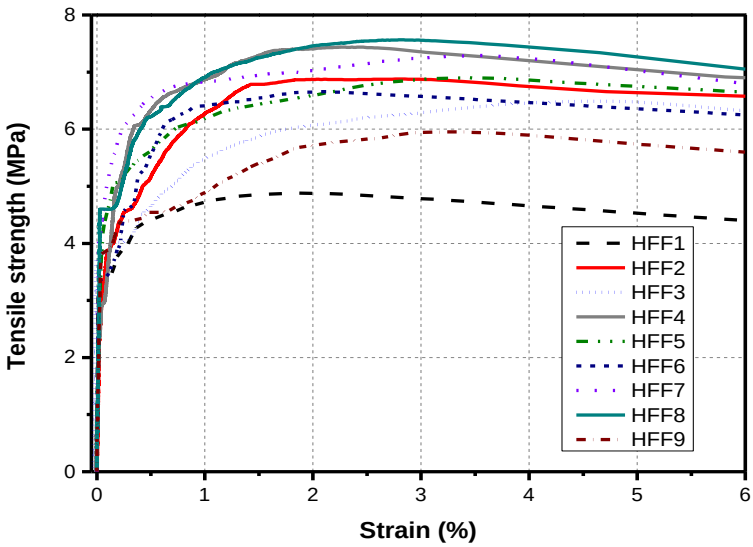

Figure 5.3 Stress–strain curves for HFF specimens with different parameters

In this study, an average maximum tensile strength value (σ_{cu}) of 6.49 MPa was measured using the results from all tested specimen. However, theoretically the tensile strength of fibre-reinforced cement-based materials is explicitly dependent on the fibre inclination angle in the matrix. Studies have discussed the effect of the inclination angle of the fibres on the tensile strength, which can be expressed through the orientation factor. The average tensile stress carried by fibres can be expressed in terms of the average tensile stress of fibres at first crack ($\sigma_{f,cr,avg}$), the fibre orientation factor (α_f) and the fibre content (V_f) (Lee, Cho and Vecchio 2011a). This relationship will clearly be more complex with synthetic hybrid fibres, and existing orientation factors relate only to steel fibre. Moreover, the ratio of fibre length to specimen size affects the orientation factor.

5.2.2 Indirect tensile test

The indirect tensile test was conducted only on small-scale specimens. A summary of the results from 36 tested specimens is provided in Figure 5.4. These results reveal the indirect tensile stress of the hybrid mixture matrix without wire mesh reinforcement for all specimens mixed according to Table 4.2. The calculated tensile stress increased with fibre volume fraction, which may be due to the additional tensile strength of the matrix afforded by the hybrid PVA fibre. Notably, the indirect tensile strength achieved by C1 (HFF) differed by only 10% from the results obtained in the direct tensile test. Excellent performance in flexure tests were achieved by C1 and C4 compared to all other mixes. There was a drop in tensile strength by specimens with 1.0% V_f, which was on average 4.9% less than that of specimens with 1.5% V_f.. However, the results from the split test for fibre-reinforced HFF were only used for comparison with the uniaxial tensile test results. The values from the indirect tensile tests differed slightly from those in the direct tensile test, likely due to the different mixture proportions and the test method.

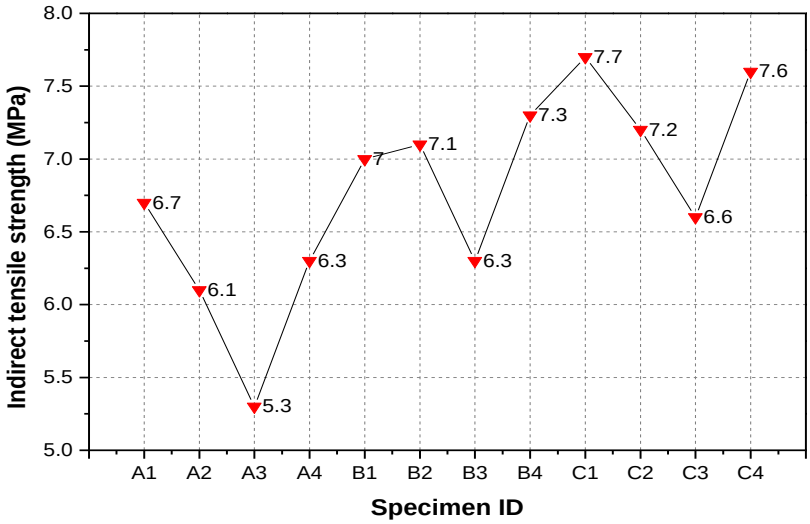

Figure 5.4 Indirect tensile strength in split tests

5.2.3 Flexural strength capacity

Two different mixtures of HFF were used in this investigation. The compressive strengths of HFF2 (containing FA and SF; see Table 4.8) and HFF2* (100% cement without FA or SF) were 66 and 53 MPa respectively. The equivalent flexure strength *vs*. deflection is shown in Figure 5.5. HFF2 samples exhibited the same strength capacity as samples without FA and SF (HFF2*). The relatively high flexural strength capacity of the HFF may be related to the additional tensile strength of wire mesh; the additional tensile capacity of the PVA fibres contributes to the overall strength performance. Moreover, crack formation is retarded by the fibre bridging effect associated with shorter fibres resisting small crack formation and longer PVA fibres bridging large cracks. This occurs where the panel is hindered by being split, which results in high deflection and increased stress capacity (Trueb 2011).

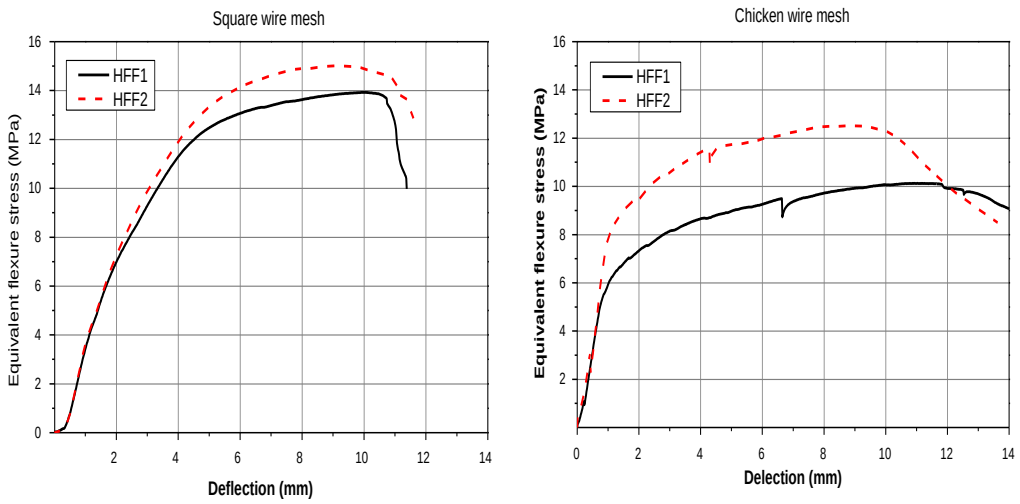

Figure 5.5 Equivalent stress–deflection of HFF panels using 1.5% fibre volume fraction with different mixture materials and wire mesh type

5.2.4 Shear behaviour of HFF panels

The focus of the research is explicitly on structural performance in response to intense shear loading. A motivation for testing HFF panels under shear load is to investigate the effect of hybrid fibres on the failure mode.

A total of 15 HFF panels were tested in bending for shear in an Instron test machine with a 500-kN-capacity loading frame. The tests were conductedat a load rate of 0.381 mm/min. The panels were fixed between U-shaped frames on either end as shown in Figure 5.6. A Teflon® plate was used between the panel and the fixing point to ensure free movement in the load direction of the panel.

The variables tested in this investigation were panel thickness, reinforcement type and applied load. The plates were designed using the mixture proportions as in Chapter 4 (mixture C1) with 1.5% hybrid fibre and four layers of wire mesh. Three panels were reinforced with a single steel tie (ϕ 8 mm) on the bottom side. The test variables were (1) panel thickness, (2) load type, using a uniform distributed line load applied through a steel disk with a diameter D = 125 mm, and (3) reinforcement, by supporting the panels with an additional bottom reinforcement rebar used as a tie (see Table 5.1).

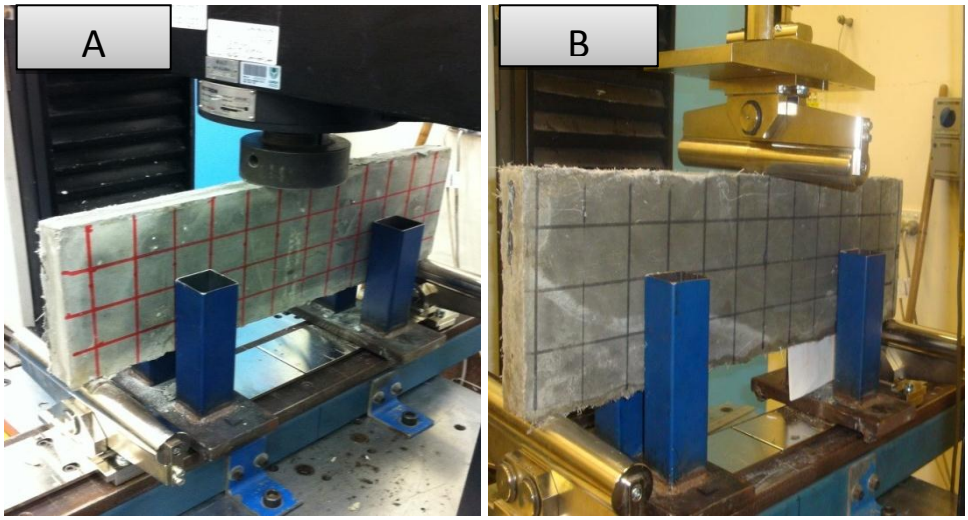

Figure 5.6 Shear test setup and load types

Table 5.1 Specimen ID and variables

Specimen ID	Size (mm)	Reinforcement	Load type
S-40	600×200×40	Wire mesh	A
S-30	600×200×30	Wire mesh	A
S-25	600×200×30	Wire mesh	A
SR-40	600×200×40	Wire mesh and tie	A
SL-40	600×200×40	wire mesh	B

The responses of the tested plates with different thicknesses are illustrated by the load–deflection curves in Figure 5.7. The ductility behaviour of all tested panels was similar. As expected, under the same load conditions, load-carrying capacity increased with increasing panel thickness.

The use of hybrid PVA fibre to reinforce the mortar is likely to increased resistance to tensile load in the tension zone at the plate bottom. Additionally, using hexagonal wire mesh instead of steel reinforcement in tension creates a straightening effect due to resistance of the mortar matrix. This led to a further tension-stiffening effect. This interaction increases the ductility compared to conventional ferrocement, which has been studied extensively by Ibrahim (2011a). Embedding a steel tie in the bottom of a panel significantly increased its load and deflection capacity (see Figure 5.8). The use of a steel tie significantly increases the tension strength resistance and forces the load transfer in a diagonal direction, forming compression studs as

described in ACI (2011) and as seen in Figure 5.9. According to this principle, the nodes (load point and supports) are classified as C–C–C, where all nodes resist compression, and C–C–T, where two nodes resist compression and one, tensile force. Note that the load values for HFF plates with ties are higher than those for regular wire mesh-reinforced HFF panels. An apparent shear failure was observed in these samples.

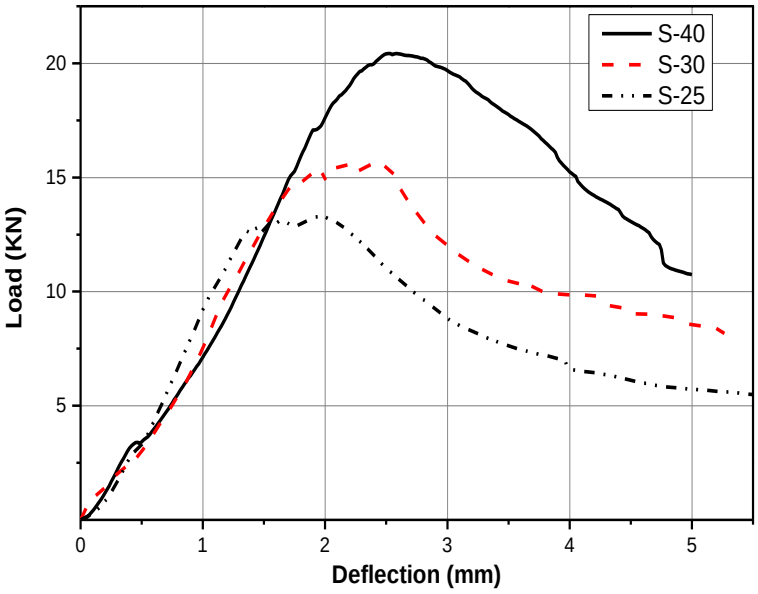

Figure 5.7 Flexure response of HFF panels with different thicknesses

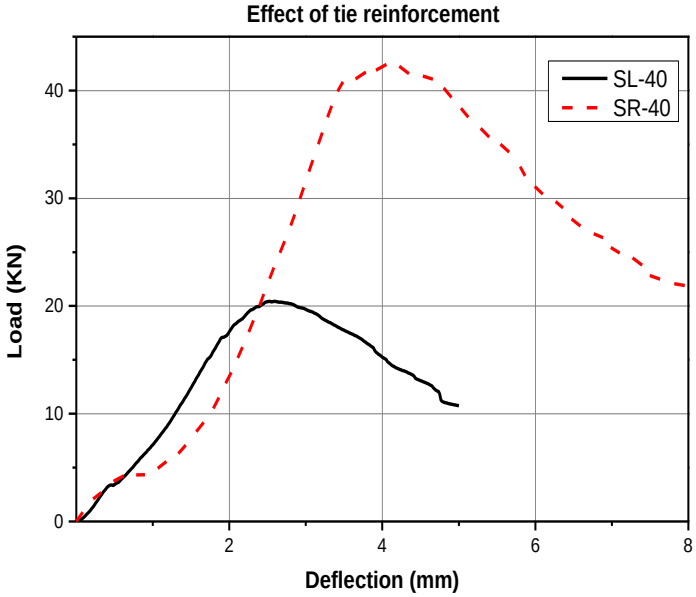

Figure 5.8 Comparing the shear response of specimens with and without tie reinforcement

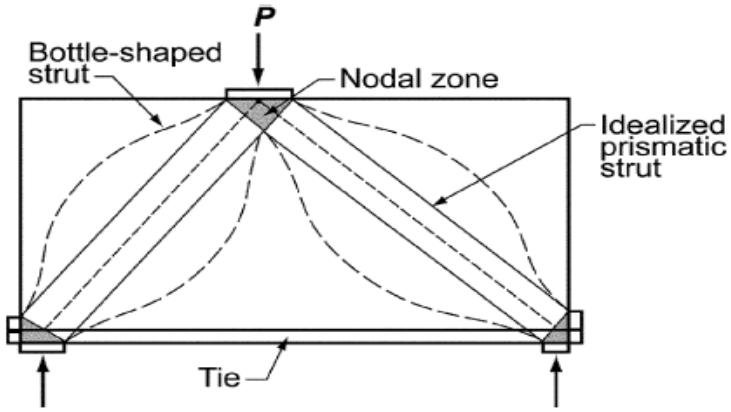

Figure 5.9 Load transfer struts (adopted from ACI 2011)

The mechanism of load transfer was through the presser struts built into the area between the load point and the supports, as seen in Figure 5.9. The consequence of this is shear in the form of splitting tensile cracks. In this failure type, the tensile stress normal to the crack is significantly higher than the ultimate tensile strength of the mortar matrix with hybrid fibre. This has a significant effect in the form of a diagonal crack. Note that this crack was only detected when the steel disk was used for uniform load distribution; flexure crack failure was observed for plates that were single point loaded. This couldbe associated with large deflections due to the large clear span of the panels. Another possible reason is the effect of using hybrid fibre, which may increase the resistance of diagonal transfer loads by applying a concentrated point load. Initiation of cracks was seen as the specimens were being loaded. The final crack patterns of the panels are shown in Figure 5.10.

Further comprehensive observations were made by testing HFF panels under an applied load using the steel disk and a concentrated load point, which revealed that the applied load type affects the strength capacity as well as the failure mode. Note that the point load results were at the lower end of the load and deflection capacities, than were values for panels tested using the loaded disk. This might be due to the larger area of the nodal zone using the 125-mm load disk. The load–deflection curves are shown in Figure 5.11.

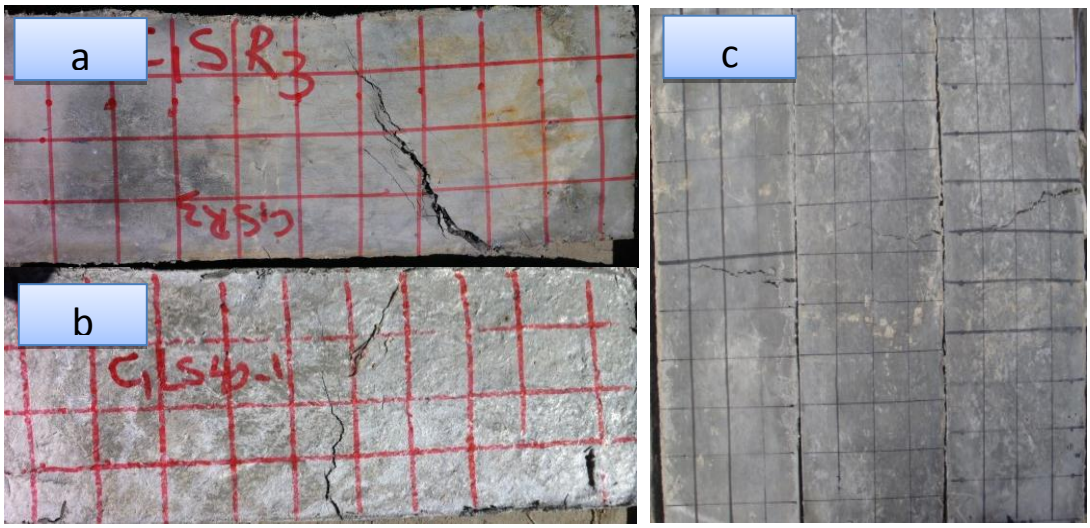

Figure 5.10 Crack patterns of tested HFF panels: a) panel with an additional tie under uniform load; b) panel without a tie and uniform load; c) panels without ties under point load

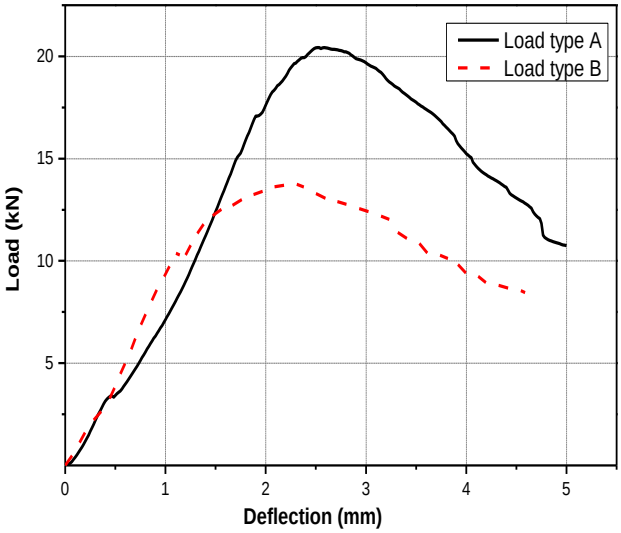

Figure 5.11 Load deflections of HFF plates under two different load types

In general, test results revealed that a pure shear capacity exists at the centre of the specimen under single load, because the maximum crack occurred in the middle of the sample, as seen in Figure 5.10(c). In contrast, samples tested using the loaded disk exhibited shear crack development diametrically along the struts. As experimentally determined and demonstrated in the load–deflection curve, in this case, the cracking load was assumed to be the ultimate shear load. The cracking strength of all tested panels wascompared with the experimentally obtained

maximum shear load. The maximum allowed load that could be sustained at the onset of diagonal cracking with a strut of different widths was calculated for HFF panels with and without tie reinforcement according to the strut–tie model (ACI 2011). The cracking angle (θ) was determined as 45.6º for panels loaded with the steel disk (uniform load), and 38.4º for panels loaded with a concentrated load (point load). The design of struts, ties and nodal zones was based on the following equation:

$$\emptyset\, F_{ns} \geq F_u \qquad (5.1)$$

where F_u is the factored force acting on a strut, and F_{ns} is the nominal strength of the strut, which is calculated from:

$$F_{ns} = f_{ce} A_{ce} \qquad (5.2)$$

where A_{ce} is the cross-sectional area at one end of the strut and f_{ce} is the characteristic strength, determined by:

$$f_{ce} = 0.85\, \beta_s f_c' \qquad (5.3)$$

The compressive strength f'_c was held constant at ~39 MPa for all tested samples, and the factor β_s was dependent on satisfactory web reinforcement. The results in Table 5.2 indicate that the load ratio, in all cases other than SL-40, fulfils Equation 5.1. In general, the strut–tie model predicted well the ultimate shear strength of the tested samples, especially those that failed in diagonal shear and that were subjected to a uniformly distributed load. Application of the equations showed that test results for panels tested under point load deviated from the calculated ultimate shear strength. According to Ibrahim (2011a), the strut–tie model is less suitable for conventional ferrocement than for modified ferrocement with hybrid PVA fibre (as used here), which supports its applicability for HFF composites.

Table 5.2 Comparison of experimental and maximum allowable failure loads

ID	Shear load		Load ratio	Shear strength
	Experiment (F_u) (kN)	Strut–tie model (F_{ns}) (kN)		(MPa)
S-40	20.4	22.2	0.92	3.8
S-30	15.6	16.7	0.94	2.9
S-25	13.3	13.9	0.96	2.5
SR-40	42.4	44.4	0.95	8.0
SL-40	13.8	9.3	1.49	2.6

5.2.5 Compressive strength behaviour of HFF materials

The stress–strain response of the HFF composite under compression load is another mechanical property that could provide significant information on the material's behaviour. HFF cubes were tested to experimentally characterise stress–strain behaviour under compression. A typical stress–strain curve for the HFF matrix is presented in Figure 5.12.

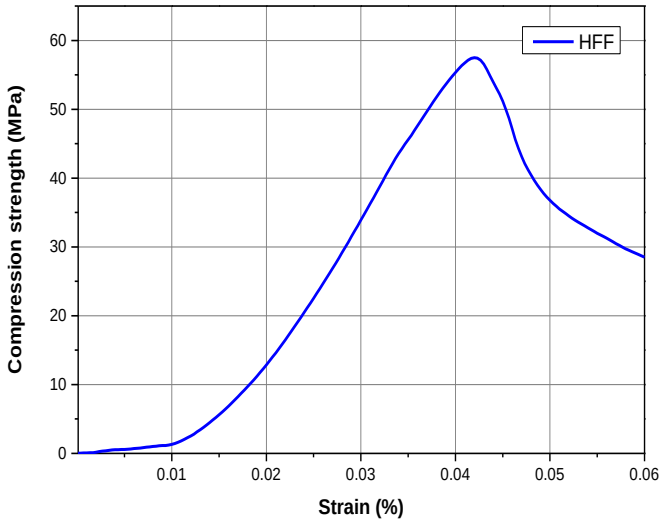

Figure 5.12 Typical compressive stress–deflection curve of the HFF composite

Importantly, the stress–strain curve of the HFF composite loaded under compression was characterised by a slight initial strength increase, followed by a significant strength increase until maximum strength was reached. In the initial stages of the loading in compression, at pressures less than 1.3 MPa, any microcracks in the matrix did not propagate further. With increasing load, however, microcracks grew into macrocracks in the matrix as a result of its stiffness to stress. At maximum peak load, the macrocracks became unstable and led to matrix failure. After localisation, the curve underwent a softening behaviour due to the crack growing. The overall compressive strength of all tested mixtures in this research was in the range of 53–68 MPa, with and without additives, and containing 1.5% fibre volume fraction.

Remarkably, the hybrid fibre performed in a similar way in terms of crack resistance caused by compression load, as it did to flexure. When fracture occurred,

the matrix did not split into small pieces as is typical for brittle, cement-based materials such as concrete or plain mortar. The fibres bridged the cracked segments and stopped them from separating. The fibre in HFF activated a crack resistance mechanism due to its random distribution in the matrix. The deformation of tested HFF cubes of size 50×50×50 mm resulted in the compressed shape illustrated in Figure 5.13.

Figure 5.13 HFF cubes after being subjected to compression load

5.2.6 Pullout testing of single PVA fibre on the HFF mixture matrix

The pullout test measures the force required to extract the fibres out of a mortar matrix. Determining the pullout behaviour of fibre-reinforced cement-based materials is necessary to understand the bond strength, which can be calculated using average shear stress caused by an applied pullout load on a single fibre (Wille and Naaman 2013). In this investigation, different fibre lengths was treated as a study parameter. The test results were used to govern the equivalent bond strength using PVA fibre. Pullout tests were conducted using an extension control of 6 mm/min. The test setup and the specimen structure were as shown in Figure 5.14. The mix proportions were as in B2 mixture in Table 4.8. Ice cube moulds were used to cast the specimens, so the maximum fibre-free length was 1.5 mm for the long PVA fibre, and 4 mm for the short fibre. The fibres tested were PVA1 and PVA4 (see Table 3.3).

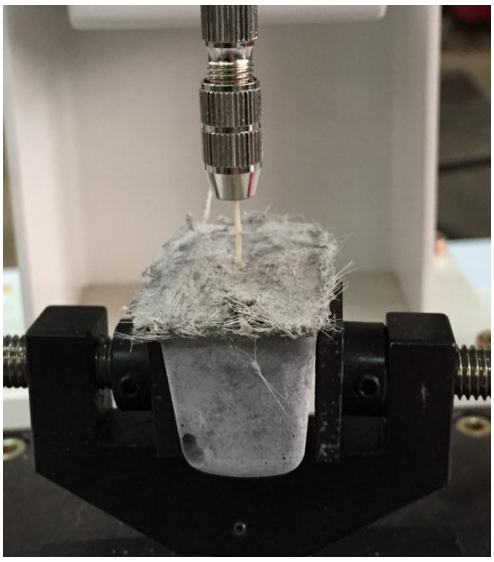

Figure 5.14 Fibre pullout test

Usually, each fibre pullout test is described by plotting the pullout load–slip relationship. However, the testing machine used here could not be connected to a data requisition system. The maximum pullout force P_{max} was measured at the point of failure. The value of P_{max} divided by the fibre cross-sectional area A_f provides the maximum tensile stress $\sigma_{f,max}$ induced in the fibre by the pullout load as a function of slip (s) (Wille and Naaman 2012). This is equal to:

$$\sigma_{f,max} = \frac{P_{max}}{A_f} = \frac{4 \times P_{max}}{\pi \times d_f^2} \; in \; MPa \qquad (5.4)$$

where d_f is the fibre diameter. The average bond strength τ_{av} is based on the maximum pullout load and the initially inserted length (L_E) is given by:

$$\tau_{av} = \frac{P_{max}}{\pi \times d_f \times L_E} \; in \; MPa \qquad (5.5)$$

The test results providing $P_{max,}$ and its associated results from applying Equations 5.4 and 5.5, are shown in Table 5.3. It is evident that L_E is strongly affected by the tensile strength and bond strength of the fibre–matrix interface. Although the longer fibre achieves higher tensile strength than the shorter one, the shorter fibre shows a better bond strength capacity. This may explain the relatively high first crack tensile strength in the tensile test. The results agree well with those of Kandal and Li (1998), if considering the different matrix proportions.

Table 5.3 Pullout test results and calculated tensile and bond strength

Experiment number	Long fibre test			Short fibre test		
	P_{max} (N)	$\sigma_{f,max}$ (MPa)	τ_{av} (MPa)	P_{max} (N)	$\sigma_{f,max}$ (MPa)	τ_{av} (MPa)
1	43.1	83.1	1.4	0.9	28.8	1.8
2	41.1	79.2	1.3	1.0	32.8	2.1
3	47.2	91.1	1.5	0.7	24.8	1.5
4	49.2	94.9	1.6	0.7	22.8	1.4
5	40.6	78.4	1.3	1.0	31.8	2.0
6	42.1	81.2	1.4	0.9	31.2	1.9
7	48.8	94.1	1.6	0.9	29.8	1.9
8	43.9	84.6	1.4	0.9	29.5	1.8
9	44.7	86.2	1.4	0.6	21.4	1.3
10	F*	-	-	1.2	41.2	2.6
11	47.74	92.1	1.5	0.7	24.1	1.5
12	F*	-	-	1.2	39.9	2.5
Av	44.8	86.5	1.4	0.9	29.9	1.9

F* failure between matrix and fibre

5.3 HFF material classification

Consideration of structural performance is important in the design of construction materials, and this is facilitated by material classification enabling understanding of structural behaviour. The classification of HFF materials requires the study of their tensile strain behaviour, flexure response, toughness and energy absorption. It is usual for materials exhibiting quasi-brittle behaviour to strain harden, and this is the case for almost all fibre-reinforced cement-based materials; thus, compressive strength is insignificant with respect to performance behaviour.

To assign the HFF composites to a material class, a test series was conducted with a focus on indicators of HPFRCC behaviour. A tensile test, as described in Chapter 3, was performed on dogbone specimens. To determine toughness, flexure tests were performed on a four-point bending setup, ensuring a constant bending moment zone. The applied load was under displacement control at a rate of 1 mm/min for all tested panels. The load was transferred as an equivalent elastic bending stress, to allow for the assumed uncracked section behaviour. In addition, to classify the mixture matrix, a four-point

loading test for testing the flexure behaviour of a non-mesh-reinforced beam was conducted. Moreover, to determine the mixture toughness with respect to specimen size, tests were carried out according to ASTM C 1609 (ASTM 2013). The specimen size and test setup for these toughness test were described in Section 3.5.2.

5.3.1 Strain hardening behaviour

Strain hardening behaviour is mostly detected using mechanical classification methods, by observing the tensile stress–strain behaviour (Li, Wang and Wu 2001). Strain hardening is indicated by the stress–strain curve: if the curve shows a linear elastic behaviour, first crack is occurring at a certain load capacity. This is followed by increased strain for large deformation and inelastic stress–strain behaviour, which continues until the maximum strength capacity of the specimen is reached. From this point, strain softening can be observed (e.g. see Figure 5.15). An important classification trait for strain hardening behaviour judged from the curve is that the maximum strength must be higher than the stress at first crack.

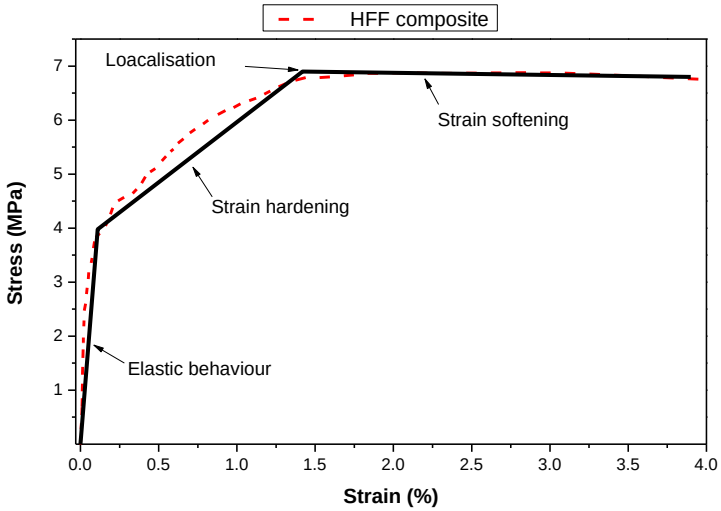

Figure 5.15 Tensile stress–strain curve of HFF composite showing strain hardening behaviour

Similarly, bending test results show deflection hardening in the equivalent stress–deflection curve after the first crack. The mixture and materials used were described in Section 5.2.3. Unusually, samples with square mesh showed multiple-linear behaviour in the idealised model, as seen in Figure 5.16. Both the tensile and

flexure test observations indicate that HFF composites exhibit strain hardening behaviours.

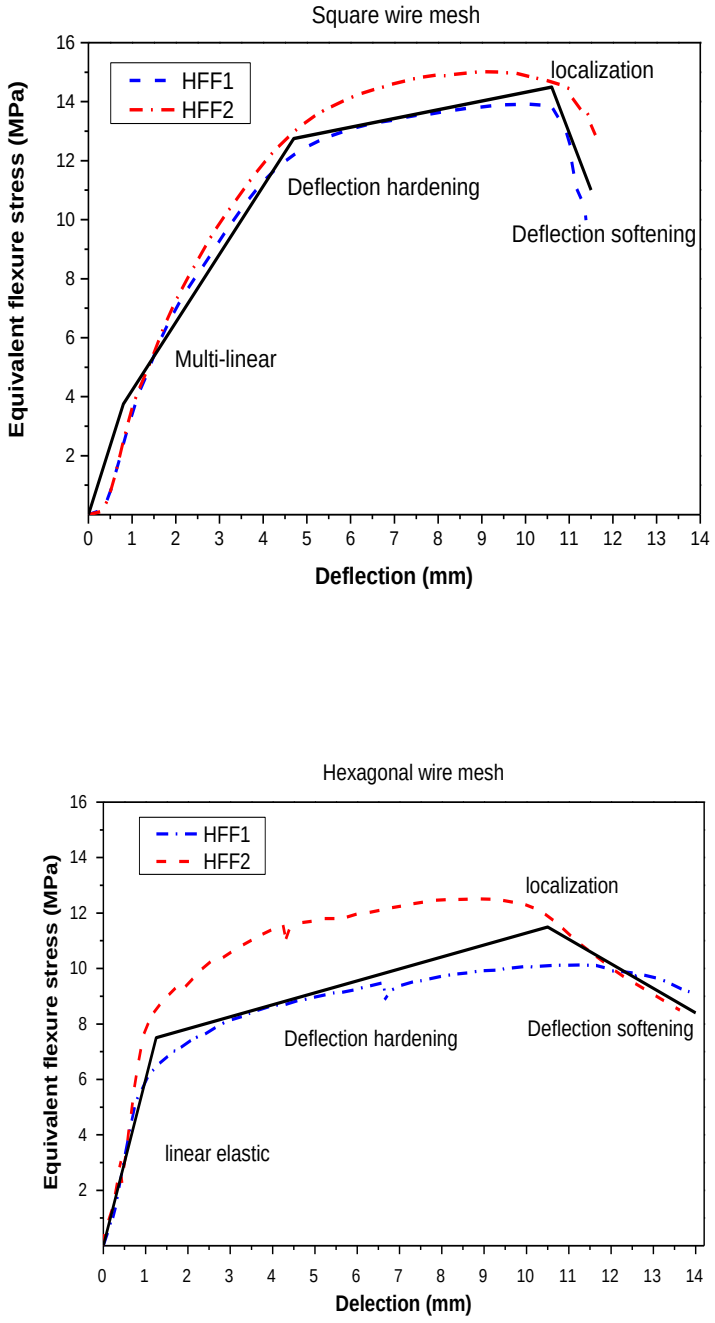

Figure 5.16 Idealised flexure response of HFF panels using a constant fibre content of 1.5% volume fraction with different mixture materials and wire mesh type

5.3.2 Classification using the toughness index

A bending test illustrating deflection hardening can be used in conjunction with toughness to classify cementitious fibre-reinforced composites regardless of whether they behave as high performance materials (Naaman 2003a). A test of HFF materials with mixture proportions as in C1 (HFF1), C4 (HFF4) and CN (HFF2) is similar to the test described in Sections 4.2.1 and 4.3. The fibre composition is as in Table 4.1. Additional samples were made with the same mix proportions as HFF1 (T1) and HFF2 (T2), but without wire mesh reinforcement. The ASTM C1609 Standard test method for flexural performance of FRC uses a beam with third-point loading. Thus, the ASTM (2013) defines the toughness index as the area under the load–deflection curve up to a specified deflection divided by the area under the same curve up to first cracking. Naaman and Reinhardt (1995) pointed out that toughness indices of I_5>5, I_{10}>10 and I_{20}>20 are reliable indicators of fibre-reinforced composites with quasi-strain hardening material behaviour.

The calculation of toughness indices I_5, I_{10} and I_{20} was explained in detail by Barr et al (1996). According to those authors, toughness indices should be calculated based on the location of deflection (δ) as seen in Figure 5.17. Therefore, toughness indices I_5, I_{10} and I_{20} can be determined by considering the first crack curves (grey area). The load–deflection curves are determined by multiples of the first crack deflection so that I_5 is associated with 3.5 δ, I_{10} with 5.5 δ and I_{20} with 10.5 δ.

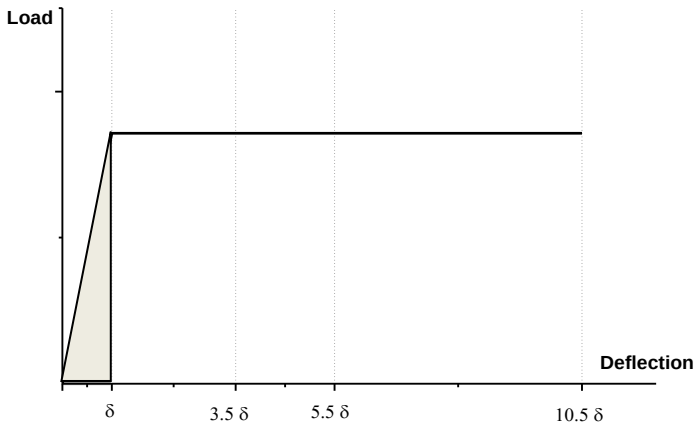

Figure 5.17 Toughness indices according to ASTM C 1018

The toughness indices of hybrid fibre composites HFF1, HFF2, HFF4, T1 and T2 are provided in Table 5.4. All tested samples contained a PVA fibre volume fraction of 1.5%. The first three toughness indices (I_5, I_{10} and I_{20}) were calculated from the net load–deflection curves from the flexural tests, as described above. The results shown in Table 5.4 meet the toughness criteria according to Naaman and Reinhardt (1995).

Table 5.4 Toughness indices of tested specimens

Mix type	Wire mesh type	Toughness indices (N*mm)		
		I_5	I_{10}	I_{20}
HFF1	Square	12.7	22.2	57.7
HFF2		13.1	27.2	58.6
HFF1	Chicken	6.8	12.3	27.2
HFF2		12.6	23.45	44.5
HFF4		5.9	10.4	20.0
T1	None	7.7	10.2	-
T2		6.7	10.1	-

5.3.3 Multiple crack formation

The SHCCs developed multiple cracks during flexure tests. In the ferrocement panels, the first relatively small crack transpired at an earlier stage of the applied load. Further increases of the load widened the cracks, and in some cases caused multiple cracks to form. At this stage, the load is carried principally by the mesh. The deflection subsequently increases rapidly and the main crack can spread further through the thin depth of the ferrocement panel until reaching the compression area on the top surface of the panel. In HFF panels with hexagonal wire mesh and 1.5% volume fraction fibre, multiple cracks were formed. The small cracks closed considerably after removal of the load.

The importance of fibres in crack control was investigated by Swamy and Hussin (1990). After first cracking, the multiple cracking stages led to a strain hardening effect while the load was increased to the maximum state. Similar behaviour was found in the tested samples with hybrid fibre. In contrast, the

ferrocement panel (marked F in Figure 5.18) showed only a single dominant crack, which occurred after the maximum flexure load was reached.

Although HFF panels had multiple crack lines, the number depended on the fibre content, as discussed in Chapter 4. The crack width was significantly reduced by increasing the fibre volume fraction. The ductility of the specimens increased because of the simultaneous activation of the longer fibres and the wire mesh to bridge the growing microcracks at the origin of the higher residual forces. Among the panels tested, PVA hybrid composites showed greater yield deflection capacities than ferrocement (Figure 4.6). Due to the additional tensile strength of shorter PVA fibres associated with small crack formation, wide cracks were bridged by the longer PVA fibres without being split, which results in high deflection capacity and relatively low strength-loss rate after the maximum load was reached.

Additional strong evidence of high performance in cementitious composite materials comes from the designated multiple cracking behaviour (Naaman 2007; Ahmed, Maalej and Paramasivam 2007b). The stress after first cracking increases with strain and multiple cracking occurs up to the maximum post-cracking stress. This occurs in the zone of first cracks up to the maximum post-cracking stress. Some examples of multiple crack patterns seen in tested panels are provided in Figure 5.18.

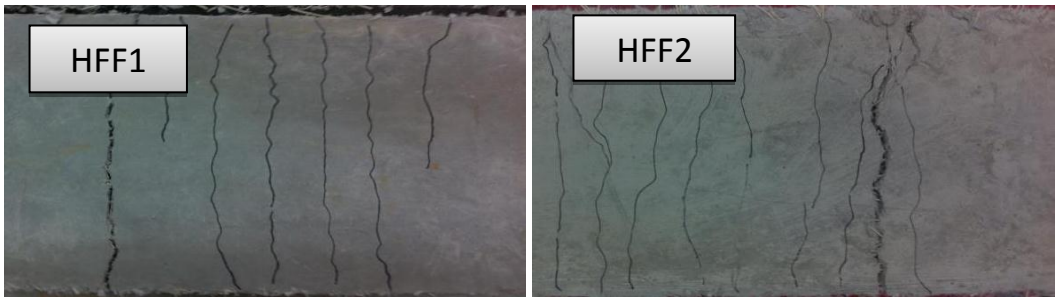

Samples with hexagonal wire mesh

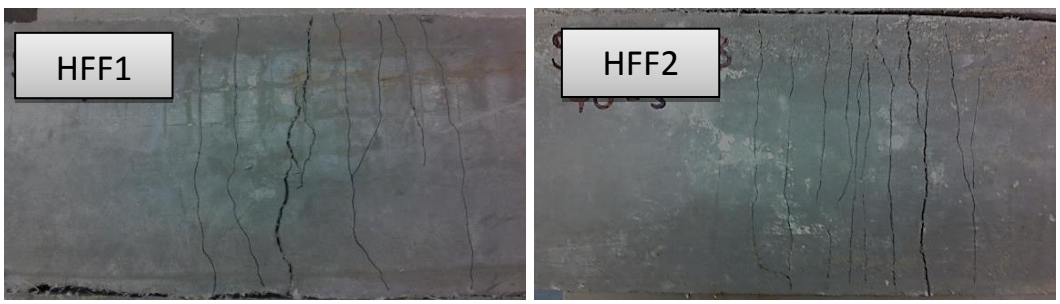

Samples with square mesh

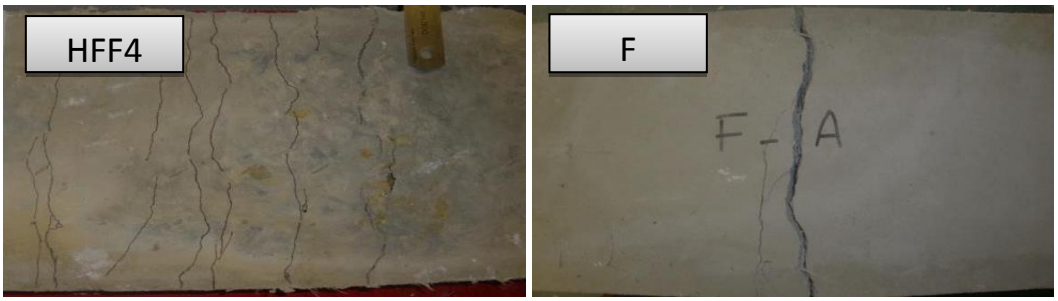

Figure 5.18 Multiple crack behaviour of tested panels

HPFRCC material behaviour is concluded when three indicators the toughness indices, multiple crack behaviour and hardening behaviour—are observed (Naaman and Reinhardt 1995). In the present work, all three indicators were demonstrated for the HFF panels. Based on the toughness test, using wire mesh to reinforce hybrid fibre composites in general increases their energy absorption compared to non-mesh-reinforced specimens.

5.4 Micromechanical behaviour of HFF composites

The development of pseudo-strain hardening properties in HFF composites employs the micromechanical specifications behind their structural performance. Thus, structural properties are reproduced through the micromechanical material specification established due to the structural projection of the tensile and flexure responses. However, the enhanced performance of HFF is the result of its mechanical properties, which are driven by its micromechanical properties at the nanoscale level.

To increase understanding of the mechanical properties of HFF at the nanoscale level, tests are required to observe the nanostructure and the matrix surrounding the PVA fibre. SEM was used to analyse elemental images showing the general morphology of the HFF matrix. Further, the nanoindentation techniques developed have been employed widely to provide information about the nanoscale mechanical properties of cement-based materials (Whitney, Broz and Cook 2007; Vandamme and Ulm 2009; Vandamme, Ulm and Fonollosa 2010). In the present work, nanoindentation experiments were used to provide a detailed description of the elastic moduli, matrix packing density and matrix hardening across the fibre–matrix.

5.4.1 Microstructural composition of HHF composites

The main binding phase in the cement paste made from OPC is the composition of the calcium silicate hydrates (C–S–H), driven by the fibre–matrix interface initiating the matrix structural performance resisting the crack formation (Sakulich and Li 2011). To observe the C–S–H hydrates, SEM scans of the HFF2 mixture matrix were conducted on the surface of the specimens, which was gold coated. High-resolution surface inspections of samples were carried out. In the early stage of hydration, needle-shaped crystals of calcium trisulfoaluminate hydrate, or ettringite, were formed, developing into large prismatic crystals of calcium hydroxide and minuscule fibrous crystals of calcium silicate hydrate (C–S–H). After the matrix was fully hydrated, the ettringite decomposed to hexagonal plates, as seen in Figure 5.19.

The micro PVA fibre was easily located at the ultrafine scale of ~100–500 nm, as shown in Figure 5.20. Initial microcracks near the PVA fibre were also observed at this scale, suggesting that PVA fibres bridge the microcracks, with which they were well matched in terms of size. This has the advantage of enhancing overall mechanical properties. Further observation of the PVA fibres showed a relatively high density surrounding matrix. This led to an increase in the adhesive elastic shear bond, which had the effect of improving the mechanical bond between the fibre and the matrix. The relative high density of the matrix was achieved by using SF particles in the mixture matrix.

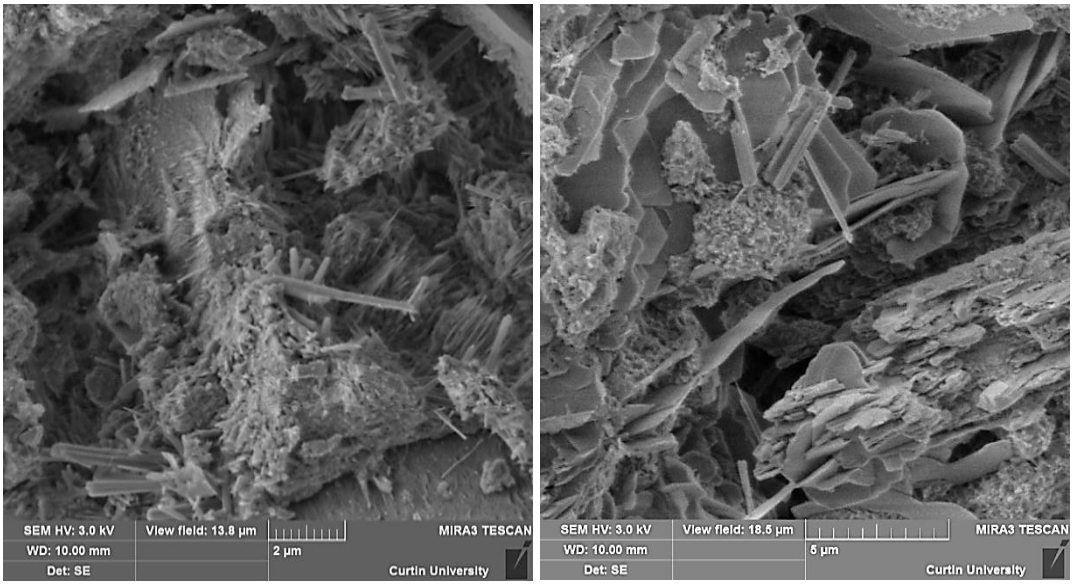

a) Early hydration stage b) Full hydration stage

Figure 5.19 SEM of the HFF matrix showing the microstructure of C–S–H

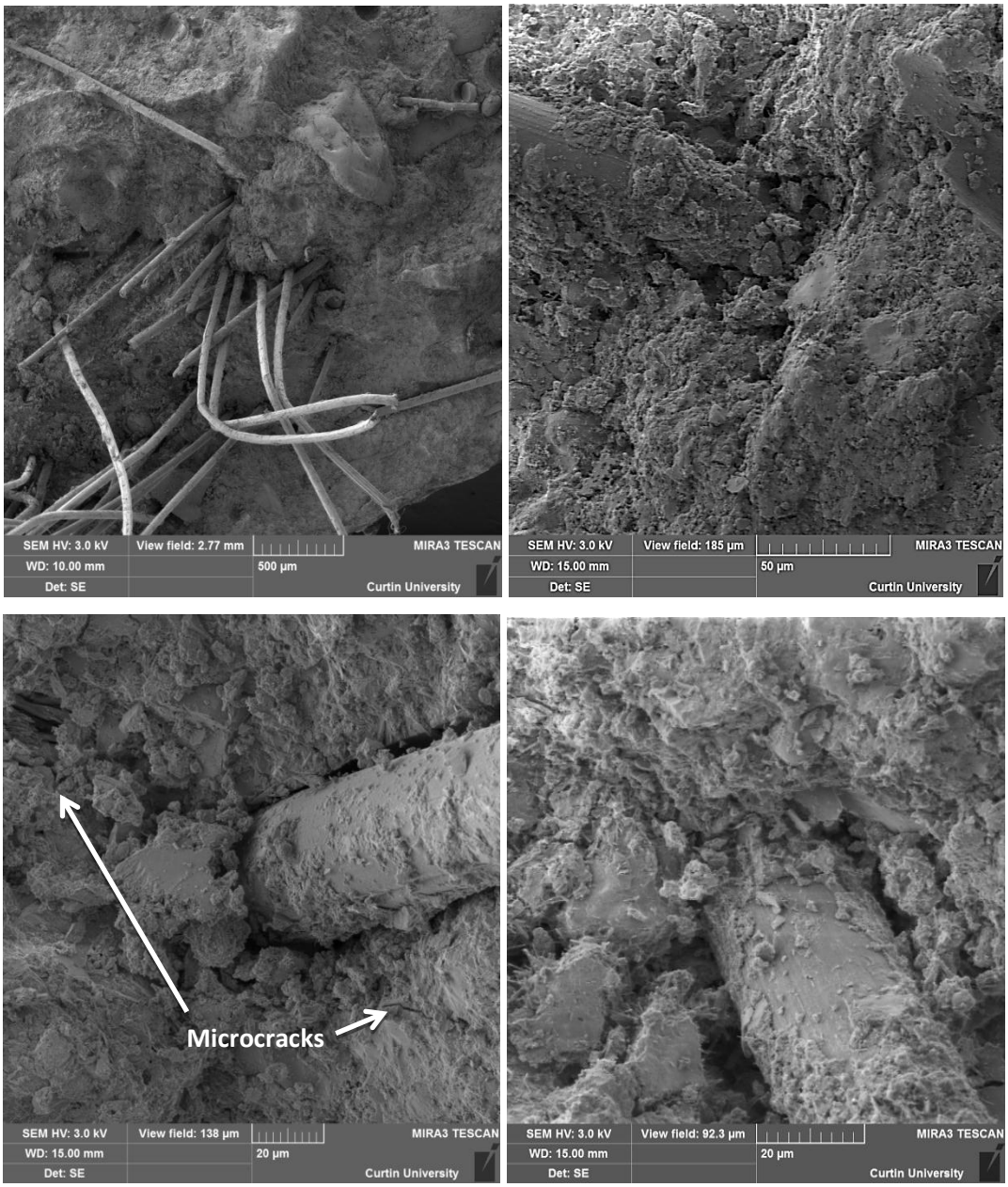

Figure 5.20 SEM images of PVA fibres surrounded by the cement matrix

5.4.2 Nanoindentation of the HFF mixture matrix

Nanoindentation tests were performed using a device equipped with a Berkovich tip indenter. The desired mechanical properties were automatically determined by recording the load (P) and displacement (h) relationship. The displacement measures the depth h of penetration into the specimen, which produces a P–h curve (Constantinides and Ulm 2004; Constantinides, Ulm and van Vliet 2003). The SNT

is used to analyse the results obtained from the nanoindentation, by engaging the deconvolution method. The procedure is based on an estimate of the mean and standard deviation of indentation modulus and hardness for each mechanical phase. The results were used to generate CDFs and probability density functions (PDF) (Ulm et al. 2007; Vandamme, Ulm and Fonollosa 2010) using a program written in MATLAB for this purpose.

The nanoindentation specimens were cut down to 10x10x8 mm segments using a diamond precision saw, as shown in Figure 5.21. The testing surface was saturated with red resin. The samples were then cast in a resin solvent. The samples were after hardening grinded with silicon carbide paper of 200, 400, 800 and 1200 grade to a total thickness of 9 mm. The surface with the dry red layer was grinded until the sample surface is exposed; the verification followed by optical microscopey. The exposed test surface was then polished with diamond suspension oils in progressive gradations of 9 μm, 6 μm, 3 μm, 1 μm, 0.25 μm and 0.1 μm. After that samples were subject to light washing with water to remove the remaining diamond fluid. The samples were then vacuumed to remove surface water, and further storage followed in a hydration inhibiting desiccator until testing.

The indentation was performed using a 3 sided pyramidal Berkovich tip. Nanoindentation used a grid technique to test 4 different sites, recording data from 500 indentations, per sample, with spacing between each indentation of 20 μm.

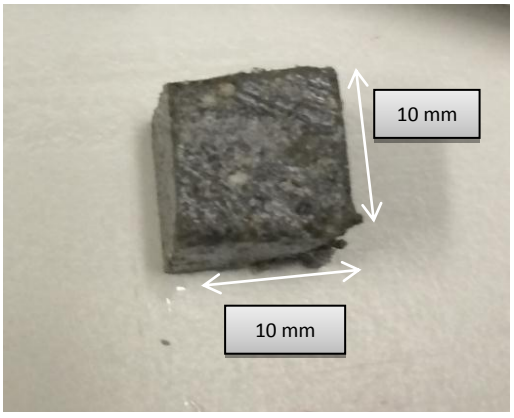

Figure 5.21 HFF samples sliced from panels for nanoindentation tests

The tests began by recording the load–depth (*P*–*h*) relationship for the tested specimen through a particular load and displacement range. A loading history curve was prescribed, defined by the loading, holding and unloading time as seen in Figure 5.22. A Berkovich indenter with a three-sided pyramidal indenter and a semi-vertical angle of 65.35° was applied. Tests were carried out by randomly choosing 500 indentation positions on the sample surface.

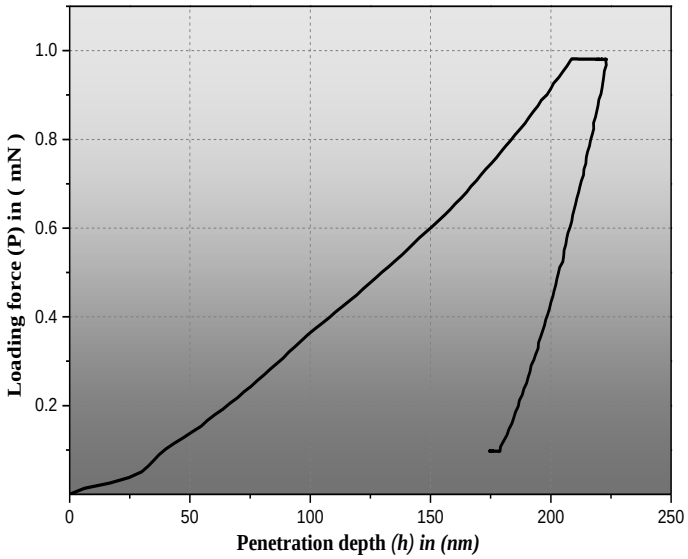

Figure 5.22 Example of typical load–depth curve obtained from a nanoindentation test on an HFF specimen

5.4.2.1 Micromechanical phase structure

In this test, two heterogeneous mixture types were used: HFF2, which represents mixture B2 in Table 4.8, and FHH2*, which has the same mixture proportions as B2 but without the addition of FA or SF. The C–S–H in cement paste appeared as a heterogeneous material, and its hydrated crystals were clearly visible at the nanoscale. The C–S–H in a cement paste is categorised as high density (HD) C–S–H or low density (LD) C–S–H depending on its mechanical properties (Vandamme, Ulm and Fonollosa 2010). The micromechanical phase and its dimensions were shown in Figure 3.19. Here, for HFF2, the C–S–H is classified into two phases: LD C–S–H and HD C–S–H featuring its mechanical properties (Constantinides and Ulm 2006). Phase 3 is due to the presence of CC. Capillary pores and air bubbles with

pore sizes between 10 nm and10 μm make up Phases 4 and 5. Powder quartz, despite having the smallest particles in the range of 0.1–100 μm, isconsidered as Phase 6. Quartz sand, granular material and fibre 150–600 μm isconsidered as Phase7. HFF2* is only a five-phase composite because there is no cement replacement using fine FA or SF.

The phase number is also dependent on the relationship between the penetration depth *h* of the indenter into the sample, the characteristic particle size *D* and the representative element volume *d*, so for $h_{max}<d$ (the indentation in the dimension of the phase), and for greater depth $h_{max}>D$, the indentation depth will be affected by different phases of the microstructure (Sorelli et al. 2008). According to this relationship and the different mixtures used in the materials, HFF2* is defined as five-phase and HFF2 as a seven-phase composite.

5.4.2.2 Packing density and hardness modulus

The packing density of the solid structure of the matrix is known to be one of the most important factors affecting the compressive strength of the whole composite. At the level of the paste material (Figure 3.19), the microscopic structure of the cement, FA and SF particles affect the structural specification of the composite matrix (De Larrard 1999). As the diameter of the smaller fibres used here is similar to those considered ‘fine particles’ in previous studies, they are predicted to influence the compactness of the whole paste material. By way of illustration, Figure 5.23 shows the results of the deconvolution technique in terms of both CDFs and PDFs for packing density for an HFF cement paste.

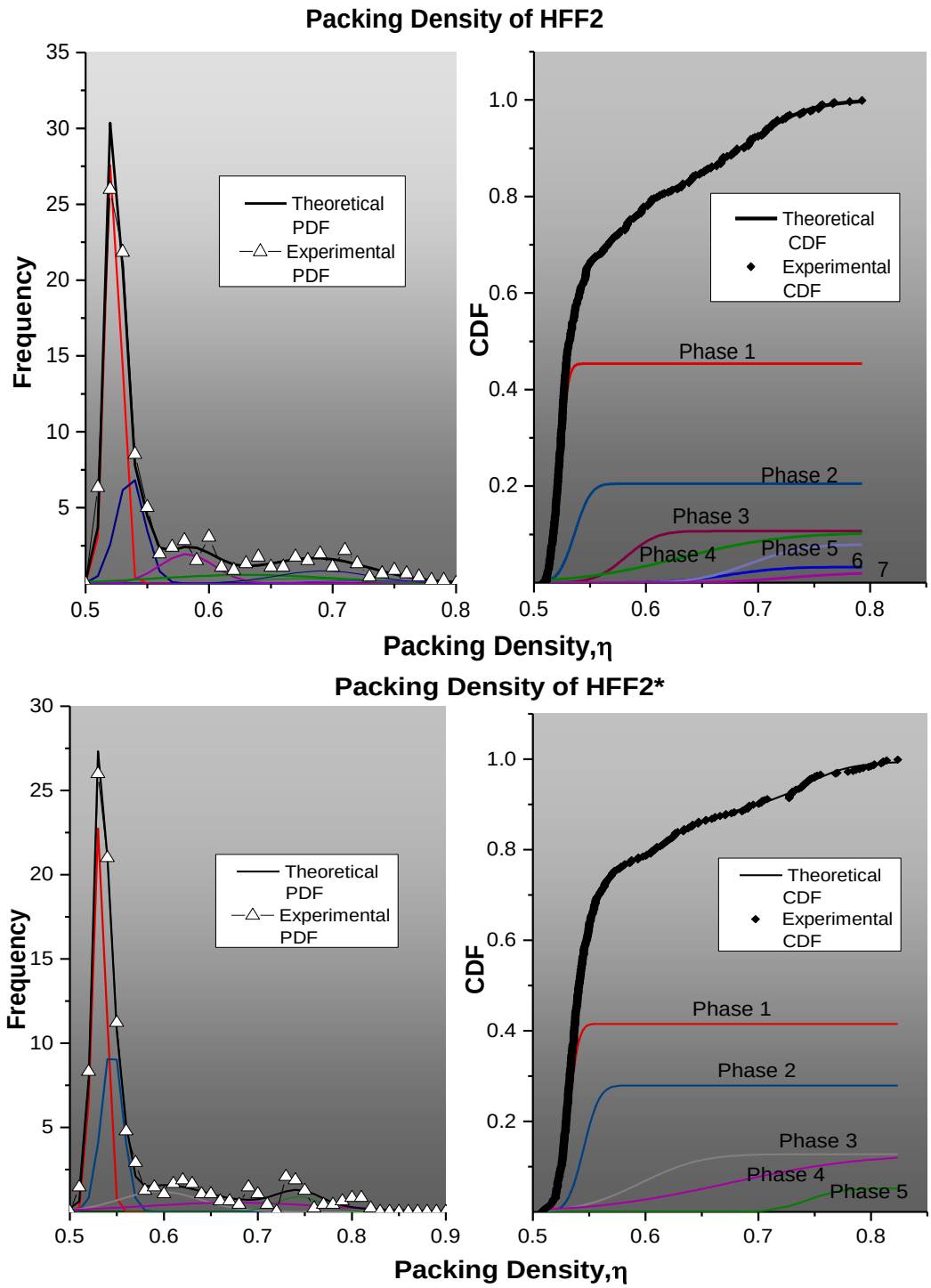

Figure 5.23 Statistical indentation analysis of two different mixtures of HFF matrix showing CDF and PDF of packing density

The Gaussian distribution PDFs, in contrast tothe packing density, have a high and a lower hydration value for each curve presented in Figure 5.23. In the two tested hybrid fibre cement paste samples, the two significant hydration phases that showed up in over 60% of all data were the same as those in similar studies on cement paste,

associated with the LD (C–S–H) phase and HD (C–S–H) phase (Constantinides, Ulm and van Vliet 2003; Constantinides and Ulm 2004; Constantinides and Ulm 2007). Therefore, the first peak in the PDF/CDF plot was attributed to the HDC–S–H phase, and the second, to the LD C–S–H phase. In contrast, the lowest characteristic packing density was attributed to air bubbles in a porous material with definite matrix–porosity structure. A solid is associated with any packing density with $0 \leq \eta \leq 1$ (Ulm et al. 2007). The phases in between are associated with FA, SF, aggregate and PVA fibre.

Figure 5.24 illustrates the relationship between indentation hardness H and packing density η for the HFF matrix is together with the deconvolution of the packing density presented. The illustration is in the form of packing density distribution plots or nanporosity distribution of the C–S–H phases (Vandamme and Ulm 2009). The plot shows that the packing density in HFF2 with fine material additives was greater through the overall mixture matrix than in HFF2*, where the density was more concentrated in the lower region of hardness. In other words, HFF2 had fewer air bubbles than HFF2*.

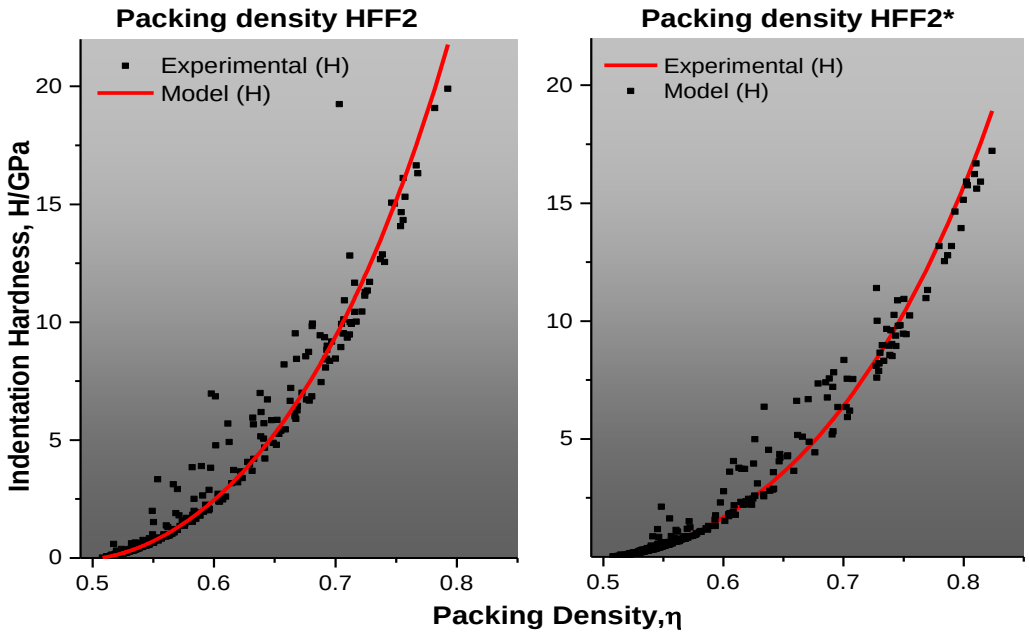

Figure 5.24 Scaling of indentation hardness with packing density for both HFF materials

The statistical analysis (CDF and PDF) of indentation hardness for two different mixtures of HFF matrix is shown in Figure 5.25. The lowest characteristic

stiffness–hardness phase had a hardness of H= 0.17± 0.08 GPa $(\mu_1 H \pm s_1 H)$ for HFF2 and H= 0.22± 0.08 GPa for HFF2*. These low values were attributed to air bubbles (pores). In relating C–S–H phases to hardness, it is evident that the HD C–S–H in HFF2 exhibited higher hardness values, and the LW C–S–H, lower values compared to those for HFF2*. In general, materials with five and seven phases had similar hardness characteristics, which was more obvious in the CDF plot.

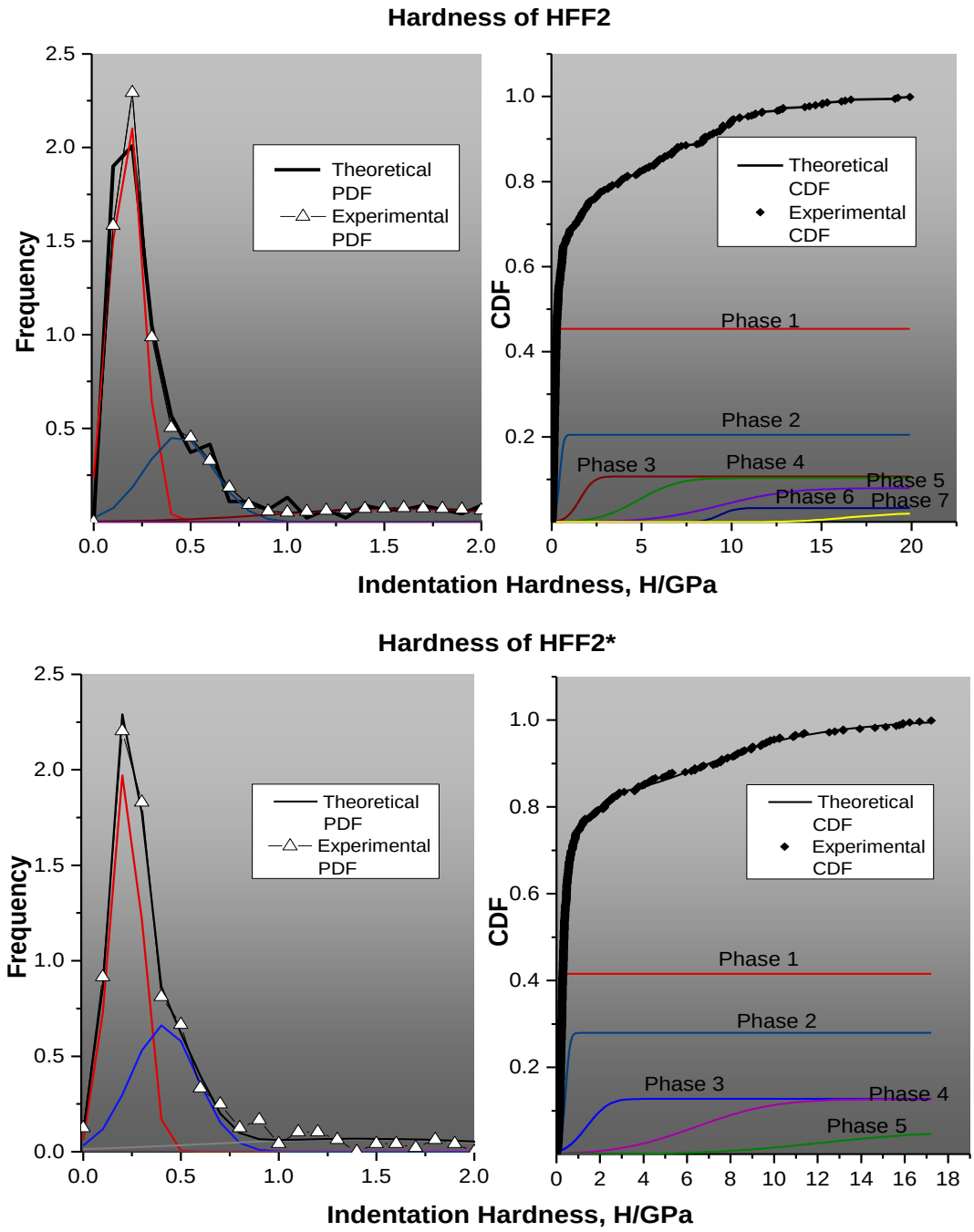

Figure 5.25 Statistical indentation analysis of two different mixtures of HFF matrix showing CDF and PDF of indentation hardness

5.4.2.3 Micromechanical elastic modulus

To perform a nanoindentation test, estimated initial Poisson's ratios are required. For simplicity, Constantinides and Ulm (2006) selected a micromechanics scheme for a characteristic range ($0.2 \leq \nu \leq 0.3$) of the multiple phase Poisson's ratios. Therefore, the ratio was assumed to be 0.25 in this test. From the *P–h* curve describing the required load to indent into the matrix, the elastic recovery was determined by analysing the unloading data according to a model for the elastic contact problem, which leads to a solution for the calculation of the elastic modulus *E* of the test area. The commonly used method is that of Oliver and Pharr (2004).

The output properties of the elastic modulus were at each phase of both indented mixtures in the PDF and CDF plotted as shown in Figure 5.26. The mean value of the indentation modulus Phase1 refers to the microporosity of the C–S–H matrix that leads to a weakening effect. An important outcome is that the volume fraction of HD of the overall volume of the C–S–H matrix in the HFF2* mixture was ~41%,whereas for HFF2 it was slightly higher (~4%). Further, the CCs of the mixtures did not differ significantly. The values obtained were in the range predicted by the theory relating to hydration reactions (Velez et al. 2001).

The CDFs and PDFs indicated the presence of seven phases in HFF, and five phases in the hardened HFF2* material system, as mentioned previously. The LD C–S–H in the HFF2 matrix was characterised by a phase modulus range of approximately $M = 7.9 \pm 2.3$ GPa $(\mu_1 M \pm s_1 M)$. This phase had a volume fraction of 45%. Similarly, the HFF2* gave values in the range of $M = 8.5 \pm 2.1$ GPa for this phase with 42% contribution to the matrix. In contrast, the HD C–S–H exhibited a phase modulus of $M = 13.8 \pm 4.2$ GPa ($\mu_2 M \pm s_2 M$) for HFF2 (20% volume fraction), and of $M = 13.9 \pm 3.3$ GPa for HFF2* matrix (volume fraction of 28%). All other phase modules obtained are summarised as average phase moduli in Table 5.5.

The elastic moduli of the different phases are an important outcome of the nanoindentation test; because they are driven by individual contributions (volume fractions), the composite elastic modulus of the whole matrix can be determined. A similar approach was taken in a study by Najm and Naaman (1995), in which the elastic modulus of fibre-reinforced cement composite was determined by using an arithmetic model considering the volume fraction (contribution) and the elastic moduli of the different components in the matrix. Table 5.5 summarises the

calculation of the composite elastic modulus from the nanoindentation results using this method.

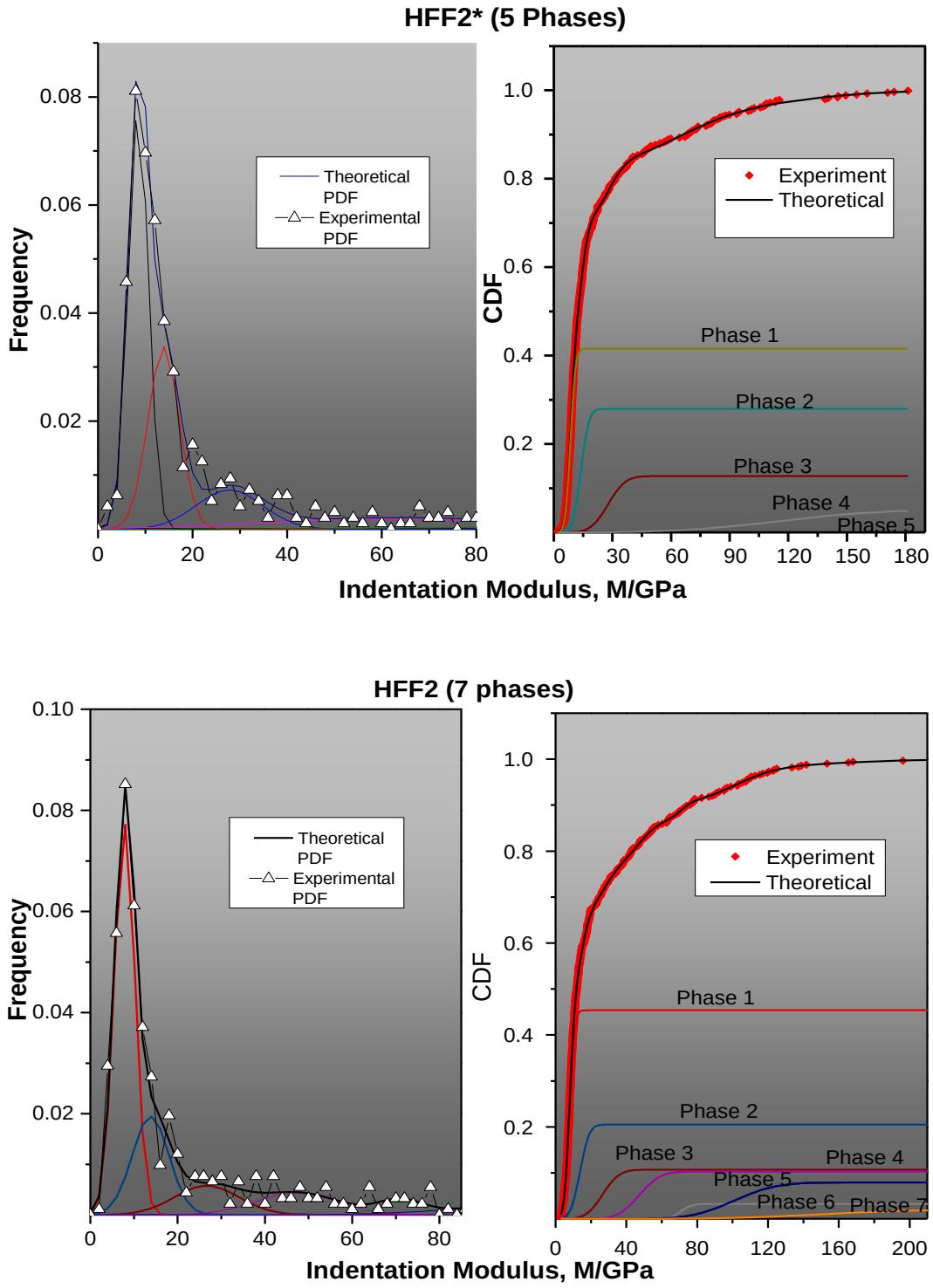

Figure 5.26 Experimental frequency plots and the best-estimated CDF and PDF evaluated from the SNT for the indentation modulus M for both mixtures

Table 5.5 Indention results describing micromechanical properties of HFF mixture

Input	HFF2*		HFF2	
	Elastic modulus E (GPa)	Volume fraction V_f (%)	Elastic modulus E (GPa)	Volume fraction V_f (%)
Phase 1	8.5	42	7.9	46
Phase 2	13.9	27	13.8	20
Phase 3	27.8	13	26.7	11
Phase 4	64	13	47.3	10
Phase 5	136.6	5	70.9	3
Phase 6	-	-	100.9	8
Phase 7	-	-	150.7	2
Outcome	**26.8**	**100**	**27.4**	**100**

5.5 HFF composite elastic modulus

Determining the elastic modulus of the whole HFF composite including wire mesh reinforcement in the calculation requires the elastic modulus of the mixture matrix. A structural and analytical approach was used to validate the results for the elastic moduli of the mixture matrix obtained from the nanoindentation test. The analytical determination of the fibre cement matrix and the validation of the final calculation using FEMs will be provided in detail in Section 5.5. Here, the elastic modulus is examined through structural testing and calculation.

5.5.1 Standard test for static modulus of elasticity and Poisson's ratio

To determine the elastic modulus, standard tests were performed for static modulus of elasticity and Poisson's ratio by testing cylinders under compression (ASTM 2010). The test setup is shown in Figure 5.27. The test proceeded via two steps: first, testing of the cylinders to obtain the average compressive strength, and second, replicating the loading and unloading process three times. The applied load was only 40% of the maximum load capacity determined in the first step. Two different test setups were used. One measured the longitudinal elongation for the elastic modulus

and the other determined the transverse elongation for calculating the Poisson's ratio. The mixtures used for the nanoindentation test were used in this investigation.

Figure 5.27 Standard test for elastic modulus and Poisson's ratio

The elastic modulus and Poisson's ratio were calculated using the following equations:

$$E = (S_2 - S_1)/\,(\varepsilon_2 - \varepsilon_1) \qquad (5.6)$$

$$\nu = (\varepsilon_{12} - \varepsilon_{11})/(\varepsilon_2 - \varepsilon_1) \qquad (5.7)$$

where E is the modulus of elasticity (MPa), S_2 is the stress corresponding to 40% of ultimate load, S_1 is the stress corresponding to the smallest longitudinal strain ε_1, and ε_2 is the longitudinal strain occurring at stress S_2. The Poisson's ratio υ was calculated by using the transverse strain (ε_{12}) at mid-height of the specimen produced by stress S_2, and the transverse strain (ε_{11}) at mid-height of the specimen produced by stress S_1. The resulting load strain curve for the tested specimen is shown in Figure 5.28. The elastic modulus and Poisson's ratio were determined by applying the data obtained from the experiment to Equations 5.6 and 5.7.

The elastic modulus obtained from the testing data was E = 27.6 GPa, and the Poisson's ratio was ν = 0.28, for HFF2. The equivalent values for HFF2* were E = 26.7 GPa and ν = 0.23. The results achieved by standard nanoindentation testing (Section 5.4.2.3) and via the FE approach (Chapter 8) are summarised in Table 5.6. The results obtained from the mechanical and FE methods were in good agreement with the elastic modulus from nanoindentation.

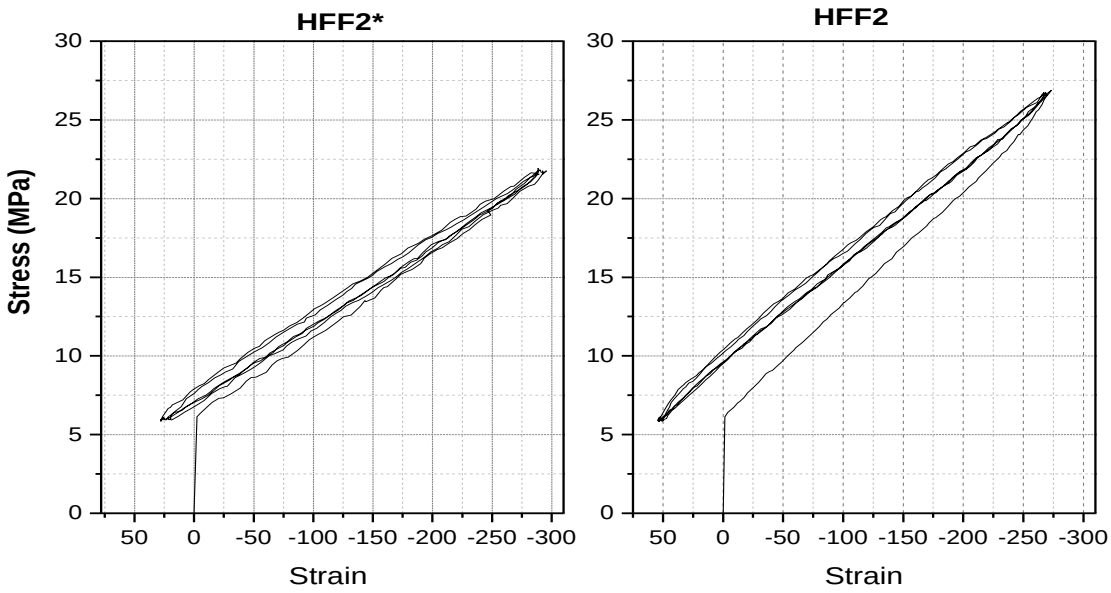

Figure 5.28 Stress *vs*. strain at 40% of the maximum load

Table 5.6 Summary of Elastic modulus and Poisson's ratio obtained by different methods

Method	HFF2*		HFF2	
	E modulus (GPa)	Poisson's ratio	*E* modulus (GPa)	Poisson's ratio
Standard test	26.7	0.23	27.6	0.23
Nanoindentation	26.8	0.25*	27.4	0.25*
Finite elements	27.6	0.29	28.2	0.29

*Assumed Poisson's ratio according to Constantinides and Ulm (2006)

5.5.2 Calculation of the composite elastic modulus

Hossain and Awal (2011) adopted a theoretical module to determine the modulus of elasticity of thin cement composite, specifically for ferrocement, using the following equation:

$$E_{com} = E_m + \varphi R_r (E_r - E_m) \qquad (5.8)$$

where in this study, E_m is the modulus of elasticity of the matrix (determined by the above methods), E_r is the elasticity modulus of reinforcement and R_r is the effective reinforcement, calculated for square mesh and hexagonal chicken wire mesh respectively as:

$$R_r = \frac{25\pi d^2 N_L}{D\ t} \quad (5.9)$$

$$R_r = \frac{25\pi d^2 N_L cos\theta}{D\ t} \quad (5.10)$$

where d is the diameter of wire, N_L is the number of layers, t is panel thickness, D is wire spacing, and θ is the angle of the wire mesh to the panel axis (59.5º for the hexagonal mesh used here). The reduction facture was taken according to Hossain and Awal (2011); φ = 0.0858 for square mesh and φ = 0.1265 for hexagonal wire mesh. Table 5.7 summarises the composite elastic modulus obtained from the input of the results from Table 5 into Equation 5.8. The composite elastic modulus of hexagonal wire mesh-reinforced specimens was lower than that of square mesh due to the lower volume fraction in its cross-section.

Table 5.7 Elastic modulus (GPa) of HFF with different wire mesh reinforcement

Type	Square wire mesh			hexagonal wire mesh		
	Standard	Nanoindentation	FE	Standard	Nanoindentation	FE
HFF2*	33.9	34.0	34.7	32.1	32.1	32.9
HFF2	34.7	34.6	35.3	32.9	32.7	33.5

5.6 Concluding remarks

In this chapter, the structural performance of the HFF composite was investigated by observing the tensile, flexural, shear and compressive response of the matrix. The HFF composite exhibited better overall structural performance than the conventional ferrocement and fibre-reinforced cement mortar. All HFF samples subjected to a tension load in a direct tensile test showed strain hardening behaviour. In general, the HFF composite achieved high performance, as classified according to deflection hardening, toughness index and multiple crack formation. Further, the tested HFF composite panels had relatively low shear capacity, but showed that the strut–tie model could be applied. In contrast, the micromechanical properties determined from a nanoindentation test clarified the effect of adding fine materials to the matrix in terms of enhancing packing density and hardness. The elastic modulus obtained using different methods for testing the materials were relatively concordant and varied in the range 26.7–28.2 GPa for both tested HFF mixtures. The structural and

mechanical properties exhibited by the material demonstrate that it is an excellent high performance material that requires further investigation in terms of durability before it might be used in structural applications.

Chapter 6: Durability of HFF Composite

6.1 Introduction

The application of the HFF composite as permanent formwork in structural concrete slabs requires a complete understanding of its structural specifications. This calls for a study of its durability to the environmental factors that most often affect HFF composites. The durability potential of HFF material is a key factor in its long-term performance, and requires detailed study. To understand parameters that may HFF composite durability, it is necessary to identify the most significant parameters that can be assessed experimentally. These include the effects of fire as one of the most likely incidents involving buildings, and several other environmental factors that may also affect structural members, such as exposure to freezing and thawing, sulphate soils or waters, or corrosion of reinforcement through the carbonation process.

The effects of elevated temperature and carbonation are examined in this study. Heat impacts are assessed using a unique test setup that allows an on-site bending test to be conducted during the heating process. The effects of higher temperature on the HFF composite, as well as its flexural response, compressive strength performance and changes in the microstructure are evaluated. Further, the effect of carbonation on its structural performance is studied in a test series to determine the changes in microstructure, chemical composition and structural performance.

6.2 Heat resistance of HFF composite

There will always be the potential for fire in buildings and other structures due to the risk of accidents or for other reasons. Generally, very high temperatures develop in less than 30 minutes after a fire begins (Purkiss 2007; Allen 2006), which damages the structure. The degradation of mechanical properties of concrete or mortar at

elevated temperatures due to fire is well established and has been widely researched (Cruz and Gillen 1980; Kodur, 2002; Kong and Sanjayan 2010; Saemann and Washa 1997; Schneider 1988). A significant form of damage to RC structures is the spalling of cover concrete during fire, which exposes the reinforcements to fire and causes substantial reduction of the load-carrying capacity and stiffness of the structure (Şahmaran et al. 2011; Balázs and Lublóy 2012). One way to reduce spalling is to use polymeric fibres in the concrete that melt at elevated temperatures and provide micro spaces inside the matrix to relieve the internal pressure associated with the evaporation of pore water (Nishida et al. 1995; Sarvaranta and Mikkola 1994).

However, the addition of fibre in ferrocement composites enhances the structural capacity of ferrocement although there are has been no detailed studies at elevated temperatures. Such data will be very useful in the design of composite slabs for fire protection of RC.

In this section, an experimental study on the flexural behaviour of HFF at various elevated temperatures is presented. The effects of hybrid PVA fibres, thickness of panels and partial replacement of cement with FA (class F) on the flexural behaviour of ferrocement panels are also evaluated in this study. Microstructural changes to the mortar and PVA fibres after exposure to elevated temperatures are also analysed by SEM. The novelty of this study lies in the measurement of *in situ* flexural load capacity of various ferrocement panels at different elevated temperatures, which is essential for their structural safety.

6.2.1 Mixture proportions and test setup

The proportions of wire mesh and PVA fibre for both mixtures are given in mixture B2 of Table 4.8. The ferrocement plate specimens made with100% cement and no FA or SF were designated ‘HFF2*’ and those containing 25% class F FA (as a partial cement replacement) and 5% additional SF by weight were designated ‘HFF2’. The mix proportions were as given in Table 6.1.

The experimental design evaluated the flexural behaviour of 54 HFF panels made with HFF2* and HFF2 at various elevated temperatures: 200, 400, 600 and 800°C. HFF panels were 620×200 mm and 25–40 cm thick (see Table 6.2).

Table 6.1 Mixture types and proportions

Mixture type	Binder		Sand	Water: Binder ratio	Silica fume	Superplasticiser	Fibre volume (%)	
	Cement	FA					PVA 1	PVA 2
HFF2*	1	-	1	0.4	-	-	0.75	0.75
HFF2	0.75	0.25	1	0.4	0.05	0.02	0.75	0.75

Table 6.2 Panels and test design

Specimen ID	Thickness (mm)	Testing temperature (°C)
HFF2*40-AMB	40	Ambient
HFF2*40-200	40	200
HFF2*40-400	40	400
HFF2*40-600	40	600
HFF2*40-800	40	800
HFF2-40-AMB	40	Ambient
HFF2-40-200	40	200
HFF2-40-400	40	400
HFF2-40-600	40	600
HFF2-40-800	40	800
HFF2-30-AMB	30	Ambient
HFF2-30-200	30	200
HFF2-30-400	30	400
HFF2-30-600	30	600
HFF2-25-AMB	25	Ambient
HFF2-25-200	25	200
HFF2-25-400	25	400
HFF2-25-600	25	600

6.2.2 Four-point bending test setup at elevated temperatures

The primary objective of these trials was to evaluate the flexure behaviour of HFF panels at elevated temperatures. A locally manufactured kiln was used to heat the HFF specimens to the desired temperature, at a heating rate of 6.67°C/min

(400°C/hour). A holding time of one hour was then applied to ensure that the panels reached the required temperature. Generally, actual fires in buildings can reach temperatures of up to 600°C in 15 minutes (Allen 2006), but heating was slower in the trials to ensure the uniformity of the temperature throughout the specimens.

Temperature was monitored using two thermocouples attached to the specimen's surface inside the oven. Two other thermocouples were also placed in the kiln to measure air temperature. All four thermocouples, a load cell and a wire LVDT were connected to a Quantum data logger to record the data. The rate of temperature increase in the air inside the kiln and on the HFF specimen's surface during heating to 800ºC is shown in Figure 6.1. A gap was evident between the specimen's surface temperature and the air temperature inside the kiln. However, this gap gradually narrowed until both air and specimen temperatures reached the target level (in this case, 800ºC), and during the one-hour holding period. A similar finding for FA-based geopolymer concrete was reported by Ahmed and Vimonsatit (2014).

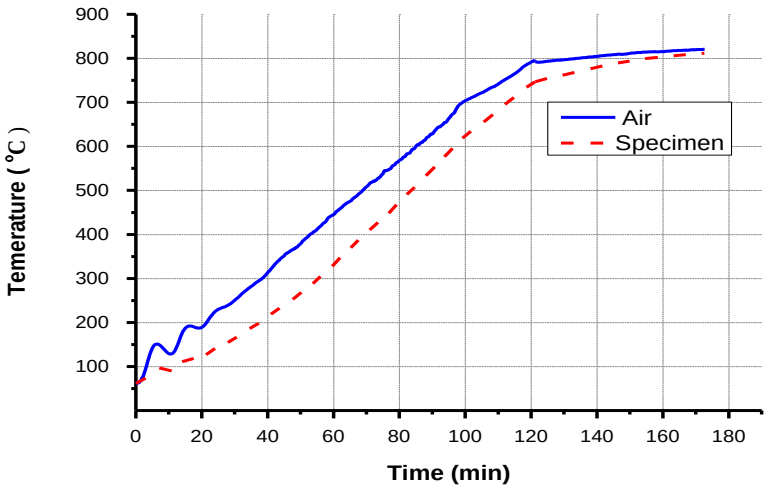

Figure 6.1 HFF specimen surface and air temperature during heating to 800°C

It should be noted that some specimens were inserted into the kiln while it was still warm from previous testing (with the temperature slightly above room temperature). In this case, the elevated starting temperature had no effect on the HFF panels because all specimens were also preheated to 100 °C (24 hours) for the drying process.

The four-point bending test setup for the HFF panels inside the kiln is shown in Figure 6.2, and a detailed schematic is shown in Figure 6.3. A clear test span of

580 mm was used for all specimens. A constant moment zone of 200 mm was used to determine the flexural strength of the panels. The kiln was positioned under a load jack with a 50-kN load cell connected to the top of a steel loading frame. A circular opening in the upper part of the kiln provided access to the loading cylinders, as can be seen in Figure 6.2. During the heating process, the hole in the kiln was sealed using rock wool to prevent heat loss.

The residual compressive strength of both mixes was also measured for 50-mm cubes after exposure to elevated temperatures of 200, 400, 600 and 800°C as well as ambient temperature.

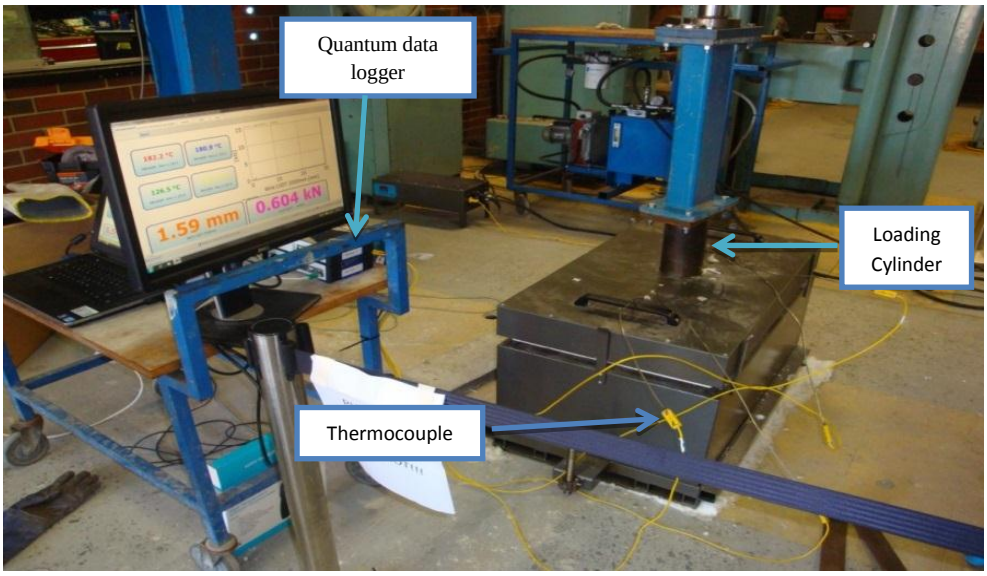

Figure 6.2 Test setup of *in situ* four-point bending test at elevated temperatures

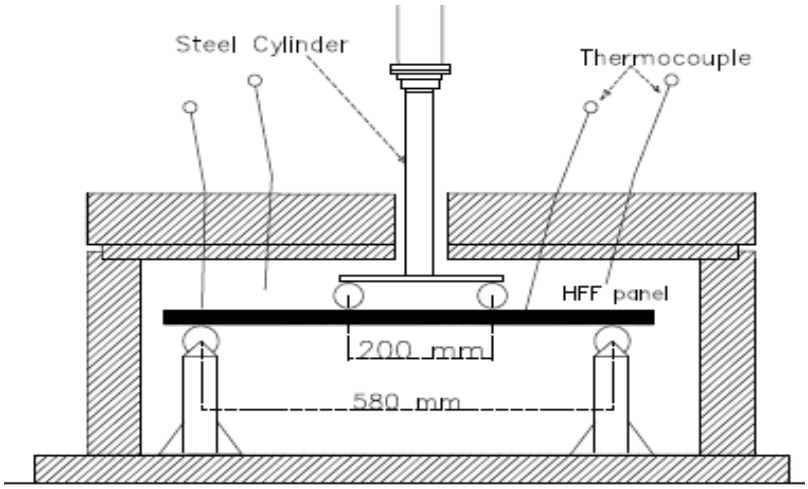

Figure 6.3 Schematic of *in situ* four-point bending test of HFF panels inside the kiln at elevated temperatures

6.2.3 Flexural behaviour of HFF panels at elevated temperatures

The flexural load–deflection behaviours of HFF2* and HFF2 mortar panels at various elevated temperatures are shown in Figure 6.4. Both panel types exhibited reduction in maximum load-carrying capacity as temperatures increased to 800ºC. However, at 200 and 400ºC, HFF2 (containing FA and SF) exhibited higher maximum load than HFF2* panels, as seen in Figure 6.4. Ductility (deflection capacity at peak load) was also improved at 200 and 400ºC, by ~16%, as a result of FA and SF in the ferrocement panels.

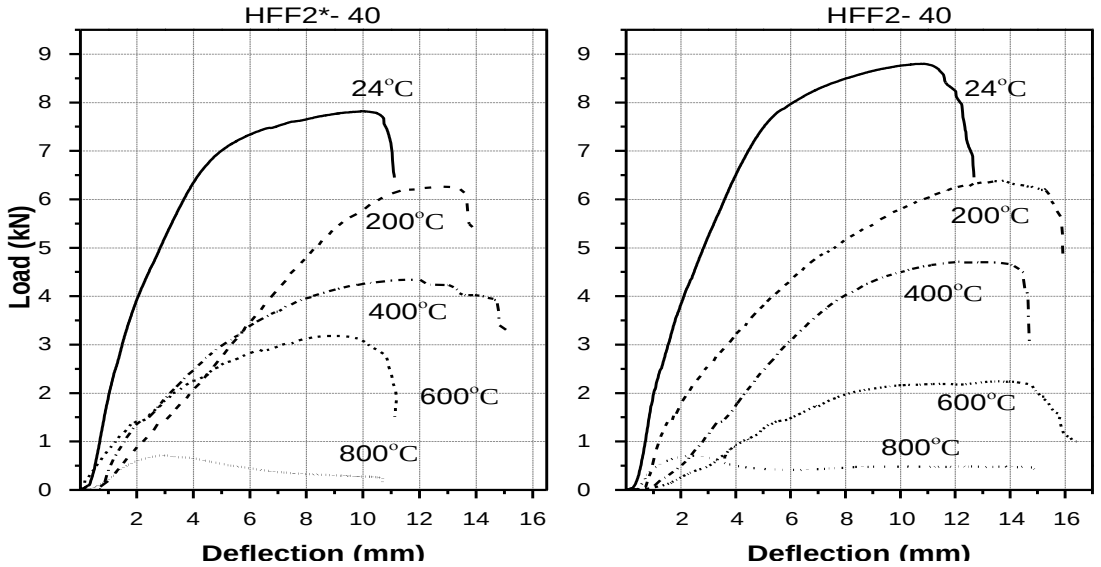

Figure 6.4 Load *vs.* deflection of HFF*2 and HFF2, 40-mm-thick samples tested at evaluated temperatures

It is clear that the steel and mortar experienced relatively large displacements during exposure to fire but had different deformation values (Purkiss 2007). This caused a geometric nonlinearity or second-order effect at those temperatures and led to increased moment and deformation capacity. It also induced microcracks in the interfacial transition zone of the fibre matrix. This zone is known to be more susceptible to damage to its flexural strength and elastic modulus than to its compressive strength (Mehta and Monteiro 2006).

One possible reason for the strength and ductility gain at higher temperatures in HFF panels containing FA and SF is the formation of tobermorite due to the addition of FA. Tobermorite is a calcium silicate hydrate mineral that forms due to a

reaction between un-hydrated FA particles and lime at elevated temperatures (Tanyildizi, Harun and Coskun. 2008). It improves the adhesion between the aggregates and the paste (Mehta and Monteiro 2006), which explains why the residual compressive strength of HFF2 mortar was higher than that of HFF2* at almost all elevated temperatures. The high resistance of HFF2 mortar at elevated temperatures was also probably due to the formation of tobermorite in the presence of FA, increasing the melting temperature of PVA fibres in the matrix. As a result, more PVA fibres survived at elevated temperatures in HFF2 than in HFF2*, providing better flexural behaviour in the ferrocement panels in the HFF2 series.

Figure 6.5 compares the maximum strength of HFF2* and HFF2 panels at various temperatures. The tested mixtures showed a steady decline in maximum strength capacity. The results at 800^{o}C indicate that FA had a negligible effect at those temperatures.

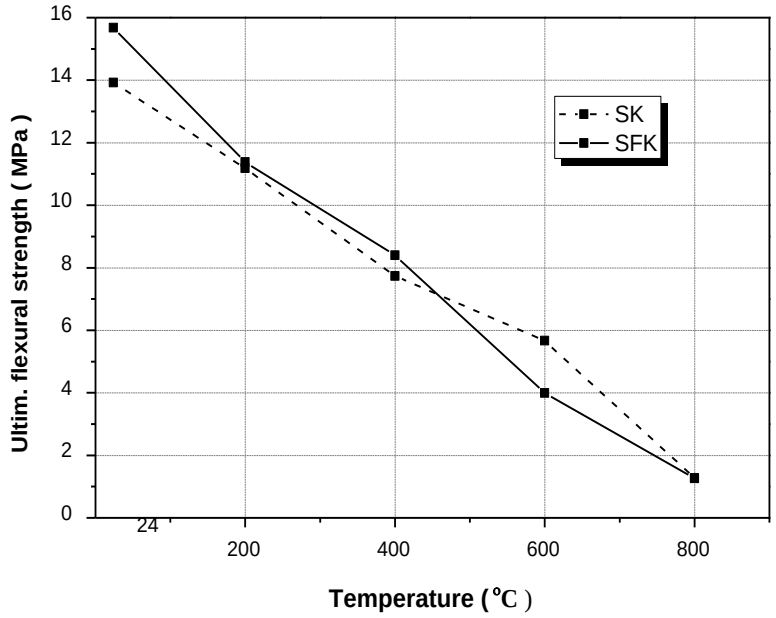

Figure 6.5 Ultimate flexure strength for HFF*2 and HFF2 panels at different temperatures

6.2.4 The effect of panel thickness on flexural behaviour of ferrocement at evaluated temperatures

The effect of differing panel thickness (25 and 30 mm) on the flexural behaviour of ferrocement specimens made with HFF2 mortar, which exhibited better flexural

behaviour at elevated temperatures, is shown in Figure 6.6. To allow direct comparison, the total fibre volume fraction and the wire mesh quantity were the same as for the 40-mm-thick ferrocement panel (Figure 6.4, HFF2 samples). The 800ºC test is not considered here because at this temperature the load-carrying capacity was relatively small.

A summary of the effects of panel thickness on maximum strength and its corresponding deflection capacities for all ferrocement panels at elevated temperatures is shown in Figure 6.7. The maximum flexural strength of HFF panels decreases with increasing temperatures up to 600ºC. However, thicker panels achieved greater maximum loads than thinner ones. The 25-mm-thick panel resisted the lowest maximum load in comparison with the 30-mm and 40-mm-thick panels, as seen in Figures 6.6 and 6.7, but due to the reduced thickness, its calculated equivalent flexural strength is the greatest, as seen in Figure 6.7(a). The 25-mm-thick ferrocement panels also exhibited better ductility in terms of higher deflection at peak load, than for the 30- and 40-mm-thick panels at all elevated temperatures, as seen in Figure 6.7(b).

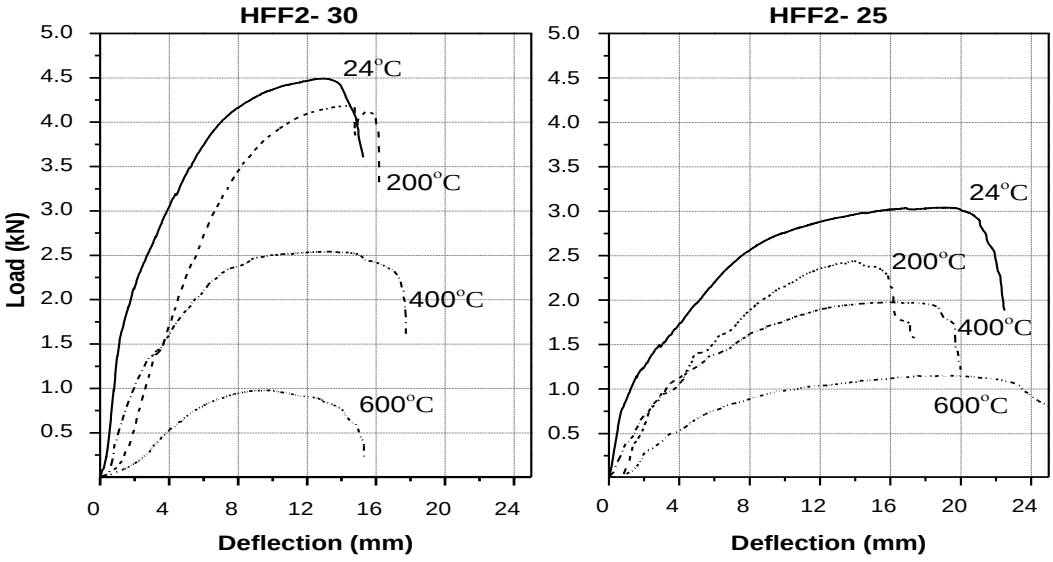

Figure 6.6 Elevated temperature effects on the load–deflection curve of panels with different thicknesses

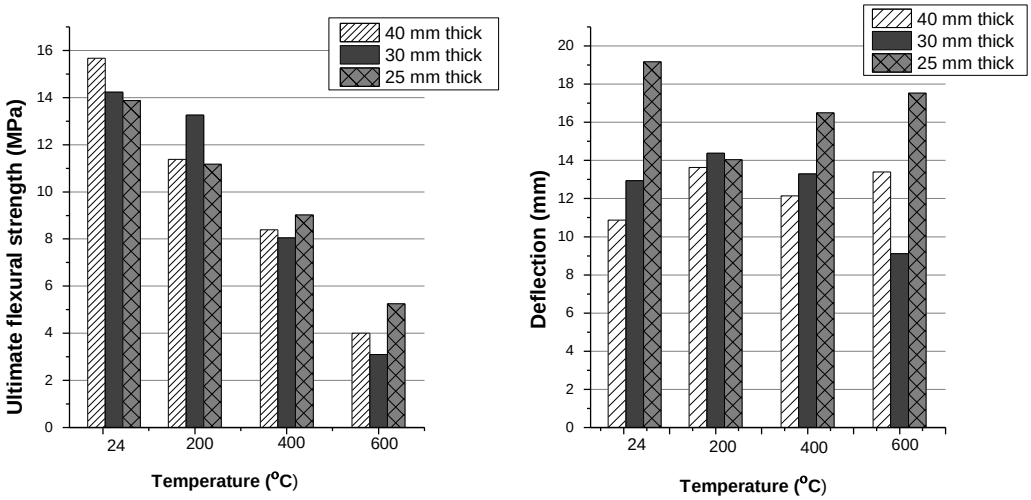

(a) Equivalent flexural strength (b) Deflection

Figure 6.7 Effects of panel thickness on ultimate strength and its corresponding deflection at elevated temperatures

6.2.5 Effect of mineral admixtures on residual compression strength of mortar at elevated temperatures

The effect of the addition of mineral admixtures on the residual compressive strength of hybrid PVA fibre-reinforced mortar at a range of elevated temperatures is shown in Figure 6.8. The residual compressive strength of the mortars was measured on a 50-mm cube that was cooled to room temperature shortly after being heated in the kiln. The residual compressive strength of hybrid PVA fibre-reinforced mortar containing mineral admixtures was higher than without mineral admixtures at all elevated temperatures. As mentioned above, the formation of tobermorite is believed to be responsible for this improvement. Tobermorite is a calcium silicate hydrate mineral that is formed due to the reaction between un-hydrated FA particles and lime at elevated temperatures (Tanyildizi, Harun and Coskun. 2008; Şahmaran et al. 2011). Tobermorite improves the adhesion between the aggregates and the paste and enhances the compressive strength, even at higher temperatures. The typical failure behaviour of the specimens after compression tests is shown in Figure 6.9.

In addition, it was suggested (Dias et al. 1990) that the addition of pulverized fly ash increases the destructive critical temperature of 400°C to 600°C for Portland

cement concrete. This was associated to the effect of fly ash in reducing the amount of $Ca(OH)_2$ present in a hydrated cement paste prior to heating.

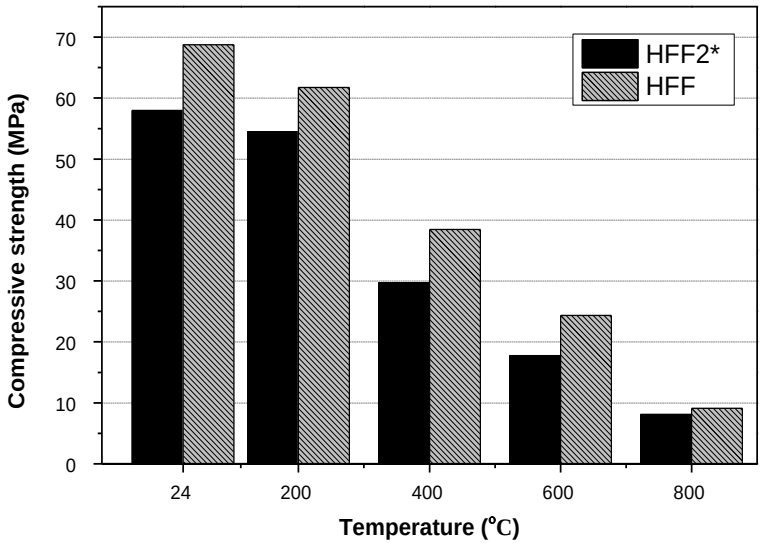

Figure 6.8 Compressive strength of HFF mixtures after exposure to different temperatures

(a) (b) (c)

(d) (e)

Figure 6.9 Failure behaviour of HFF2 mixture specimens after compression tests: (a) at ambient temperature; (b) 200 °C; (c) 400°C; (d) 600°C; and (e) 800°C

6.2.6 Microstructure changes due to elevated temperatures

Via SEM observations, a microstructural analysis was conducted on samples taken from the cores of the HFF ferrocement panels after exposure to temperatures of up to 800°C to study the behaviour of the fibre and matrix microstructure, as shown in Figure 6.10.

Figure 6.10 (a–a*) shows general views of PVA fibres in an HFF control sample at ambient temperature. Partial or minor surface damage to the PVA fibre at 200°C can be seen in Figure 6.10 (b–b*). At 400°C, the PVA fibre was in a more extensive damage stage, and had melted extensively, leaving a weak, porous skeletal structure, as can be seen in Figure 6.10(c). At 600°C, the PVA fibres had completely melted and created small channels with microcracks, as shown in Figure 6.10(d). After exposure to 800°C, the cracks in the empty channels had widened, as can be seen in Figure 6.10(e).

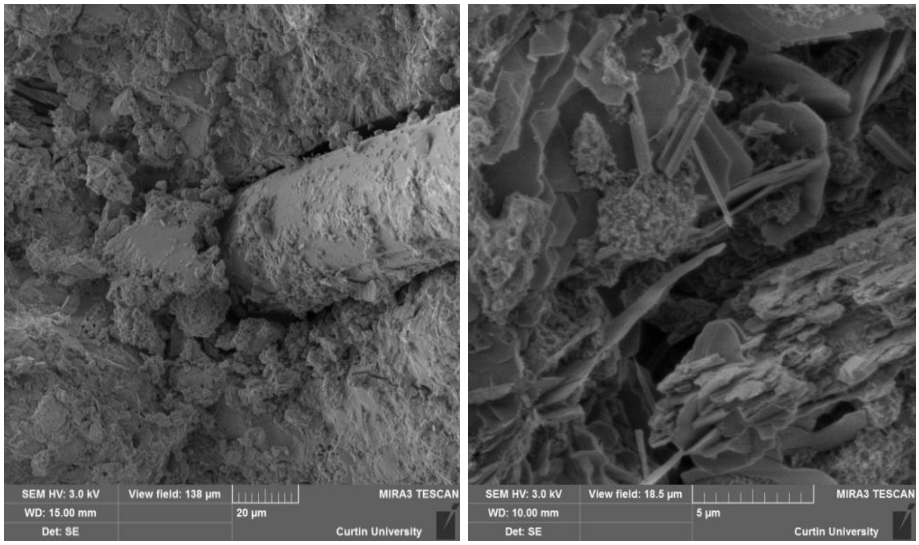

(a) (a*)

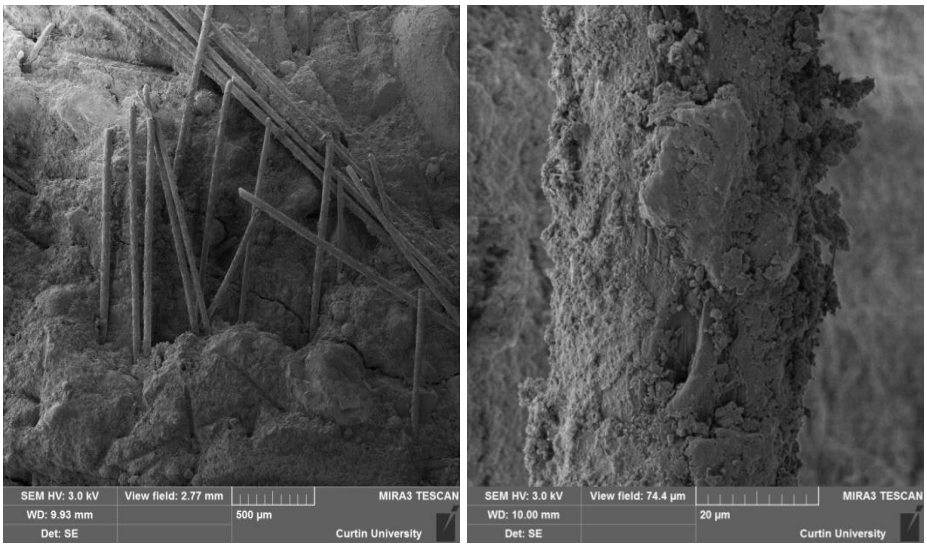

(b) (b*)

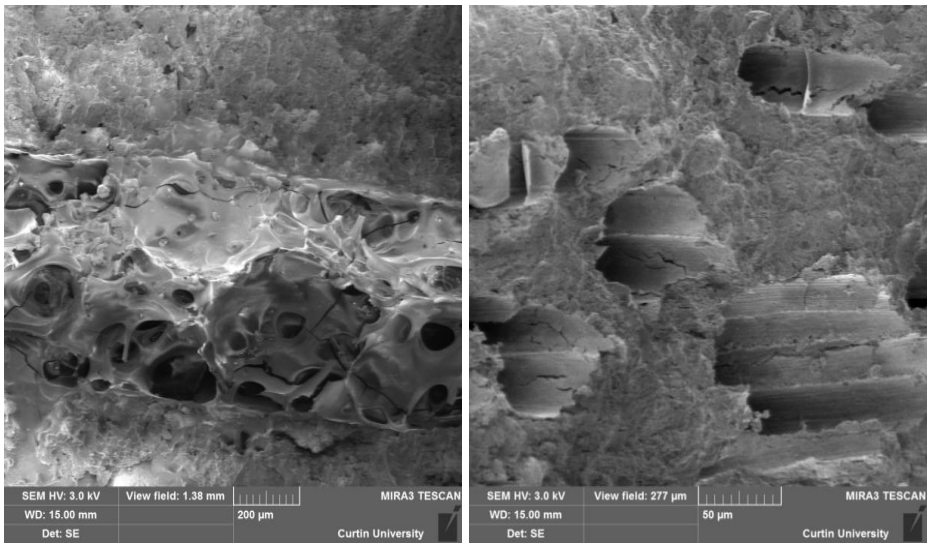

(c) (d)

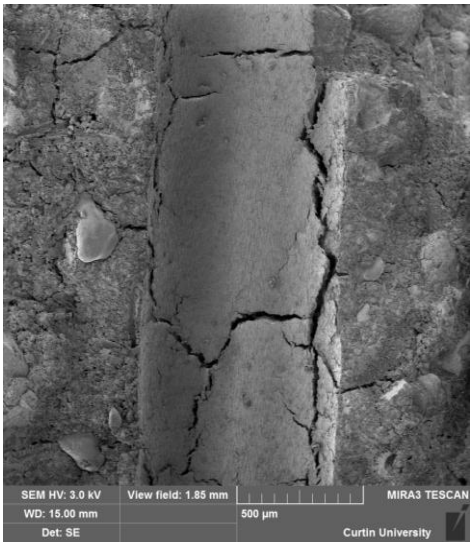

(e)

Figure 6.10 SEM micrograph of HFF2 samples at elevated temperature: (a–a*) control (ambient); and (b–b*) after 200°C; (c) 400°C; (d) and800°C exposure

6.2.7 Multiple cracking behaviour of ferrocement panels at elevated temperatures

In this study, it was observed that the loss of flexural load-carrying capacity for the ferrocement panels was significant at 400ºC and above. This can be attributed to the formation of voids in the form of empty micro-channels due to the melting of PVA fibres, the microcracking of the matrix due to the evaporation of free-bonded water in the matrix and the decomposition of calcium hydroxide crystals. In Figure 6.11, the cracking behaviour of the surface of the ferrocement panels after testing at elevated temperatures is shown. All panels tested for flexure at various temperatures showed multiple cracks. Specimens tested at 400°C and above appeared to have more complex crack structures than those tested at lower temperatures. Further, the widths of the cracks increased with temperature.

It is also evident from Figure 6.11 that the PVA fibres improved the resistance to spalling in ferrocement panels: no spalling occurred, even after the specimens were cooled down after exposure to 800°C; similar to results reported by Şahmaran et al. (2011).

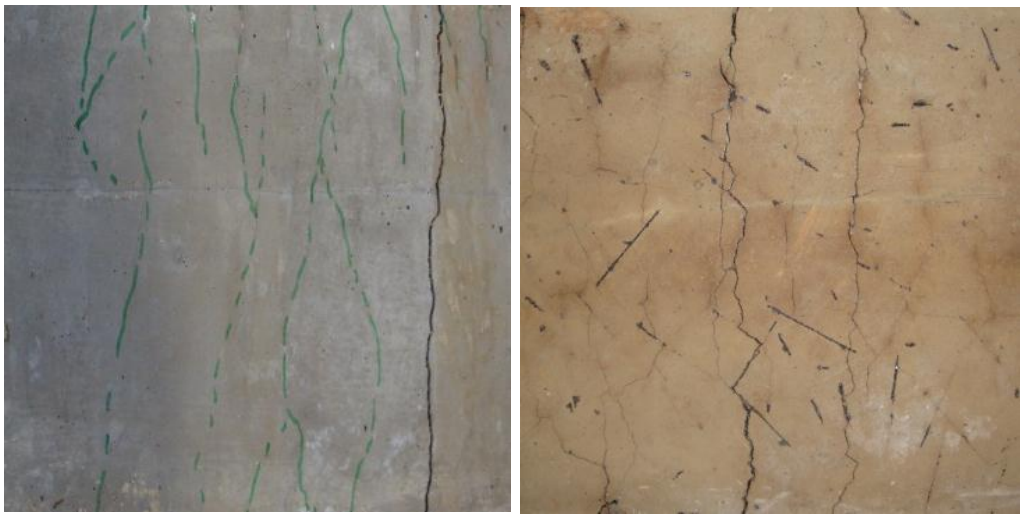

HFF-200 HFF-400

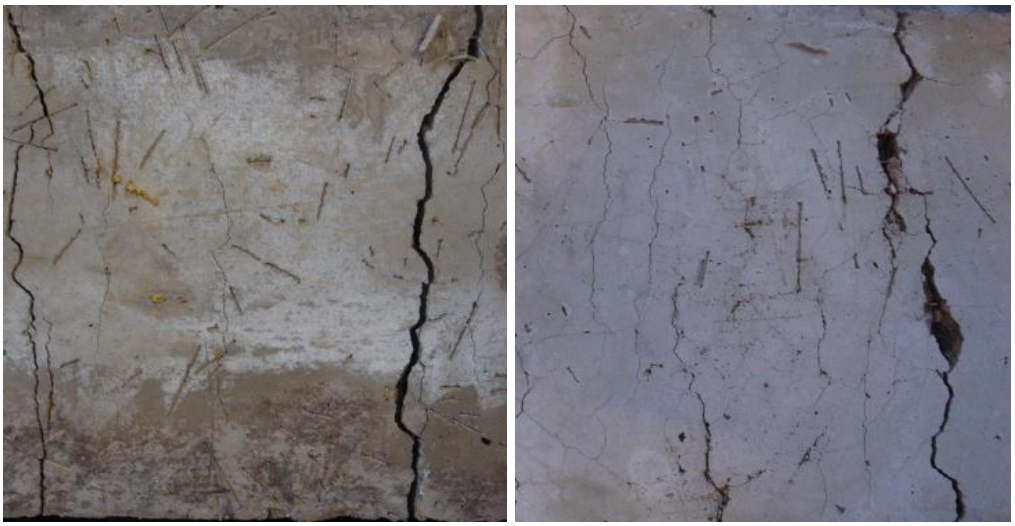

HFF2-600 HFF2-800

Figure 6.11 Cracking behaviour of hybrid PVA fibre after exposure to elevated temperature and testing under four-point bending

6.2.8 Theoretical prediction of flexural capacity of ferrocement panel

The flexural capacity of the ferrocement panels tested at elevated temperatures has been predicted theoretically. The moment capacity of FRC was calculated by Szerszen, Szwed and Li (2006), using a simplified method based on tensile reinforcement yielding. In this method, the consideration of the compatibility conditions of the cross-section and the stress–strain relationship are significant. Wang, Naaman and Li (2004) reported strong agreement between the theoretical values and their experimental results by applying this method to predict the moment capacity of mono fibre ferrocement. The significance of this approach is that the fibre's capability to bridge the cracks is considered in the tensile zone, as seen in Figure 6.12.

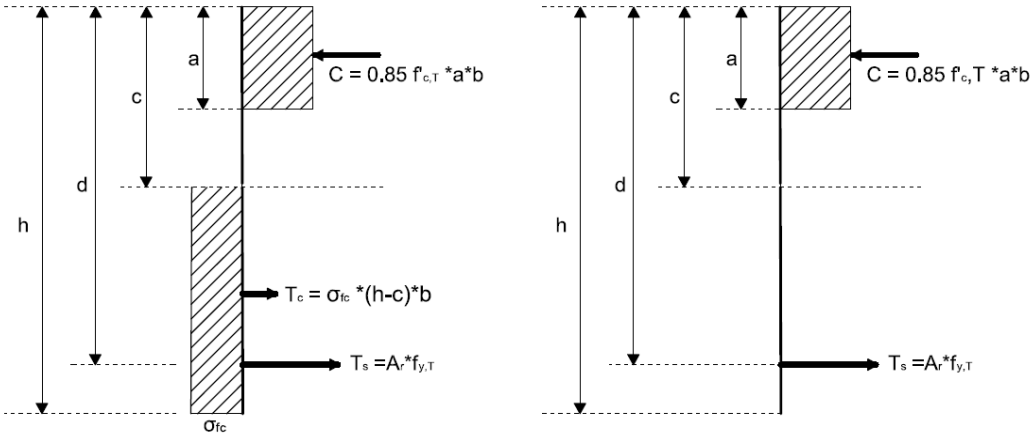

(a) **(b)**

Figure 6.12 Stress distribution in the cross-section of HFF: (a) at ambient up to 200°C and (b) for ≥ 200°C

A similar approach was used here in the prediction of the moment capacity of HFF panels at elevated temperatures to predict strength-reduction factors. The flexural load–deflection behaviour of HFF panels indicated deflection hardening behaviour. Therefore, a uniform stress distribution in the tensile zone at ambient temperature and 200°C was assumed. Because both PVA fibres reached their complete melting temperature at approximately 350°C, the uniform tensile stress of the matrix beyond 400°C was considered to be zero. For simplicity, it was further assumed that only one layer of tensile mesh was active across the wire mesh reinforcement area. This allowed the prediction of the force and moment equilibrium equations to calculate the depth of the rectangular stress block (a) and the moment M_n for various temperatures, as follows for temperatures ≤200°C (Equations 6.1 and 6.2) and >200°C (Equations 6.3 and 6.4):

$$c = \frac{\sigma_{fc,T}\, b\, h + A_r \eta_{s,T} f_{y,T}}{0.85 f'_{c,T}\, 0.66\, b + \sigma_{fc,T} b} \quad (6.1)$$

$$M_n = \frac{1}{2}(A_r f_{y,T} \eta_{s,T}(2d - a) + \sigma_{fc,T}(h - c)b(h + c - a) \quad (6.2)$$

$$c = \frac{A_s f_{y,T} \eta_{s,T}}{0.85\, f'_{c,T}\, 0.66 b} \quad (6.3)$$

$$M_n = A_s f_y \eta_{s,T} \left(d - \frac{a}{2}\right) \quad (6.4)$$

where $f'_{c,T}$ is the compressive strength of HFF at elevated temperatures, A_r is the effective area of the wire mesh (according to ACI 549.1R-93, ACI Committee 549-R93 2009) and $\eta_{s,T}$ is the steel strength-reduction factor due to temperature for steel

(according to EN 1992-1-2 (1994-1-2 2005)). The flexural strength is reported to be five times the tensile strength $\sigma_{fc,T}$ in ECC (Maalej and Li 1994), This value was applied to the equations for various temperatures to adjust the experimentally measured moment. In contrast, Equations 4 and 5 are formulated without the contribution of the mortar's tensile strength due to the melting of the fibre.

Figure 6.13 shows a comparison between the predicted and experimental moment reduction ratios, along with the concrete reduction factor, according to EN1994-1-2 (1994-1-2 2005). The curve of the moment capacity reduction from the calculated ($M_{n,T}/M_n$) and test values ($M_{u,T}/M_u$) shows a relative good agreement, except at 200°C. This could be because of insufficient effective area in the tensile zone at maximum load in Equation 3, due to minor partial damage to the fibre at 200°C, but not at ambient temperature. Moreover, the tested and predicted curves follow the same trend as the yield strength-reduction factors for the concrete material ($k_{c,\theta}$) provided in EN1994-1-2 but with much reduced factors at 400 and 600°C. This outcome indicates that the effect of elevated temperatures is greater on the structure level than on the material level in HFF panels.

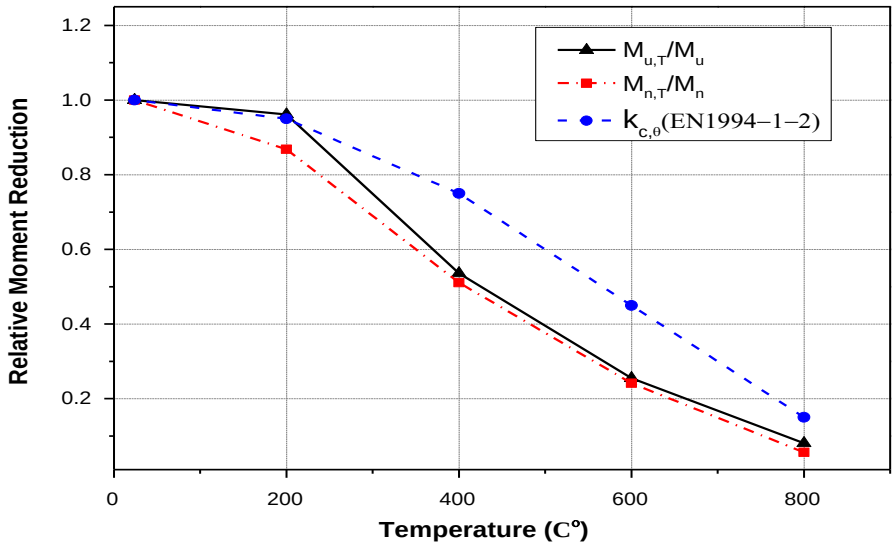

Figure 6.13 Comparison of calculated ($M_{n,T}/Mn$) and tested ($M_{u,T}/M_u$) moment reduction ratio at elevated temperatures

6.3 Carbonation effect on the structural and microstructural behaviour of HFF composite

Steel reinforcement in cement-based composites like concrete is physically and chemically protected from corrosion by the surrounding matrix, which is very alkaline (pH ~13.5) (Papadakis, Vayenas and Fardis 1991). Penetrating carbon dioxide (CO_2) dissolves and reduces the pH by reacting with the hydrates already contained in the mixture, leading to the build-up of calcium carbonates ($CaCO_3$) in ordinary Portland cementitious materials. Consequently, the reinforcement is no longer protected and is expected to corrode. This carbonation process leads to the degradation of the steel reinforcement in cement composites (Monkman and Shao 2006). The carbonation of cement composites mainly depends on the porosity of the matrix, the moisture content of the matrix and the CO_2 content in the environment. Under appropriate conditions, the calcium hydroxide ($Ca(OH)_2$) obtained from a reaction chain will carbonate according to the following reaction:

$$Ca(OH)_2 + CO_2 + H_2O \rightarrow CaCO_3 + 2H_2O \qquad (6.5)$$

Equation 6.5 shows that carbonation is a CO_2-consuming process. In general, CO_2 can be absorbed from almost all combinations of calcium and converted to stable calcium carbonates.

The focus of this investigation is on the effect of carbonation curing of HFF samples on their structural performance and the effect of time-derived carbonation on strength development for HFF materials proposed for structural applications. The tests include the determination of carbonation effects of the mixture on the PVA fibre and wire mesh—in other words, the effect of carbonation on mortar performance associated with its compressive strength, and the whole composite attributed to its flexural response after carbonation. The carbonation of the CO_2-subjected specimens was quantified using phenolphthalein solution. The reaction was characterised by examining the carbonated materials using X-ray diffraction (XRD) and SEM.

6.3.1 Test setup and mixture proportion

A plexiglass chamber was built for curing the samples in a CO_2 environment at a controlled relative humidity of 68%; the optimal humidity rate for carbonation lies between 40 and 70% (Wierig 1984). To accelerate the carbonation process on the specimens, the CO_2 supply was fixed at a constant rate of 6% for 15, 30 or 45 days. The curing chamber and the specimens subjected to the specific environment are shown in Figure 6.14.

Figure 6.14 Carbonation chamber

The mixture quantities for the materials are shown in Table 6.3. The binder (cement and FA) to sand ratio for all mixtures was 1:1. A small amount (5% *w.t.*) of SF was added to the mixtures containing FA. The cement, FA and SF components were provided in Tables 3.1 and 3.2. Only samples with wire mesh were for used in flexure tests. However, 200 cubes of size 50×50×50 mm were subjected to different compression strengths; that is, from each mix five for initial (28 days), and five for the samples placed in the carbonation chamber for 15, 30, 45 days. All cubes were placed in the chamber after the initial 28 days curing. In addition, 64 panels of size 300×150×30 mm, for mixtures HFF1, HFF2, HFF5 and HFF9 were tested for their flexural strength after 28 days curing, and 15, 30 and 45 days in the chamber. The panel size and test setup can be seen in Figure 6.15.

Table 6.3 Mixture proportion for the tested samples

Mix number	OPC	FA	PVA1	PVA2	W	Wire mesh	Total binder
	(g)	(g)	(g)	(g)	(ml)	(%)	(g)
HFF1	7,500	2,500	121.9	365.6	3,800	0.5	10,000
HFF2	7,500	2,500	243.8	243.8	4,000	0.67	10,000
HFF3	7,500	2,500	365.6	121.9	4,500	-	10,000
HFF4	8,800	1,200	243.8	243.8	3,800	-	10,000
HFF5	8,800	1,200	365.6	121.9	4,000	0.5	10,000
HFF6	8,800	1,200	121.9	365.6	4,500	-	10,000
HFF7	10,000	0	365.6	121.9	3,800	-	10,000
HFF8	10,000	0	121.9	365.6	4,000	-	10,000
HFF9	10,000	0	243.8	243.8	4,500	0.5	10,000
F	10,000	0	-	-	4,000	-	10,000

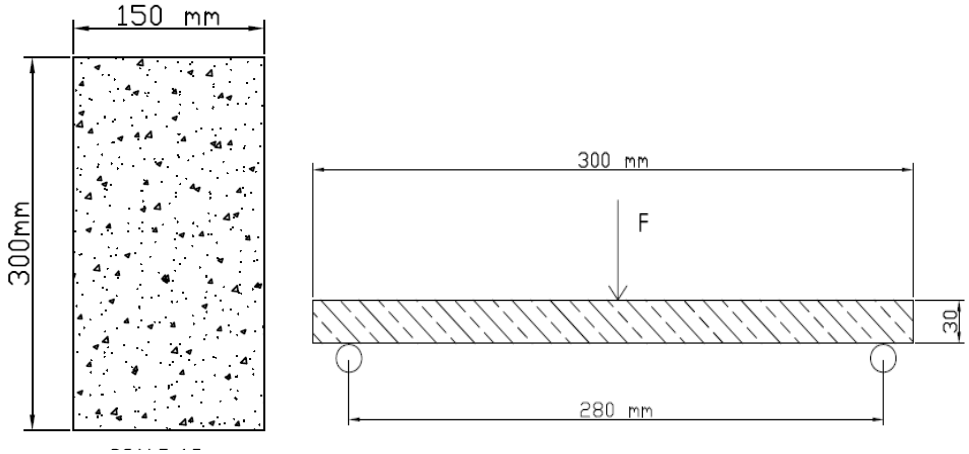

Figure 6.15 Specimen size and flexure test details

6.3.2 Assessment of carbonation of the HFF composite

Carbonation curing of HFF mixtures was an accelerated curing process due to the high humidity and the constant flow of CO_2 gas into a curing chamber at 24°C. The injection of CO_2 into the stored samples under low pressure led to transformation of CO_2 into solid $CaCO_3$ (Monkman and Shao 2006). Understanding the effect of this

chemical change on the strength behaviour and the microstructural component requires chemical, structural and microstructural evaluation.

6.3.2.1 Phenolphthalein test

Measurement of the carbonation depth and carbonated area was achieved by spraying a phenolphthalein solution onto the split surfaces of the cubes to reveal H-dependent colour change. The pH indicator range of phenolphthalein is 8.3–9.5 (Lee et al. 2012). Carbonation of specimen surfaces sprayed with the phenolphthalein solution is evident in Figure 6.16.

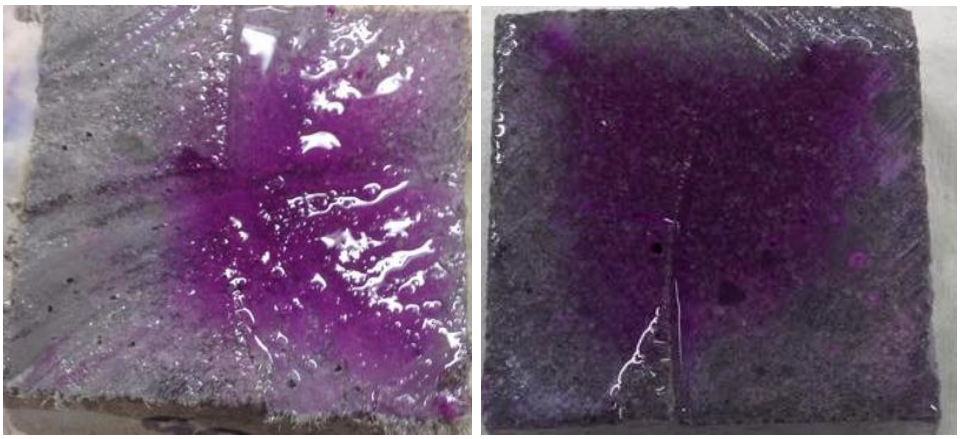

Figure 6.16 Detection of carbonation using phenolphthalein solution

Carbonation depth measurement can be achieved to an accuracy of 0.5 mm using this method. However, the change in the carbonation area after 15, 30 and 45 days curing time was conducted using the indicator method. The carbonated area (non-coloured surface of tested samples) was marked on a drawing to enable calculation of the carbonation area and the carbonation change (%) as shown in Tables 6.4 and 6.5. One disadvantage of this method is its reduced level of accuracy, although it still provides satisfactory information about the change in carbonation of the tested specimens over their total area. Therefore, the results can be used as an indication of the change in carbonation.

Table 6.4 Change in carbonation area and depth for all tested samples

Spec ID	Carbonation time		
	Day 15	**Day 30**	**Day 45**
HFF1	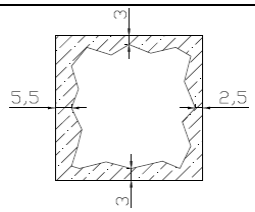	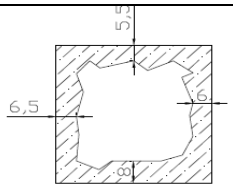	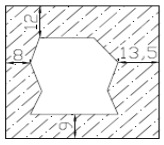
HFF2	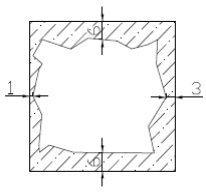	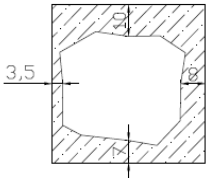	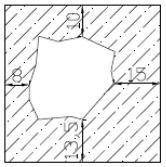
HFF3	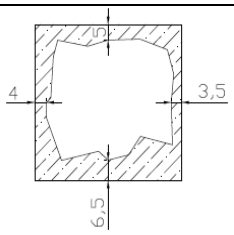	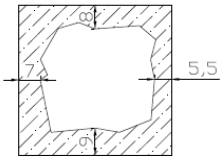	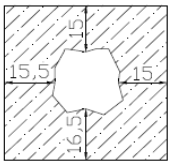
HFF4	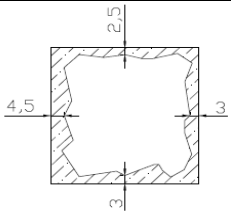	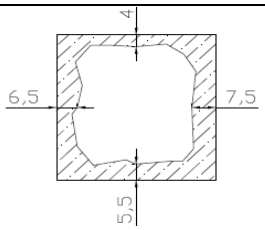	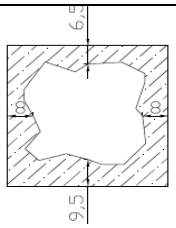
HFF5	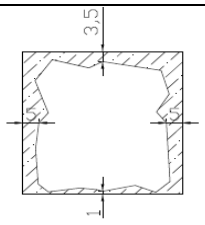	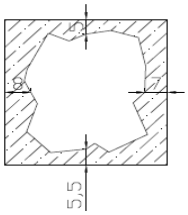	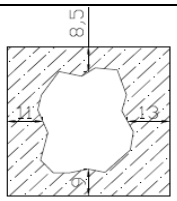
HFF6	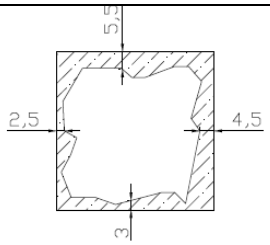	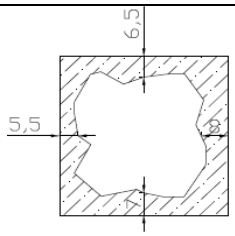	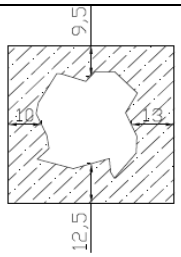

HFF7	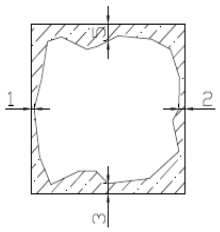	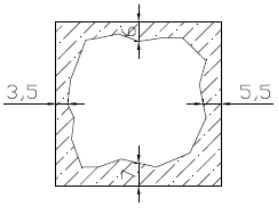	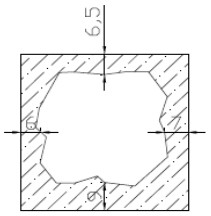
HFF8	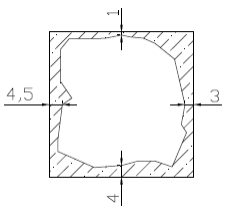	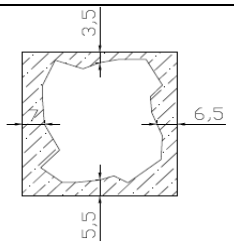	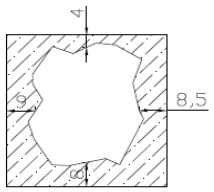
HFF9	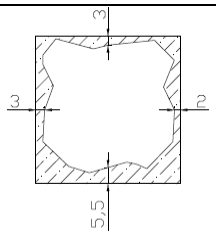	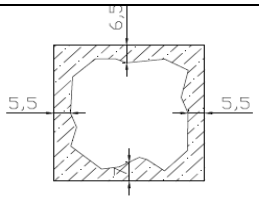	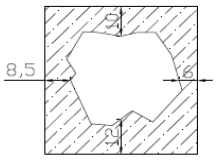
F	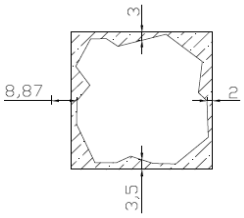	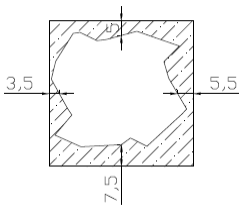	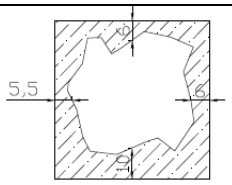

Table 6.5 Calculated carbonation area and percentage of carbonation change

ID	15 days		30 days		45 days		Final carbonation depth (45 d) (mm)
	Carbonated area (mm^2)	(%)	Carbonated area (mm^2)	(%)	Carbonated area (mm^2)	(%)	
HFF1	989.8	39.6	1252.6	50.1	1794.5	71.8	10.6
HFF2	1006.4	40.3	1280.9	51.2	1922.7	76.9	11. 6
HFF3	1081.1	43.2	1320.5	52.8	2133.4	85.3	15.5
HFF4	785.5	31.4	1081.6	43.3	1353.4	54.1	8.0
HFF5	774.1	31	1203.8	48.2	1682	67.3	10.4
HFF6	881.4	35.3	1202.9	48.1	1738.1	69.5	11.3
HFF7	755.8	30.2	1068.8	42.8	1287.8	51.5	7.1
HFF8	768.5	30.7	1072	42.9	1343.4	53.7	7.4
HFF9	762.8	30.5	1120.2	44.8	1596	63.8	9.1
Control	675.8	27	1083.7	43.3	1288	51.5	6.9

*Cross-section area 2500 mm^2

The results revealed increasing change in carbonation area with curing time. Specimens subjected to accelerated carbonation conditions exhibited a carbonation area of 64.6% on average. However, it may be necessary to take into account the relatively high carbonation depth, which affects the protection of the wire mesh from corrosion. Observations of the wire mesh in carbonated specimens (45 days) revealed minor changes on their surface, and only minimal corrosion (see Figure 6.17). However, the low level might be due to galvanised wire mesh being more resistant to corrosion. Nonetheless, the observations indicate that with increased curing time, the steel will become more corroded and damage will occur to a higher level. In contrast, there is no evidence of damage or change in the PVA fibre due to carbonation (see Figure 6.18).

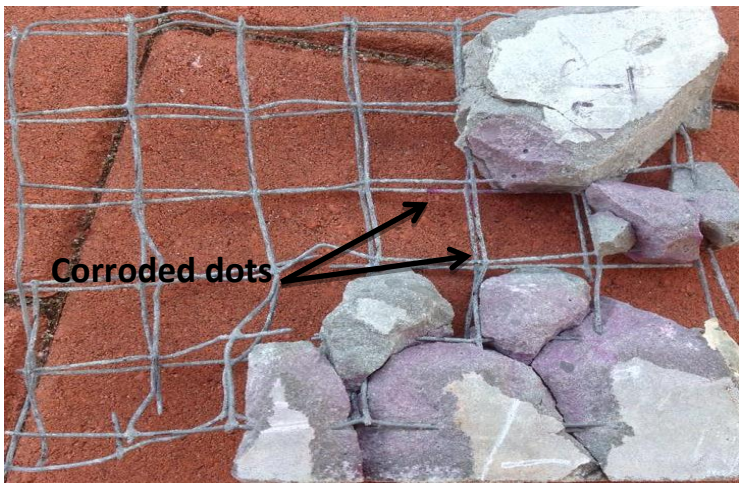

Figure 6.17 Changes in the wire mesh surface due to carbonation

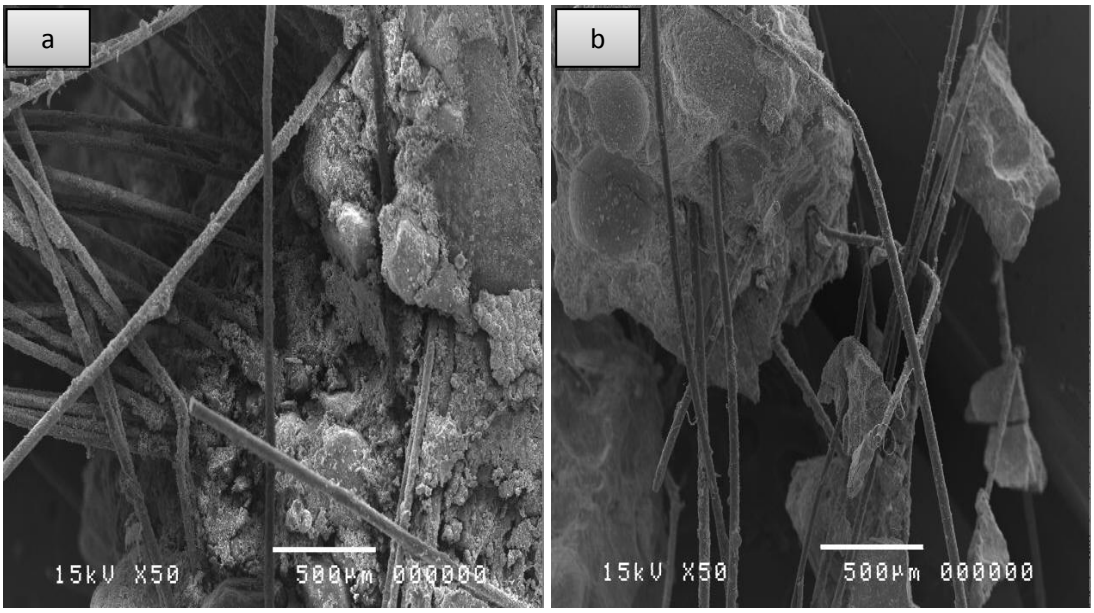

Figure 6.18 SEM images of PVA fibre in carbonated HFF specimens aftercarbonation for (a) 15 days and (b) 45 days

6.3.3 Strength development

6.3.3.1 Compressive strength development

The structural assessment of carbonation and its effect on the compressive strength is shown in Figure 6.19. All specimens showed an increase in compressive strength with curing time. Importantly, the HFF mixtures exhibited similar trends for strength increase to plain mortar (F). The compressive strength of mixtures with different water to cement ratios and FA content increased slightly, in comparison with non-carbonated specimens. The $CaCO_3$ (calcite) that was produced filled the gaps in the matrix due to its higher volume compared with the water (H_2O). In other words, the solid $CaCO_3$ serves as an infill product increasing the packing density of the matrix, which leads to increased compressive strength (Chi, Huang and Yang 2002). Moreover, among samples with similar carbonation time, those that showed higher compressive strengths exhibited smaller carbonation depths. This is logical, as carbonation and compressive strength both depend on the matrix age (Dias 2000) and structure.

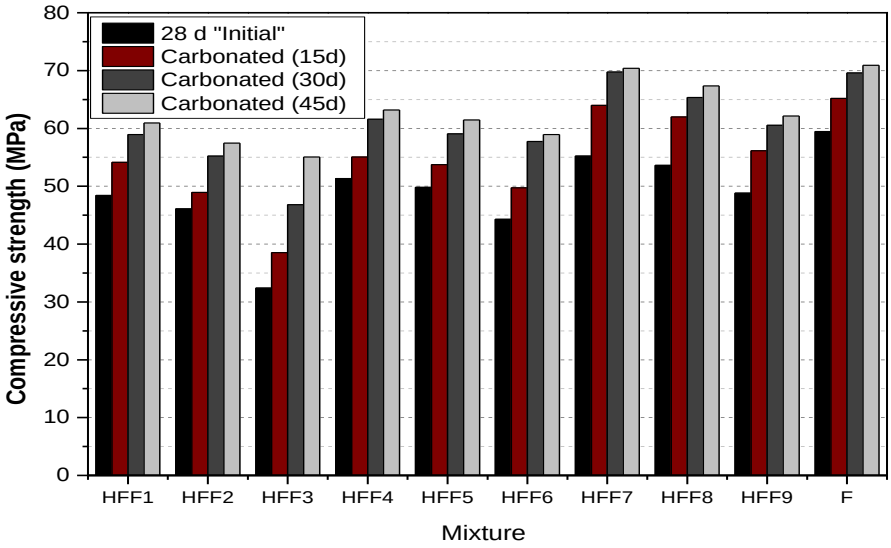

Figure 6.19 Compressive strength development of specimens initially, and after different curing times

To determine the mixture components influencing the carbonation process, the Taguchi method was used based on the fact that the production of calcite $CaCO_3$ increases the compressive strength. The difference in the compressive strength of carbonated samples (45 days) and non-carbonated samples was used as the response to the factors. In other words, the increases in compressive strength were used as the indicator for carbonation. The mix components providing higher compressive strength are more likely accelerating the carbonation process, but the factors and levels used are similar to the study discussed in Section 4.6.3.

The Taguchi results are provided in Table 6.6, and indicate the ranking of parameters affecting carbonation. The water to cement ratio was the main factor influencing the carbonation process because higher water content is required to accelerate the carbonation reaction. The PVA fibre is in the second position, which might be due to the increased porosity caused by the presence of fibre in the matrix. In contrast, it was evident that samples with FA produced the highest level of carbonation (Monkman and Shao 2006). Here, the relatively low content of the FA in the matrix (<25%) may explain its insignificant effect on the carbonation process.

Table 6.6 *S/N* ratio of increase in compressive strength

Control factor	Mean *S/N* ratio			Delta	Rank
	Level 1	Level 2	Level 3		
FA content	22.96	22.05	23.39	1.34	3
Water–cement ratio	22.36	21.74	24.31	2.57	1
PVA1 rate	22.68	21.70	24.03	2.33	2

6.3.3.2 Tensile strength behaviour of carbonated samples

The carbonation phenomenon produces an environment that leads to the corrosion of wire mesh in cement mortar. The corrosion of wire mesh might have affected the structural behaviour of the HFF composite. The flexural test results for four mixtures of non-carbonated and carbonated panels are shown in Figure 6.20. However, the flexure strength behaviour of the carbonated and non-carbonated panels showed a similar trend. Some of the tested carbonated panel samples showed an increase in flexural strength compared to non-carbonated panels of the same mixture, where as other samples exhibited lower flexural strength.

In general, there was no clear trend in terms of flexural strength development. This could be due to several factors, one being that the wire mesh was still in a relatively good condition, such that carbonation did not affect its tension resistance. Another factor may be that carbonation had no significant effect on the flexure strength in the presence of PVA fibre; the fibre was not affected due to carbonation and still performs its role in resisting tension forces.

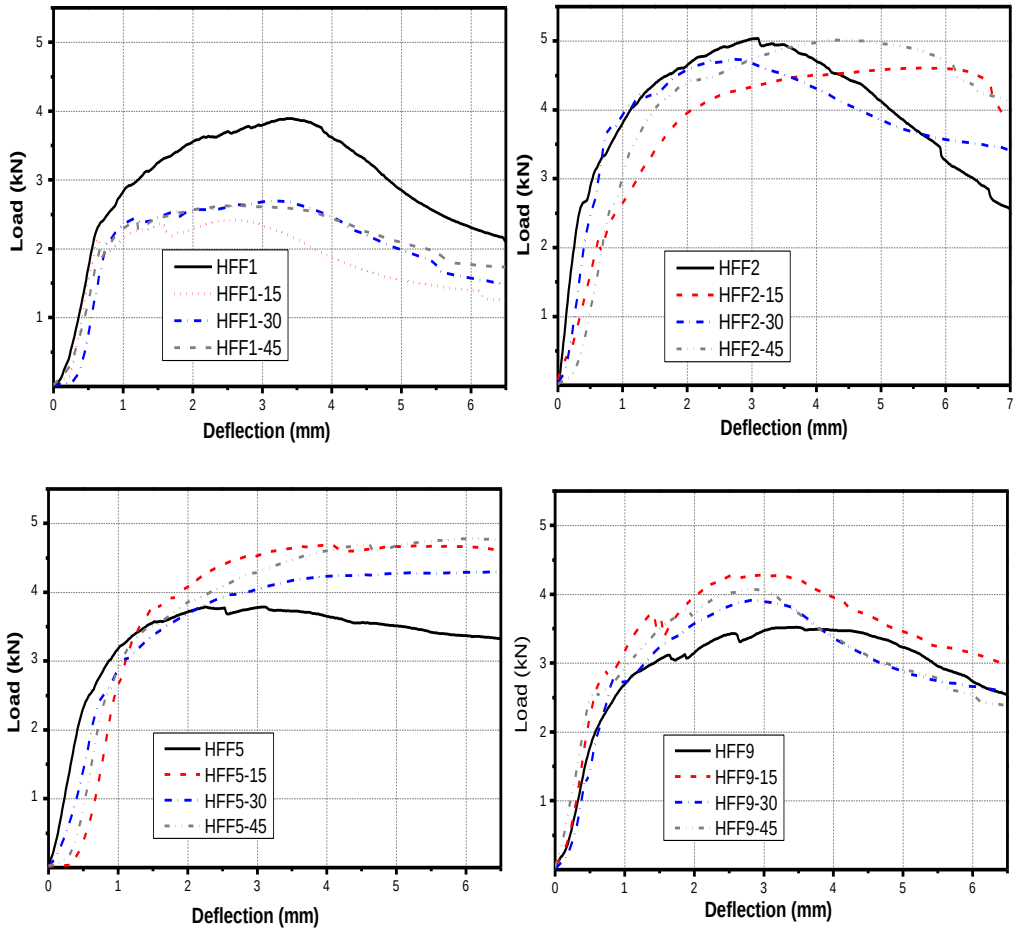

Figure 6.20 Flexural behaviour of carbonated and non-carbonated HFF panels

6.3.4 XRD analysis

The XRD test was performed to analyse the mixtures for carbonation. Figure 6.21 shows the XRD pattern of two HFF samples exposed to carbonation-accelerated conditions for 15 and 45 days (two for each curing time). There was evidence that some carbonates were present as calcite in the carbonated samples. The XRD pattern included a peak of $Ca(OH)_2$, indicating that not all of the cement paste had reacted. The presence of quartz SiO_2 (Q) and Portlandite $Ca(OH)_2$ (P) was also determined. A notable XRD pattern for the HFF mixture was that for natural calcite, which indicates that the main carbonation product was based on calcite $CaCO_3$ (C).

The carbonated HFF samples showed XRD peaks corresponding to calcite and calcium hydroxide, although the samples subjected to longer times at the accelerated environmental conditions (45 days curing time) showed a decrease in

intensity of the peaks corresponding to Portlandite. This reduction was an indication of $Ca(OH)_2$ consumption due to the carbonation reaction.

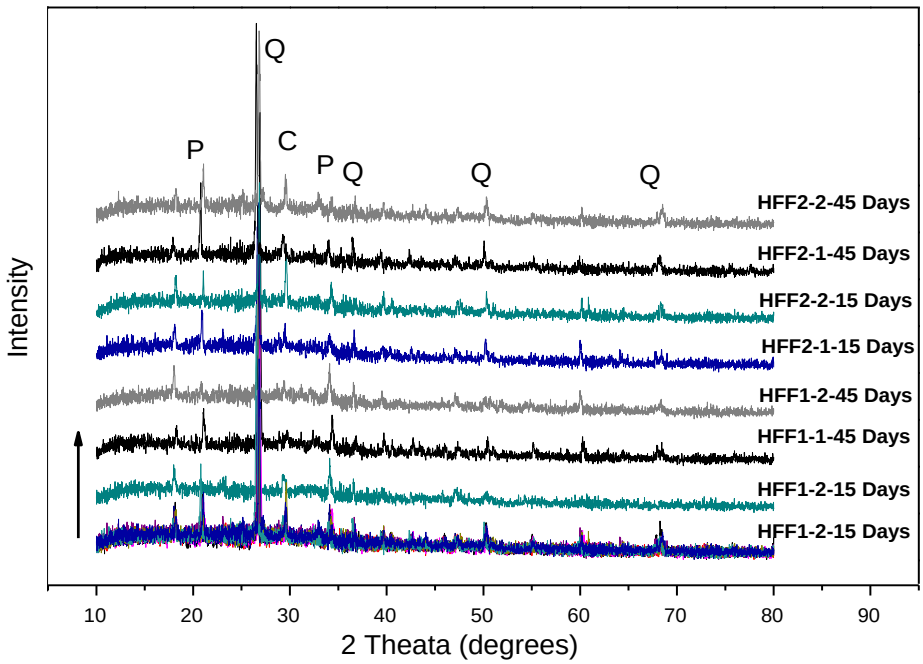

Figure 6.21 XRD patterns of carbonated HFF component: C = calcite, Q = quartz; P = Portlandite

A rough quantitative assessment of Portlandite consumption was made by comparing the sizes of XRD peaks at 2θ = 20.7° and 33.1°, as they varied in curing time and mixtures. A similar comparison for calcite at the only measured point 2θ = 29.5° was also made for assessing the increase in carbonation. The peak intensity comparisons are summarised in Table 6.7.

Table 6.7 XRD pattern ratio of HFF mixture

Peak location	**Average ratio (I45/I15)**		**Chemical product**	**Name**
(2θ °)	HFF1	HFF2		
20.7	0.89	0.87	$Ca(OH)_2$	Portlandite
29.5	1.24	1.20	$CaCO_3$	Calcite
33.1	0.95	0.96	$Ca(OH)_2$	Portlandite

The results indicate a decrease in the Portlandite, although it was not entirely depleted, suggesting that the carbonation process was not complete. On the other hand, the calcite ratio rose by ~20% with increasing carbonation time. However, the

non-carbonated content in all samples suggests that a curing time of 45 days in the chamber was much too short for completing the carbonation reaction.

SEM images of carbonated HFF mixture are provided in Figure 6.22, showing the microstructure of the scanned HFF sample near the surface of the carbonated HFF. New, irregular, flaky particles covering the matrix, with a size of approximately 1 μm, can be seen in Figure 6.22(a). The new material merged with the matrix in such a way that it was difficult to distinguish the form of the original cement product. Previous research has shown that the end product of a carbonised cement paste changes to a form of C–S–H, whose morphological structure is very difficult to identify (Berger, Youngand Leung 1972).

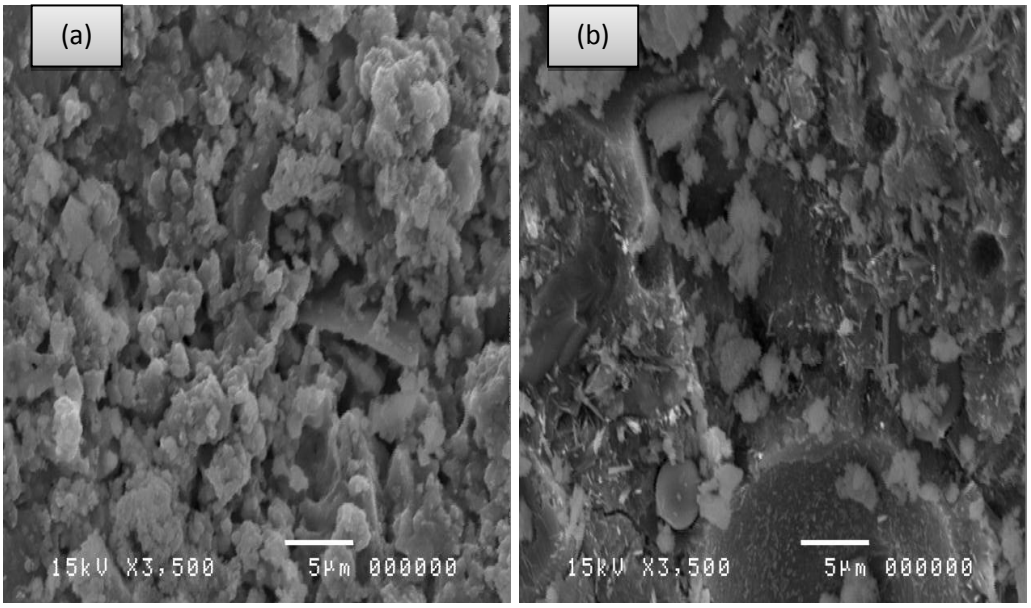

Figure 6.22 SEM photomicrograph of carbonation cured HFF mixtures; (a) after 15 days, (b) after 45 days curing in the carbonation chamber

The morphological microstructure of specimens with 45-day carbonation times (see Figure 6.22(b)) included some distinct morphological ettringite needles, which are evidence of unreacted $CaOH_2$. The sample may have been taken from a border zone between carbonated and non-carbonated area; however, the flaky products were recognised as calcite, which was observed in all other carbonated samples.

6.4 Concluding remarks

The effect of elevated temperature and carbonation were examined in this chapter. The addition of PVA fibre provided beneficial properties, including by enhancing resistance to high temperature. However, there was a small but insignificant drop in strength capacity of the composite heated to temperatures below the melting point of PVA fibre (230°C). Significant decreases in the strength capacity of the HFF panels were obvious at temperatures greater than 400°C, due to the complete melting of the PVA fibre. However, predictions of flexure capacity and strength-reduction factors using a simplified method based on tensile reinforcement yielding appear to be in good agreement with the EN1994-1-2 code.

The effect of carbonation on the strength capacity of the HFF composite was also presented in this chapter. Carbonation depth increased with exposure time to accelerated carbonation conditions. Moreover, the compressive strength of carbonated HFF mixtures was higher than that of non-carbonated samples. The bending test results revealed an insignificant effect of carbonation on the flexure behaviour of the HFF composite. However, further long-term studies may be required to provide a more complete understanding of the effects of carbonation on the flexural capacity of HFF composites.

Chapter 7: Application of HFF Panels as Permanent Formwork in One-way Concrete Slabs

7.1 Introduction

Slabs are structural elements subjected to initial and superimposed loads. One way to decrease the dead load is to use lightweight materials or lightweight infill materials such as AAC. However, the use of AAC concrete members in structural applications is very limited due to its low strength capacity compared to ordinary concrete (Vimonsatit, Mazlan and Nikraz 2011; Wahyuni, Vimonsatit and Nikraz 2012).

An alternative way to reduce weightis by employing thin cementitious composites such as ferrocement, which can be used in slabs (Nassif and Najm 2004; Hago et al. 2005; Clarke 2010; Paramasivam 2001; Anitha and Thenmozhi 2012; Aboul-Anen, El-Shafey and El-Shami 2009). The use of this material in model housing has been encouraged because of its structural performance and crack reduction behaviour (Alam et al. 2010), excellent corrosion durability due to the addition of FA (Bhikshma, Ravandekishore and Srinivas 2011) and relatively good flexural performance (Shannag and Ziyyad 2007). However, ferrocement has not been used for floor slabs because of its limited carrying capacity with respect to the loads to which floor slabs are generally subjected. Further, the mechanical specifications of ferrocement by itself are not very good when exposed to fire, because it is a thin material that only reduces spalling to a certain degree (Greepala and Nimityongskul 2008). Fibre has been added to ferrocement in efforts to improve its specifications (Wang, Naaman and Li 2004; El Debs and Naaman 1995; Pereira, Fischer and Barros 2012b), but such improved fibre-reinforced ferrocement has not been used in slab applications.

In contrast, ferrocement has been successfully used as permanent formwork in solid slabs, which means that it remains in place after casting and may not behave

as a composite fragment of the whole structural member (Spanos, Ravindrarajah and Swamy 2012). Therefore, the primary function of formwork is to create the required shape and to carry the weight of fresh concrete during casting of horizontal structural members such as slabs and beams. After the concrete has hardened, the formwork becomes part of the structure. The control of total composite behaviour is assured through the interaction between distinguished elements in their performance contribution to bearing applied loads. Applications of ferrocement as permanent formwork can be seen in columns (Katsuki 2003), beams (Fahmy et al. 2014) and slabs (Al-Kubaisy and Jumaat 2000; Yardim et al. 2013). The ferrocement cover provides a superior crack control mechanism, and increases stiffness and flexural strength capacity compared to solid slabs without this cover.

In the research described in the current chapter, HFF panels are used as permanent formwork in combination with one-way concrete slabs using AAC block as infill material. For simplicity, the tested slabs are abbreviated to 'HFF–OWC'. Weight reduction is achieved by the use of AAC blocks as infill material. AAC blocks do not have any structural function and could be replaced with any lightweight material. This investigation differs from previous studies (Yardim et al. 2013; Spanos, Ravindrarajah and Swamy 2012) in its use of HFF panels instead of conventional ferrocement; one-way concrete slab; AAC blocks as infill material; and a lower total slab height. The experiments focus on determining the effect of HFF panel height and using shear studs to connect slabs. The purpose of this study is to develop a double advantage (permanent formwork and weight reduction) structural construction system that enhances structural performance and durability in terms of fire resistance.

7.2 Test programme and materials description

The main test programme was conducted by testing 13 HFF–OWC slabs with a total depth of 155 mm. All slabs except for the control slab were modified with panels at the bottom of the concrete slab (tension zone). The slabs were 1220×1000 mm and simply supported. The test specimens were designed to cover four research variables; therefore, the specimens were arranged in three groups (S, C and T). Group S includes two control specimens, one being a conventional one-way concrete slab and the other

being modified with a conventional ferrocement panel in the tensile zone area. Group C consists of HFF panels with different connection studs to the one-way concrete slabs. The third group (T) contains slabs with different HFF panel thicknesses: 40, 30 and 25 mm.

The mortar mixture for the HFF panels contained 400 kg/m^3 cement, with a ratio of 0.75:0.025:0.40:1:0.05 by weight of cement, FA, water, sand and SF respectively. This was similar to mix B2 in Table 4.8, with a total fibre volume fraction of 1.5% but with compression strength of 63 MPa. In addition, the mixture proportions for the concrete were as described in Chapter 3: a cement:sand:aggregate ratio of 1.0:2.1:3.2 and a water-cement ratio of 0.45. The concrete mix was designed to have compression strength of 30 MPa at 28 days.

Shear stud connections were constructed using an M12 rebar with grade strength of 500 MPa. The 120-mm long rebar was welded to a steel flat bar (2.5×20 mm). Three types of shear studs were made as seen in Figure 7.1, and inserted into the last wire mesh layer during HFF panel preparation.

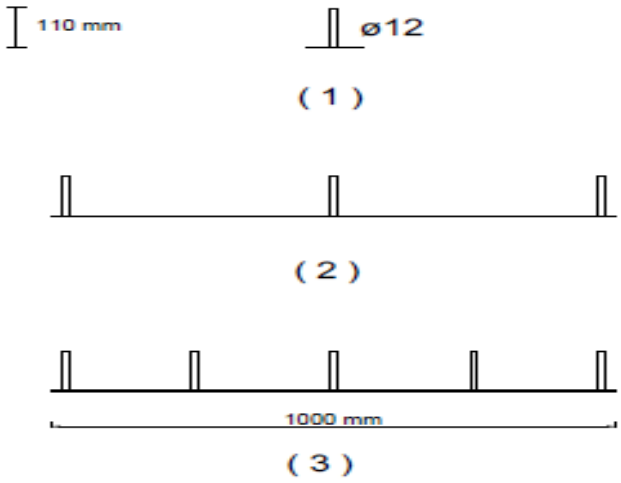

Figure 7.1 Shear stud connection types

The weight of the AAC blocks used was around one-quarter of the weight of normal concrete, which provides remarkable fire resistance and excellent sound and thermal insulation (Yardim 2008). Three AAC blocks of size 600×200×75 mm were tested to determine their flexural strength. The average maximum flexural strength was 0.7 MPa. Cubes of size 50×50×50 mm were cut to conduct a compression test. The average compressive strength was only 3.5 MPa, suggesting that the AAC blocks would have a negligible structural effect on the slab and are only acting as

infill. Thus, the AAC could be totally removed or replaced using any other lightweight infill material. However, the excellent insulation properties of AAC are an additional advantage in this slab concept. A slab cross-section is seen in Figure 7.2.

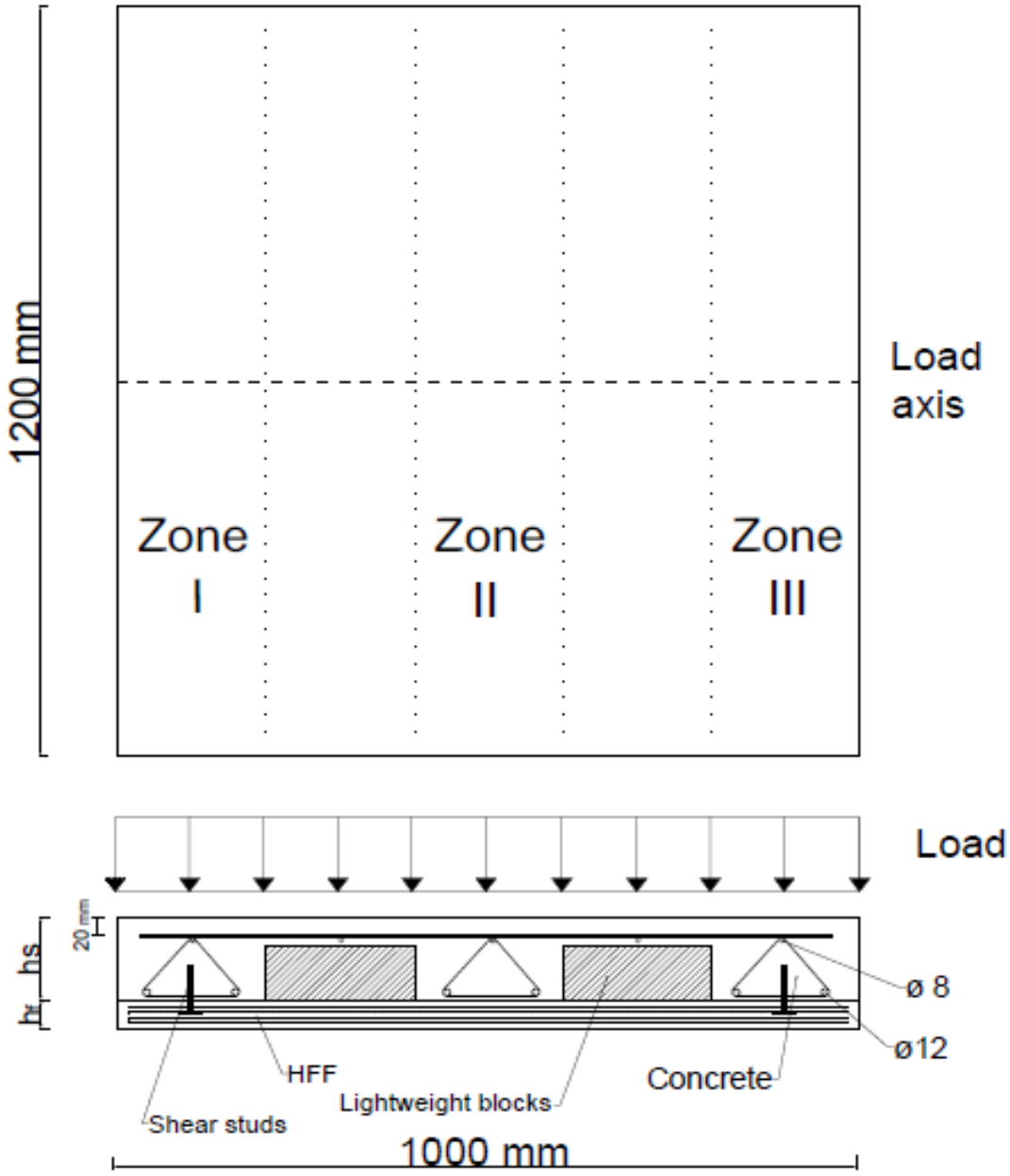

Figure 7.2 Slab cross-section, zone location of shear studs and load direction

7.3 Construction steps and system advantages

To determine the behaviour of HFF–OWC composite slabs in a bending test, 13 slabs of size 1220×1000×155 mm were constructed. The fabrication of the specimens

occurred in four stages: (1) placing the required wire mesh in the moulds and placing the shear studs under the top wire mesh layer; (2) casting the fibre-reinforced mixture and using a vibration tool to reduce air bubbles. The vibration process caused the fibre to set and ensures full penetration of the fibre matrix through the wire mesh. After a short time, the AAC blocks were placed in position in the wet mortar. The blocks adhered to the cement paste, which avoided any lift up during concrete casting; (3) placing the reinforcement with its required spacing; and (4) concrete casting and surface finishing work. Figure 7.3 shows the slabs during the typical fabrication process.

Figure 7.3 Slab construction and fabrication process

A potential benefit of using HFF panels in the tension zone of the concrete composite slab before casting is that they act as a form for the wet concrete, which remains permanently in place. This function contributes significantly to total cost reduction for *in situ* construction of floor slabs. Eliminating the cost of formwork removal drives the total slab production cost down. In particular, the total cost of

construction of multiple-storey buildings can be reduced due to the reduced time and production costs involved in applying this construction concept. Further labour hours can be saved by using precast panels that are precisely tailored to the project, and savings in material quantities could be achieved due to the decrease in slab thickness and the replacement of the concrete portion with infill material. The consequent weight reduction can have a chain effect on material reduction in other concrete structural members such as columns and beams, due to reduction in the acting superimposed loads.

7.4 Slab identification and test setup

Specimen identification according to their group and shear stud connection is shown in Table 7.1 and Figure 7.4. In this study, slabs are classified according to shear stud type. Here, the AAC block-free area is where the reinforcement and shear studs are placed. The total slab thickness including both the HFF panel and the concrete slab is 155 mm. The panel thickness is 40, 30 or 25 mm, which causes variation in the concrete slab thickness as seen in Table 7.1.

Table 7.1 Slab identification based on shear stud type and position

Group	Specimen ID	Panel thickness (mm)	Concrete slab thickness (mm)	Shear stud type	Zone	Location
S	S	-	155	-	-	-
	FS1	40	115	1	I, III	Corner
C	HFF–OWC2	40	115	1	I, III	Corner
	HFF–OWC3	40	115	2	II	Mid-area
	HFF–OWC4	40	115	2	I, III	Side area
	HFF–OWC5	40	115	3	II	Mid-area
	HFF–OWC6	40	115	3	I, III	Sidearea
	HFF–OWC7	40	115	1	I, III	Sidearea
	HFF–OWC10	40	115	Steel wire	I-III	Random
	HFF–OWC11	40	115	1	II	Mid- area
	HFF–OWC12	40	115	1	II	Mid-area
T	HFF–OWC8	25	130	1	I, III	Corner
	HFF–OWC9	30	125	1	I, III	Corner

The projected structure in this test contained two layers: PVA HFF panels and one-way RC. The slabs were simply supported; however, two Teflon® sheets (see Appendix B) were used on one support to ensure horizontal free movement on the support. The load was applied in the form of a uniform line load across the width of the slab, which appears from the front perspective as a point load. The clear testing span was 1000 mm to simplify calculations with respect to width, for comparisons of the test results with the control specimen. Twelve LVDTs (six for the top (concrete) and six for the bottom slab (HFF panel)) were used to measure deflection at a spacing of 200 mm in the slab's longitudinal direction. A 400-kN load cell and all LVDTs were connected to a Quantum data logger to record the test results. The test setup is shown in Figure 7.5.

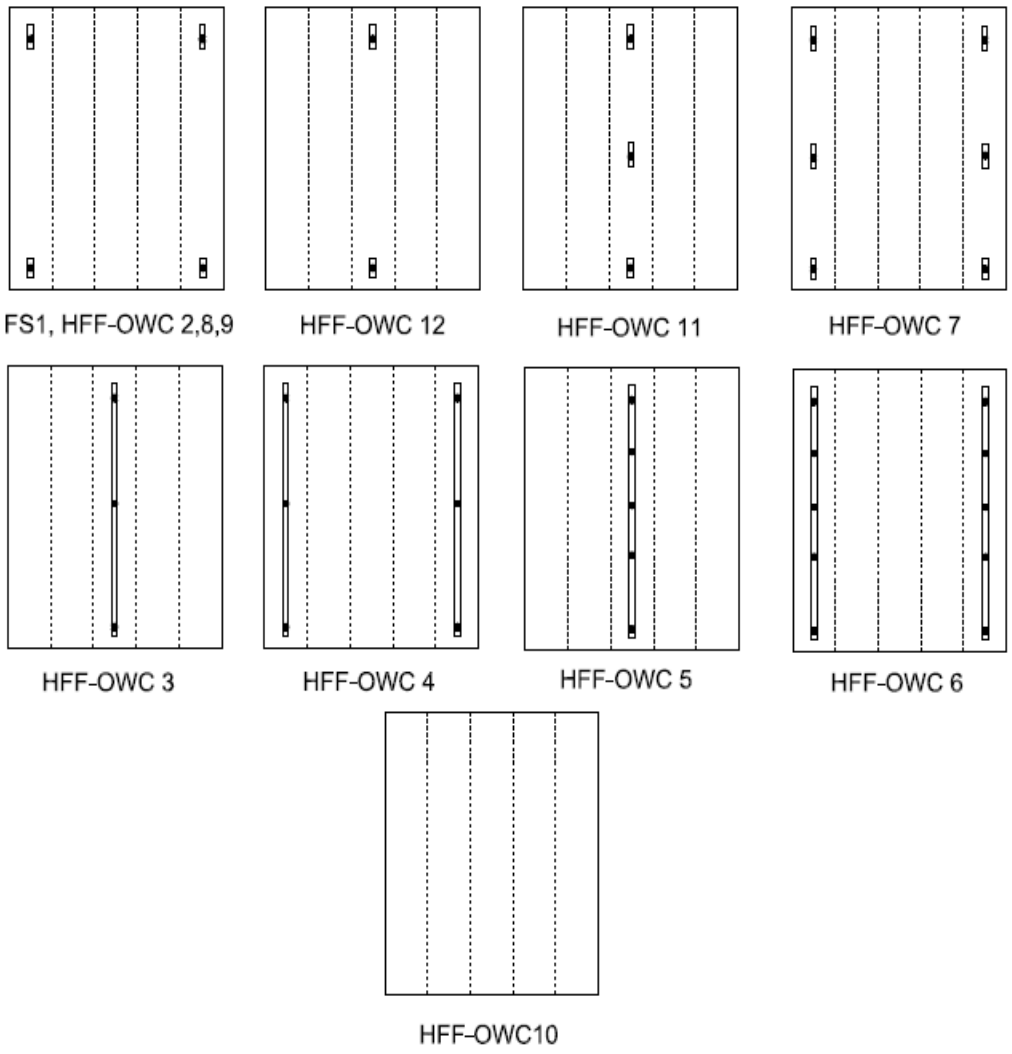

Figure 7.4 Shear stud type and position in all slabs

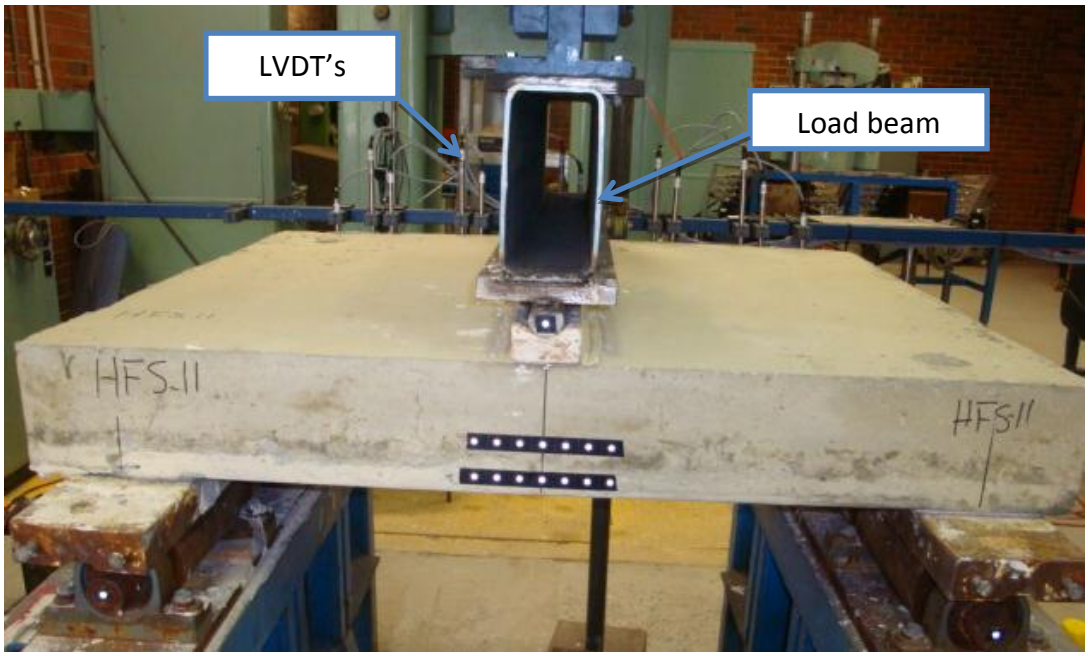

Figure 7.5 Slab test setup

7.5 Load–deflection behaviour of tested composite slabs

The load–deflection curves for control slabs (group S) were examined and compared with those for the HFF-OWC slabs (group C). All slabs had similar connection systems (shear stud type 1) except for slab S1, which had no permanent formwork on its bottom side. The resulting load–deflection curves are shown in Figure 7.6. The maximum load of slab HFF–OWC2 was greater than that for both control slabs. The hybrid fibre in the ferrocement apparently improved strength performance and ductility for the slabs, as seen from the load *vs*. deflection curve. However, the maximum load capacities were 245 kN for HFF–OWC2, 205 kN for slab S and 196 kN for FS1; an 18–20% increase compared with HFF–OWC2. The ductility of specimens with HFF and ferrocement cover was substantially better than that of the control slab, as seen in Table 7.2. However, the slab with the modified HFF plate exhibited the greatest ductility value, likely due to the PVA fibres maintaining their ability to increase the deflection capacity of the composite because of their relative low stiffness (Ahmed, Maalej and Paramasivam 2007b).

The overall better performance of HFF slabs in the tensile zone of this particular composite slab was due to the capability of the fibres in bridging crack formations, as reported in previous studies (Pereira, Fischer and Barros 2012b; Li,

Wang and Wu 2001; Wang, Naaman and Li 2004; Suwannakarn 2009) and in Chapter 4 here. Shorter fibres are activated at small crack formation and bridge the cracks at that scale. With increasing load the cracks extend and the crack openings grow until shorter fibres reach their maximum strength capacity and ruptured. The longer fibres then become active and bridge the larger cracks (Trueb 2011). At the same time, the wire mesh carries the increased tensile load until maximum load, when failure occurs with wire mesh rupture. This mechanism makes the use of HFF panels suitable for their proposed application as permanent formwork, due to their excellent ductility and strength performance. Importantly, the test results indicated strain hardening behaviour for the HFF panels tested as a composite slab in the tension zone. This enhanced strain behaviour increased overall performance and delayed first crack formation.

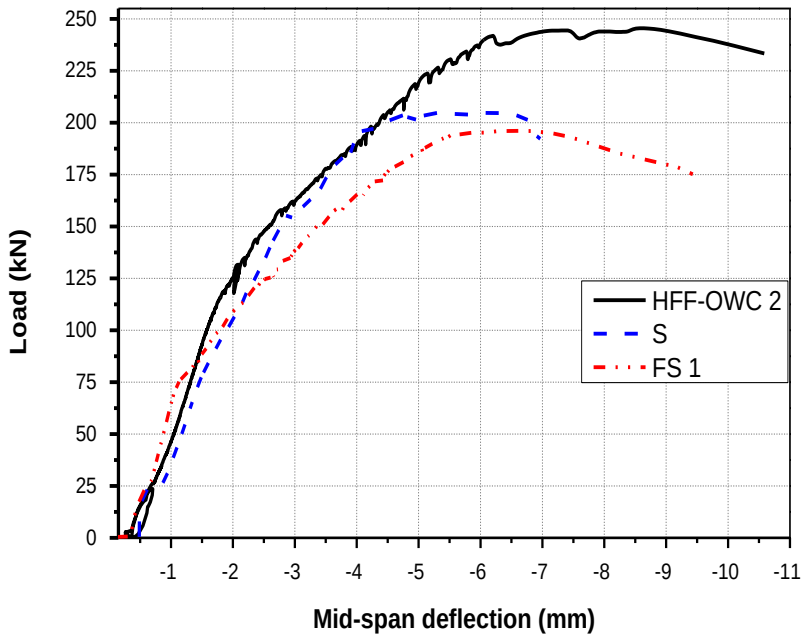

Figure 7.6 Load *vs*. deflection of control slab group S compared with HFF-OWC2, and FS1

Table 7.2 Ductility of the specimen

Specimen ID	Deflection at yielding (mm)	Deflection at maximum load (mm)	Ductility ($\partial u/\partial y$)
S	2.6	4.8	1.8
FS1	1.6	6.6	4.1
HFF-OWC2	1.9	8.6	4.6

7.6 Bending moment behaviour and failure mode using different shear stud connections

As shown in Figure 7.1, three types of shear stud connections and only one slab used simple wire ties (ϕ= 1.3 mm) to connect slabs. The load–deflection of the slab is shown in Figure 7.7. The higher load capacity in slabs using connection types 2 and 3 in comparison with slabs using type 1 was due to the additional tension resistance of the flat bar in those particular connection systems. The maximum load capacity of slabs using connection type 1 was still remarkable. The maximum load increase was achieved by increasing the volume fraction of this shear stud connection type. Specifically, the use of flat bars (stud types 2 and 3) increased performance through additional tensile capacity. In contrast, the location and number of shear studs (type1) had an insignificant effect on overall slab performance in comparison with slabs HFF–OWC2 and HFF–OWC13 (see Figure 7.7). Notably, all HFS slabs performed better and showed better ductility compared with the control slab S1. All tested slabs modified with HFF panels showed deflection hardening behaviour, which is an additional indication of high performance of HFF plates in a multifunctional application.

Table 7.3 summarises the moment capacity, ductility and failure mode of the slabs. All slabs showed excellent moment capacities and satisfactory ductility of over 2.4 (Yardim et al. 2013). The shear stud connection increased the load and, therefore, the moment capacity, implying that connectivity contributes significantly to overall slab performance (Al-Kubaisy and Jumaat 2000; Degtyarev 2014b). This was confirmed by comparing the carrying moment capacity of the wire-connected slab (HFF–OWC10) with the slabs in which connection studs were used to integrate panels with the upper concrete part.

Here, ductility was defined as the ratio of deflection at maximum load to that at yielding load. Therefore, it appears that the type of connectivity has a significant effect on the ductility: specimens using stud type1 exhibited respective increases of ~41 and 24% in ductility compared to slab specimens using connection systems 2 and 3. Slabs HFF–OWC3 and HFF–OWC5 gave unexpected results, so both slabs were re-fabricated and tested, with similar results as in the first test.

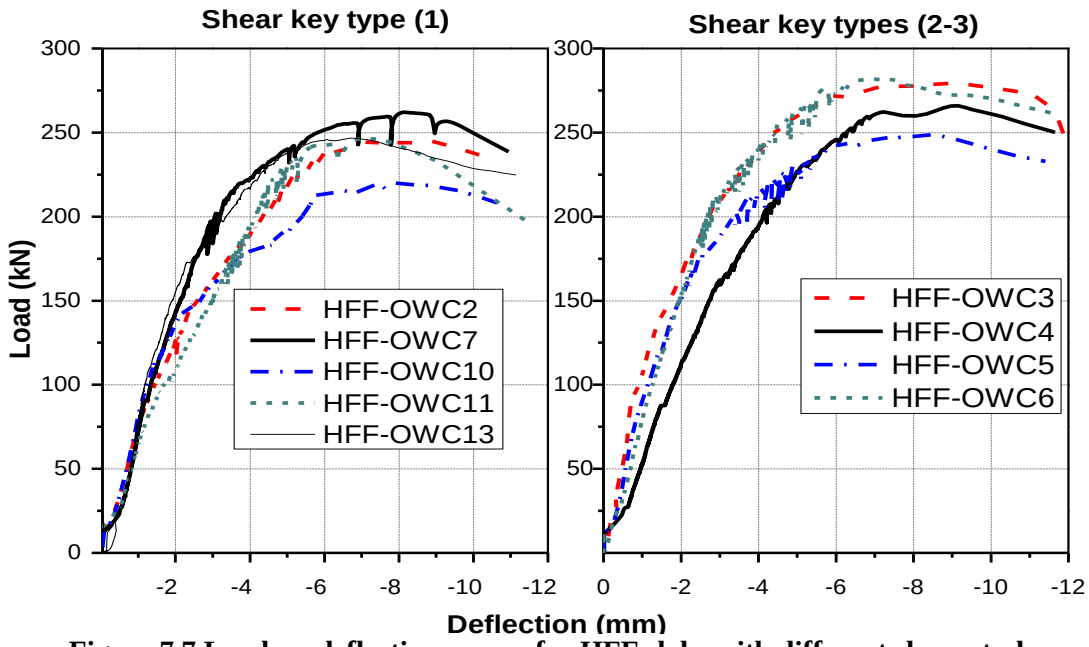

Figure 7.7 Load vs. deflection curves for HFF slabs with different shear stud connections

Table 7.3 Ductility of specimens

ID	Moment (kNm/m)		Moment ratio	Deflection (mm)		Ductility	Failure mode
	M_{cr} (Crack)	M_u(ultimate)	M_{cr}/M_u	At yieldload ∂y	At maximumload ∂u	$\partial u/\partial y$	
HFF–OWC10	23	55	0.4	1.9	6.4	3.4	Flexure
HFF–OWC2	27	61	0.4	1.9	8.6	4.6	Flexure-shear
HFF–WOC7	23	66	0.3	1.8	8.2	4.6	Flexure-shear
HFF–OWC11	21	62	0.3	1.8	7.4	4.1	Flexure-shear
HFF–OWC12	18	62	0.3	2.3	6.8	2.9	Flexure-shear
HFF–OWC3	24	70	0.3	2.7	6.7	2.5	Flexure-shear
HFF–OWC4	22	66	0.3	2.9	9.2	3.1	Flexure-shear
HFF–OWC5	30	62	0.5	2.2	8.4	3.9	Flexure
HFF–OWC6	16	70	0.2	2.4	6.9	2.8	Flexure

Crack patterns at the failure of some composite slabs are shown in Figure 7.8. In all slabs with the HFF panel, the first crack occurred in the HFF panel, followed by the development of multiple cracks in the mid-zone of the HFF panel. Further cracks extended the cracks developed in the de-laminated overlay of the upper concrete slab interface. Those cracks were an extension of the first cracks formed in the HFF panel; with increasing load, shear cracks appeared. At this stage, failure occurred in the slab composite so that the overlay one-way concrete slab failed by shear and the HFF panel by flexure. Importantly, all HFF panels exhibited multiple cracks at failure stage, as can be seen in Figure 7.9. All high performance indications such as deflection hardening and multiple crack formation were observed in slabs with HFF panels used in this study.

Notably, shear cracks along the interface of both slabs were only observed after failure and not at any other load stage. However, shearing occurred at the interface due to the continuing applied load after failure, which allowed further observations after the localisation points on both slabs. This might be because the HFF and concrete components of the composite slabs exhibited different failure modes, as seen in Figure 7.8 for slab HFF–OWC3. Further figures showing the crack pattern are seen in Appendix B.

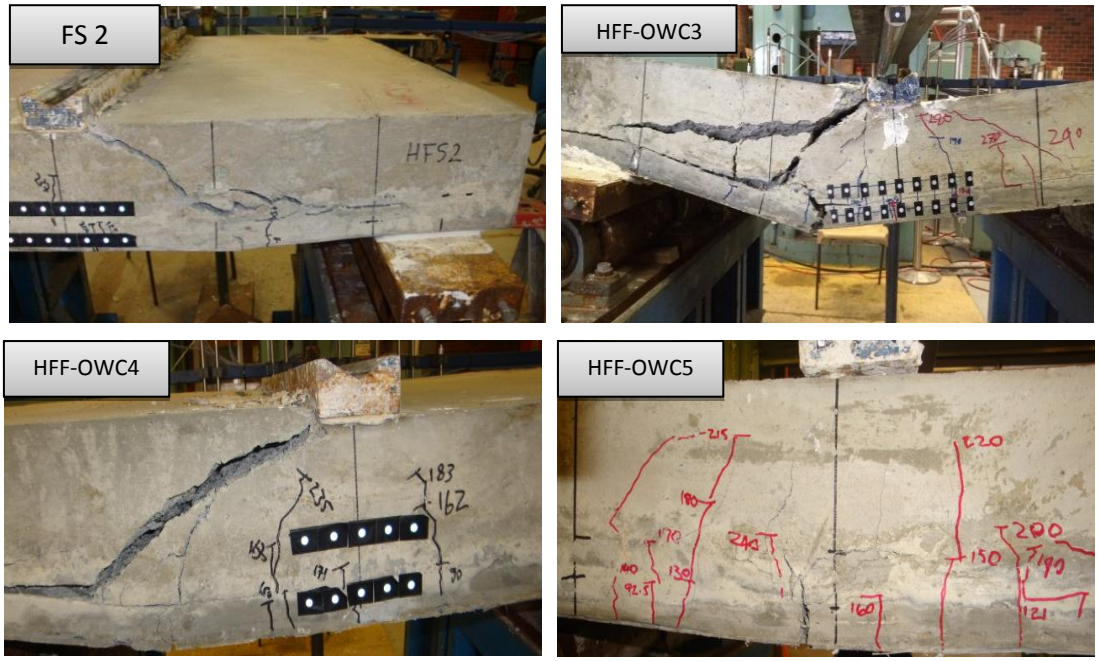

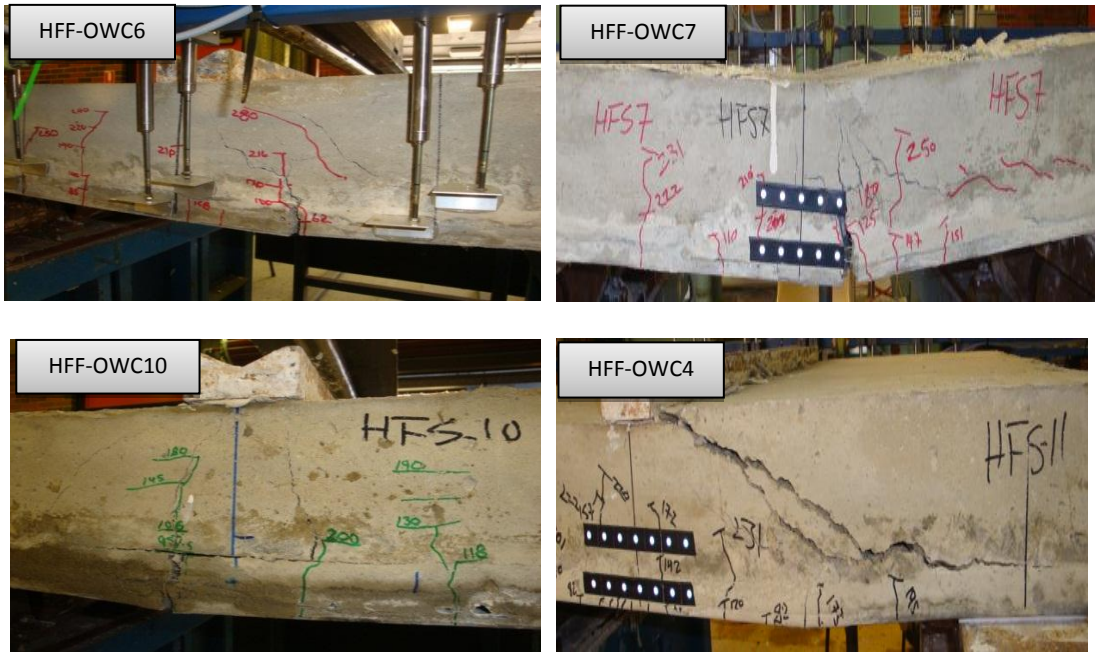

Figure 7.8 Crack pattern showing the failure mode of different slabs with different connection types

A flexural failure mode governs slabs with a low percentage of reinforcement. The use of shear studs prevents the composite slab from slipping, and the failure mode of the tested slabs is independent of the type of connection. Slabs with shear stud types 1 and 2 failed in flexure-shear, as seen in Table 7.3 and Figure 7.8; slab HFF–OWC10, which used only tie wire, failed in flexure only. However, the flexure-shear failure in slabs with shear stud types 1 and 2 might be related to the shear transfer resistance provided by the shear studs, with shear resistance being insufficient to avoid flexure-shear failure because of the lower volume fraction of the shear studs. Also, specimens with denser shear stud content (type 3) achieved optimal shear resistance and therefore failed in flexure only. The slabs with tie wires had negligible shear transfer resistance and failed in flexure (slab HFS 5 and 6). This may be due to slight slippage at the interface of the slabs at the failure load.

Figure 7.9 Examples of multiple cracks in the HFF panel

7.7 Effect of HFF panel thickness

Increasing the slab thickness increased stiffness but decreased ductility. Consequently, the total slab thickness in this experiment was kept constant, but the HFF panel in the tensile zone varied in thickness to increase the upper concrete depth. This was designed to examine the effect of using different HFF panel thicknesses in the tension zone.

Comparison of the results for maximum load and deflection in Figure 7.10 shows that the results differ for 40, 30 and 25-mm-thick panels. The maximum load was very similar for HFF–OWC slabs with 30 and 40-mm thicknesses of HFF, whereas the slab with 25 mm exhibited smaller maximum load and deflection capacities, which could be due to the increased cross-sectional area of brittle concrete. Slabs with 40 and 30 mm produced similar results for both of these parameters, although the slab with 30 mm HFF panel values were slightly larger.

In contrast, slabs HFF–OWC8 (25 mm bottom panel) and HFF–OWC9 (30 mm bottom panel) failed in flexural mode under load despite the fact that they developed shear cracks; the thinner HFF panels failed first in flexure. The failure patterns of both slabs are shown alongside HFF–OWC2 in Figure 7.11. The failure mode changed to flexure failure as the thickness increase to 40 mm. Therefore, slab thickness is a significant determinant of failure mode.

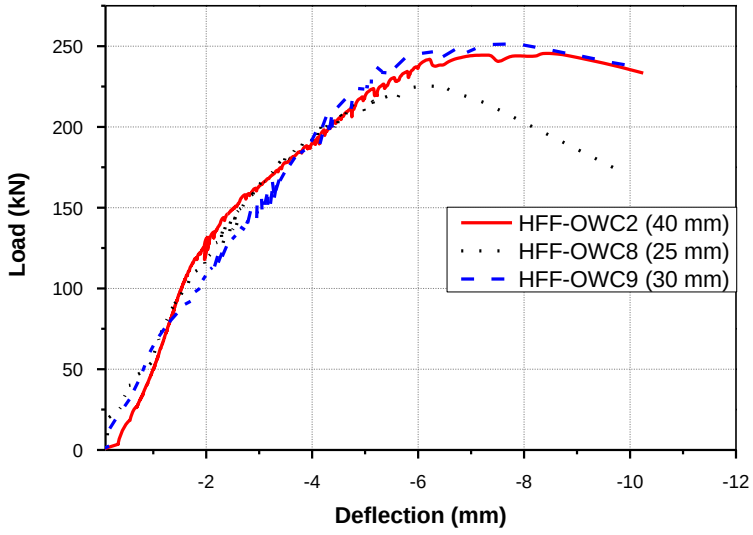

Figure 7.10 Comparing the load–deflection curve of slabs with different HFF panel thicknesses

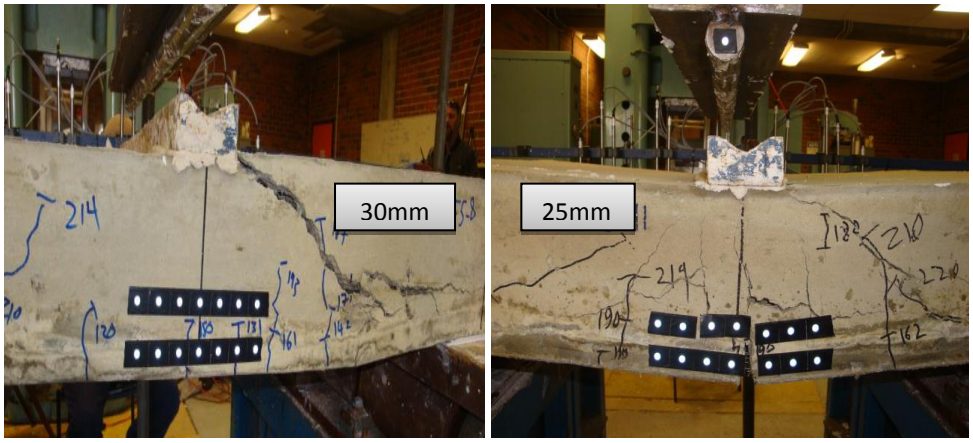

Figure 7.11 Crack pattern of HFF-OWC 8 (right) and HFF-OWC 9 (left) slabs

7.8 Behaviour of the composite slab at maximumload

Horizontal shear forces developed at the interface between the HFF panel and the one-way concrete slab. The shear studs crossing the interface of both slabs acted as shear reinforcement (Alam et al. 2010). The forces acting on the slab composite and flexural-strain distribution are shown in Figure 7.12. Horizontal shear forces abbreviated the bottom of the concrete slab and elongated the upper surface of the HFS panel so that both interfaces deformed together; this property allows the use of different segment thicknesses in a composite. It is important to transfer the acting shear forces across the connection area of both slabs to attain composite behaviour. The horizontal shear forces were transferred through friction and dowel action generated from the shear studs. As the composite action was achieved, negligible slip arose between both slabs. A load increase led the connected slabs to slip relative to each other, generating tensile loads that were carried by the shear stud reinforcement. Longitudinal slip initially occurred between the HFF panel and the concrete in the positive bending moment regions of the concrete slab. As tension arose in the shear studs, compression force normal to the surface was activated and transferred to friction between the two slab surfaces; by achieving the maximum load with insufficient shear stud reinforcement, the top slab developed shear cracks in a diagonal direction starting from the load point, and failure occurred. The flexure in multiply cracked, thinner HFF slabs on the bottom side reached the carrying load capacity and failed in flexure due to the lower stiffness.

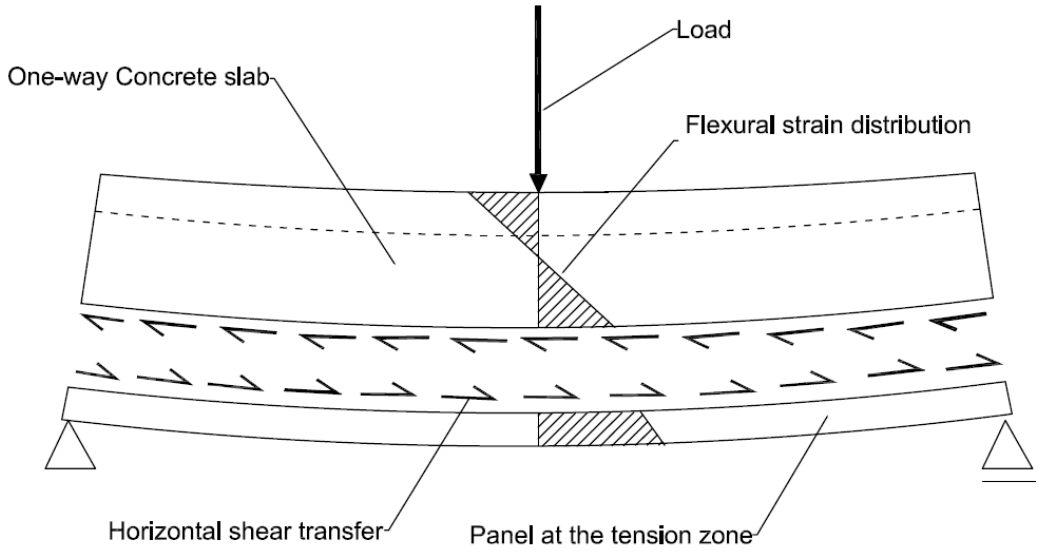

Figure 7.12 Action at the composite slab

7.9 Slab deflection and design load

A deflection profile along the slab length of the HFF–AAC concrete one-way slab is shown in Figure 7.13. The deflection shown is only for the apparent load span of the slab. The deflection rate at the mid-span increased up to failure at maximum load for all slabs. The profiles at this load were relatively linear between the load point and the longer sides. A very limited zone near the support points showed rotations causing a deflection in the positive direction at the free edges behind the support points. The deflection of both composites at the span between support and load point did not completely match. This was due to the different crack patterns that developed at maximum load. All tested slabs exhibited a good composite action. This became more obvious through the slip measurement. Only slab HFF-OWC10 showed a minuscule slip, which may explain the deviation of the deflection at maximum load.

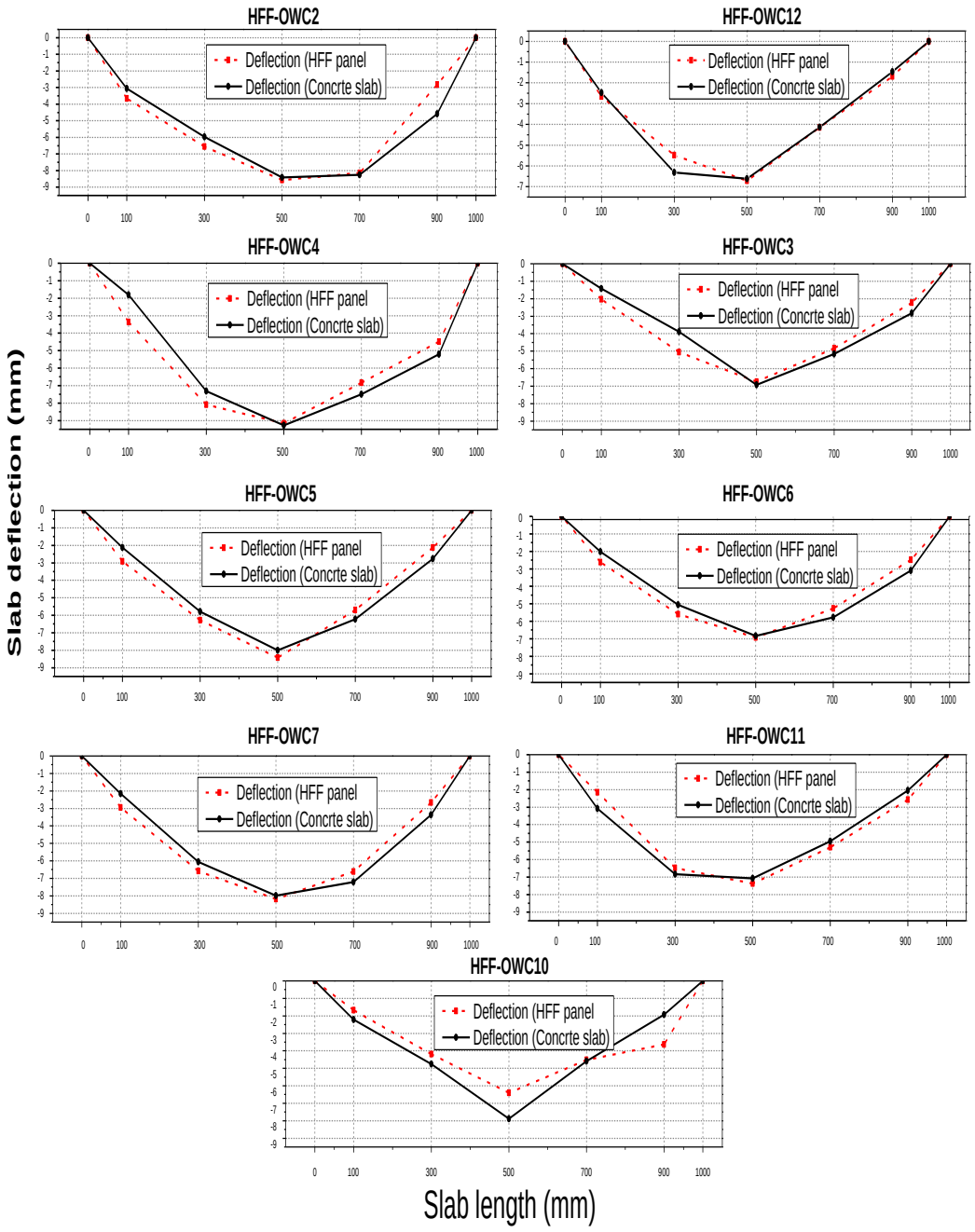

Figure 7.13 Deflection at maximum load along the slab length

As expected, the deflection of all slabs at the first crack, as seen in Figure 7.14, showed relatively low values compared to the deflection at maximum loads. The largest deflection at first cracking for any slab was 1.8 mm for slab HFF–OWC4. The deflection at this stage was only 23% of the total deflection capacity of this slab; however, similar ratios were observed for all tested slabs. This behaviour of the composite slabs could be used as a reference for a possible design prediction of the HFF–OWC slabs.

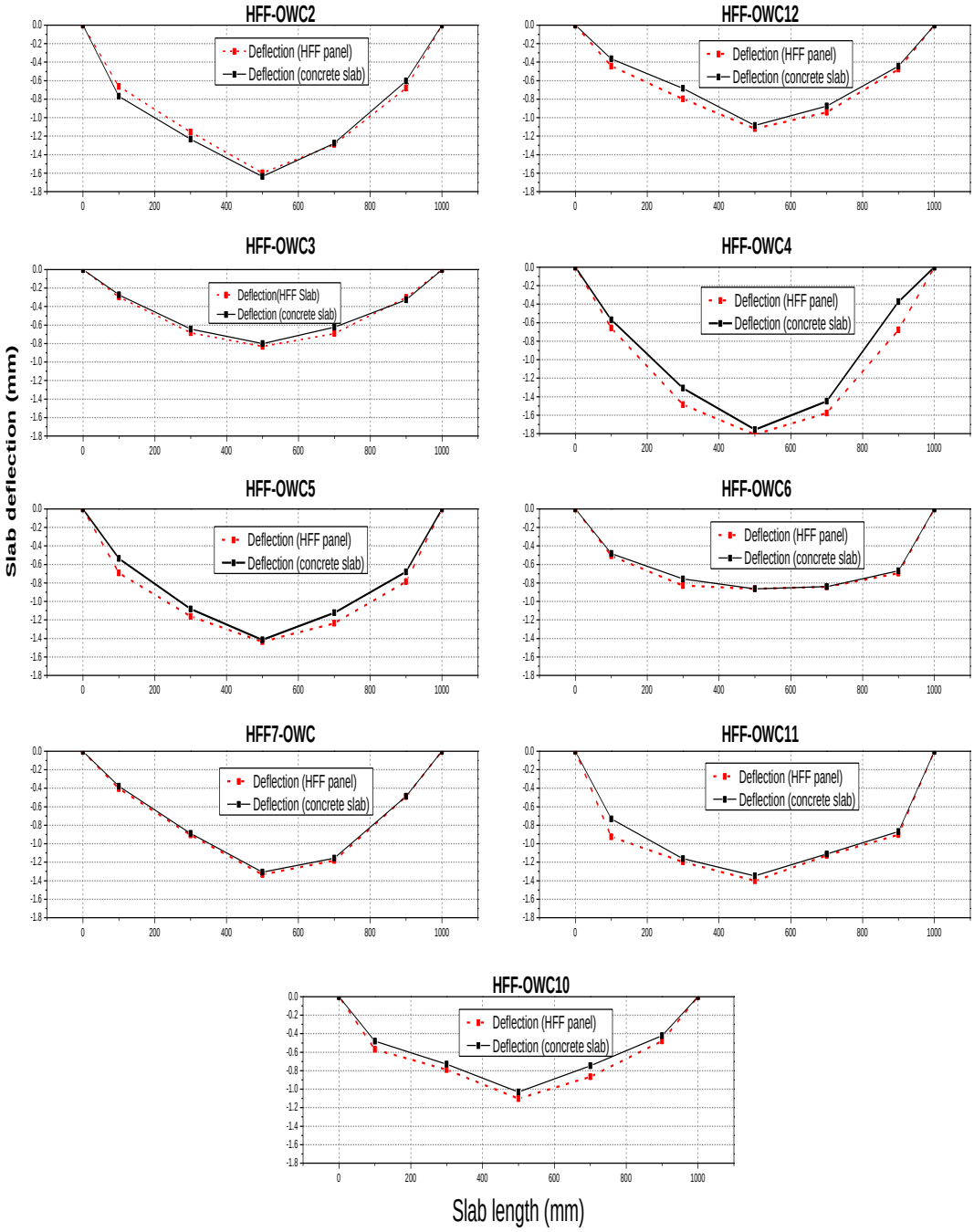

Figure 7.14 Deflection at first crack load over the slab length

The idea here was to evaluate slab deflection in light of the permissible deflection in one-way slabs according to the ACI 318-M11 (2011). The permissible deflection in a structural system is mainly governed by the amount that can be sustained in a way that the aesthetic appearance and the supporting members are not

affected. A tolerable deflection covers a wide range and depends on several parameters relating to the building's function, the use of supporting structures and the distance across the floor from other structural elements. All these factors substantially drive the limitations on deflection. This means that the service load is key to limiting the deflection of slabs. As structural elements are designed with respect to maximum load, the deflection performance at serviceability must be controlled to avoid immediate or long-term destruction. The ACI 318-M11 (2011) code (see Table 9.5(b)) lists the permissible deflection in terms of the total deflection caused through short- and long-term deflection.

Table 7.4 provides the deflection of the HFF panels at the first crack (δ_{cr}), and at maximum load (δ_u) and its related loads. The load at the permissible span deflection (P_{ACI}) according to the ACI 318 (2011) (see Table 9.5(b)) dictates the maximum span deflection for a 1000-mm test span—in this case, L/360 = 2.77 mm. Table 7.4 presents the percentage of the maximum load of the load at permissible deflection, calculated according to the ACI (ΔP_u). The AS 3600 value for the maximum allowed deflection of L/250 = 4 mm appears to be very conservative. Therefore, the carrying load at the deflection allowed according to the ACI was used for the evaluation of the tested HFF–OWC slabs. However, the load at permissible deflection according to the ACI code is on average 67% of the maximum load for slabs with shear stud type 1, and approximately 71% for slabs with shear stud type 2 and 3. It is worth mentioning that this rate does not consider variables such as shear stud type or quantity. Moreover, the experimentally determined load–deflection relationship only considers the deflection at the total applied load and does not distinguish between short- and long-term deflections. Therefore, it is recommended that this rate be used only as an indicator of the allowed deflection range, and not as a design value.

Table 7.4 Permissible deflection and suggestion of design load

ID	Experimental				ACI	
	δ_{cr} (mm)	P_{cr} (kN)	δ_U (mm)	P_U (kN)	$P_{U,ACI}$ (kN)	ΔP_U (%)
HFS2	1.64	109.7	8.57	245.5	158.0	64.4
HFS12	1.12	72.8	6.81	246.6	186.2	75.5
HFS3	0.83	95.2	6.75	279.1	206.8	74.1
HFS4	1.81	87.6	9.16	265.9	151.6	57.0
HFS5	1.43	119.8	8.42	248.7	196.4	79.0
HFS6	0.86	64.1	6.92	281.8	207.2	73.5
HFS7	1.33	90.6	8.18	262.1	186.2	71.0
HFS11	1.40	85.1	7.37	246.4	140.9	57.2
HFS10	1.10	90.7	6.40	220.1	153.8	69.9

7.10 Digital image correlation for determination of slip between the slab composites

Slab deformation was measured using the digital image correlation system, an optical method to determine surface displacement (Alam et al. 2010). This method evaluates and compares two images using reflecting marks or points in a grey scale recorded before and after deformation. The first image, of the initial undeformed position, is called the reference and the second is the deformed image. The displacement field is then in an area defined as the correlation area.

Here, reflecting points or target points were located at the mid-span of the slab (Figure 7.15) in a way that the slip resulting from the acting loads could be observed and compared at different load values. Initial locations of the reflecting points were recorded before the load was applied and compared with images from other load stages. During the test, images were logged at an increasing load step of 10 kN up to failure. Figure 7.15 shows one of the recorded photogrammetric images. The images were analysed using the photogrammetry-based Australis software to locate the coordinate system of the reflective dots at different load stages.

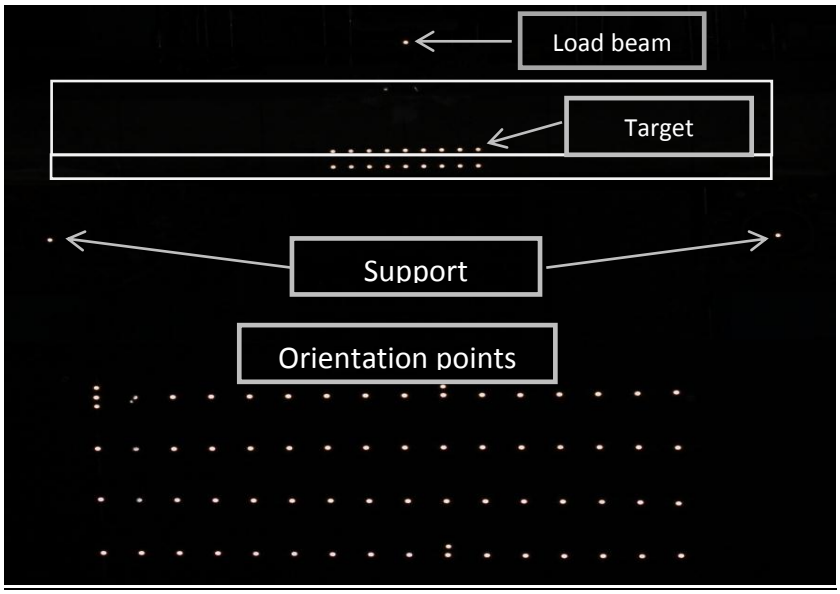

Figure 7.15 Photogrammetry image showing reflective points used in this method

The plot of the target reflective points at the initial and maximum load of slabs HFF–OWC2 and HFF–OWC10 is shown in Figure 7.16. Note that the different target point positions of the graphs are due to different camera angles during the test setup. Moreover, only the horizontal movement (*x*-direction) of the reflecting points, or 'target points', are as shown in Figure 7.16, which allows simplified observation of the slippage between the slabs. As the composite action is achieved, minimal negligible horizontal movement between the slabs was observed in HFF-OWC2. This slippage was determined to be at the micrometre scale and was therefore considered insignificant as it could be related to analysis errors or be part of the slab deformation. In contrast, the slab with wire ties (HFF–OWC10) showed a larger slip at maximum load compared to the slab with shear studs in the edges, which eliminated slippage between the slabs. The average slip was 0.5 mm, which still has an insignificant effect on the composite action in large-scale slabs. Consequently, the anchorage carried by the shear studs limited slippage between the slab segments. This increased the carrying capacity and ductility, and enhanced overall slab performance. A magnified graph showing a zoom in of two reflecting points before and after testing is as seen in Figure 7.17 to illustrate how the slip was measured.

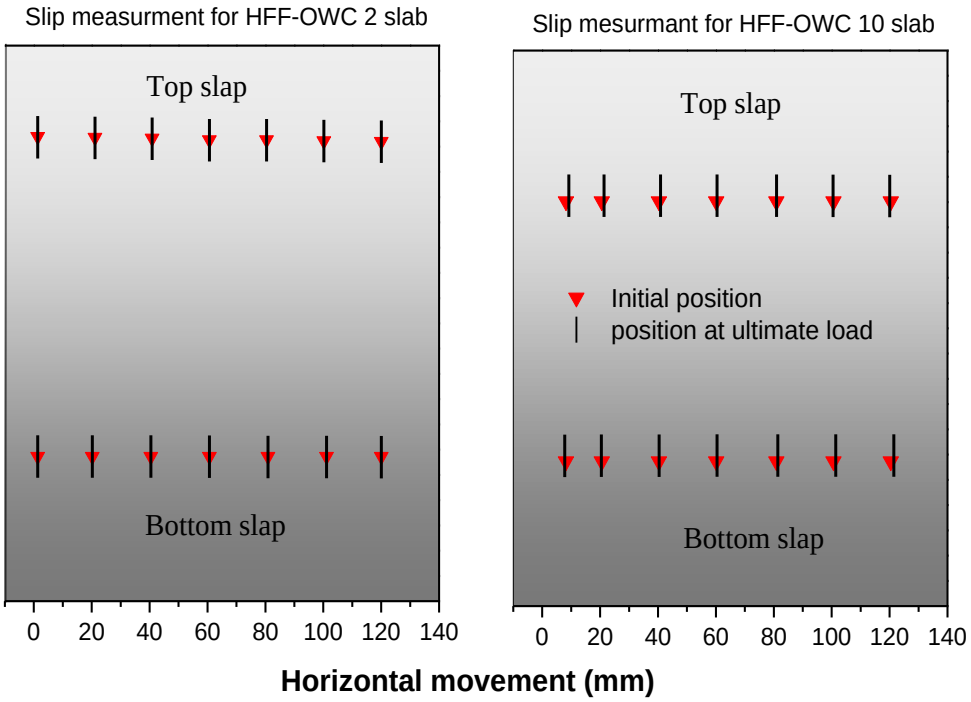

Figure 7.16 Comparing the slab slip of slabs with (HFF–OWC2) and without (HFF–OWC10) shear studs

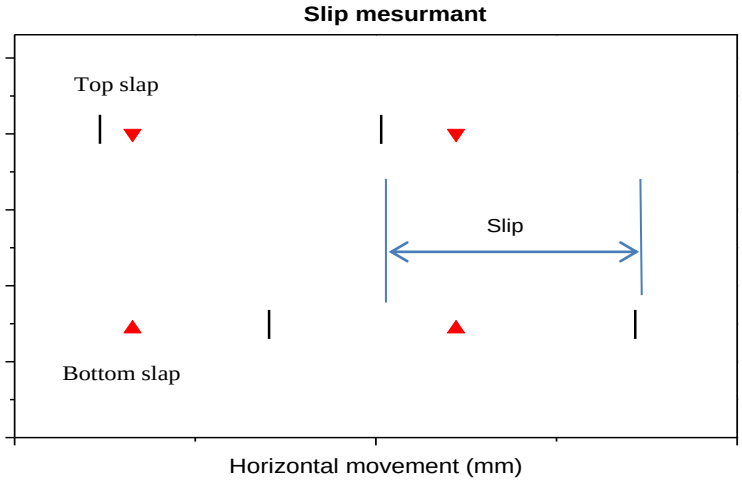

Figure 7.17 Magnified target point area for determining the slip of the composite slab

7.11 Prediction of the horizontal shear bond load

To obtain the moment capacity of HFF–OWC slabs, calculations were performed based on tensile reinforcement yielding. Calculations employed the equilibrium method on the phase-acting forces. A critical section diagram of a slab section and its corresponding forces is provided in Figure 7.18. A similar approach determining the shear force and shear bond for composite slab systems, to simulate the horizontal shear bond stress and the end slip of the steel deck and concrete slab composites, was developed by (Abdullah and Easterling 2009). The method used here is similar, except that it considers the effect of wire mesh and fibre in the HFF panel in addition to steel reinforcement of the concrete slab. As the method is dependent on the slip determined in the tests, only the maximum shear force for slab HFF–OWC10 was used in the calculations.

The friction at the support was assumed to be a significant contributor to the shear bond force (V_{max}). It is also important in this model to consider interaction behaviours between the concrete slab and the HFF panels, because the HFF panel carries a significant part of the applied load due to the steel wire mesh and the fibre, in the form of bending about its one axis. The shear force (V_{max}) can be calculated by equilibrium of the loads as follows:

$$V_{max} = \frac{(P_{max}L_S - M_r)}{Z} \qquad (7.1)$$

where, L_s is the shear span; P_{max} is the maximum applied load and Z is the lever arm between tension and compression forces. The bending moment resistance M_r can then be calculated from the deflection relationship of the deformed slab by:

$$M_r = \frac{48\,\delta_i}{L_s^2} E_d I_d \qquad (7.2)$$

E_d is the modulus of elasticity (determined in Chapter 5 to equal 34.2 GPa for square wire mesh samples), and I_d is the moment of inertia of the HFF panel, calculated as $bh^3/12$.

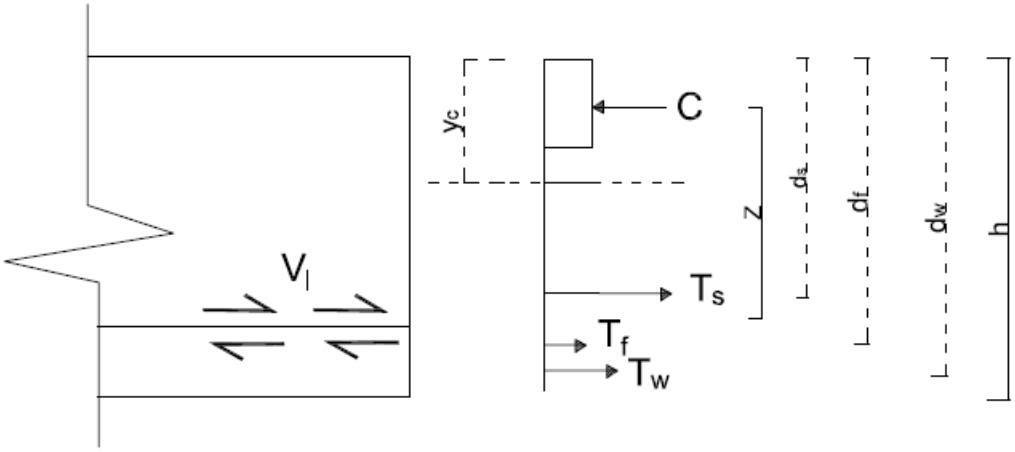

Figure 7.18 Stress and internal force diagram at the composite slab interaction phase

Z, considered as the distance from the neutral axis of the composite section to the top of slab y_c, is obtained as follows:

$$z_i = d - \frac{1}{2} y_c; \text{ where } y_c = \frac{S_i L_s}{\delta_i} \qquad (7.3)$$

where S_i is the measured slip; and d is the effective depth of the slab section, which in this case for simplicity is determined from the contribution (interpolation) of the three tension reactions due to the steel reinforcement (T_s), wire mesh (T_w) and tension through the PVA fibre (T_f), as seen in Figure 7.18. Therefore, d for slab composite HFF–OWC10 was calculated as 112 mm. Substituting slip s = 0.48 mm and L_s = 500 mm into Equations 7.1–7.3, the maximum shear force V_{max} is calculated as 88.3 kN. The relatively high value may be related to the wire tie resistance of the generated horizontal shear load in friction and dual loads.

In contrast, the ACI 318 Building Code and Commentary (2011) covers composite concrete flexural members because linear design method equations are applicable to determine their horizontal shear load and shear strength. The approach used here is based on factoring in the ultimate shear force (V_u), using the following equation:

$$V_u \leq \emptyset V_{nh} \qquad (7.4)$$

where the reduction factor ∅ is equal to 0.75, and because ties are applied to connect the slab composite, the nominal horizontal shear strength (V_{nh}) is considered as:

$$V_{nh} \leq (1.8 + 0.6\, \rho_V\, f_y)\, \lambda\, b_v\, d \qquad (7.5)$$

In this case, ρ_v is area of reinforcement crossing the interface (which is $Av/(b_v s)$, where b_v *is* the width of the interface); λ = 1.0 for normal weight concrete; and *d* is

the distance of the extreme phase. The nominal horizontal shear strength V_{nh} will be not greater than 3.5 $b_v d$. The resulting horizontal shear stress is calculated by:

$$v_h = \frac{V_u}{b_v d} \qquad (7.6)$$

The results are provided in Table 7.5 and are compared with the horizontal shear load and shear stress obtained from the test results. The results from the ACI code exhibited higher values, because the shear load from the experimental data did not include the slab's own weight and is not factored into any design safety factors.

Table 7.5 Horizontal shear and shear stress

ID	ACI code 318			Experiment	
	V_{nh}(kN)	V_u(kN)	v_h(MPa)	V_E(kN)	v_{Eh}(MPa)
HFF–OWC2	205.40	154.05	1.38	123.2	1.10
HFF–OWC3	209.19	156.90	1.40	139.56	1.25
HFF–OWC4	209.19	156.90	1.40	132.96	1.19
HFF–OWC5	220.58	165.44	1.48	124.35	1.11
HFF–OWC6	220.58	165.44	1.48	140.88	1.26
HFF–OWC7	209.19	156.90	1.40	131.03	1.17
HFF–OWC11	209.19	156.90	1.40	122.75	1.10
HFF–OWC2	205.40	154.05	1.38	123.2	1.10

7.12 The strength increase due to the studs

In composite slabs, shear studs were used as a resistance mechanism for longitudinal slip and for connecting slabs. All tested slabs with shear studs exhibited greater strength capacities than those without. This strength increase was achieved through the effect of the studs resisting the longitudinal shear that causes the slip. The relationship between the studs and the increase in strength can be calculated in the form of a coefficient known as the coefficient of strength increase, which is an important factor determining the strength of the whole composite slab performance resulting from the use of shear studs (Degtyarev 2014a). The coefficient strength increase due to the end anchorage (k_s) was defined as the ratio of the calculated maximum load for a composite slab with end studs to the calculated maximum load for a similar composite slab without studs (Degtyarev 2014b). Here, the loads were

applied from the test results. Figure 7.19 shows the effect of the number of shear studs in relation to the strength increase coefficient calculated from the following equation:

$$k_s = \frac{P_{u\,(studs)}}{P_{u\,(without\ studs)}} \qquad (7.7)$$

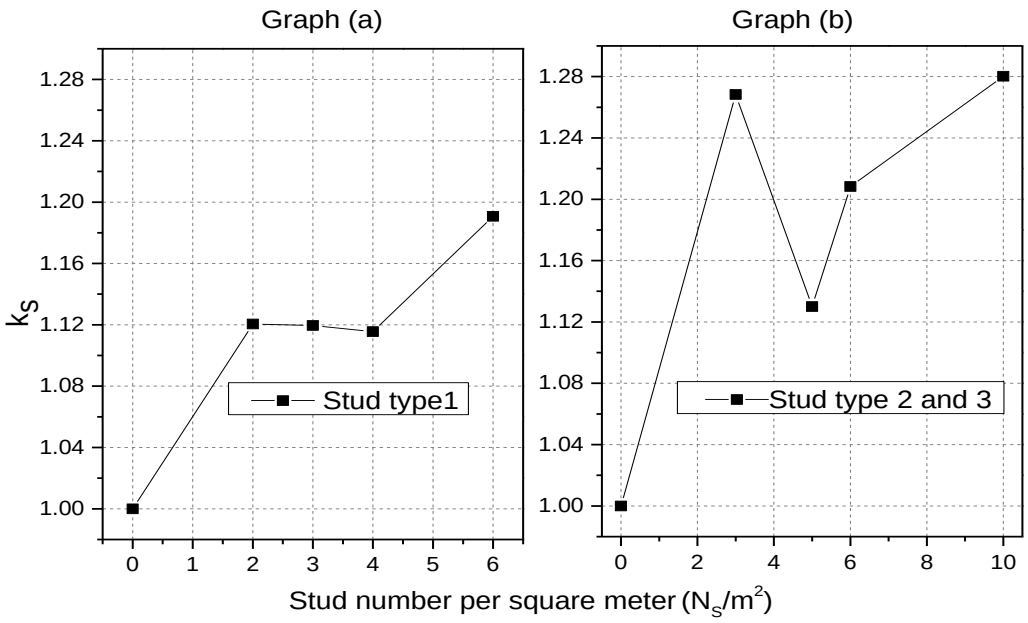

Figure 7.19 Effect of shear stud number on slab strength increase (k_s) due to the studs

The values applied in Equation 7.7 were the maximum load of the slabs with studs for each slab and the maximum load resulting from slab HFS10, for which no studs were used (see Figure 7.19). The use of studs led to an increase in the strength capacity of the composite slabs. The use of single studs (stud type 1), as seen in Figure 7.19(a), produced an increase of ~12% in strength capacity. The use of two to four studs per square metre appears to add insignificantly to the strength. However, the use of six single studs (type 1) produced the highest strength increase and was the most significant effect enhancing the strength capacity of the slab composite.

In contrast, using studs with the flat bar system gave controversial results, particularly for slabs in which three and five connecting studs were used (Figure 7.19 (b)). These two slabs, HFF–OWC3 and HFF–OWC5, were each tested twice, with similar results. However, the highest strength increase (28%) was related to the improved tension resistance due to the flat bars.

7.13 Concluding remarks

The application of the HFF panels produced excellent and increased strength and deflection behaviour compared to slabs without the panel in the tension zone, or by using conventional ferrocement in the tension zone. The tests showed that the concept of using the panels as permanent formwork is realistic in terms of structural performance. Further, the variation in HFF panel thickness (25–40 mm) barely affected overall slab performance; however, with reduced HFF panel thickness the slab weight, and therefore the amount of dead load, might increase. In general, the slabs behaved as one slab, which recorded excellent composite action due to minimal slip and evidence for splitting. However, the use of shear studs provided substantial strength increase, and preferable load-carrying capacities and deflection values. The effect of stud types and the number of studs on the strength capacity requires more intense investigation.

Chapter 8: Numerical Modelling of HFF Composites and HFF–AAC Block Composite Slabs

8.1 Introduction

Numerical modelling of fibre-reinforced materials is a significant aspect of research that is used to validate test data and to provide better understanding of the structural and mechanical behaviour of such composites. Among the substantial literature on numerical modelling of concrete, there is only a handful of publications on the structural scale simulation of FRCC. The complexity of modelling fibre-reinforced cement-based material lies in its behaviour: the transition from linear elastic to inelastic and strain hardening behaviour, followed by strain softening. However, methods for simulating the structural response of hybrid fibre cement-based elements subjected to real loads and stresses are more sophisticated and can only be undertaken by making certain assumptions. In the following sections, microstructural and structure-scale models for HFF composite and its applications are presented.

8.2 Microscale modelling

Several cementitious composites are quasi-brittle, or exhibit strain hardening and complex strength and deformation behaviour. A numerical model of HFRCC that applies the material properties obtained from mechanical testing was developed by Pereira, Fischer, and Barros (2012b). Developing an FEM including hybrid fibres in HFF composites is a very complex issue. Randomly distributed fibre shows transversely isotropic behaviours (Barbero 2014; Barbero and Luciano 1995), and avariety of assumptions are necessary to take into account unknown material properties of the matrix. The determination of hybrid fibre amounts requires a vast effort. Also, predicting the fibre inclination angle in a hybrid fibre matrix is more

difficult than in a mono composite. All these difficulties make it necessary to use an approach that reduces the effort needed for a material specification study.

A three-dimensional FEM was created, which characterises a valuable effect to calculate the dominant micromechanical properties using a RVE. Microstructural features such as the size distribution of fibres and flaws in the matrix (the sites where cracks are initiated) have a substantial influence on ductility (Li and Wang 2006); therefore, the assumption here was that the modelled RVE was representative of the whole composite.

Two different fibre types and a cement mortar property were modelled using a commercial FE programme (ANSYS 2014a) to determine the composite elastic modulus. An element capable of exhibiting plastic deformation, cracking in three orthogonal directions and crushing was used to model and perform a calculation to determine the elastic modulus of the matrix containing cement paste and fibre. The approach considered only the mortar and fibre properties. The equations to accomplish the elastic modulus and the Poisson's ratio were from Barbero (2014).

8.2.1 Theoretical approach

The fibre in HFF composite is randomly distributed, and its mechanical properties are not straightforward to predict. A large number of fibre composites show anisotropic material properties. However, the analysis of an FE using micromechanical properties was performed using several methods. A mathematical equation is available for isotropic fibre-arranged materials. Performing an analysis to predict the three-dimensional stress of anisotropic materials requires a large number of elastic properties that are difficult to quantify. Conversely, all micromechanics analyses proposed for isotropic fibre composites are easily modified to take into account anisotropic fibre. This can be done by assuming that the fibres are transversely isotropic (Whitney 1967). This method of calculation reduces the properties required to determine the necessary elasticity specifications.

For simplicity, the theoretical determination of the strain is in relation to a state of plain stress ($\sigma_z = \tau_{xy} = \tau_{yz} = 0$), which is two dimensional for isotropic linear elastic material and formulated as follows (Roylance 2000):

$$\varepsilon_x = \frac{1}{E}\left(\sigma_X - \upsilon\sigma_y\right) \qquad (8.1)$$

$$\varepsilon_y = \frac{1}{E}\left(\sigma_y - \nu\sigma_x\right) \quad (8.2)$$

$$\gamma_{xy} = \frac{1}{G}\tau_{xy} \quad (8.3)$$

The three elastic constants for isotropic material properties—modulus of elasticity *E*, Poisson's ratio *v* and the shear modulus *G*—are related as follows:

$$G = \frac{E}{2\,(1+\upsilon)} \quad (8.4)$$

Applying Equations 8.1–8.3 in a matrix notation gives:

$$\begin{Bmatrix}\varepsilon_x\\ \varepsilon_y\\ \gamma_{xy}\end{Bmatrix} = \begin{bmatrix}1/E & -\nu/E & 0\\ -\nu/E & 1/E & 0\\ 0 & 0 & 1/G\end{bmatrix}\begin{Bmatrix}\sigma_x\\ \sigma_y\\ \tau_{xy}\end{Bmatrix} \quad (8.5)$$

By expressing the stress in terms of strain and applying Equation 8.4 in Equation 8.5, the following equation will apply:

$$\begin{Bmatrix}\sigma_x\\ \sigma_y\\ \tau_{xy}\end{Bmatrix} = \frac{E}{1-\upsilon^2}\begin{bmatrix}1 & \nu & 0\\ \nu & 1 & 0\\ 0 & 0 & (1-\nu)/2\end{bmatrix}\begin{Bmatrix}\varepsilon_x\\ \varepsilon_y\\ \gamma_{xy}\end{Bmatrix} \quad (8.6)$$

If considering the three definitional stresses applying to an RVE element, the stress in the *z–y* plane will no longer be zero. The matrix considering the three-dimensional stresses in a computational form regarding the transversely isotropic conditions (Barbero 2014) will be:

$$\begin{Bmatrix}\sigma_1\\ \sigma_2\\ \sigma_3\\ \sigma_4\\ \sigma_5\\ \sigma_6\end{Bmatrix} = \begin{bmatrix}C_{11} & C_{12} & C_{12} & 0 & 0 & 0\\ C_{12} & C_{22} & C_{23} & 0 & 0 & 0\\ C_{12} & C_{23} & C_{22} & 0 & 0 & 0\\ 0 & 0 & 0 & 1/2(C_{22}-C_{23}) & 0 & 0\\ 0 & 0 & 0 & 0 & C_{66} & 0\\ 0 & 0 & 0 & 0 & 0 & C_{66}\end{bmatrix}\begin{Bmatrix}\epsilon_1\\ \varepsilon_2\\ \varepsilon_3\\ \varepsilon_4\\ \varepsilon_5\\ \varepsilon_6\end{Bmatrix} \quad (8.7)$$

More explanation determining the equation are in Appendix C. The elastic modulus in fibre direction and Poisson's ratio are calculated by:

$$E = [C_{11}(C_{22}+C_{23}) - 2C_{12}^2] * (C_{22}-C_{23})/(C_{11}C_{22}-C_{12}^2) \quad (8.8)$$

$$\nu = [C_{11}C_{23} - C_{12}^2]/(C_{11}C_{22}-C_{12}^2) \quad (8.9)$$

Performing a calculation in the FEM using Equations 8.8 and 8.9 provides the required elastic modulus and the Poisson's ratio of the HFF composite.

8.2.2 Determining the elastic modulus through modelling of RVE

It was assumed that a transversely isotropic material behaviour was a unidirectional distribution of the fibre in the chosen cross-section of the specimen with randomly

distributed fibre, as seen in Figure 8.1. This made it possible to obtain an axis of symmetry to construct a transversal isotropic RVE (Barbero 2014; Maligno, Warriorand Long 2008). The fibre contribution in the matrix was assumed to be equal for each type, which provides a better support for the assumption of transversely isotropic behaviour. For simplicity, the elastic modulus of both fibres in the chosen RVE was taken as the average of the elastic moduli given in Table 3.3 for PVA1 and PVA4. The advantage of assuming transversely isotropic behaviour was the convenience it afforded when calculating the elastic constants, because the fibre was considered to be parallel to one axis. Here, a SOLID 65 element was applied to the RVE model. This element will be further described in Section 8.3.3.

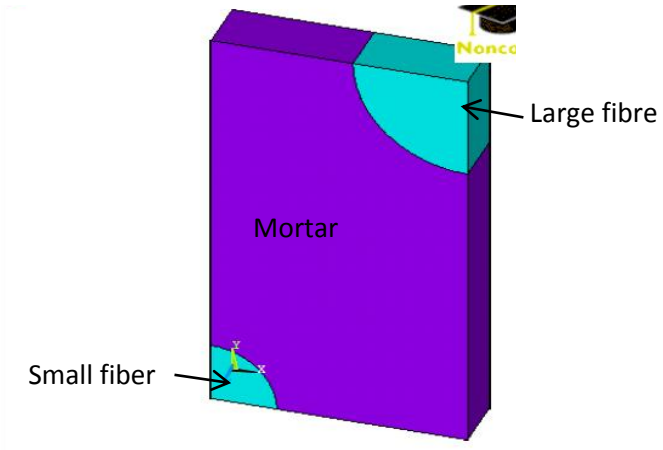

Figure 8.1 Symmetry module of the RVE of HFF composite

The FEM and the calculations performed are shown in Appendix C. The elastic modulus and Poisson's ratios obtained after performing an analysis using Equations 8.8 and 8.9 via the numerical FE program can be seen in Table 5.6.

8.3 Structural scale modelling

In this section, the modelling of HFF composite and its application as composite slabs at the structural level is illustrated. The consideration of material behaviour and performance is important in achieving the desired structural response. Therefore, the important theoretical and experimental results determining overall performance must be defined to allow accurate modelling of HFF. The difficulty lies in the method for modelling, which takes into account the effect of long and short fibre, and the wire mesh embedded in the mortar matrix.

8.3.1 Theoretical considerations of material specification of HFF composite

The significant improvements to the material behaviour of ferrocement were achieved via the increase of tensile strength through the addition of hybrid PVA. This fibre had a significant effect by stopping or constraining the growth and widening of microcracks. The efficiency of the shorter fibres in resisting the microcracks and the longer fibres in bridging the extended cracks at the macro level was established in Chapter 4. The small fibre and its dispersion in the matrix substantially increased the first crack strength. These two factors also had an effect on slowing down the propagation of microcracks growth (Mobasher, Stang and Shah 1990; Akkaya, Shah and Ankenman 2001). The transition to macrocracks occurs by extending the microcrack openings, known as the first crack point. The small fibres bridge the cracks until they rupture or are pulled out, at which point the crack propagation has exceeded the small fibre size, and the longer fibres become activated. This important behaviour of crack bridging needs to be considered in the analytical model.

However, fibre size is not the only parameter influencing bridging characteristics; fibre spacing is also not possible to calculate if different types are used and their dispersion influences crack bridging behaviour. The crack bridging behaviour and specific tensile strength are to some extent dependent on fibre orientation, which is expressed through the orientation factor (α_f) (Lee, Cho and Vecchio 2011a). The fibre inclination angle not only influences tensile stress, but also the quality of the fibre–matrix bond in terms of pullout performance (Lee, Choand Vecchio 2011b). Nevertheless, considering the influence of all these aspects on the composite is not simple and depends on the modelling method used to simulate the behaviour of HFF.

To model fibre as a separate element included in the matrix is not simple and requires considerable effort. The modelling in this section is performed with respect to the definition and consideration of fibre cohesion and the bridging effect of this fibre type as part of the mixture specification.

8.3.2 Theoretical method application to model

To determine material behaviour for the designated HFF composite, it was necessary to consider its structural performance with respect to compression, flexure and tensile strength. For instance, the analytical results required to simulate HFF composite in tension include a stress *vs*. strain curve that exhibits an elastic phase until the first crack. Strain hardening, inelastic behaviour comes next. At localisation, strain softening behaviour until failure is the final step. All these stages are essential to successfully model an HFF composite.

Another important aspect of the modelling strategy is the consideration of the failure surface in cement-based materials. A plasticity models for combined tension and compression model can be used. The tensile part is described in this approach by the yield condition, whereas another yield condition describes the compressive part. Tensile behaviour in these models is associated with the rotating smeared crack concept (Kullaa 1997). The initial method was developed for the triaxial failure surface of plain concrete, by Willam and Warnke (1974). The three-dimensional failure surface for concrete is shown in Figure 8.2, where the stresses are ordered such that $\sigma_1 \geq \sigma_2 \geq \sigma_3$. The most important aspect of this order is representation of the projection of non-zero principal stresses in the *x* and *y* directions in the form of $\sigma_{xp}$and σ_{yp} respectively. The failure surface is separated into hydrostatic (change in volume) and deviatoric (change in shape) sections in what is known as the three-parameter model. The deviatoric trace is described by the polar coordinates as formulated. The hydrostatic and deviator are shown in Figure 8.3.

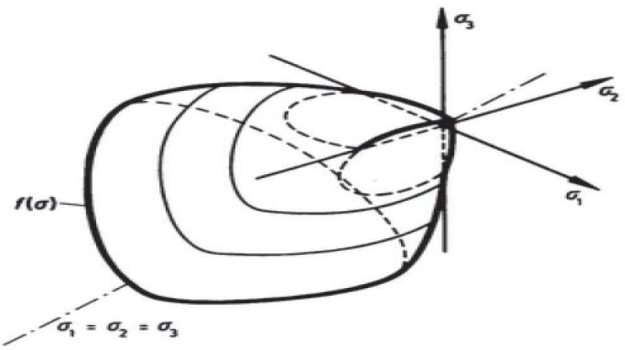

Figure 8.2 Initial failure surface (Willam and Warnke 1974)

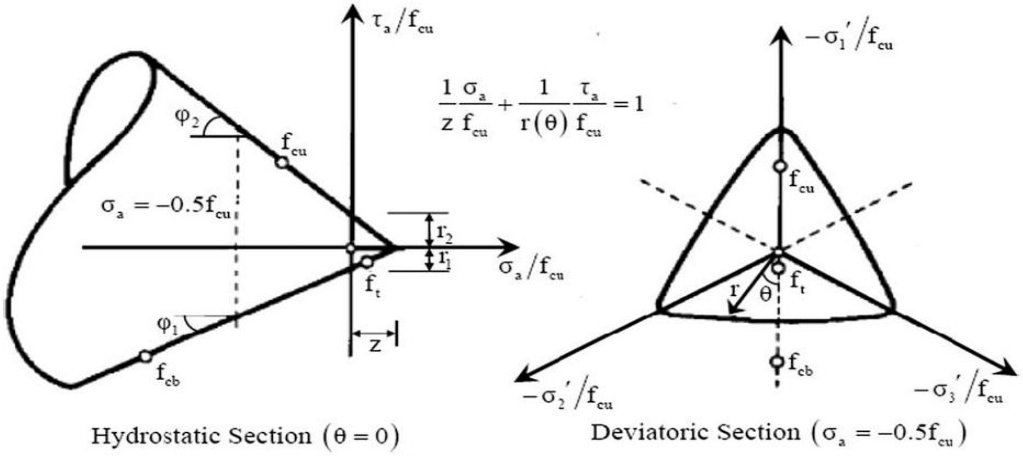

Figure 8.3 The three-parameter model (Willam and Warnke 1974)

Based on the failure criteria, a suitable model for concrete can be expressed. The yield condition can be estimated by three to five parameters that differentiate between elastic and inelastic deformations. In the transition phase from elastic to plastic behaviour, two arithmetical approaches were recommended. The first method subdivides the load into proportions, one for the elastic and the otherfor the inelastic stage in a form that governs the failure surface using integration. The other method is the normal penetration, which allows the interaction of the elastic path with the yield surface at the normal intersection. Both methods provide satisfactory stress values that fulfil the constraint condition (Özcan et al. 2009).

8.3.3 Applied element

SOLID 65 is a solid element used to model the concrete and the HFF matrix with or without rebar reinforcement, as seen in Figure 8.4. The element allows cracking in tension and crashing in compression (Rots and Blaauwendraad 1989). A significant advantage of this element is its capacity for nonlinear material treatment. The element has eight nodes with isotropic material properties, three degrees of freedom at each node and translations in the nodal *x*, *y* and *z*-directions.

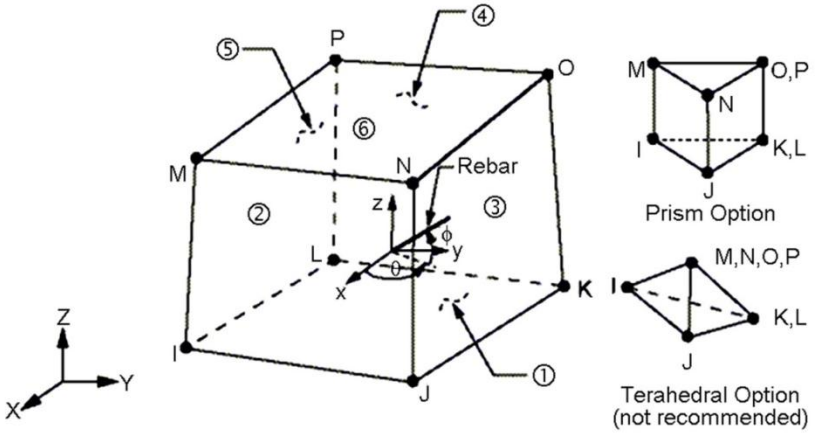

Figure 8.4 Geometry of a SOLID 65 element taken from ANSYS (2009)

There are three methods to model the reinforcement in cement-based composites: smeared modelling, the embedded rebar method and the discrete model. The smeared approach is limited due to its requirement for uniform distribution of reinforcement through the element. The embedded rebar model provides an advantage compared to the smeared method: it is possible to control reinforcement locations, and their orientations can be randomly distributed through the element. In the discrete model, reinforcement is represented in the form of a separate member (Chang et al. 1987), the only disadvantage being that the nodes of the FE mesh must match with all other nodes from contacting elements (Trueb 2011). This method allows a simple representation of the reinforcement and a detailed observation of the reinforcement behaviour in a test simulation. Here, the reinforcement of wire mesh, bar and stirrups were simulated using the discrete model by applying a LINK 180 element as seen in Figure 8.5. The three-dimensional spear element is a uniaxial tension–compression element with three degrees of freedom at each end.

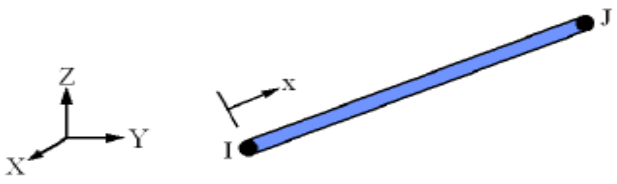

Figure 8.5 LINK 180 element geometry (ANSYS 2009)

8.3.4 Model parameters and material properties

The materials applied in this model were for the fibre cement composite, and the concrete in the composite slab were based on the constitutive modelling approach. The HFF material parameters were from the test results. In particular, the material properties of the HFF composite and the one-way concrete slab are further described.

8.3.4.1 Material properties of the HFF panels

To simulate the HFF composite, the multilinear isotropic material was modelled using the Willam and Warnke (1974) failure criterion. The elastic modulus of the HFF composite and the Poisson's ratio was determined in Chapter 5. Multilinear behaviour was used to support the convergence algorithm with a nonlinear solution. The multiaxial state of stress in HFF composite due to the presence of fibre was simulated by applying of the typical stress–strain behaviour of HFF (Figure 8.6) in the form of multilinear isotropic hardening behaviour as seen in Table 8.1.

The tensile test was conducted on HFF matrix without wire mesh reinforcement. The tensile stress–strain relationship is shown in Figure 8.7. The average maximum tensile strength of three tested plain composites was 4.9 MPa. Therefore, based on the tensile behaviour, a nonlinear elasticity model was considered for the HFF composite containing fibre.

The shear condition at the crack face was represented due to the transfer coefficient for open cracks (β_t). The value of β_t ranges from 0 to 1. Investigations have shown that the value of the shear transfer varies between 0.05 and 0.30 (Huyse, Hemmaty and Vandewalle 1994; Hemmaty 1998). Here, the shear transfer coefficient was assumed to be 0.3, whereas the shear transfer coefficient for closed cracks (β_c) was assumed to be 0.9 (Padmarajaiah and Ramaswamy 2002).

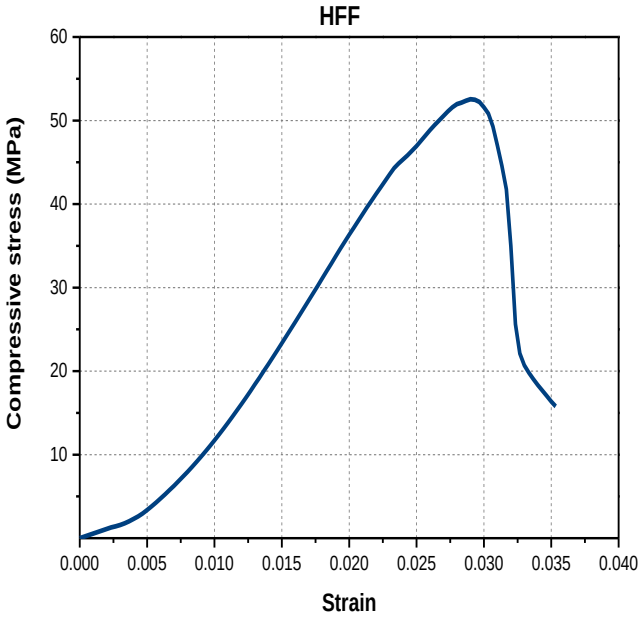

Figure 8.6 Uniaxial stress *vs*. strain curve for HFF composite

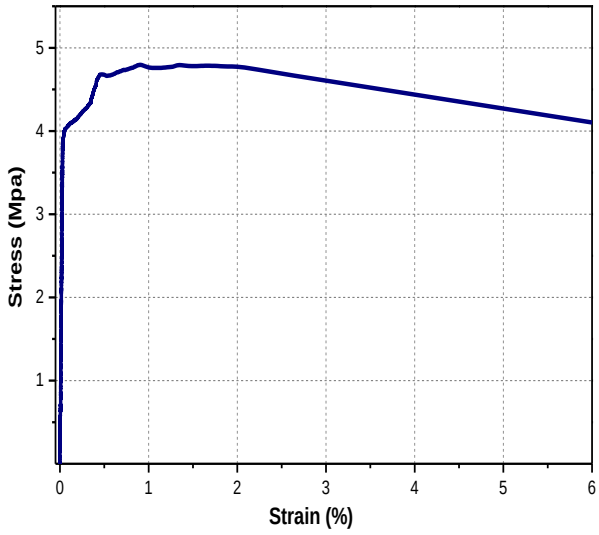

Figure 8.7 Tensile stress *vs*. strain of HFF matrix without wire mesh

Steel properties were assigned to the wire mesh using an elastic modulus of 200 GPa. The fibre properties applied in the model were from Table 3.3. All material properties implemented in the model are summarised in Table 8.2.

Table 8.1 Stress–strain of the HFF composite

HFF2*		HFF2	
Strain (%)	Stress (MPa)	Strain (%)	Stress (MPa)
0.0001	2.7	0.0001	2.9
0.0002	5.4	0.0002	5.7
0.0006	15.9	0.0006	16.8
0.0010	25.5	0.0010	27.1
0.0020	43.1	0.0020	47.3
0.0030	51.2	0.0030	58.5
0.0035	52.7	0.0040	62.2
0.0039	53.0	0.0044	63.0
0.0040	53.0	0.0050	63.0

Table 8.2 Material properties for HFF composites

	Cement-based mixture						Wire mesh		
Material	E (GPa)	f_c'(MPa)	f_t (MPa)	v	β_t	βc	E_s (GPa)	f_y (MPa)	v
HFF *2	27.1	53	4.9	0.29	0.3	0.9	200	350	0.3
HFF 2	28.5	63	4.9	0.29	0.3	0.9	200	350	0.3

8.3.4.2 Material properties of concrete

A uniaxial stress–strain curve was not tested, but the modulus of elasticity of concrete based on ACI (2011) was calculated as follows:

$$E_c = 4700\sqrt{f_c'} \tag{8.10}$$

with compressive strength of 30 MPa and Poisson's ratio assumed to be 0.2. The uniaxial compressive stress–strain relationship for concrete can be plotted using the following equations (MacGregor 1992):

$$f = \frac{E_c \varepsilon}{1+(\frac{\varepsilon}{\varepsilon_0})^2} \tag{8.11}$$

$$\varepsilon_0 = \frac{2f_c'}{E_c} \tag{8.12}$$

where f is the stress at any localised strain ε and ε_0 is the strain at maximum compressive strength. The resulting uniaxial stress–strain curve for concrete is given in Figure 8.8. However, the multilinear isotropic hardening behaviour of the stress–strain data obtained (Table 8.3) involves the initial elastic modulus, according to Hooke's law.

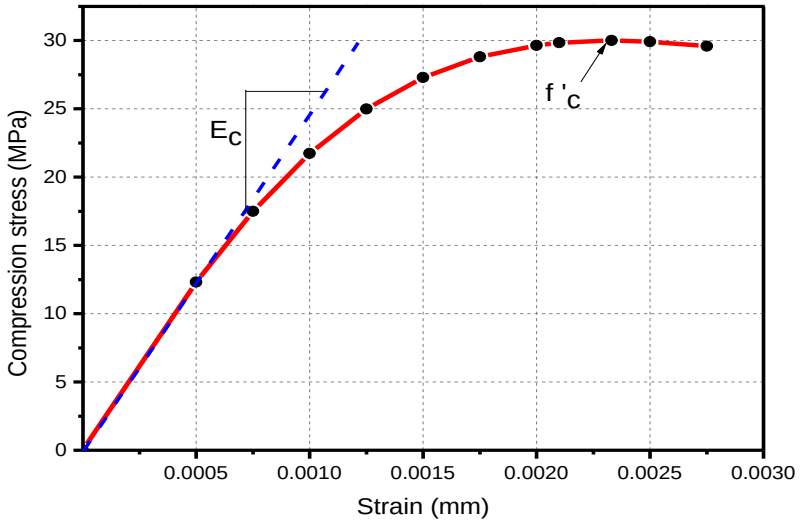

Figure 8.8 Uniaxial stress *vs*. strain curve for concrete

FE modelling requires tensile strength capacity in the material model. The concrete tensile strength was given from the equation below (AS-3600 2001):

$$f_t = 0.4\sqrt{f_c'} \qquad (8.13)$$

The compressive strength of the AAC block was 3.5 MPa. This compressive strength is similar to that experimentally obtained by Vimonsatit, Wahyuni and Nikraz (2011). Equations 8.10–8.13 were used for the concrete and AAC blocks. The multilinear isotropic stress–strain parameters for concrete and AAC are provided in Table 8.3.

The steel reinforcement consisted of wire mesh in the HFF composite and rebar in the concrete slab. The reinforcement steel simulated in the FEMs was an elastic plastic identical in tension and compression material. A Poisson's ratio of 0.3 was used. The summary of all material properties used in the FE modelling is provided in Table 8.4.

Table 8.3 Stress–strain of the slab component

Concrete		AAC	
Strain (%)	Stress (MPa)	Strain (%)	Stress (MPa)
0.00075	17.50	0.0003	2.31
0.0010	21.74	0.0004	2.81
0.0015	27.31	0.0005	3.15
0.00175	28.81	0.0006	3.36
0.0020	29.65	0.0007	3.47
0.0021	29.84	0.00075	3.49
0.002331	30.00	0.000796	3.50
0.0025	29.93	0.0008	3.50

Table 8.4 Applied material specification in the FEM of the HFF–OWC slab

	Cement-based mixture						Reinforcement		
Material	E_c(GPa)	f_c' (MPa)	f_t (MPa)	v	β_t	βc	E_s (GPa)	f_y (MPa)	v
HFF	28.5	63	4.9	0.29	0.3	0.9	200	350	0.3
Concrete	24.6	30	2.3	0.2	0.4	0.9	200	350	0.3
AAC blocks	8.6	3.5	0.8	0.2	0.4	0.9	-	-	-

8.4 Modelling and results

The FEM was conducted using the ANSYS program. The HFF panels of size 600×200×40 mm were modelled under a four-point bending test as shown in Figure 8.9. A SOLID 65 element was used to model the mortar composite. The fibre was assigned to the SOLID 65 element using the smeared method through the real constant.

The steel wire mesh was modelled with LINK 180 elements with a wire diameter of 1.24 mm and 25×25 square meshes. Here, a reliability check was also conducted using a BEAM 188 element. The LINK 180 element results were more consistent with the test results.

Mesh size in the model was selected to match the real wire mesh sizing. The panel was divided into six horizontal segments to simulate the wire mesh layers. The

panel length and depth were meshed into 25-mm elements according to the wire mesh opening size. Mesh size reliability checks were performed by meshing the entire panel with 5-mm elements. However, the chosen mesh sizing exhibited reasonable results.

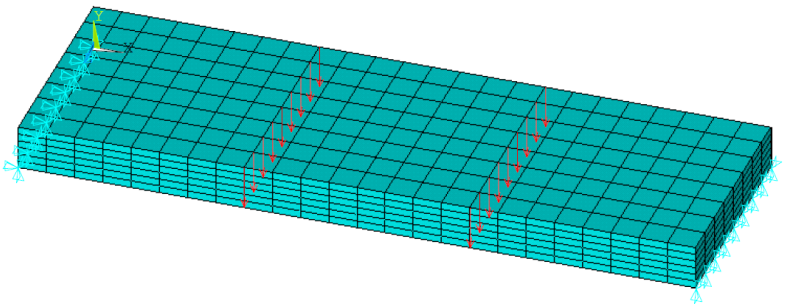

Figure 8.9 Geometrical FEM of the HFF panel

The model was validated by the elastic modulus obtained for the HFF matrix in the analysis reported in Chapter 5. Two different elastic moduli determined by the nanoindentation (Table 5.6) were used. The results were then compared with the test results shown in Section 5.2.3. The load–deflection from the flexure test was compared with the FE results in Figure 8.10. The experimental and FE results agreed well with one another. There was an insignificant change in the curve fitting using the elastic modulus for the fibre mortar, from Table 5.6. In general, the load–deflection curve for the panel obtained from the FE analyses differed only slightly from the experimental curve at the initial elastic stage. The perfect bond between the mortar and fibre assumed in the FE analysis might not be realistic for the tested panels. Also, the stress and strain calculated in the FE program due to integration points of the applied solid element might not match the true crack direction. However, multiple crack behaviours were also achieved in this model, as seen in Figure 8.11.

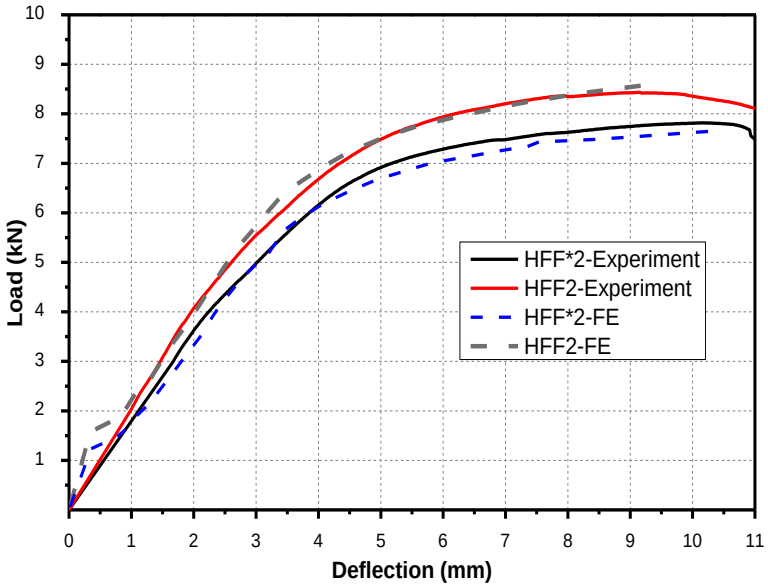

Figure 8.10 Load *vs.* deflection comparison for experimental and FEM results

The excellent results obtained in this study were only possible after a lengthy parametric study. All results obtained in Chapter 5 such as the elastic modulus and the Poisson's ratio showed excellent agreement between the FE and test results. However, the strain softening of the load–deflection curve has not yet been considered in the model, which explains why the FE curves end at the localisation point. The program stops calculating due to deficiency of convergence at this point.

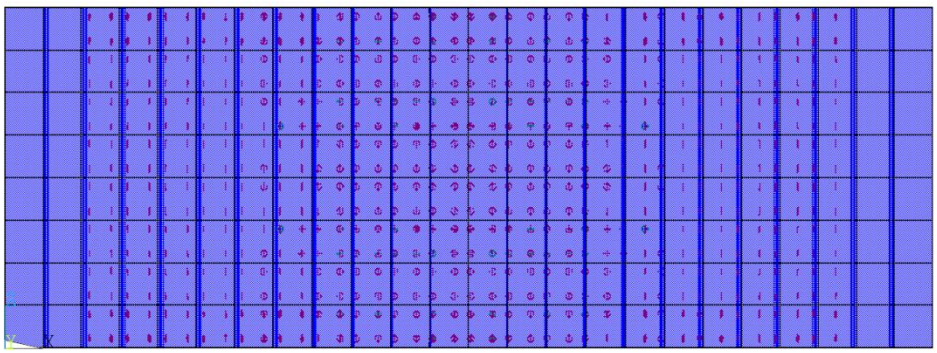

Figure 8.11 Multiple crack pattern of an HFF model

The HFF–OWC slab was modelled according to the slab size and components described in Chapter 7. The concrete, HFF composite and AAC blocks were modelled with the SOLID 65 element. All reinforcement used in the slab composite

was modelled with the LINK 180 element. The meshed geometry and load were as shown in Figure 8.12.

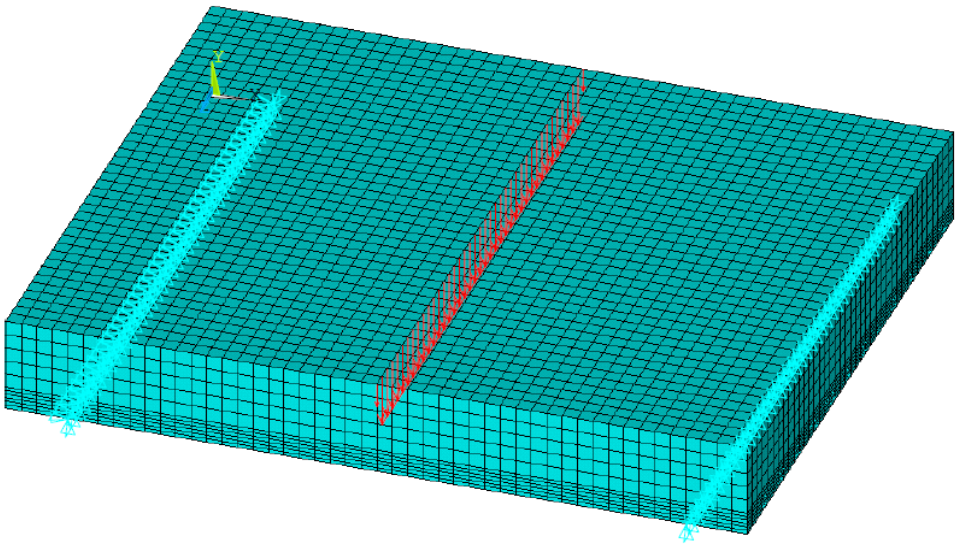

Figure 8.12 Geometry and load for the HFF–OWC slab

Several convergence issues occurred during the nonlinear calculation. One reason was the very low elastic modulus and strength capacity of the AAC blocks compared to concrete and HFF composite. The large variation in material properties led to geometrical nonlinearity. To achieve convergence in the calculation, large deformations must be considered, which can be accomplished by activating calculations with the large deformation mode in the program. However, the interface area between the top and bottom slabs requires a contact element; to simulate real conditions, a contact element with rough conditions was used. The friction applied was 0.65.

The FE results were compared with the experimental load *vs*. deflection as seen in Figure 8.13. The FE results showed a slightly different trend that is more typical for concrete. Importantly, similar load values were achieved for first crack and maximum loads. The lower stiffness in the FEM might be due to the lower strength properties of the AAC material, which interacts with the other materials. However, the FEM exhibited similar crack patterns as observed in the tested slabs. Multiple cracking was also detected in the HFF panels in the slab composite (e.g. see Figure 8.14). The deviation in the deflection behaviour could be due to the insufficient definition of the contact areas in providing the load transfer between the

different materials. Therefore, further investigation is required to assess the stress transfer between the HFF and AAC elements. This part of the work is beyond the scope of this research.

The crack behaviour of the FE model exhibited similar crack patterns observed in the tested slabs. Multiple cracking are also in the HFF panels in the slab composite detected.

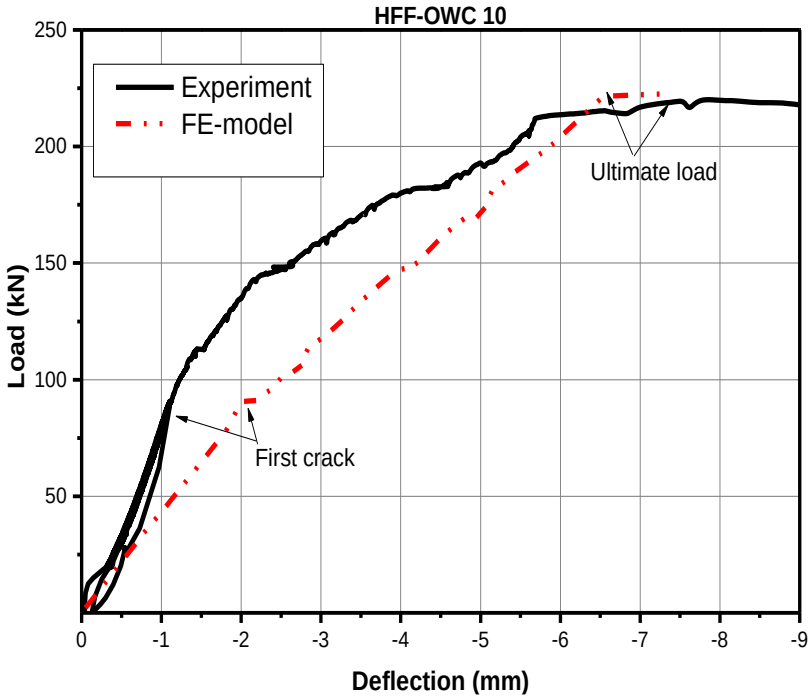

Figure 8.13 Load–deflection curves for HFF–OWC slab composite

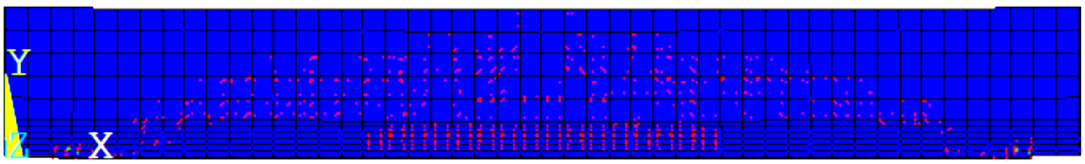

Figure 8.14 Crack pattern in HFF–OWC slab

The horizontal shear in the interface zone between the concrete slab and the HFF panels did not show any concentrated stresses (see Figure 8.15), which indicates that the slab did not fail due to the forces generated from the shear transfer between the contact areas. The shear transfer values are given in Figure 8.15.

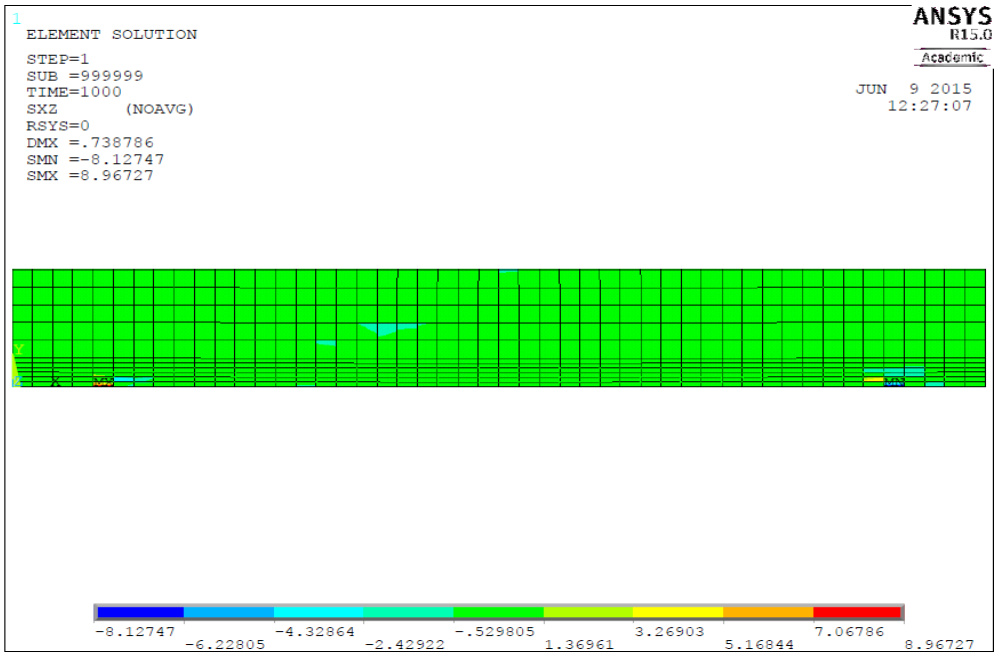

Figure 8.15 Horizontal shear results for the slab composite

8.5 Concluding remarks

Numerical analyses using the FEM were presented in this chapter. The modelling of an RVE representing the HFF matrix was used to determine the elastic modulus and Poisson's ratio. The results obtained were then applied in a structural model and showed a relative good match. However, the best results were obtained by simulating the flexure test of the HFF panels using an elastic modulus of 26.8 GPa for HFF2* and 27.4 GPa for HFF2, obtained from the nanoindentation tests performed earlier. Importantly, the modelling of the HFF composite with its strain hardening behaviour due to the influence of hybrid fibre was considered by applying the stress–strain behaviour of the composite. The fibre in the composite was also considered in the model by using the smeared method.

The slab composite was also modelled using the constitutive modelling method, and the results were compared with the experimental data. The curve trend achieved deviated slightly from the test results, but still exhibited satisfactory results. The crack pattern of the FEM was in good agreement with real crack patterns in the tested slabs. In general, the FEM showed that the slab composite did not fail due to shear transfer in the interface zone. However, further investigation in the contact zone of the different materials is required for result obtimazation.

Chapter 9: Conclusions and Recommendations

9.1 Summary

The research presented in this thesis focused on the development and utilisation of HFF. The results have provided fresh insights into understanding of the mechanisms for HFF. Experimental and analytical researches were carried out that produced quantitative data on the basic properties of HFF. The models for predicting the flexure response, tensile stress–strain behaviour and the occurrence of multiple cracking in HFF were all conducted using data collected under laboratory conditions. The experimental data were maximum tensile stress, strain at maximum stress, equivalent flexural stress, deflection and energy at maximum stress, toughness, strain data, fibre pullout and crack observations.

Experimental studies included the material composition in term of fibre combination, wire mesh content, additives to mortar and panel thickness. The parameters were statistically analysed to determine the effect of each component on the strength capacity of the HFF composite. The material was qualitatively classified based on its tensile stress–strain, flexure strength deflection and compressive strength. The study also addressed the microstructure and micromechanical properties using the nanoindentation approach.

Two important potential environmental impacts—fire and carbonation—were a significant part of the durability study. The bending test uniquely developed during the heating process was successful in testing specimens with different mixtures and panels thicknesses. The carbonation effect at the material and structural levels was also tested.

The improved ferrocement was then applied as permanent formwork in a one-way concrete slab containing AAC blocks as infill. The tests included several parameters such as formwork thickness, and shear stud quantity and location for connecting the top slabs. This investigation was followed by a numerical modelling

of the tests performed to validate the results obtained. Analytical models were developed to predict the micromechanical elasticity constants of HFF composite at the micro level. Further numerical models for the structural level were developed, including the flexural response of the HFF panels and the HFF–OWC slab.

9.2 Conclusions on material composition of the HFF composite

Flexure tests were carried out on panels using ferrocement with the hybrid fibre combination. Four different types of PVA fibres were used: two short and two long fibres in different combinations of long and short. The flexure tests applied in the study were chosen because of the proposed application of the panels as permanent formwork for slabs. The experimental study included three different fibre volume fractions: 0.75, 1.00 and 1.50%. In addition, various mixtures were designed to investigate the workability of the composite. Other parameters such as panel thickness and wire mesh content were tested for their ability to enhance performance. The material constituents providing the best strength and ductility performance were identified using a statistical approach. The experimental results were obtained from direct tensile tests and compression tests. The method also identified the different mobilisation stages of the hybrid reinforcement in the various crack phases. Based on all results from the experimental investigations, the following conclusions can be drawn:

1. The presence of PVA fibre effectively improves flexural performance compared to conventional ferrocement and hybrid fibre mortar. The enhancement was observed in flexure strength capacity and deflection performance. Comparisons of hybrid fibre with mono fibre ferrocement showed that the HFF exhibits better performance and capacities.
2. With respect tothe fibre content tested in this study, for the same fibre and wire mesh content, panels combining PVA1 (shorter fibre) and PVA4 (longer fibre) have overall better structural performance than all other combinations. Another hybrid fibre type combination using PVA2 (short) and PVA3 (long) fibre in the mix also showed excellent strength performance. Therefore, the

best hybrid fibre combination, in terms of high-strength capacity and ductility, consists of both short and long fibres.

3. Increasing the content of PVA fibres up to 1.5% volume fraction, leads to a noticeable structural improvement. The enhancement includes flexure strength capacity, ductility and energy absorption of the composite material, compared to 1.00 or 0.75% fibre content.
4. The addition and partial replacement of cement by FA (25%) and SF (5%), a water-cement ratio of 0.38 and superplasticisers (600 ml in 1 $m^3$of mortar) substantially increase the workability (mixture flow). This is a critical factor when using two fibres, as it allows the mixture to fully penetrate between the relatively dense wire mesh. This is not possible with a very stiff mixture, and hence air bubbles are formed, causing defects at those locations and leading to a reduction in the overall performance of the composite.
5. The reinforcement optimisation of wire mesh content leads to a general increase in flexural strength, tensile ductility and energy dissipation of HFF composites. Four layers of 40-mm thick panels exhibited excellent strength, deflection capacities and energy absorption values.
6. Thickness reduction and simultaneous adjustment of wire mesh content increases strain hardening, toughness and energy absorption levels, particularly for thinner panels. This leads to a general weight reduction of the sheets without affecting the strength capacity of the HFF composites.
7. Remarkable strength and energy absorption results were achieved using a wire mesh volume fraction of 0.69–0.80% with different panel thicknesses: 25, 30 and 40 mm.
8. The addition of hybrid fibre to ferrocement panels is extremely desirable to improve tensile strength capacity and ductility, and confers strain hardening properties.
9. The proportions of the components are individual and depend on the intended application for the material. The function of the applied structure element is an essential factor in choosing the proportions. In other words, the material constituents for members requiring high tensile strength performance will differ from those for members requiring more flexibility and excellent strain capacities. Specifically, the proportions to be considered in members subjected to tension forces are the short and long fibre amount, and wire

mesh content. Therefore, the material quantities can be designed according to the loads acting on the composite.

10. Shorter fibre is activated according to its propagation at the crack scale, showing a higher contribution during the strain at first crack, whereas longer fibre is mobilised at maximum strength. This indicates that shorter fibres contribute to bridging microcracks and longer fibres, to bridging cracks at the localisation period.
11. Longer fibre efficiently contributes to deflection capacity, and both fibre types contribute equally to flexural strength.
12. The wire mesh also has a significant effect on maximum tensile strength and the strain at the first crack, which contributes to the overall performance of HFF composite, whereas PVA fibre contributes to the strain at maximum strength and has less effect during the first crack.
13. Moderate amounts of FA appear not to decrease ultimate flexure and tensile strength.

9.3 Conclusions on structural behaviour and mechanical properties of the HFF composite

The structural and micromechanical material specification have been determined. At the structural level, tests were conducted to determine tensile, flexure and compressive strengths, and shear behaviour. A composite classification approach was used to define the material behaviour. The method was based on the tensile stress–strain behaviour and the toughness index obtained from the bending test. The multiple crack observation was included in the evaluation. In addition, a micromechanical analysis was performed using the nanoindentation results. The results were statistically analysed to determine the packing density, hardness and micromechanical elastic modulus. The elastic modulus obtained was compared with other results from a compression test and later by using a numerical FE simulation. In general the following specific conclusions can be drawn:

1. Hybrid PVA fibre composites show greater ultimate strength and yield strain capacity at maximum load than those of the control specimens.

2. Given the specimen preparation and testing procedure used, the optimum volume fraction of fibre was ~1.5%. The highest direct tensile stress observed was 6.5 MPa.
3. The maximum stress and ductility of the HFF composite are significantly improved by the presence of fibre in the matrix. However, no consistent correlation could be established between direct tensile strength and indirect tensile strength due to the different mixtures, specimen sizes and test procedures.
4. In the tensile test, not all tested specimens exhibited clear multiple cracking behaviour, regardless of the amount of each fibre type. A single large crack was generally observed. In contrast, almost all dogbone-shaped samples showed multiple cracking during direct tensile tests. The behaviour described might be attributed to the self-healing properties of fibre-reinforced materials.
5. The equivalent flexure stress showed improvement using welded square mesh rather than hexagonal chicken mesh.
6. In the shear test, the increase in panel thickness increased the carrying load capacity of HFF plates. However, thinner panels showed relatively good shear stresses.
7. The shear strut–tie model was successfully applied. The applied load affected the crack formation behaviour in the samples tested for shear. This could be related to the extended area in a nodal zone using uniformly distributed line load. In general, a state of pure shear exists at the centre of the specimen under single load and specimens show flexure failure modes. The maximum crack occurs at the middle of the sample. In contrast, samples tested using the loaded disk showed shear crack development in a diametrical direction along the struts.
8. The pullout test was conducted to measure the average bond strength as an indication of crack bridging capacity. The measurement included the pullout load, which is important in calculating the shear bond. The pullout strength of the shorter fibre was 1.4 MPa, and of the longer fibre, 1.87 MPa.
9. Using wire mesh with hybrid PVA fibre led to higher energy absorption in comparison with non-wire-reinforced specimens.
10. Strain hardening behaviour was inferred from the mechanical classification using toughness index and multiple cracking formation. The HFF composite

with 1.5% PVA fibre volume fraction and four layers of wire mesh was classified as a high performance material.

11. The nanoindentation method provided satisfactory values for the elastic modulus of the composite mixture. The experimental method using the standard compressive strength also showed good results in determining the elastic modulus, in comparison with the nanoindentation method.
12. The elastic modulus obtained for the HFF matrix was 26.8 GPa for samples without FA and SF. There was a slight increase to 27.4 GPa in the elastic modulus for the composite matrix containing 25% FA and 5% SF. However, the deviation between the elastic modulus achieved using both methods was less than 1%. The FE method did not match precisely with the test results but it showed a good indication of the data validity.
13. The elastic modulus of the whole composite was obtained using a method relevant to ferrocement. The total elastic modulus was in the range of 32.1–34.7 GPa depending on the wire mesh type, mixture proportion and test method. Moreover, the reinforcement volume fraction in the cross-section substantially affected the composite modulus.
14. There were no significant changes in the packing density and hardness due to the relatively small amount of fine particle addition to the composite. This could be because of the low quantity of SF (only 5%). In particular, the packing density could be significantly influenced by adding fine particle materials.

9.4 Conclusions from the elevated temperature and carbonation effect tests of the HFF composite

Fire resistance was inferred based on the structural performance of the HFF composite when subjected to high temperatures. The *in situ* flexure load–deflection of HFF panels at temperatures up to 800 °C was used as the primary measurement indicator. The comparison was made with panels tested at ambient temperature. The effects of different thicknesses of ferrocement panels, the use of 25% replacement of cement with FA and the addition of 5% SF in the matrix mixtures were also evaluated. The applicability of the simplified design method based on tensile

reinforcement yielding to predict the capacity reduction due to the effect of fire was also evaluated and compared with Euro code EN1994:2005(1994-1-2 2005).

The carbonation effect on the composite matrix was assessed as a part of the durability study, through the evaluation of structural performance and chemical composition before and after carbonation. Based on those results, the following conclusions can be drawn:

1. The partial replacement of cement with 25% FA and the addition of 5% SF improved flexural strength, ductility and compressive strength of ferrocement at temperatures up to 400^{o}C.
2. The reduction of HFF thickness increased the ductility and capacity in terms of equivalent flexural strength at all elevated temperatures.
3. The microstructural analysis of SEM images confirmed the damage to PVA fibres at 200^{o}C, and complete melting at 400^{o}C and beyond.
4. Cracking of the fibre–matrix interface at temperatures of 600 and 800^{o}C was observed in the HFF, indicating inferior flexural behaviour at those temperatures.
5. Multiple cracking behaviours with no sign of spalling of mortar in HFF under bending were observed at all elevated temperatures. The widths of multiple cracks increased with temperature.
6. Neglecting the tensile strength contribution of PVA fibre-reinforced mortar in the tension zone of ferrocement in predicting the maximum moment capacity provided results that agreed well with experimental values beyond 200^{o}C. The equation used for determining the moment capacity of HFF at elevated temperatures below 200^{o}C needs to be optimised through a reduction factor of the fibre tensile strength. This is because at 100^{o}C, the fibre begins to be affected by the heat and its maximum tensile capacity decreases.
7. The exposure of the specimens to an accelerated carbonation environment led to carbonation depth increases with an increase in exposure time, resulting in higher carbonation depth for all mixtures.
8. The compressive strength of carbonated HFF mixture was slightly higher than that of HFF composites without carbonation.
9. Tests on the carbonation of the HFF composite showed an increase in the compressive strength similar to the plain cement mortar. The carbonation increased compressive strength due to an increase in calcium carbonate

(Calcite). However, the growth of the calcium carbonate negatively affected the flexure strength results. The acidic component of calcium carbonate made changes to the pH of the mortar, so the protective cover over the wire mesh was eliminated and the wire mesh could corrode, reducing the composite's strength capacity under tension.

9.5 Conclusions from the application of the HFF panels as permanent formwork in the slab composite

The high performance HFF panels were used as permanent formwork in the tensile zone of concrete one-way slabs with AAC blocks as infill material. The slabs were tested in flexure, and the following specific conclusions can be made:

1. The use of hybrid PVA fibre in the tensile zone of one-way concrete slabs provides better overall strength and ductility performance compared to conventional one-way slabs or slabs using ferrocement panels.
2. The investigation showed that HFF cover can be successfully used for its proposed application as permanent formwork in one-way concrete slabs using AAC blocks as an infill material.
3. All tested slabs showed full composite action, so the proposed composite slabs can be used as structural flooring in residential buildings.
4. The use of shear studs as connectors between HFF–OWC slabs improved the composite action between the concrete and HFF slabs and contributed to the strength and ductility of the slabs.
5. The reduction of HFF panel thickness to 25 mm decreased the performance of the slab system studied in this investigation.
6. Using shear studs with flat bars had only a slight effect on increasing flexure strength.
7. The slip of slabs with shear studs was negligible and had insignificant effects on the strength capacity and ductility of the composite slabs.
8. The preliminary investigation showed that the permissible deflection according to the ACI building code can be applied as a design indication. However, further investigations to confirm the initial test results are required.

9.6 Conclusions from the FE modelling

The numerical modelling included the micro and structural levels. The following conclusions were drawn from this part of the study:

1. The FEM simulating the RVE (microstructural model) to determine the elastic modulus to some extent validated the experimental results. The FE simulation exhibited slightly higher values in term of elastic modulus. The deviations of the obtained values were less than 4% compared to the experimental results. This was a strong indication that the experimentally determined elastic modulus is in good agreement with the FE model.
2. The application of the numerical model to the HFF panel under flexure showed excellent results compared with experimental data using the elastic modules obtained from the nanoindentation test.
3. The FE simulation of the HFF–OWC slab showed good composite action and lack of failing due to horizontal shear transfer.

9.7 Main conclusions

An extensive experimental programme was carried out in this research to develop conventional ferrocement. Improvements were due to the addition of short and long PVA fibre. The panels were applied in the proposed one-way concrete slabs. The significant overall conclusions are:

1. Conventional ferrocement was successfully developed to be a high performance material. The addition of hybrid fibre resulted in excellent strength and strain capacity. The composite showed strain and deflection hardening behaviour, and multiple crack formation.
2. The composite material proportion can be designed to suit an application and its structural function. The short and long fibre and the wire mesh contributed differently to strength capacity and its corresponding deformation. However, shorter fibre and high wire mesh content were responsible for the high tensile strength, whereas the shorter fibre contributed significantly to strain at first crack. The influence of the longer fibre was on the strain at maximum strength.

3. The HFF panels are ideal for an application as permanent formwork for one-way concrete slabs. The material exhibited excellent structural and durability performance. The addition of fibre improved structural behaviour in the face of high temperatures and carbonation. The excellent structural performance following subjection to environment influences was in conjunction with the addition of PVA fibre. Therefore, the composite is suitable for its application in terms of the viability and survivability.

9.8 Recommendations for future work

After completing the experimental research programme, research in the following areas is recommended:

1. The effect of hybrid PVA fibre ratio (short to long fibre) on the structural performance of HFF panels requires further investigation.
2. Maintaining material costs at a suitable level for developing countries where material expenses are a key factor in construction costs. This is the main reason for not increasing the packing density using additional fine materials. The effects of enhancing packing density and simultaneously increasing toughness would be of great interest, particularly for the application of safety structural elements that require ultra-high performance.
3. Regarding the application of the HFF panels as permanent form work, the deflection analysis of HFF panels under their own weight and that of the fresh concrete immediately and after casting needs to be studied to determine deflection limits and design loads that ensure requirements are met for reshoring and support during *in situ* production of slabs.
4. Further studies are recommended in terms of material saving limitations of the composite slabs: determination of the minimum required reinforcement and concrete slab thickness will be a beneficial cost saving contribution.
5. The composite slabs examined exhibited an average load rate at the permissible deflection of 51.4% of the maximum load, which at this stage can only be considered as an indication of the load at permissible deflection according to the ACI code. To obtain a more reasonable and precise value, large-scale and intensive studies of the different slab types are required.

6. To obtain more detailed design guidelines for the HFF–OWC, further intensive experimental work is recommended. The tests should include the optimum concrete slab reinforcement, the minimum required concrete slab height and the use of alternative infill materials.

Further intensive experimentation must be undertaken to determine the necessary design parameters for the composite slab. The slip–block test developed in Australia, which is internationally recognised and recommended for determining mechanical resistance due to the coefficient of friction between both slabs, needs to be tailored in such a way that it could be applied to the proposed permanent formwork concept.

References

Abdullah, Redzuan and Samuel Easterling. W. 2009. "New Evaluation and Modeling Procedure for Horizontal Shear Bond in Composite Slabs." *Journal of Constructional Steel Research* 65 (4):891–899. doi: http://dx.doi.org/10.1016/j.jcsr. 2008.10.009.

Abdullah, and Mansur, M.A. 2001. "Effect of Mesh Orientation on Tensile Response of Ferrocement." *Journal of Ferrocement* 31 (4):289–298.

Aboul-Anen, Boshra, Ahmed El-Shafey and Mostafa El-Shami. 2009. "Experimental and Analytical Model of Ferrocement Slabs." *International Journal of Recent Trends in Engineering* 1 (6):25–29.

Abushawashi, N., Vimonsatit, V. and Hopkins, G. 2012. "Shotcrete prefabricated ferrocement panels by using WA mixture materials." Research, Development, and Practice in Structural Engineering and Construction, Perth, Australia.

ACI 318. 2011. Building Code Requirements for Structural Concrete. Detroit, USA.

ACI Committee 549-R97. 1997. *State-of-the-Art Report on Ferrocement*. Detroit: ACI.

ACI Committee 544. 2002. Manual of Concrete Practice. In *State-of-the-Art Report on Fiber Reinforced Concrete*. Detroit: ACI.

ACI Committee 549.2 R-04. 2004. Report on Thin Reinforced Cementitious Products. Detroit: ACI.

ACI Committee 549-R93. 2009. Guide for the Design, Construction, and Repair of Ferrocement. Detroit: ACI.

Adajar, Jose. C., Hogue, T and Jordan, C. 2006. "Ferrocement For Hurricane-prone State of Florida." *Structural Faults and Repair conference*, Edinburgh, Scotland UK.

Ahmed, S.F.U., Maalej, M. and Paramasivam, P. 2003. "Strain hardening Behaviorof Hybrid Fiber Reinforced Cement Composites." *Ferrocement* 3 (33):172–82.

Ahmed, Shaikh Faiz Uddin, Maalej, M. and Paramasivam, P. 2007a. "Analytical Model for Tensile Strain Hardening and Multiple Cracking Behavior of Hybrid Fiber-Engineered Cementitious Composites " *Journal Of Materials In Civil Engineering* 19:527–539. doi: 10.1061/ ASCE 0899-1561 2007 19:7 527

Ahmed, Shaikh Faiz Uddin, Maalej, M. and Paramasivam, P. 2007b. "Flexural Responses of Hybrid Steel–Polyethylene Fiber Reinforced Cement Composites Containing High Volume Fly Ash." *Construction and Building Materials* 21 (5):1088–1097. doi: 10.1016/j.conbuildmat.2006.01.002.

Ahmed, S.F.U. and Maalej, M. 2009. "Tensile Strain Hardening Behaviour of Hybrid Steel–Polyethylene Fibre Reinforced Cementitious Composites."*Construction and Building Materials* 23 (1) : 96–106 .

Ahmed, Shaikh Faiz Uddin and Mihashi, H. 2011. "Strain Hardening Behavior of Lightweight Hybrid Polyvinyl Alcohol (PVA) Fiber Reinforced Cement Composites." *Materials and Structures* 44:1179–1191. doi: 10.1617/s11527-010-9691-8.

Ahmed, S.F.U. and Vimonsatit, V. 2014. "Compressive Strength of Fly-Ash-Based Geopolymer Concrete at Elevated Temperatures." *Fire and Materials*. 39 (2): pp. 174-188. doi: 10.1002/fam.2240.

Akkaya, Yilmaz. Surendra Shah, P. and Ankenman, B. 2001. "Effect of Fiber Dispersion on Multiple Cracking of Cement Composites." *Journal of Engineering Mechanics* 127 (4):311–316. doi: doi:10.1061/(ASCE)0733-9399(2001)127:4(311).

Al-Kubaisy, M. A. and Jumaat, M. Z. 2000. "Flexural Behaviour of Reinforced Concrete Slabs with Ferrocement Tension Zone Cover." *Construction and Building Materials* 14 (5):245–252. doi: http://dx.doi.org/10.1016/S0950-0618(00)00019-2.

Ali, M. A., Majumdar, A.J. and Rayment, D.L. 1972. "Carbon Fibre Reinforcement of Cement." *Cement and Concrete Research* 2 (2):201–212. doi: http://dx.doi.org/10.1016/0008-8846(72) 90042-7.

Allen, C. 2006. *Fire Protection Engineering for New and Existing Tunnels in Concrete Solutions to Fire*. International Tunnelling Association: London.

Alsadey, Salahaldein. 2012. "Influence of Superplasticizer on Strength of Concrete." *International Journal of Research in Engineering and Technology* 1 (3):164–166.

Altun, Fatih, Tefaruk H. and Kamura, A. 2007. "Effects of Steel Fiber Addition on Mechanical Properties of Concrete and RC Beams." *Construction and Building Materials* 21 (3):654–661. doi: http://dx.doi.org/10.1016/j.conbuildmat.2005.12.006.

Alwan, J.M., Naaman, A.E. and Hansen, W. 1991. "Pull-out Work of Steel Fibers From Cementitious Composites: Analytical Investigation." *Cement and Concrete Composites* 13:247–255.

Anitha, M. and Thenmozhi, R. 2012. "Behaviour of Hybrid Ferrocement Slabs Subjected to Impact." *International Journal of Emerging trends in Engineering and Development* 4 (2):465–474.

ANSYS. 2009. Ansys element reference guide. In *Ansys*. Swanson Analysis System, US.

ANSYS Mechanical APDL 15. 2015. Swanson Analysis System, US.

Arif, M., Akhtar, S., Masood, A., Basit, F. and Garg, M. 2001. "Flexural Behaviour of Fly Ash Mortar Ferrocement Panels for Low Cost Housing." *Journal of Ferrocement* 31 (2):125–135.

Arif, M., Pankaj, P. and Kaushik, S. K. 1999. "Mechanical Behaviour of Ferrocement Composites: An Experimental Investigation." *Cement and Concrete Composites* 21 (4):301–312. doi: http://dx.doi.org/10.1016/S0958-9465(99)00011-6.

AS-3600. 2001. Concrete Structures. In *Standard Association of Australia*. Sydney.

ASTM Standard. 1997. Standard Test Method for Flexural Toughness and First Crack Strength of Fiber Reinforced Concrete (using Beam with Third-point Loading). American Society for Testing and Materials.

ASTM Standard. 2011a. Standard Specification for Fiber-Reinforced Concrete. United States: ASTM International.

ASTM Standard. 2011b. Standard Specification for Steel Fibers for Fiber Reinforced Concrete. United States: ASTM International.

ASTM. 2010. Standard Test Method for Static Modulus of Elasticity and Poisson's Ratio of Concrete in Compression.

ASTM. 2012. Standard Test Method for Flexural Performance of Fiber-Reinforced Concrete (using Beam with Third-point Loading). In *C1609/C1609M*: ASTM.

ASTM. 2013. Standard Test Method for Flexural Performance of Fiber-Reinforced Concrete (using Beam with Third-point Loading). In *ASTM C1609/C1609M − 12*.

Australian Standard. 1993. Specification for Test Sieves. In *AS 1152*: Standard Australia.

Australian Standard. 2000a. Determination of Indirect Tensile Strength of Concrete Cylinders ('Brazil' or Splitting Test). In *AS 1012.10*: Standard Australia.

Australian Standard. 2000b. Method for Making and Curing Concrete—Compression and Indirect Tensile Test Specimens. In *AS 1012.8.1*: Standard Australia.

Australian Standard. 2010. General Purpose and Blended Cements. In *AS 3972*: Standard Australia.

Aveston, J., Cooper G.A. and Kelly, A. 1971. *Single and Multiple Fracture*. The Properties of Fibre Composites: Guildford.

Bahr, David F. and Morris, D. J. 2008. *Springer Handbook of Experimental Solid Mechanics*. Springer.

Balázs, György. L. and Lublóy, É. 2012. "Reinforced Concrete Structures in and After Fire." *Concrete Structures*:72–80.

Banthia, Nemkumar. 1992. "Pitch-based Carbon Fiber Reinforced Cements: Structure, Performance, Applications, and Research Needs." *Canadian Journal of Civil Engineering* 19 (1):26–38. doi: 10.1139/l92-003.

Banthia, N. and Bhargava, A. 2007. "Permeability of Stressed Concrete and Role of Fiber Reinforcement." *ACI Materials Journal* 104 (1):303–309.

Banthia, Nemkumar, Bindiganavile, V. Jones, J. and Novak, J. 2012. "Fiber-reinforced Concrete in Precast Concrete Applications: Research Leads to Innovative Products." *PCI Journal*: Vol.57(3): 33–46.

Banthia, N.and Gupta, R. 2004. "Hybrid Fiber Reinforced Concrete (HyFRC): Fiber Synergy in High Strength Matrices." *Materials and Structures* 37 (274):707–716.

Banthia, N., F. Majdzadeh, F. Wua, J. and Bindiganavile, V. 2014. "Fiber Synergy in Hybrid Fiber Reinforced Concrete (HyFRC) in Flexure and Direct Shear." *Cement and Concrete Composites* 48:91–97.

Banthia, N. and Nandakumar, N. 2003. "Crack Growth Resistance of Hybrid Fiber Reinforced Cement Composites." *Cement and Concrete Composites* 25 (1):3–9. doi: http://dx.doi.org/10.1016/S0958-9465(01)00043-9.

Barbero, E. J. 2014. *Finite Element Analysis of Composite Materials using Ansys*, 2nd ed. Boca Raton: CRC Press.

Barbero, E. J.and Luciano, R. 1995. "Micromechanical Formulas for the Relaxation Tensor of Linear Viscoelastic Composites with Transversely Isotropic Fibers." *International Journal of Solids and Structures* 32 (13):1859–1872. doi: http://dx.doi.org/10.1016/0020-7683(94)00233-M.

Barr, B., Gettu, R. Al-Oraimi, S.K.A. and Bryana, L.S. 1996. "Toughness Measurement—the Need to Think Again." *Cement and Concrete Composites* 18 (4):281–297. doi: http://dx.doi.org/10.1016/0958-9465(96)00021-2.

Barr, B.I.G., Liu, K. and Dowers, R.C. 1982. "A Toughness Index to Measure the Energy Absorption of Fibre Reinforced Concrete." *International Journal of Cement Composites and Lightweight Concrete* 4 (4):221–227. doi: http://dx.doi.org/10.1016/0262-5075(82)90025-2.

Bentur, A., Diamond, S. and Berke, N.S. 1997. *Steel Corrosion in Concrete: Fundamentals and Civil Engineering Practice*. London: E & FN Spon.

Berger, R.L., Young, J.F. and Leung, K. 1972. "Acceleration of Hydration of Calcium Silicates by CarbonDioxide Treatment." *Nature Phys. Sci. (London)* 240:16–18.

Betterman, L.R., Ouyang, C. and Shah, S.P. 1995. "Fiber–Matrix Interaction in Microfiber-Reinforced Mortar." *Advanced Cement Based Materials* 2 (2):53–61. doi: http://dx.doi.org/10.1016/1065-7355(95)90025-X.

Bhikshma, V., Ravandekishore, B. and Srinivas, R. 2011. "Durability of Polymer and Fly Ash Modified Ferro Cement Elements." *Procedia Engineering* 14 (0):2642–2649. doi: http://dx.doi.org/10.1016/j.proeng.20 11.07.332.

Bindiganavile, Vivek, Banthia, N and Aarup, B. 2002. "Impact Response of Ultra-High-Strength Fiber-Reinforced Cement Composite." *ACI Materials Journal* 99 (6):543–548.

Brown. 1973. *Ferrocement Applications in Developing Countries*, edited by National Academy of Sciences. Washington. D.C.

Chang, T.Y. Asce, M. Taniguchi, H. and Chen, W.F. 1987. "Nonlinear Finite Element Analysis of Reinforced Concrete Panels." *Journal of Structural Engineering* 113 (1):122–140. doi: doi:10.1061/(ASCE)0733-9445(1987)113:1(122).

Chatterjee, Abhijit and Das, D. 2013. "Assessing Flow Response of Self-compacting Mortar by Taguchi Method and ANOVA Interaction." *Materials Research*. 16 (5): 1084-1091.

Chen, Bing and Liu, J. 2004. "Residual Strength of Hybrid-Fiber-Reinforced High-Strength Concrete after Exposure to High Temperatures." *Cement and Concrete Research* 34 (6):1065–1069. doi: http://dx.doi.org/10.1016/j.cemconres.2003.11.010.

Chi, Jack M., Huang, R. and Yang, C.C. 2002. "Effects of Carbonation on Mechanical Properties and Durability of Concrete Using Accelerated Testing Method." *Journal of Marine Science and Technology* 10 (1):14–20.

Clarke, Richard P. 2010. "Study of Full-scale Elements of a Ferrocement Roof System for Caribbean Application." *Construction and Building Materials* 24 (3):221–229. doi: http://dx.doi.org/10.1016/j.conbuildmat.2009.09.003.

Constantinides, Georgios and Ulm, F.-J. 2004. "The Effect of Two Types of C–S–H on the Elasticity of Cement-based Materials: Results from Nanoindentation and Micromechanical Modeling." *Cement and Concrete Research* 34 (1):67–80. doi: http://dx.doi.org/10.1016/S0008-8846(03)00230-8.

Constantinides, G. and Ulm, F.-J. 2006. The Elastic Properties of Calcium Leached Cement Pastes and Mortars: a Multi-scale Investigation.Report, MIT CEE.

Constantinides, G. and Ulm, F.-J. 2007. "The Nanogranular Nature of C–S–H." *Journal of the Mechanics and Physics of Solids* 55 (1):64–90.

Constantinides, G., Ulm, F.-J. and van Vliet, K. 2003. "On the Use of Nanoindentation for Cementitious Materials." *Materials and Structures* 36:191–196.

Cruz, C.R. and Gillen, M. 1980. "Thermal Expansion of Portland Cement Paste, Mortar and Concrete at High Temperatures." *Fire and Materials* 2 (4): 66-70.

Dazio, Alessandro, Buzzini, D and Trüb, M. 2008. "Nonlinear Cyclic Behaviour of Hybrid Fibre Concrete Structural Walls." *Engineering Structures* 30 (11):3141–3150. doi: http://dx.doi.org/10.1016/j.engstruct.2008.03.018.

De Larrard, F. 1999. *Concrete Mixture Proportioning: a Scientific Approach*, *Modern Concrete Technology Series*. E&FN Spon, London

Degtyarev, V.V. 2014a. "Strength of Composite Slabs with End Anchorages. Part I: Analytical Model." *Journal of Constructional Steel Research* 94 (0):150–162. doi: http://dx.doi.org/10.1016/j.jcsr.2013.10.005.

Degtyarev, V.V. 2014b. "Strength of Composite Slabs with End Anchorages. Part II: Parametric Studies." *Journal of Constructional Steel Research* 94 (0):163–175. doi: http://dx.doi.org/10.1016/j.jcsr.2013.10.004.

Deluce, Jordon R. and Vecchio, F.J. 2013. "Cracking Behavior of Steel Fiber-Reinforced Concrete Members Containing Conventional Reinforcement." *ACI Structural Journal* 110 (3):481–490.

Desayi, Prakash and EI-Kholy, S.A. 1991. "Lightweight Fibre-Reinforced Ferrocement in Tension." *Cement and Concrete Composites* 13:37–48.

Dias, W. P. S.G., Khoury, A. and Sullivan, P. J. E. 'Mechanical Properties of Hardened Cement Paste Exposed to Temperatures up to 700 C (1292 F)', *Materials Journa*l, 87, No 2, March – April 1990. Pp 160 - 166.

Dias, W. P. S. (2000). 'Reduction of concrete sorptivity with age through carbonation', *Cement and Concrete Research*, 30(8), 1255-1261.

El Debs, M.K. and Naaman, A.E. 1995. "Bending Behavior of Mortar Reinforced with Steel Meshes and Polymeric Fibers." *Cement and Concrete Composites* 17 (4):327–338. doi: http://dx.doi.org/10.1016/0958-9465(95)00031-7.

Euro code 1994-1-2, EN. 2005. Eurocode 4: Design of composite steel and concrete structures – Part 1–2.

Fahmy, Ezzat, Yousry, H. Shaheen, B.I. Abdelnaby, A. and Abou Zeid, M.N. 2014. "Applying the Ferrocement Concept in Construction of Concrete Beams Incorporating Reinforced Mortar Permanent Forms." *International Journal of Concrete Structures and Materials* 8 (1):83–97. doi: 10.1007/s40069-013-0062-z.

Fischer-Cripps A, Nicholson D, Reviewer. Nanoindentation. *Mechanical Engineering Series*. ASME. Appl. Mech. Rev. 2004;57(2):B12. doi:10.1115/1.1704625.

Fischer, G. 2004. "Characterization of Fiber-reinforced Cement Composites by their Tensile Stress Strain Behavior and Quantification of Crack Formation." *6th RILEM Symposium on Fiber-Reinforced Concretes (FRC)*, 20-22 September 2004, Varenna, Italy.

Fischer, G. 2010. "Application of Engineered Cementitious Composites (ECC) in Prefabricated Modular Housing." *ACI Special Publication* 268 (2):17–28.

Fischer, Gregor and Li, C.V. 2002a. "Effect of Matrix Ductility on Deformation Behavior of Steel Reinforced ECC Flexural Members under Reversed Cyclic Loading Conditions." *ACI Structural Journal* 99 (6):781–90.

Fischer, Gregor. and Li, V.C. 2002b. "Influence of Matrix Ductility on Tension-Stiffening Behavior of Steel Reinforced Engineered Cementitious Composites (ECC)." *ACI Structural Journal* 99 (1):104–111.

Fischer, G. and 2003a. "Ultra-ductile Engineered Cementitious Composites for Seismic Resistant Structures." *FIB Symposium*, Athens, Greece.

Fischer, Gregor and Li, C.V. 2003b. "Deformation Behavior of Fiber-Reinforced Polymer Reinforced Engineered Cementitious Composite (ECC) Flexural Members under Reversed Cyclic Loading Conditions." *ACI Structural Journal* 100 (1):25–35.

Fischer, G. and Li, C.V. 2007. "Effect of Fiber Reinforcement on the Response of Structural Members." *Engineering Fracture Mechanics* 74 (1-2):258–272.

Fukuyama, H., Matsuzaki, Y. Nakanoand, K. Sato, Y. 1999. "Structural Performance of Beam Elements with PVA–ECC." *3rd International RILEM Workshop on High Performance Fiber Reinforced Cement Composites*.

Garboczi, E.J. and J.G. Berryman. 2001. "Elastic Moduli of a Material Containing Composite Inclusions: Effective Medium Theory and Finite Element Computations." *Mechanics of Materials* 33 (8):455–470.

Greepala, Vatwongand Nimithyongskul. P. 2006. "Structural Integrety and Insulation Property of Ferrocement Exposed to Fire." *Journal of Ferrocement* 36 (4):939.

Greepala, Vatwong and Nimithyongskul. P. 2008. "Structural Integrity of Ferrocement Panels Exposed to Fire." *Cement and Concrete Composites* 30 (5):419–430. doi: http://dx.doi.org/10.1016/j.cemconcomp.2007.08.007.

Greepala, Vatwong, Parichatprechaand, R. Tanchaisawat, T. 2011. Specific Heat Capacity of Ferrocement Using Inverse Thermal Analysis. RSID6- STR-10, http://fscieng. csc. ku. ac. th/~ce/images/stories/paper/vatwong_rsid_str100.pdf.

Grübl, P., Weigler, H. and Karl, S. 2001. *Beton, Arten, Herstellung und Eigenschaften*. Vol. 2.Ernst & Sohn:Berlin.

Hago, A.W., Al-Jabri, K.S. Alnuaimi, A.S. Al-Moqbali, H. and Al-Kubaisy, M.A. 2005. "Ultimate and Service Behavior of Ferrocement Roof Slab Panels." *Construction and Building Materials* 19 (1):31–37. doi: http://dx.doi.org/10.1016/j.conbuildmat. 2004.04.034.

Hemmaty, Y. 1998. "Modelling of the Shear Force Transferred Between Cracks in Reinforced and Fibre Reinforced Concrete Structures." *Proceedings of the ANSYS*.

Hikasa, J., Genbaand, T and Mizobe, A. 1986. "Replacement for Asbestos in Reinforced Cement Products." *Man-Made Fibers Congress*, Dornbirn, Austria.

Horikoshi, T., Ogawa, A. Saito, T and Hoshiro, H. 2006. "Properties of Polyvinylalcohol Fiber as Reinforcing Materials for Cementitious Composites." *International RILEM Workshop on HPFRCC in Structural Applications*.

Hossain, M.Z and Awal, A.S.M.A. 2011. "Experimental Validation of a Theoretical Model for Flexural Modulus of Elasticity of Thin Cement Composite." *Construction and Building Materials* 25:1460–1465.

Hossain, Z., Rokonuzzaman, M and Inoue, S. 2005. "Flexural Behavior of Cement Composites Panels Reinforced with Different Types of Meshes." *30th Our World in Concrete & Structures*, Singapore, 23–24 August 2005.

Huyse, L., Hemmaty, Y and Vandewalle, L. 1994. "Finite Element Modeling of Fiber Reinforced Concrete Beams." *Proceedings of the ANSYS Conference*, Pittsburgh, Pennsylvania.

Ibrahim, Hassan M.H. 2011a. "Shear Capacity of Ferrocement Plates in Flexure." *Engineering Structures* 33 (5):1680–1686. doi: http://dx.doi.org/10.1016/j.engstruct.2011.02.004.

Ibrahim, Hassan Mohamed 2011b. "Experimental Investigation of Ultimate Capacity of Wired Mesh-reinforced Cementitious Slabs." *Construction and Building Materials* 25:251–259.

Jayakumar, Jothi, V and Anandan, S. 2014. "Composite Strain Hardening Properties of High Performance Hybrid Fibre Reinforced Concrete." *Advances in Civil Engineering* 2014:1–9.

Japanese Industrial Standard. 2006. Method of Making and Curing Concrete Specimens.

Juárez, C. Valdez, P. Durán, A and Konstantin Sobolev. 2007. "The Diagonal Tension Behavior of Fiber Reinforced Concrete Beams." *Cement and Concrete Composites* 29 (5):402–408. doi: http://dx.doi.org/10.1016/j.cemconcomp.2006.12.009.

Kanda, T., Lin, Z and Li, V.C 2000. "Tensile Stress–Strain Modeling of Pseudostrain Hardening Cementitious Composites." *Journal of Materials in Civil Engineering* 12 (2):147–156. doi: doi:10.1061/(ASCE)0899-1561(2000)12:2(147).

Kandal, Tetsushi and Li, V.C 1998. "Interface Property and Apparent Strength of High-Strength Hydrophilic Fiber in Cement Matrix." *Journal of Materials in Civil Engineering* 10 (1):5–13. doi: doi:10.1061/(ASCE)0899-1561(1998)10:1(5).

Kanit, T., Forest, S. Galliet, I. Mounoury, V and Jeulin, D 2003. "Determination of the Size of the Representative Volume Element for Random Composites: Statistical and Numerical Approach." *International Journal of Solids and Structures* 40 (13–14):3647–3679. doi: http://dx.doi.org/10.1016/S0020-7683(03)00143-4.

Katsuki, T. 2003. Ferrocement Permanent Formwork. Google Patents.URL: WO2003102317 A1

Kaufmann, J.P 2014. "Durability Performance of Fiber Reinforced Shotcrete in Aggressive Environment." *Proceedings of the World Tunnel Congress*, Brazil.

Kesner, K.E., Billington, S.L and Douglas, K.S 2003. "Cyclic Response of Highly Ductile Fiber-Reinforced Cement-Based Composite." *ACI Materials* 100 (5):381–390.

Kodur, V.K.R. 2002. "Fire Resistance Evaluation of Large Scale Structural System." *Fire Resistance Determination and PerformancePrediction Research Needs Workshop: Proceedings N: 002. 2002.* .

Kong, D.L.Y. and Sanjayan, J.G 2010. "Effect of Elevated Temperatures on Geopolymer Paste, Mortar and Concrete." *Cement and Concrete Research* 40 (2):334–339.

Kong, H.J. Bike, S.G. and. Li, V.C 2003. "Constitutive Rheological Control to Develop a Self-consolidating Engineered Cementitious Composite Reinforced with Hydrophilic Poly(Vinyl Alcohol) Fibers." *Cement and Concrete Composites* 25 (2):333–341.

Kullaa, J. 1996. "Analysis of Elastic Fibre Bridging in the Multiple Cracked Composite." *Journal of materials science* 31:61–70.

Kullaa, J. 1997. *Finite Element Modelling of Fibre-reinforced Brittle Materials*. Delft, The Netherlands: Civil Engineering and Geosciences.

Kullaa, J. 1998. "Micromechanics of Multiple Cracking." *Journal of Materials Science* 33:4213–24.

Kumar Mehta, P. and Monteiro, P.J.M 2006. *Concrete,Microstructure, Properties, and Materials*. 3rd ed.: McGraw-Hill. New York. DOI: 10.1036/0071462899

Lee, Ho Jae, Do Gyeum Kim, Jang Hwa Lee and Myoung Suk Cho. 2012. " A Study for Carbonation Degree on Concrete using a Phenolphthalein Indicator and Fourier-Transform Infrared Spectroscopy." In Proceedings of World Academy of Science, Engineering and Technology, 184-90. Çanakkale, Italy. WASET

Lee, Seong-Cheol, Jae-Yeol Cho and Frank J. Vecchio. 2011a. "Diverse Embedment Model for Steel Fiber-Reinforced Concrete in Tension: Model Development." *ACI Materials Journal* 108 (5):516–525.

Lee, Seong-Cheol, Jae-Yeol Cho and Frank J. Vecchio. 2011b. "Diverse Embedment Model for Steel Fiber-Reinforced Concrete in Tension: Model Verification." *ACI Materials Journal* 108 (5):526–235.

Li, G.Q. Zhao, Y. Pang, S.S and Li, Y.Q. 1999. "Effective Young's Modulus Estimation of Concrete." *Cement and Concrete Research* 29 (9):1455–1462.

Li, Victor. C. 1993. "From Micromechanics to Structural Engineering—the Design of Cementitious Composites for Civil Engineering Applications." *Struct Mechanics Earthquake Eng. -JSCE* 10(2):37–48.

Li, Victor. C. 1997. *Engineered Cementitous Composittes (ECC) Tailored Composites through Micromechanical Modeling*. Fiber Reinforced Concrete: Canada.

Li, Victor. C. 2003. "On Engineered Cementitious Composittes (ECC) A Review of the Material and Its Applications." *Advanced Concrete Technology* 1 (3):215–230.

Li, Victor. C. 2008. "Engineered Cementitious Composites (ECC)—Material, Structural, and Durability Performance."In *Concrete Construction Engineering Handbook*,edited by E. Nawy, CRC Press.

Li, V and Leung, C. 1992. "Steady-State and Multiple Cracking of Short Random Fiber Composites." *Journal of Engineering Mechanics* 118 (11):2246–2264. doi: doi:10.1061/(ASCE)0733-9399(1992)118:11(2246).

Li, Victor C., Mishra, D. K. Naaman, A. E. Wight, J. K. LaFave, J. M. Wu, H.-C and Inada, Y. 1994. "On the Shear Behavior of Engineered Cementitious Composites." *Advanced Cement Based Materials* 1 (3):142–149. doi: http://dx.doi.org/10.1016/1065-7355(94)90045-0.

Li, Victor. C., Horii, H. Kabele, P. Kanda, T and Lim, Y.M. 2000. "Repair and Retrofit with Engineered Cementitious Composites." *Engineering Fracture Mechanics* 65:317–334.

Li, Victor. C. and Kanda, T. 1998. "Engineered Cementitious Composites for Structural Applications." *Journal of Materials in Civil Engineering* 10 (2):66–69.

Li, Victor. C. Lepech, M. Wang, S. Weimann, M and Keoleian, G. 2004a. "Development of Green ECC for Sustainable Infrastructure Systems." *International Workshop on Sustainable Development and Concrete Technology*, Iowa State University.

Li, Victor. C., Lepech, M. Wang, S. Weimann, M and Keoleian, G. 2004b. "Development of Green Engineered Cementitious Composites for Sustainable Infrastructure Systems." *International Workshop on Sustainable Development and Concrete Technology*, Beijing, China.

Li, Victor C. and Maalej, M 1996a. "Toughening in Cement Based Composites. Part I: Cement, Mortar, and Concrete." *Cement and Concrete Composites* 18 (4):223–237. doi: http://dx.doi.org/10.1016/0958-9465(95)00028-3.

Li, Victor C. and Maalej, M 1996b. "Toughening in Cement Based Composites. Part II: Fiber Reinforced Cementitious Composites." *Cement and Concrete Composites* 18 (4):239–249. doi: http://dx.doi.org/10.1016/0958-9465(95)00029-1.

Li, V.C., and Stang, H. 2004. "Elevating FRC Material Ductility to Infrastructure Durability." To appear in proceedings of BEFIB, Varenna, Italy.

Li, Victor C., Wang, S and Wu, S. 2001. "Tensile Strain-Hardening Behavior of Polyvinyl Alcohol Engineered Cementitious Composite (PVA–ECC)." *ACI Materials Journal* 98 (6):463–472.

Li, Victor C. and Wang, S. 2006. "Microstructure Variability and Macroscopic Composite Properties of High Performance Fiber Reinforced Cementitious Composites." *Probabilistic Engineering Mechanics* 21:201–206.

Li, Victor C., Wu, S. Wang, S. Ogawa, A and Saito, T 2002. "Interface Tailoring for Strain Hardening Polyvinyl Alcohol Engineered Cementitious Composite (PVA–ECC)." *ACI Materials Journal* 99 (5):463–72.

Lim, D.H. and B.H. Oh. 1999. "Experimental and Theoretical Investigation on the Shear of Steel Fibre Reinforced Concrete Beams." *Engineering Structures* 21 (10):937–944. doi: http://dx.doi.org/10.1016/S0141-0296(98)00049-2.

Lin, Zhong and Li, Victor C. 1997. "Crack Bridging in Fiber Reinforced Cementitious Composites with Slip Hardening Interfaces." *Journal of the Mechanics and Physics of Solids* 45 (5):763–87.

Lukovic, Mladena, Savija, B. Dong, H, Schlangen, E and Ye, G 2014. "Micromechanical Study of the Interface Properties in Concrete Repair System." *Journal of Advanced Concrete Technology* 12:320–339.

Maalej, M., Hashida, T and 1995. "Effect of Fiber Volume Fraction on the Off-Crack-Plane Fracture Energy in Strain Hardening Engineered Cementitious Composites." *Journal of American Ceramics Society* 78 (12):3369–3375.

Maalej, M. and Li, V.C 1994. "Flexural—Tensile Strength Ratio in Engineered Cementitious Composites." *Journal of Materials in Civil Engineering* 6 (4): 513-528.

Maalej, Mohamed and Li, V.C 1995. "Introduction of Strain Hardening Engineered Cementitious Composites in Design of Reinforced Concrete Flexural Members for lmproved Durability." *ACI Structural Journal* 92 (2):167–76.

Maalej, M., Quek, S.T. Ahmed, S.F.U. Zhang, J. Lin V.W.J and Leong, K.S 2012. "Review of Potential Structural Applications of Hybrid Fiber Engineered Cementitious Composites." *Construction and Building Materials* 36 (0):216–227. doi: http://dx.doi.org/10.1016/j.conbuildmat.2012.04.010.

MacGregor, J.G. 1992. *Reinforced Concrete Mechanics and Design*. Englewood Cliffs: Prentice-Hall.

Maligno, A.R., Warrior, N.A and Long, A.C 2008. "Finite Element Investigations on the Microstructure of Fibre-reinforced Composites." *eXPRESS Polymer Letters* 2 (9):665–676. doi: 10.3144/expresspolymlett.2008.79.

Mansur, A., Maalej, M. and Ismail, M. 2008. "Study on Corrosion Durability of Ferrocement." *ACI Materials Journal* 105 (1): 28-34.

Mansur, M.A. and Paramasivam, M 1985. "Ferrocement under Combined Bending and Axial Loads." *The International Journal of Cement Composites and Lightweight Concrete* 7 (3):151–158.

Markovic, I. 2006. "High Performance Hybrid-Fiber Concrete." PhD thesis, Delft University of Technology.

Markovic, I. Walraven, J.C. and van Mier, J.G.M 2003. "Development of High Performance Hybrid Fibre Concrete." *4th International RILEM Workshop on High Performance Fiber Reinforced Cement Composites (HPFRCC4)*.

Masood, A., Arif, M. Akhtar, S and Haquie, M 2003. "Performance of Ferrocement Panels in Different Environments." *Cement and Concrete Research* 33 (4):555–562. doi: http://dx.doi.org/10.1016/S0008-8846(02)01003-7.

Memon, Noor Ahmed, Sumadi, S.R. and Ramli, M 2007. "Ferrocement Encased Lightweight Aerated Concrete: A Novel Approach to Produce Sandwich Composite." *Materials Letters* 61 (19–20):4035–4038. doi: http://dx.doi.org/10.1016/j.matlet.2007.01.039.

Mihashi, H. and Ohno, Y 2007. "Toughening Mechanism of Hybrid Fiber Reinforced Cement Composites." Fracture Mechanic of Concrete and Concrete Structures—High Performance Concrete, Brick Masonry and Environmental Aspects.

Mobasher, B., Stang, H and Shah, P 1990. "Microcracking in Fiber Reinforced Concrete." *Cement and Concrete Research* 20 (5):665–676. doi: http://dx.doi.org/10.1016/0008-8846(90)90001-E.

Monkman, Sean and Shao, Y 2006. "Assessing the Carbonation Behavior of Cementitious Materials." *Journal of Materials in Civil Engineering*18:768–776. doi: 10.1061/ASCE0899-1561200618:6768.

Naaman, A.E. 1999. Optimized Geometries of Fibre Reinforcement of Cement, Ceramic and Polymeric Based Composites. US: Patent No: 5989713.

Naaman, A.E. 2000. *Ferrocement and Laminated Cementitious Composites*. Michigan: Techno Press 3000.

Naaman, A.E. 2003a. "Strain Hardening and Deflection Hardening Fiber Reinforced Cement Composite." *4th International RILEM Workshop on High Performance Fiber*.

Naaman, A.E. 2003b. "Engineered Steel Fibers with Optimal Properties for Reinforcement of Cement Composites." *Journal of Advanced Concrete Technology* 1 (3):241–252. doi: 10.3151/jact.1.241.

Naaman, A.E. 2005. "Thin Cement Composites: Performance Comparison Between Steel and Textile Reinforcements." Composites in Construction, University of Lyon, France.

Naaman, A.E. 2006. "Ferrocement: Four Decades of Progress." *Journal of Ferrocement* 36 (1):741–756.

Naaman, A.E. 007. "High Performance Fiber Reinforced Cement Composites: Classification and Applications." CBM-CI international workshop, Karachi, Pakistan.

Naaman, A.E. 2013. "Evolution in Ferrocement and Thin Reinforced Cementitious Composites." *Arab Journal of Scince and Engineering* 37:421–441.

Naaman, A.E. and Jeong, S.M 1995. "Structural Ductility of Beams Prestressed with FRP Tendons." *Proceedings 2nd International Symposium on Non-Metallic (FRP) Reinforcement for Concrete Structures*, Belgium.

Naaman, A.E., Moavenzadeh, F and McGarry, F 1974. "Probabilistic Analysis of Fiber Reinforced Concerete." *Journal of Engineering Mechanics Division* 100 (EM 2):397–413.

Naaman, A.E., Namur, G. Najm, H and Alwan, J 1989. "Mechanisms in Fiber Reinforced Cement-based Composites." Report of the US Department of Civil Engineering, The University of Michigan.

Naaman, A.E., Namur, G.G.,. Alwan, J.M and Najm, H.S 1991. "Fiber Pullout and Bond Slip. I: Analytical Study." *Journal of Structural Engineering* 119:2769–2790.

Naaman, A.E. and H.W. Reinhardt. 1995. "Characterization of High Performance Fiber Reinforced Cement Composites." *Proceedings of the second international RILEM workshop*, U.S.A, June 1995.

Naaman, A.E. and H.W. Reinhardt. 2006. "Proposed Classification of HPFRC Composites Based on their Tensile Response." *Materials and Structures* 39:547–555. doi: 10.1617/s11527-006-9103-2.

Najm, H.S. and Naaman, A.E 1995. "Prediction Model for Elastic Modulus of High Performance Fiber Reinforced Cement-Based Composites." *ACI Materials Journal* 92 (3):304–314.

Nanni, Antonio and Zollo, R.F. 1987. "Behavior of Ferrocement Reinforcement in Tension." *ACI Materials Journa.* 84(4):273–277.

Nassif, Hani H. and Najm, H 2004. "Experimental and Analytical Investigation of Ferrocement–Concrete Composite Beams." *Cement and Concrete Composites* 26 (7):787–796. doi: http://dx.doi.org/10.1016/j.cemconcomp.2003.08.003.

Nishida, A., Yamazaki, N. Inoue, H. Schneider, U and Diederichs, U 1995. "Study on the Properties of High Strength Concrete with Short Polypropylene Fibers for Spalling Resistance." Conference of the Concrete Under Severe Environment.

Oliver, W.C. and Pharr, G.M 2004. "Measurement of Hardness and Elastic Modulus by Instrumented Indentation: Advances in Understanding and Refinements to Methodology." *Journal of Materials Research* 19 (1): 3-20.

Özbay, E., Karahan, O. Lachemi, M. Hossain, K.M.A and Atis, C.D 2012. "Investigation of Properties of Engineered Cementitious Composites Incorporating High Volumes of Fly Ash and Metakaolin." *ACI Materials Journal* 109 (5):565–571.

Özbay, Erdoğan, Oztas, A. Baykasoglu, A and Ozbebek, H 2009. "Investigating Mix Proportions of High Strength Self Compacting Concrete by using Taguchi Method."

Construction and Building Materials 23 (2):694–702. doi: http://dx.doi.org/10.1016/j.conbuildmat.2008.02.014.

Özcan, D. Mehmet, Bayraktar, A. Şahin, A. Haktanir, T and Türker, T 2009. "Experimental and Finite Element Analysis on the Steel Fiber-reinforced Concrete (SFRC) Beams Ultimate Behavior." *Construction and Building Materials*23(2):1064–1077.Doi:http://dx.doi.org/10.1016/j.conbuildmat 2008.05.10.

Padmarajaiah, S.K. and Ramaswamy, A 2002. "A Finite Element Assessment of Flexural Strength of Prestressed Concrete Beams with Fiber Reinforcement." *Cement and Concrete Composites* 24 (2):229–241. doi: http://dx.doi.org/10.1016/S0958-9465(01)00040-3.

Papadakis, V.G., Vayenas, C.G and Fardis, M.N. 1991. "Physical and Chemical Characteristics Affecting the Durability of Concrete." *ACI Materials Journal* 8 (2):186–196.

Paramasivam, P. 2001. "Ferrocement structural applications." 26th Conference on Our World in Concrete & Structures, Singapore.

Paramasivam, P. and Nathan, G.K 1984. "Prefabricated Ferrocement Water Tank." *ACI Journal* 8 (81):582–586.

Paramasivam, P. and Ravindrarajah, R.S 1988. "Effect of Arrangements of Reinforcements on Mechanical Properties of Ferrocement." *ACI Structural Journal* 85 (1): 3-11.

Park, Seung Hun, Kim, D. J. Gum Sung Ryu and Kyung Taek Koh. 2012. "Tensile Behavior of Ultra High Performance Hybrid Fiber Reinforced Concrete." *Cement and Concrete Composites* 34 (2):172–184. doi: http://dx.doi.org/10.1016/ j.cemconcomp.2011.09.009.

Parra-Montesinos, G. and Wight, J 2000. "Seismic Response of Exterior RC Column-to-Steel Beam Connections." *Journal of Structural Engineering* 126 (10):1113–1121. doi: doi:10.1061/(ASCE)0733-9445(2000)126:10(1113).

Paul, B.K and Pama, R.P1978. *Ferrocement*. Bangkok: IFIC.

Pereira, E.B., Fischer, G. and Barros, J.A.O 2012a. "Effect of Hybrid Fiber Reinforcement on the Cracking Process in Fiber Reinforced Cementitious Composites." *Cement and Concrete Composites* 34 (10):1114–1123. doi: http://dx.doi.org/10.1016/j.cemconcomp.2012.08.004.

Pereira, Eduardo B., Joaquim, G.F. Barros A.O 2012b. "Direct Assessment of Tensile Stress–Crack Opening Behavior of Strain Hardening Cementitious Composites (SHCC)." *Cement and Concrete Research* 42 (6):834–846. doi: 10.1016/j.cemconres.2012.03.006.

Prakash, Desayi and EI-Kholy, S.A 1991. "Lightweight Fibre-Reinforced Ferrocement in Tension." *Cement & Concrete Composites* 13:37–48.

Purkiss, John A. 2007. *Fire Safety Engineering Design of Structures*, 2nd ed. Great Britain: Elsevier.

Ranade, Ravi, Li, V.C. Stults, M.D. Todd S. Rushing, Jason Roth and Heard, F.W 2013. "Micromechanics of High-Strength, High-Ductility Concrete." *ACI Materials* 110 (4):375–384.

Rao, Samruddhi, Pragati Samant, Athira Kadampatta and Reshma Shenoy. 2013. "An Overview of Taguchi Method-Evolution, Concept and Interdisciplinary Applications." *International Journal of Scientific & Engineering Research* 4 (10): 622-626.

Ravichandran, A., Suguna, K. and Ragunath, P.N 2009. "Strength Modeling of High-Strength Concrete with Hybrid Fibre Reinforcement." *American Journal of Applied Sciences* 6 (2): 219–223.

Ross, P.J 1996. *Taguchi Techniques for Quality Engineering*, 2nd ed. New York: McGraw.

Rots, J.G and Blaauwendraad, J 1989. "Crack Models for Concrete: Discrete or Smeared? Fixed, Multi-directional or Rotating?" In *HERON:* Delfet University of Technology.

Roylance, David. 2000. Laminated composite plates. Cambridge: Department of Materials Science and Engineering, Massachusetts Institute of Technology.

Saemann. J.G.and Washa. G.W 1997. "Variation of Mortar and Concrete Properties and Temperature." *ACI Proceedings* 5 (54):385–97.

Şahmaran, Mustafa, Lachemi, M and Li, V.C 2010. "Assessing Mechanical Properties and Microstructure of Fire-Damaged Engineered Cementitious Composites." *ACI Materials Journal* 107 (3):297–304.

Şahmaran, Mustafa and Li, V.C 2008. "Durability of Mechanically Loaded Engineered Cementitious Composites under Highly Alkaline Environments." *Cement & Concrete Composites* 30:72–81.

Şahmaran, Mustafa, Erdoğan Özbay, Hasan Yücel, Mohamed Lachemi and Li, V.C 2011. "Effect of Fly Ash and PVA Fiber on Microstructural Damage and Residual Properties of Engineered Cementitious Composites Exposed to High Temperatures." *Journal Of Materials in Civil Engineering* (23):1735–1745.

Sakulich, Aaron Richard and Li, V.C 2011. "Nanoscale Characterization of Engineered Cementitious Composites (ECC)." *Cement and Concrete Research* 41 (2):169–175. doi: http://dx.doi.org/10.1016/j.cemconres.2010.11.001.

Saleem, M.A. and Ashraf, M 2008. "Low Cost Earthquake Resistant Ferrocement Small House." *Pakistan Journal of Engineering and Applied Sciences* 2: 59-64.

Sarvaranta, L. and Mikkola, E 1994. "Fibre Mortar Composites in Fire." *Fire Mater* 18 (1):45–50.

Sasiekalaa, K. and Malathy, R 2012. "A Review Report on Mechanical Properties of Ferrocement with Cementitious Materials." *International Journal of Engineering Research & Technology (IJERT)* 1 (9). ISSN: 2278-0181.

Schneider, U. 1988. "Concrete at High Temperatures—a General Review." *Fire Safety Journal* 13 (1988): 55 - 68.

Shakor, Pshtiwan N. and Pimplika, S.S 2011. "Glass Fibre Reinforced Concrete Use in Construction." *International Journal of Technology and Engineering System* 2 (2).

Shannag, M. Jamal. 2008. "Bending Behavior of Ferrocement Plates in Sodium and Magnesium Sulfate Solutions." *Cement & Concrete Composites* 30:597–602.

Shannag, Jamal M. and Bin Ziyyad, T 2007. "Flexural Response of Ferrocement with Fibrous Cementitious Matrices." *Construction and Building Materials* 21 (6):1198–1205. doi: http://dx.doi.org/10.1016/j.conbuildmat.2006.06.021.

Shannag, M. Jamal, Brincker, B and Hansen, W 1997. "Pullout Behavior of Steel Fibers from Cement-based Composites." *Cement and Concrete Research* 27 (6):925–936. doi: http://dx.doi.org/10.1016/S0008-8846(97)00061-6.

Shri, S. Deepa and Thenmozhi, R 2012. "An Experimental Investigation on the Flexural Behavior of SCC Ferrocement Slabs Incorporating Fibers." *International Journal of Engineering Science and Technology* 4 (5):2146–2158.

Sorelli, Luca, Constantinides, G. Ulm, F.-J. and Toutlemonde, F 2008. "The Nano-mechanical Signature of Ultra High Performance Concrete by Statistical Nanoindentation Techniques." *Cement and Concrete Research* 38:1447–1456.

Soroushian, Parviz, Khan. A and Hsu, J.-W 1992. "Mechanical Properties of Concrete Materials Reinforced with Polypropylene or Polyethylene Fibers." *ACI Materials Journal* 89 (6):535–40.

Spanos, A., Sri Ravindrarajah, R and Swamy, R.N 2012. "Material and Structural Implicationsof using ferrocement as Permanent Formwork." *Indian Concrete Journal*:9–23.

Staehli, P. and Van Mier, J.G.M 2007. "Manufacturing, Fibre Anisotropy and Fracture of Hybrid Fibre Concrete." *Engineering Fracture Mechanics* 74:223–242.

Stang, H. 2004. "Toughness in Testing and Design, the FRC Experience." Fracture Mechanics of Concrete Structure. *6th International RILEM Symposium on Fibre-Reinforced Concretes* (FRC) BEFIB. September 2004, Veerna, Italy.

Stang, Henrik and Li, V.C 2004. "Classification of Fibre Reinforced Cementitious Materials for Structural Applications." *6th RILEM Symposium on Fiber-Reinforced Concretes (FRC)*, September 2004,Varenna, Italy.

Suhaendi, Sofren Leo and Horiguchi, T 2006. "Effect of Short Fibers on Residual Permeability and Mechanical Properties of Hybrid Fibre Reinforced High Strength

Concrete after Heat Exposition." *Cement and Concrete Research* 36 (9):1672–1678. doi: http://dx.doi.org/10.1016/j.cemconres.2006.05.006.

Sujivorakul, C. 2012. "Model of Hooked Steel Fibers Reinforced Concrete under Tension." In: Parra-Montesinos, G., Reinhardt, H. & Naaman, A. E. (eds.) High Performance Fiber Reinforced Cement Composites 6. Reports 2:19-26. Springer.

Suwannakarn, Supat W 2009. "Post-cracking Characteristics of High Performance Fiber Reinforced Cementitious Composites." Doctor of Philosophy, Civil Engineering, University of Michigan.

Swamy, N.R. and Hussin, M.W 1990. "Flexural Behavior of Thin Fiber Reinforced and Ferrocement Sheets." *ACI Special Publication* 124:323–356.

Szerszen, Maria M., Szwed, A and Li, C.V 2006. *Flexural Response of Reinforced Beam with High Ductility Concrete Material*. Brittel Matrix Composites 8, Warsaw.

Tanyildizi, Harun. 2013. "Variance Analysis of Crack Characteristics of Structural Lightweight Concrete Containing Silica Fume Exposed to High Temperature." *Construction and Building Materials* 47 (0):1154–1159. doi: http://dx.doi.org/10.1016/j.conbuildmat.2013.05.060.

Tanyildizi, Harun and Coskun, A. 2008. "The Effect of High Temperature on Compressive Strength and Splitting Tensile Strength of Structural Lightweight Concrete Containing Fly Ash." *Construction and Building Materials* 22 (11): 2269–2275.

Tejchman, Jacek and Kozicki, J 2010. *Experimental and Theoretical Investigations of Steel-Fibrous Concrete*. Berlin: Springer-Verlag.

Tjiptobroto, Prijatmadi and Will Hansen. 1991. "Mechanism for Tensile Strain Hardening in High Performance Cement-based Fiber Reinforced Composites." *Cement and Concrete Composites* 13 (4):265–273. doi: http://dx.doi.org/10.1016/0958-9465(91)90032-D.

Trueb, M.C. 2011. "Numerical Modeling of High Performance Fiber Reinforced Cementitious Composites." Doctor of Sciences, Civil engineering, ETH Zurich (19437).

Ulm, Franz-Josef, Vandamme, M. Bobko, C and Ortega, J.A 2007. "Statistical Indentation Techniques for Hydrated Nanocomposites: Concrete, Bone, and Shale." *Journal of the American Ceramic Society* 90 (9):2677–2692. doi: 10.1111/j.1551-2916.2007.02012.x.

UNHCR. 2006. "Large Ferro-Cement Water Tank." Technical Support Section Division of Operational Support.

van Mier, J.G.M. 2003. "High Performance Fibre Reinforced Concrete." *9th Betontagung*

van Mier, J.G.M. 2004. "Cementitious Composites with High Tensile Strength and Ductility through Hybrid Fibres." *6th International RILEM Symposium on Fibre Reinforced Concretes*.

Vandamme, M. and Ulm, F.-J 2009. "Nanogranular Origin of Concrete Creep." *Proceedings of the National Academy of Sciences* 106:10552–10557.

Vandamme, Matthieu, Ulm, F.-J and Fonollosa, P 2010. "Nanogranular Packing of C–S–H at Substochiometric Conditions." *Cement and Concrete Research* 40 (1):14–26. doi: http://dx.doi.org/10.1016/j.cemconres.2009.09.017.

Velez, K., Maximilien, S., Damidot, D. Fantozzi, G., Sorrentino, F., Determination by nanoindentation of elastic modulus and hardness of pure constituents of portland cement clinker, Cem. Concr. Res. 31 (4) (2001) 555–561.

Vimonsatit, V. Wahyuni, Ade S. and Nikraz, N 2012. "Reinforced Concrete Beams with Lightweight Concrete Infill." *Scientific Research and Essays* 7 (14): 2370-2379.

Vimonsatit, V. Wahyuni, Ade S. and Nikraz, N 2011. "Behavior and Strength of Lightweight Sandwich Reinforced Concrete Beams." *Modern Methods and Advances in Structural Engineering and Construction*, International Structural Engineering and Construction Conference. June 21-26, 2011. Zürich.

Vimonsatit, V., Mazlan, M.A and Nikraz, H 2011. "Use of Lightweight Concrete as Infill of Reinforced Concrete Sections." *Incorporating Sustainable Practice in Mechanics of Structures and Materials*, Sujeeva Setunge (eds):245–250. Taylor and Frances, London.

Wahyuni, Ade S., Vimonsatit, V and Nikraz, N 2012. "Shear Behaviour of Ligthweight Sandwich Reinforced Concrete Slabs." *Advances in Structural Engineering* 15. DOI: http://dx.doi.org/10.1260/1369-4332.15.10.1705

Wang, S. and Li, V.C 2003. "Lightweight Engineered Cementitious Composite (ECC)." *HPFRCC4*, USA.

Wang, S. and Li, V.C 2006. "Polyvinyl Alcohol Fiber Reinforced Engineered Cementitious Composites: Material Design and Performances." *Proceedings of International RILEM Workshop on HPFRCC in Structural Applications*.

Wang, S., Naaman, A.E and Li, V.C 2004. "Bending Response of Hybrid Ferrocement Plates with Meshes and Fiber." *Journal of Ferrocement*34 (1):275–288.

Wang, Youjiang, Li, V.C and Backer, S 1990. "Experimental Determination of Tensile Behavior of Fiber Reinforced Concrete." *ACI Materials Journal* 87 (5):461–468.

Ward, R.J. and Li, V.C 1991. "Dependence of Flexural Behaviour of Fibre Reinforced Mortar on Material Fracture Resistance and Beam Size." *Construction & Building Materials*5 (3):151–61.

Wegian, F.M. 2010. "Strength Analysis of Fibrous Ferrocement Concrete and Effect of Using Superplasticiser." *Australian Journal of Structural Engineering* 11 (2):155–162

Whitney, Donna L. Broz, M and Cook, R.F. 2007. "Hardness, Toughness, and Modulus of Some Common Metamorphic Minerals." *American Mineralogist* 92 (2–3):281–288. doi: 10.2138/am.2007.2212.

Whitney, J.M.1967. "Elastic Moduli of Unidirectional Composites with Anisotropic Filaments." *Journal of Composite Materials*1 (2):188–193.

Wierig, H. 1984. "Long Time Studies on the Carbonation of Concrete under Normal Outdoor Exposure." *RILEM Seminar*, Hanover.

Willam, K.J. and Warnke, E.P 1974. "Constitutive Model for Triaxial Behaviour of Concrete." Seminar on Concrete Structures Subjected to Triaxial Stresses, Bergamo, Italy.

Wille, Kayand. Naaman, A.E 2012. "Pullout Behavior of High-strength Steel Fibers Embedded in Ultra-High-Performance Concrete." *ACI Materials Journal* 109 (4):479–87.

Wille, Kay and Naaman, A.E 2013. "Effect of Ultra-High-Performance Concrete on Pullout Behavior of High-Strength Brass-Coated Straight Steel Fibers." *ACI Materials Journal* 110 (4):451–61.

Wille, K., Naaman, A.E, El-Tawil, S and Parra-Montesinos, G 2012. "Ultra-high Performance Concrete and Fiber Reinforced Concrete: Achieving Strength and Ductility without Heat Curing." *Materials and Structures* 45 (3):309–324. doi: :http://dx.doi.org/10.1617/s11527-011-9767-0

Wua, Min, Johannesson, B and Geiker, M 2012. "A Review: Self-healing in Cementitious Materials and Engineered Cementitious Composite as a Self-healing Material." *Construction and Building Materials* 28:571–583.

Xu, B.W., Ju, J.W and Shi, H.S 2011. "Progressive Micromechanical Modeling for Pullout Energy of Hooked-end Steel Fiber in Cement-based Composites." *International Journal of Damage Mechanics*20:922–38.

Xu, Yi, Jiang, L. Xu, J and Li, Y 2012. "Mechanical Properties of Expanded Polystyrene Lightweight Aggregate Concrete and Brick." *Construction and Building Materials* 27 (1):32–38. doi: http://dx.doi.org/10.1016/j.conbuildmat.2011.08.030.

Yang, En-Hua, Wang, S. Yang, Y and. Li, V.C 2008. "Fiber-bridging Constitutive Law of Engineered Cementitious Composites." *Journal of Advanced Concrete Technology* 6 (1):181–193. doi: 10.3151/jact.6.181.

Yang, Yingzi, Lepech, M.D. Yang,E.-H. and Li, V.C 2009. "Autogenous Healing of Engineered Cementitious Composites under Wet–Dry Cycles." *Cement and Concrete Research* 39:382–90.

Yao, Wu, Li, J and Wu, K 2003. "Mechanical Properties of Hybrid Fiber-Reinforced Concrete at Low Fiber Volume Fraction." *Cement and Concrete Research* 33 (1):27–30. doi: http://dx.doi.org/10.1016/S0008-8846(02)00913-4.

Yardim, Yavuz. 2008. "Structural Performance of a Lightweight Composite Slab System." Doctor of Philosophy Civil engineering, Putra Malaysia (FK 200865).

Yardim, Yavuz, Waleed, Abdulmalik Thanoon Mohamad Saleh. Jaafar and Jamaloddin Noorzaie. 2011. "Composite Aerated Concrete and Ferrocement Lightweight Slab." *5th International Conference on Autoclaved Aerated Concrete*, Bydgoszcz, Poland.

Yardim, Yavuz, Waleed, A.M.T. Jaafar, M.S and Laseima, S 2013. "AAC-concrete Light Weight Precast Composite Floor Slab." *Construction and Building Materials* 40 (0):405–410. doi: http://dx.doi.org/10.1016/j.conbuildmat.2012.10.011.

Yasir Alam, S., Lenormand, T. Loukili, A. and Regoin, J.P 2010. "Measuring Crack Width and Spacing in Reinforced Concrete Members." *7th International conference on Fracture Mechanics of Concrete and Concrete Structures*, Seoul.

Zhanga, Jun and Li, V.C. 2002. "Monotonic and Fatigue Performance in Bending of Fiber-reinforced Engineered Cementitious Composite in Overlay System." *Cement and Concrete Research* 32:415–423.

Zhou, Jian, Qian, S. Ye, G. Copuroglu, O. van Breugel K and Li, V.C 2012. "Improved Fiber Distribution and Mechanical Properties of Engineered Cementitious Composites by Adjusting the Mixing Sequence." *Cement and Concrete Composites* 34 (3):342–348. doi: 10.1016/j.cemconcomp.2011.11.019.

Appendix (A)

Tagouchi and ANOVA method

Tensile strength test of HFF composites

Example for the calculation of signal to noise for first crack (Tensile test)

Exp No.	First crack strength			mean	S	S/N (Cal.)	S/N (Minitab)
1	3.69	3.14	3.04	3.29	0.28	10.25	10.25
2	2.38	3.07	4.84	3.43	0.33	9.64	9.64
3	3.51	3.69	4.34	3.85	0.21	11.60	11.60
4	3.44	2.91	5.88	4.08	0.23	11.12	11.12
5	4.04	4.21	3.99	4.08	0.18	12.21	12.21
6	3.85	3.30	2.92	3.35	0.28	10.35	10.35
7	4.15	4.06	5.27	4.49	0.15	12.88	12.88
8	5.13	4.54	3.33	4.33	0.18	12.30	12.30
9	3.09	3.81	4.70	3.87	0.22	11.37	11.37
				3.86	mean	3.86	

Example for the calculation of signal to noise for ultimate tensile strength (Tensile test)

Exp No.	Tensile			mean	S	S/N (cal.)	S/N (mini tab)
1	5.03	4.88	4.58	4.83	0.13	13.66	13.66
2	6.55	6.88	6.52	6.65	0.07	16.45	16.45
3	5.85	6.49	7.15	6.49	0.07	16.16	16.16
4	7.09	7.44	7.49	7.34	0.06	17.3	17.3
5	6.39	6.9	6.33	6.54	0.07	16.29	16.29
6	7.19	6.66	5.92	6.59	0.07	16.29	16.29
7	7.29	7.22	6.7	7.07	0.06	16.97	16.97
8	6.17	7.57	7.46	7.06	0.06	16.87	16.87
9	5.38	5.95	6.09	5.81	0.09	15.24	15.24
				6.49	mean	6.49	

S/N ratio of tensile strength at first crack strength

Levels	Factors			
	FA/C	***W/C***	***PVA1/PVAtot %***	***Wire %***
1	10.50	11.42	10.97	11.28
2	11.22	11.38	10.71	10.95
3	12.18	11.11	12.23	11.68
Delta	1.69	0.31	1.52	0.72
Rank	1.00	4.00	2.00	3.00

S/N ratio of ultimate tensile strength

Levels	Factors			
	FA/C	*W/C*	*PVA1/PVAtot %*	*Wire %*
1	15.42	15.98	15.61	15.06
2	16.63	16.54	16.33	16.57
3	16.36	15.90	16.47	16.78
Delta	1.21	0.64	0.87	1.71
Rank	2.00	4.00	3.00	1.00

Flexural strength test of HFF composites

Example for the calculation of signal to noise for first crack strength (Bending test)

Exp No.	First crack strength			mean	S	S/N (cal.)	S/N (Minitab)
1	7.62	7.19	8.67	7.83	0.05	17.79	17.79
2	7.12	8.38	8.32	7.94	0.05	17.92	17.92
3	7.93	8.03	5.12	7.03	0.07	16.35	16.35
4	7.86	8.31	7.87	8.01	0.05	18.07	18.07
5	7.86	8.21	8.24	8.10	0.05	18.17	18.17
6	7.98	8.24	5.75	7.32	0.06	16.94	16.94
7	6.87	8.93	6.64	7.48	0.06	17.26	17.26
8	8.96	9.88	11.94	10.26	0.03	20.04	20.04
9	8.24	9.67	7.30	8.40	0.04	18.31	18.31
				8.04	mean	8.04	

Example for the calculation of signal to noise for ultimate strength (Bending test)

Exp No.	Ultimate flexure strength			mean	S	S/N (cal.)	S/N (Minitab)
1	11.79	12.11	12.80	12.23	0.02	21.74	21.74
2	14.48	13.69	15.68	14.61	0.01	23.26	23.25
3	10.55	12.02	12.30	11.63	0.02	21.25	21.25
4	13.78	16.39	16.90	15.69	0.01	23.81	23.81
5	9.10	11.78	8.98	9.96	0.03	19.77	19.76
6	12.89	11.98	15.85	13.58	0.02	22.48	22.48
7	9.69	11.93	9.06	10.23	0.03	20.02	20.02
8	15.76	14.03	16.30	15.37	0.01	23.68	23.68
9	10.69	10.97	11.48	11.04	0.03	20.85	20.85
				12.7	mean	12.7	

S/N ratio of flexure strength at first crack

Levels	Factors			
	FA/C	*W/C*	*PVA1/PVA2 %*	*Wire %*
1	17.35	17.71	18.26	18.09
2	17.73	18.71	18.10	17.37
3	18.54	17.20	17.26	18.15
Delta	1.18	1.51	1.00	0.78
Rank	2	1	3	4

S/N ratio of ultimate flexure strength

Levels	Factors			
	FA/C	*W/C*	*PVA1/PVA2 %*	*Wire %*
1	22.08	21.85	22.63	20.78
2	22.02	22.23	22.64	21.92
3	21.52	21.53	20.34	22.91
Delta	0.56	0.71	2.29	2.13
Rank	4.00	3.00	1.00	2.00

Compressive strength test of HFF composites

Example for the calculation of signal to noise for compressive strength

Exp No.	compressive					mean	S	S/N (calc.)	S/N (Minitab)
1	50.0	52.0	48.0	48.0	44.0	48.4	0.002	33.66	33.66
2	46.4	46.8	45.6	45.6	46.0	46.08	0.002	33.27	33.27
3	30.4	31.6	35.2	32.0	32.4	32.32	0.005	30.16	30.16
4	52.0	50.0	52.0	51.0	51.3	51.26	0.002	34.19	34.19
5	44.0	55.2	52.0	48.0	49.0	49.64	0.002	33.84	33.84
6	44.0	46.8	42.0	43.0	44.6	44.08	0.003	32.87	32.87
7	57.6	58.0	48.4	56.8	55.0	55.16	0.002	34.77	34.77
8	56.0	52.0	56.4	50.0	53.0	53.48	0.002	34.54	34.54
9	54.4	48.8	47.2	44.8	48.8	48.8	0.002	33.72	33.72
					mean	47.69		33.45	33.45

S/N ratio of compressive strength

Levels	Factors		
	FA/C	*W/C*	*PVA1/PVAtot %*
1	34.34	34.21	33.69
2	33.63	33.88	33.73
3	32.36	32.25	32.92
Delta	1.98	1.96	0.80
Rank	1.00	2.00	3.00

Appendix (B)

Material and tests

Mortar mixture of the HFF matrix (mixture CN)

Tensile test specimens after test

Elevated temperature test

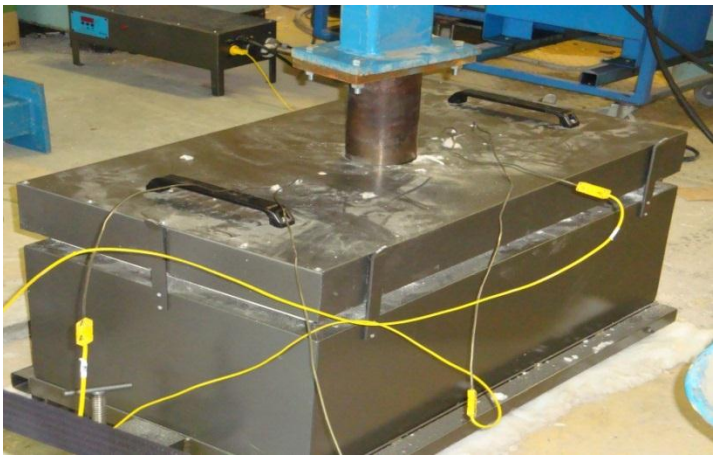

Kiln oven during flexure test after specimen achieved the designated temperature

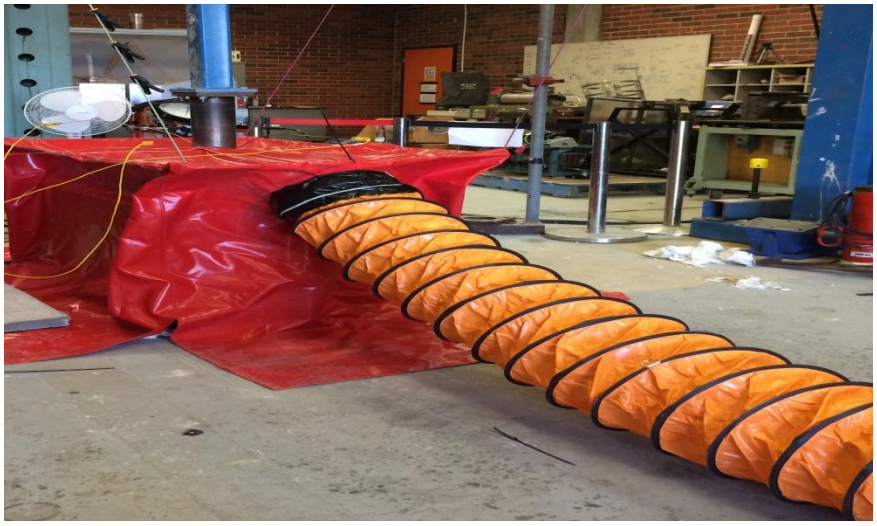

Smoke absorption system during the heating process (elevated temperature test)

HFF panel cross section after testing for flexure at 400ºC

PVA fibre full evaporation at 600ºC

Composite slabs

Teflon plates in the left support area

HFF-OWC 3 at failure

HFF-OWC 5 at failure

HFF-OWC 13 at failure

Appendix (C)

Transversely isotropic equation

The concept of the constitutive equation for the numerical analysis is based on the Hooke's law:

$$\{\sigma\} = [C]\{\varepsilon\}$$

where the stiffness matrix [C] is defined by the transformation matrix as follow:

$$[C'] = [T]^T[C'][T]$$

and

$$[C'] = [T][C][T]^T$$

the Hooke's law in three dimensions (3D) for anisotropic materials takes the form

$$\sigma_{ji} = C_{jilk}\varepsilon_{lk}$$

Since the stress- strain tensor are symmetric it is to mention that

$$C_{ijkl} = C_{jikl} = C_{ijlk} = C_{jilk}$$

This lead to 6x6 matrix in a contracted written form as follow:

$$\begin{Bmatrix}\sigma_1\\ \sigma_2\\ \sigma_3\\ \sigma_4\\ \sigma_5\\ \sigma_6\end{Bmatrix} = \begin{bmatrix}C_{11} & C_{12} & C_{13} & C_{14} & C_{15} & C_{16}\\ C_{12} & C_{22} & C_{23} & C_{24} & C_{25} & C_{26}\\ C_{13} & C_{23} & C_{33} & C_{34} & C_{35} & C_{36}\\ C_{14} & C_{24} & C_{34} & C_{44} & C_{45} & C_{46}\\ C_{15} & C_{25} & C_{35} & C_{45} & C_{55} & C_{56}\\ C_{16} & C_{26} & C_{36} & C_{46} & C_{56} & C_{66}\end{bmatrix} \begin{Bmatrix}\varepsilon_1\\ \varepsilon_2\\ \varepsilon_3\\ \gamma_4\\ \gamma_5\\ \gamma_6\end{Bmatrix}$$

A random distributed fibre in a cross-section can be considered an axis of symmetry which describes transversely isotropic materials (Barbero, 2014). In transversely isotropic materials the plane of symmetry is the plane containing the fibre direction. Therefore, the axis of symmetry is the fibre direction (1-direction), and the 3D constitutive equation reduces to equation 8.7, which is described by five constants as follow:

$$\begin{Bmatrix}\sigma_1\\ \sigma_2\\ \sigma_3\\ \sigma_4\\ \sigma_5\\ \sigma_6\end{Bmatrix} = \begin{bmatrix}C_{11} & C_{12} & C_{12} & 0 & 0 & 0\\ C_{12} & C_{22} & C_{23} & 0 & 0 & 0\\ C_{12} & C_{23} & C_{22} & 0 & 0 & 0\\ 0 & 0 & 0 & 1/2(C_{22} - C_{23}) & 0 & 0\\ 0 & 0 & 0 & 0 & C_{66} & 0\\ 0 & 0 & 0 & 0 & 0 & C_{66}\end{bmatrix} \begin{Bmatrix}\epsilon_1\\ \varepsilon_2\\ \varepsilon_3\\ \varepsilon_4\\ \varepsilon_5\\ \varepsilon_6\end{Bmatrix}$$

FE- model of RVE

```
/TITLE,Elastic modulus of HFF
!Define variables for parametric Model of RVE
rf1=8                    ! fiber 1 radius in microns
rf2=33.0                 ! fiber 2 radius in microns
a2=73.9                  !Length in Microns
a3=128                   !a2*tan60
a1=a2/4                  !Length in Micron
/PREP7
MP,EX,1,26.5
MP,NUXY,1,0.25
MP,EX,2,30.7
MP,NUXY,2,0.2
ET,1,SOLID65             !Mortar Matrix Element
BLOCK,0,a2,0,a3,0,a1     !Geometry
CYLIND,rf1,,0,a1,0,90
WPOFF,a2,a3
CYLIND,rf2,,0,a1,180,270
VOVLAP,all
NUMCMP,all
/DEVICE,VECTOR,1
/VIEW,1,1,2,3
/ANG,1
/PNUM,VOLU,1
/PNUM,MAT,1
/REPLOT
LSEL,U,LOC,Z,A1          !Mesh process
LSEL,U,LOC,Z,0
LESIZE,ALL,,,2
VSEL,S,,,1,2
ASLV,S
LSLA,S
LESIZE,ALL,,,6
LSEL,S,LOC,Y,A3
LSEL,A,LOC,Y,0
LESIZE,ALL,,,3
ALLSEL,ALL
LESIZE,ALL,,,12
MAT,1
VMESH,1,2
MAT,2
VSWEEP,3
EPLOT
FINISH                   !Finishing mash process
/SOLU
ANTYPE,STATIC            ! Analysis type Structure
LSCLEAR,ALL              !BOUNDARY CONDITION COLUMN1
```

```
ASEL,S,LOC,X,0
ASEL,A,LOC,X,A2
DA,ALL,UX,0
ASEL,S,LOC,Y,0
ASEL,A,LOC,Y,A3
DA,ALL,UY,0
ASEL,S,LOC,Z,0
DA,ALL,UZ,0
ASEL,S,LOC,Z,A1
DA,ALL,UZ,A1
ASEL,ALL
LSWRITE,1              !Writes load and load step option data to a file
LSCLEAR,ALL            !Boundary condition for column 2
ASEL,S,LOC,X,0
DA,ALL,UX,0
ASEL,S,LOC,X,A2
DA,ALL,UX,A2
ASEL,S,LOC,Y,0
ASEL,S,LOC,Y,A3
DA,ALL,UY,0
ASEL,S,LOC,Z,0
ASEL,S,LOC,Z,A1
DA,ALL,UZ,0
ASEL,ALL
LSWRITE,2
LSCLEAR,ALL             ! Boundary condition for column 3
ASEL,S,LOC,X,0
ASEL,A,LOC,X,A2
DA,ALL,UX,0
ASEL,S,LOC,Y,0
DA,ALL,UY,0
ASEL,S,LOC,Y,A3
DA,ALL,UY,A3
ASEL,S,LOC,Z,0
ASEL,A,LOC,Z,A1
DA,ALL,UZ,0
ASEL,ALL
LSWRITE,3
LSSOLVE,1,3
FINISH                  !End of boundary conditions

                                !APDL TO COMPUTE AVERAGE STRESS IN "RVE"
*CREATE,SRECOVER   !,mac     !MACRO TO CALCULATE AV STRESS
/NOPR
ETABLE, ,VOLU,                  !Fill a table of element values for further processing
ETABLE, ,S,X
ETABLE, ,S,Y
ETABLE, ,S,Z
ETABLE, ,S,XY
ETABLE, ,S,XZ
ETABLE, ,S,YZ
ETABLE, ,S,YZ
```

```
SMULT,SXV,VOLU,SX,1,1,       !Stress by Element
SMULT,SYV,VOLU,SY,1,1,
SMULT,SZV,VOLU,SZ,1,1,
SMULT,SXYV,VOLU,SXY,1,1,
SMULT,SXZV,VOLU,SXZ,1,1,
SMULT,SYZV,VOLU,SYZ,1,1,
SSUM
*GET,TOTVOL,SSUM,,ITEM,VOLU
*GET,TOTSX,SSUM,,ITEM,SXV
*GET,TOTSY,SSUM,,ITEM,SYV
*GET,TOTSZ,SSUM,,ITEM,SZV
*GET,TOTSXY,SSUM,,ITEM,SXYV
*GET,TOTSXZ,SSUM,,ITEM,SXZV
*GET,TOTSYZ,SSUM,,ITEM,SYZV
SXX0=TOTSX/TOTVOL          !Compute average Stress
SYY0=TOTSY/TOTVOL
SZZ0=TOTSZ/TOTVOL
SXY0=TOTSXY/TOTVOL
SXY0=TOTSXY/TOTVOL
SYZ0=TOTSYZ/TOTVOL
/GOPR
*END                         !SRECOVER
/POST1
/DEVICE,VECTOR,0
PLESOL,S,Z,1
SET,1                        !First column
*USE,SRECOVER
C11=Szz0
C21=Sxx0
C31=Syy0
set,2
*use,srecover                !second column
C12=Szz0
C22=Sxx0
C32=Syy0
SET,3                        !Third column
*USE,SRECOVER
C13=sZZ0
C23=SXX0
C33=Syy0
EL= C11-2*C12*C21/(C22+C23)                                  !Longitudinal E1 modulus
nuL=C12/(C22+C23)
ET=(C11*(C22+C23)-2*C12)*(C22-C23)/(C11*C22-C12*C21)   !12 possion ratio
nuT=(C11*C23-C12*21)/(C11*C22-C12*C21)                       !23 possion ratio
GT=(C22-C23)/2                                               !Shear stiffness
FINISH
```